

**CRUSTAL EVOLUTION OF THE NEOPROTEROZOIC MOZAMBIQUE BELT
ROCKS IN MATUU-MASINGA AREA, CENTRAL KENYA: AN IMPLICATION TO
THEIR TECTONIC SETTING AND POTENTIAL MINERALIZATION**

**THIS THESIS HAS BEEN ACCEPTED FOR
THE DEGREE OF...PH...D... 1999...
AND A COPY MAY BE PLACED IN THE
UNIVERSITY LIBRARY.**

By

Christopher Munyao Nyamai

**A thesis submitted to the Faculty of Science in fulfillment of the requirements for the
Degree of Doctor of Philosophy (Geology).**

Department of Geology, University of Nairobi.

PO Box 30197, Nairobi, Kenya.

In Nairobi, July 1999.

DECLARATION

I hereby declare that this is my own work and has not been submitted for a degree at any other University. All sources of information have been specifically acknowledged by means of references.

I am indebted to my colleagues and staff at the Department for all the assistance given to me and for the facilities and firm support which was critical to the successful completion of this project. My special thanks go to my supervisors and technical assistants provided by the following organizations towards the completion of the present research work.

Signed C.M. Nyamai Date 2/10/99

This Ph.D. Thesis has been submitted for examination with our knowledge as University supervisors.

Signed Prof. S.J. Gaciri Date 4/10/99

DEPARTMENT OF GEOLOGY

Signed Dr. N. Opiyo-Akech Date 6/10/99

DEPARTMENT OF GEOLOGY

ACKNOWLEDGMENTS

This work was mainly carried out at the Department of Geology, University of Nairobi, under the guidance of Prof. S.J. Gaciri and Dr. Opiyo-Akech. Both supervisors followed with keen interest the development of this thesis from its infancy to maturity. I wish to express my deep gratitude to them for all the support they gave me throughout this study. Their constructive criticism on various drafts of the thesis proved quite valuable.

I am indebted to my colleagues and staff at the Department for all the assistance given to me and for the friendly and warm atmosphere which was conducive to the successful completion of this work. I acknowledge with profound thanks the financial and technical assistance provided by the following organizations towards the completion of the present research work:

- (i) The Deans Committee, University of Nairobi, for providing financial assistance for carrying out the fieldwork exercise and partial analysis of the research data.
- (ii) The Japan Co-operation Development Agency (JICA) for sponsoring a one-year training programme in Metallurgy and Mineral Processing Techniques at the Institute of Advanced Materials, Tohoku University, Japan.
- (iii) To United Nations Education, Scientific and Cultural Organization (UNESCO) for providing funds to carry out isotope analysis of the research samples.

I am grateful to Prof. H. Fujimaki, of the Institute of Mineralogy, Petrology and Economic Geology, Tohoku University for Rb/Sr isotope determinations; to Prof. K. Itagaki, of the Institute of Advanced Materials, Tohoku University for introducing me to high temperature gas-phase equilibria systems; to Bo Johanson, of the Geological Survey of Finland, and Y. Sato, of Tohoku University, for mineralogical microprobe analyses. The encouraging discussions and literature support from Prof. S. Muhongo of the Geology Department, University of Dar-Es-Salaam, are gratefully acknowledged.

My understanding of the geology of Matuu-Masinga area was greatly increased by discussions with colleagues at the Mines and Geological Department, regional office in Embu. I acknowledge the fruitful discussions I held with Peter Mosley of the British Geological Survey, with whom we made a number of study visits to the survey area. Special thanks are due to

Shedrack Kimomo, Justus MRagwa and Mwaura Mwendia for their co-operation in the field. There are other colleagues who, though unnamed, assisted me in various ways towards the completion of the present study. A special word of gratitude goes to them.

I express my warmest thanks to my wife, Elizabeth Koki, for her patience and support, and our children who helped to keep our feet firmly on the ground during the course of this study. Finally and greatest of all, I thank God for his countless blessings and sustenance.

ABSTRACT
DEDICATION

The first research study was carried out in 1970 at the University of Toronto, Canada. The study was carried out in order to understand the relationship between the structure and properties of the polymer. The study was carried out in order to understand the relationship between the structure and properties of the polymer.

In memory of my parents, **Jones and Beatrice Munyao**, who installed patience and hope in my research of the planet earth.

The study was carried out in order to understand the relationship between the structure and properties of the polymer. The study was carried out in order to understand the relationship between the structure and properties of the polymer.

The study was carried out in order to understand the relationship between the structure and properties of the polymer. The study was carried out in order to understand the relationship between the structure and properties of the polymer.

The study was carried out in order to understand the relationship between the structure and properties of the polymer. The study was carried out in order to understand the relationship between the structure and properties of the polymer.

The study was carried out in order to understand the relationship between the structure and properties of the polymer. The study was carried out in order to understand the relationship between the structure and properties of the polymer.

The study was carried out in order to understand the relationship between the structure and properties of the polymer. The study was carried out in order to understand the relationship between the structure and properties of the polymer.

ABSTRACT

The Matuu-Masinga study area, located about 70 km north-east of Nairobi, lies at the intersection of latitude $1^{\circ} 10'S$ and longitude $37^{\circ} 30'E$. The area is predominantly underlain by rocks of the Mozambique Belt (MB) in central Kenya. The MB itself exhibits a general N-S trend extending from Mozambique in the South, through East Africa and beyond to Ethiopia in the North.

The MB has a complex history of superimposed deformation and metamorphism which consists of a high grade reworked or reactivated basement. Presently this trans-continental belt is regarded as a product of continent-continent collision. This mobile belt is believed to be polyorogenic, with the latest Neoproterozoic (the Pan-African) orogeny being superimposed onto the Mesoproterozoic (Kibaran) and Palaeoproterozoic (the Ubendian) orogenies.

The study area offers a striking geological region composed of granitoids, ultramafic/mafic rocks and the field association of granulite-(meta)-anorthosite-amphibolite rocks. These rocks are of greater importance insofar as the understanding of the tectonic evolution of the belt and petrogenesis of the deep continental crust is concerned. The present study has drawn evidence from trace element and isotope geochemistry of the rocks and from analysis of the characteristics and sequence of the structures.

The Matuu-Masinga area firstly experienced regional prograde granulite facies metamorphism which was later retrograded to the amphibolite and greenschist-facies. The structural trend varies from NNW-SSE to NW-SE with westerly dips ranging from 50° to the vertical. Several shear zones, various foliation surfaces, linear structures and complex folds suggest a complex tectonic history of the region with at least three phases of deformation.

Distribution of aluminum among the tetrahedral and octahedral sites in the pyroxene analyses from dioritic rocks shows the clinopyroxenes to have crystallized under higher pressure than their corresponding iron rich orthopyroxenes. The almost equal amounts of the jadeite (Al^{VI}) and Ca-Tschermak (Al^{IV}) in the clinopyroxenes of gabbroic rocks are interpreted to be as a result of the combined effects of high pressure and high temperature. The characteristic coronas around clinopyroxene crystals are interpreted to have developed under metamorphic conditions.

Thermobarometric PT calibrations obtained from various mineral pairs range from 750 $^{\circ}C$ and pressures between 6.55 to 6.98 kbar for the amphibolite rocks, to temperatures

between 879-904 °C and pressures between 5.89 to 6.31 kbars for the gabbroic rocks, to temperatures between 843-854 °C and pressure of 15 kbar for the dioritic rocks. The use of the Al-in-amphibole thermo-barometry data for the granitic rocks gave an average equilibrium temperature of 750 °C and a pressure of 5.97 kbar.

The rocks of the study area are mainly metaluminous to slightly peraluminous. Geochemical data indicate the granites are of magmatic origin with calc-alkaline affinity. The data indicate a dominantly island arc-tectonic setting with subordinate within-plate environment. A Rb-Sr whole rock age of 558 +/- 16 Ma is given on the Mavoloni hills granite. From the low initial $^{87}\text{Sr}/^{86}\text{Sr}$ ratio of 0.70398 recorded from the granite, the age is interpreted to indicate the time of original emplacement for granite magma from a juvenile mantle-derived material.

The relatively high concentration of Cu (av. 1960 ppm) and zinc (av. 155 ppm) in the mafic rocks of the study area compared with the average for ultramafic rocks of 30 and 50 ppm respectively invokes further exploration of their ore minerals. The granites and diorites in the study area are of potential economic use as dimension stone in the construction and building industry.

Keywords: Mozambique Belt, Tectonic evolution, Petrography, Mineral chemistry, Thermo-barometry, Geochemistry, Geochronology, Structures, Metamorphism, Mineralization, Matuu-Masinga area.

TABLE OF CONTENTS

	1.0 REGIONAL GEOLOGICAL SETTING	iv
	1.0.1 Regional Geology	iv
	1.0.2 Tectonic History of the Kenya Tectonic Province	page iv
Title	1.0.3 The Potential and Current Role of the Kenya Geological Survey	(i)
Declaration	Foreword	(ii)
Acknowledgments	Foreword of the Director General of the Kenya Geological Survey	(iii)
Dedication	Committee Members	(v)
Abstract	Kenya Geological Survey Commission Commission	(vi)
Table of Contents	Kenya Geological Survey Commission Commission of Survey of Kenya	(viii)
List of Figures	Kenya Geological Survey Commission Commission of Survey of Kenya	(xiii)
List of Plates	Kenya Geological Survey Commission Commission of Survey of Kenya	(xv)
List of Tables	Kenya Geological Survey Commission Commission of Survey of Kenya	(xviii)
List of Appendices	Kenya Geological Survey Commission Commission of Survey of Kenya	(xix)
	1.0.4 Kenya Geological Survey Commission Commission of Survey of Kenya	iv
 CHAPTER 1: INTRODUCTION		
1.1	Statement of the problem and Aim of the study	1
1.2	1.1.1 Objectives of the study	3
1.3	Laboratory Methods	5
1.4	Sampling	6
1.5	LOCAL GEOLOGICAL SETTING	6
	1.5.1 Local Framework	6
	1.5.1 (a). Location	6
	1.5.1 (b). Physiography and climate	8
	1.5.1 (c). Previous Geological work	10

1.6	REGIONAL GEOLOGICAL SETTING	13
1.6.1	Regional Framework	13
1.6.2	Tectonic Features of the Kenya-Tanzania Province	16
1.6.3	The Foreland and External zone of the Kenya-Tanzania Province	19
1.6.4	The Internal zone of the Kenya-Tanzania Province	20
1.6.4.1	Granulite Complexes	20
	(a). North-Central Kenya Granulite Complex	20
	(b). The Proterozoic Granulite Terranes of Eastern Tanzania	23
	(c). Central Granulite Complexes of Tanzania	25
	(d). The Kurase and Kasigau Groups of Kenya	26
1.6.4.2	Ophiolitic Rocks	27
	(a). Sekerr and Itiso Ophiolite	27
	(b). Baragoi Ophiolite	28
	(c). Moyale Ophiolite	29
	(d). Pare Mountains Ophiolite	29
1.6.5	Geodynamic Model of the Mozambique Belt	32
1.7	MINERALIZATION WITHIN THE KENYAN SEGMENT OF THE MOZAMBIQUE BELT.	33
1.7.1	Ores related to Intermediate Magmatic rocks	33
1.7.2	Ophiolite-related Ores and Minerals	35
1.7.3	Metamorphogenic Minerals	35
1.7.4	Pegmatite Ores and Minerals	36
1.7.5	Syngenetic Stratiform Ores	37

1.7.6	Industrial raw Materials	37
1.7.7	Potential Mineralization	38
1.7.8	Conclusion	39
CHAPTER 2:		
PETROGRAPHY, MINERAL CHEMISTRY AND THERMOBAROMETRY OF		
THE MOZAMBIQUE BELT INTRUSIVE ROCKS OF MATUU-MASINGA		
AREA, CENTRAL KENYA		
2.0	INTRODUCTION	40
2.1	PETROGRAPHY AND MINERAL CHEMISTRY	41
2.1.1.	The Mafic Rocks	41
2.1.1.1	Petrography of the meta-diorite rock	43
2.1.1.2	Mineral chemistry of the meta-diorite rock	48
2.1.1.3	Petrography of the meta-gabbro rock	55
2.1.1.4	Mineral chemistry of the meta-gabbro rock	59
2.1.1.5	Petrography of the anorthositic gabbro	64
2.1.1.6	Petrography of the hornblende gneiss	65
2.1.1.7	Mineral chemistry of the hornblende gneiss	71
2.1.1.8	Petrography of the biotite gneiss	73
2.1.1.9	Petrography and mineral chemistry of the minor mafic intrusives:	74
	(a). Syeno-diorite rock	74
	(b). Mafic granulite (plagioclase-pyroxene-garnet) gneiss	75
2.1.2	The granitic rocks	80
2.1.2.1	Petrography of the granitoid gneiss	81

2.1.2.2	Petrography of the porphyritic granite gneiss	81
2.1.2.3	Petrography of the pink granite	81
2.1.2.4	Petrography of the grey granite	83
2.1.2.5	Mineral chemistry of the granitic rocks	86
2.2	ESTIMATES OF METAMORPHIC CONDITIONS	89
2.2.1	Condition of pyroxene crystallization	89
2.2.2	Thermo-barometric conditions of formation of the mafic rocks	90
2.2.2.1	Amphibolite rocks	91
2.2.2.2	The Gabbroic and meta-diorite rocks	91
2.2.2.3	Mafic granulite (plagioclase-pyroxene-garnet) gneiss	94
2.2.3	Thermo-barometric conditions of formation of the granitic rocks	94
2.3	DISCUSSION AND CONCLUSION	95
2.3.1	Mafic rocks	95
2.3.2	Granitic rocks	98
2.3.3	Metamorphic grade	98
CHAPTER 3:		
GEOCHEMISTRY AND TECTONOMAGMATIC AFFINITIES OF THE		
MOZAMBIQUE BELT INTRUSIVE ROCKS IN MATUU-MASINGA AREA,		
CENTRAL KENYA.		
3.0	INTRODUCTION	101
3.1	STRUCTURAL SETTING	101
3.2	PETROGRAPHY	102

3.3	GEOCHEMISTRY AND TECTONOMAGMATIC AFFINITIES	105
3.3.1	Alteration effects	105
3.3.2	Geochemical characteristics	105
3.3.3	Spidergram characteristic patterns for the mafic rocks	112
3.3.4	Spidergram characteristic pattern for the granitic rocks	112
3.4	ISOTOPE GEOCHEMISTRY	116
3.5	DISCUSSION: Petrogenesis and Tectonic setting	116
3.6	CONCLUSION	119

CHAPTER 4:

**STRUCTURES, METAMORPHISM AND GEOCHRONOLOGY OF THE
MOZAMBIQUE BELT INTRUSIVE ROCKS IN MATUU-MASINGA
AREA, CENTRAL KENYA.**

4.0	INTRODUCTION	120
4.1	STRUCTURAL SETTING OF MATUU-MASINGA AREA	122
4.1.1	Structures	122
4.1.2	Metamorphism	130
4.2	GEOCHRONOLOGICAL STUDIES	132
4.2.1	Nature of samples	132
4.2.2	Analytical method	132
4.2.3	Results	133
4.2.4	Interpretation	135
4.3	CONCLUSIONS	136

CHAPTER 5:	CONCLUSIONS	81
5.1	Petrography	137
5.2	Structural Evolution	138
5.3	Metamorphism	139
5.4	Mineral Chemistry	140
5.5	Thermobarometric Conditions	141
5.6	Geochronology	142
5.7	Geochemistry	143
5.8	Economic Mineral Potential	144
5.9	Recommendations for further work	145
	REFERENCES	145
	APPENDICES	161
	List of Figures	
	Chapter 1	
Fig. 1.1	The study area superimposed on the geological map of Kenya.	2
Fig. 1.2	Geological Map of Matuu-Masinga area, central Kenya.	7
Fig. 1.3	Structural trends in the Mozambique belt.	14
Fig. 1.4	Structural and stratigraphic sketch map of the Mozambique belt.	18
Fig. 1.5	Geological Map of Northern Kenya (Samburu-Marsabit area).	21
Fig. 1.6	Representative geochemical patterns for the Baragoi lavas.	30
Fig. 1.7	Zr/Y versus Zr discriminant diagram for basic rocks from Baragoi and	30
Fig. 1.8	Moyale ophiolite zones.	30
Fig. 1.8	Ti-Zr-Y discriminant diagram for basic rocks from Baragoi and Moyale	31
	ophiolite belts	31

Fig. 1.9	Pre-drift reconstruction of Gondwana showing Pan-African belts.	34
Chapter 2		
Fig. 2.1	Rock samples from Matuu-Masinga area plotted on $(\text{Na}_2\text{O} + \text{K}_2\text{O})$ vs SiO_2 variation diagram.	42
Fig. 2.2	X-ray diffraction pattern for diorite rock from Matuu-Masinga area, central Kenya.	49
Fig. 2.3	Plot of clinopyroxenes given in Tables 2.1 & 2.2 on part of triangular diagram in terms of Ca: Mg : Fe atomic percent.	51
Fig. 2.4	Nomenclature of calcic amphibole from Matuu-Masinga area.	53
Fig. 2.5	Biotites in the diagram $\text{Fe}/(\text{Fe}+\text{Mg})$ vs $\text{Al}^{\text{IV}}-2$.	54
Fig. 2.6	X-ray diffraction pattern for gabbroic rock from Matuu-Masinga area central Kenya.	58
Fig. 2.7	Comparative diffraction pattern between alkali pink granite and porphyritic granite, Matuu-Masinga area, central Kenya	85
Chapter 3		
Fig. 3.1	Diagram for assessing alteration of magmatic rocks of the Matuu-Masinga area, central Kenya.	106
Fig. 3.2	Major element discrimination diagram distinguishing ortho- and para-gneiss in high grade metamorphic terrain in Matuu-Msinga area, central Kenya.	107
Fig. 3.3	Composition of mafic and granitic rock suites projected onto $(\text{FeO}^* + \text{TiO}_2) - \text{Al}_2\text{O}_3 - \text{MgO}$ and $\text{FeO}^* - (\text{Na}_2\text{O} + \text{K}_2\text{O}) - \text{MgO}$ diagrams.	109

Fig. 3.4	(a). Plot of SiO_2 versus A/CNK molar ratio for mafic and granitic rocks of Matuu area.	109
Fig. 3.5	(b). Alumina saturation-silica diagram for granitic rocks of Matuu area.	109
Fig. 3.5	SiO_2 variation diagrams for Rb, Nb and Y on Matuu-Masinga granitic rocks.	110
Fig. 3. 6	Rb-(Y+Nb) variation diagram for the Matuu-Masinga granitic rocks.	111
Fig. 3.7	Spidergram of the averages of some mafic rocks from Matuu-Masinga area.	113
Fig. 3.8	Patterns for some granitic rocks from Matuu-Masinga area, central Kenya, normalized to ocean ridge granite (ORG) .	114
Chapter 4		
Fig. 4.1	Orientation diagram of foliation poles in the Matuu-Masinga area.	124
Fig. 4.2	Rb-Sr Isochron diagram for granite from Matuu area, central Kenya.	134
List of Plates		
Plate 1.1	Field photograph of Nzukini the Needles granite hills.	9
Plate 2. 1	(a). Photomicrograph of clinopyroxene with exsolved orthopyroxene, amphibole and zoned plagioclase in meta-diorite.	44
Plate 2.1	(b). Photomicrograph of elongated crystals of apatite occurring within interstices of plagioclase, clinopyroxene, and orthopyroxene in meta-diorite	44
Plate 2.2	(a). Photomicrograph of clinopyroxene being replaced by a corona of amphibole in contact with plagioclase in meta-diorite	46

Plate 2.2	(b). Photomicrograph of magnetite with exsolved ilmenite lamellae in meta-diorite	46
Plate 2.3	Photomicrograph of plagioclase in contact with clinopyroxene, orthopyroxene and amphibole in gabbro.	56
Plate 2.4	Photomicrograph of clinopyroxene in optical continuity with and being replaced by amphibole in anorthositic gabbro.	66
Plate 2.5	Photomicrograph of hypersthene inclusion in plagioclase in anorthositic gabbro.	66
Plate 2.6	Photomicrograph of secondary hornblende in plagioclase crystal crevices in anorthositic gabbro.	67
Plate 2.7	(a). Photomicrograph of optically oriented plagioclase and amphibole in anorthositic gabbro.	67
Plate 2.7	(b). Photomicrograph of secondary plagioclase from the leucocratic layer in anorthositic gabbro.	68
Plate 2.8	Photomicrograph of spinel-hornblende-plagioclase reaction zoning in anorthositic gabbro.	68
Plate 2.9	Photomicrograph of amphibole alternating with plagioclase showing lineation texture in hornblende gneiss.	69
Plate 2.10	Field photograph of foliated biotite gneiss, Matuu-Masinga area.	69
Plate 2.11	(a). Photomicrograph of mafic granulite showing recrystallized garnet traversing plagioclase and in contact with pyroxene and epidote.	77
Plate 2.11	(b). Photomicrograph of mafic granulite showing garnet in contact with plagioclase	77
Plate 2.12	Field photograph of outcrops of porphyritic granite in Matuu area.	82

Plate 2.13	Photomicrograph of microcline porphyroblast with exsolved plagioclase in contact with quartz in porphyritic granite.	82
Plate 2.14	Photomicrograph of partially sericitized plagioclase, biotite, microcline and quartz in pink alkali granite.	84
Plate 3.1	Field photograph showing migmatitic folds, Matuu-Masinga area.	103
Plate 3.2	Field photograph showing mafic dykes of doleritic composition intruding the basement, Matuu-Masinga area, central Kenya	103
Plate 4.1	Field photograph showing the general topography of Matuu-Masinga area.	121
Plate 4.2	Field photograph of foliated biotite gneiss, Matuu-Masinga area.	121
Plate 4.3	Field photograph showing migmatitic folds, Matuu-Masinga area.	125
Plate 4.4	Field photograph showing isoclinal folds, Matuu-Masinga area.	125
Plate 4.5	Field photograph showing open folds, Matuu-Masinga area.	126
Plate 4.6	Field photograph showing mafic dykes intruding the basement.	126
Plate 4.7	Field photograph showing a rotated hornblende boudin in psammitic gneiss affected by a sinistral shear zone.	128
Plate 4.8	Field photograph showing longitudinal and a-c joints within psammitic gneiss Matuu-Masinga area, central Kenya.	128
Plate 4.9	Field photograph showing a zoned and faintly deformed pegmatite.	129
Plate 4.10	Field photograph showing a deformed pegmatite vein with marked fracture cleavage conformable with the regional foliation planes.	129
List of Tables		
Table 2A.	Modal composition of representative dioritic and gabbroic rock samples from Matuu-Masinga area, central Kenya.	45

Table 2. 1	Microprobe analyses of orthopyroxene, clinopyroxene, plagioclase,biotite, amphibole and apatite from meta-diorite rock, Matuu-Masinga area.	50
Table 2.2	Microprobe analyses for orthopyroxene, clinopyroxene, plagioclase, amphibole and biotite occurring in representative gabbroic rocks, Matuu-Masinga area.	60
Table 2.3	Microprobe analysis of amphibole, plagioclase and biotite occurring in amphibolite rocks, Matuu-Masinga area.	72
Table 2B.	Modal analysis of representative biotite gneisses from Matuu-Masinga area.	74
Table 2.4	Mean microprobe analyses of K-feldspar, plagioclase, amphibole and biotite occurring in syeno-diorite rock, Matuu-Masinga area.	76
Table 2.5	Electron microprobe analysis of garnet, plagioclase, clinopyroxene and sphene from plagioclase-pyroxene-garnet granulite gneiss, Matuu-Masinga area.	78
Table 2C.	Modal composition of representative granitic rock samples from Matuu-Masinga area, central Kenya.	80
Table 2.6	Microprobe analyses of K-feldspar, plagioclase, biotite, amphibole and chlorite occurring in granitic rocks of Matuu-Masinga area, central Kenya.	87
Table 2.7	K_p values for seven co-existing pyroxene pairs from Matuu-Masinga mafic rocks.	89
Table 2.8	Thermobarometric data for intrusive rocks from Matuu-Masinga area.	92
Table 3.1	Rb-Sr analytical data for representative rocks from Matuu-Masinga area.	116
Table 4.1	Chemical analysis of granite rock samples from Mavoloni hill, Matuu-Masinga area, central Kenya.	132
Table 4.2	Rb-Sr analytical data for granite samples from Matuu-Masinga area.	133

List of Appendices

- Appendix 1: Geological Map of Matuu-Masinga area, central Kenya.
- Appendix 2: Microprobe Mineral Analyses.
- Appendix 2.1 Clinopyroxene compositions in the gabbroic and dioritic rocks of Matuu-Masinga area, central Kenya.
- Appendix 2.2 Orthopyroxene compositions in the gabbroic and dioritic rocks of Matuu-Masinga area, central Kenya.
- Appendix 2.3 Plagioclase compositions from rocks of the Matuu-Masinga area.
- Appendix 2.4 Amphibole compositions from rocks of the Matuu-Masinga area.
- Appendix 2.5 Biotite compositions from rocks of the Matuu-Masinga area, central Kenya.
- Appendix 2.6 K-feldspar compositions from rocks of the Matuu-Masinga area.
- Appendix 2.7 Garnet, sphene and rutile compositions from rocks of the Matuu-Masinga area, central Kenya.
- Appendix 2.8 Apatite, calcite, ilmenite and magnetite compositions from rocks of the Matuu-Masinga area, central Kenya.
- Appendix 2.9 Chlorite and epidote compositions from rocks of the Matuu-Masinga area.
- Appendix 3: Whole-rock Geochemical Analysis
- Appendix 3.1 Geochemical analyses of the Mozambique belt intrusive rocks from Matuu-Masinga area, central Kenya.

CHAPTER 1

INTRODUCTION

1.1 Statement of the Problem and Aim of the study

Up until now, the Mozambique belt has still not been completely understood in spite of appreciable mapping and scientific research carried out since it was first defined in 1948 by Holmes (1951). Our knowledge of the belt has lagged behind most other orogens of similar size and importance partly because the belt cuts across many developing countries where it is difficult to work or which lack enough economic resources to carry out regional research programmes.

The Mozambique Belt contains numerous usually small ultramafic bodies, frequently associated with mafic rocks and generally concordant to strike and dip of the country rocks. These rocks are deformed and metamorphosed to the same degree as their country rocks. Some of them may be tectonically reduced ophiolites (Shackleton, 1977; Pohl, 1979; Pohl et al. 1980; Vearncombe, 1983) while others, which are associated with granulites, are possibly fragments of subcontinental mantle (Prochaska and Pohl, 1983). In the absence of distinctive geological features in the belt, Frisch and Pohl (1986) have suggested that petrochemical methods have to be used for a tentative genetic attribution of these rocks.

In the Matuu-Masinga study area, which occurs in the central part of the Kenyan segment of the Mozambique orogenic belt (Fig. 1.1), little is known about its crustal and tectonic evolution. This area, underlain by the Neoproterozoic migmatitic basement, is a striking geological region composed of granitic and mafic rocks. These rocks can be used to test the petrogenetic evolution of the lithologies in the area. For the less understood Mozambique belt, it is envisaged that a proper understanding of the crustal evolution and tectonic environment of

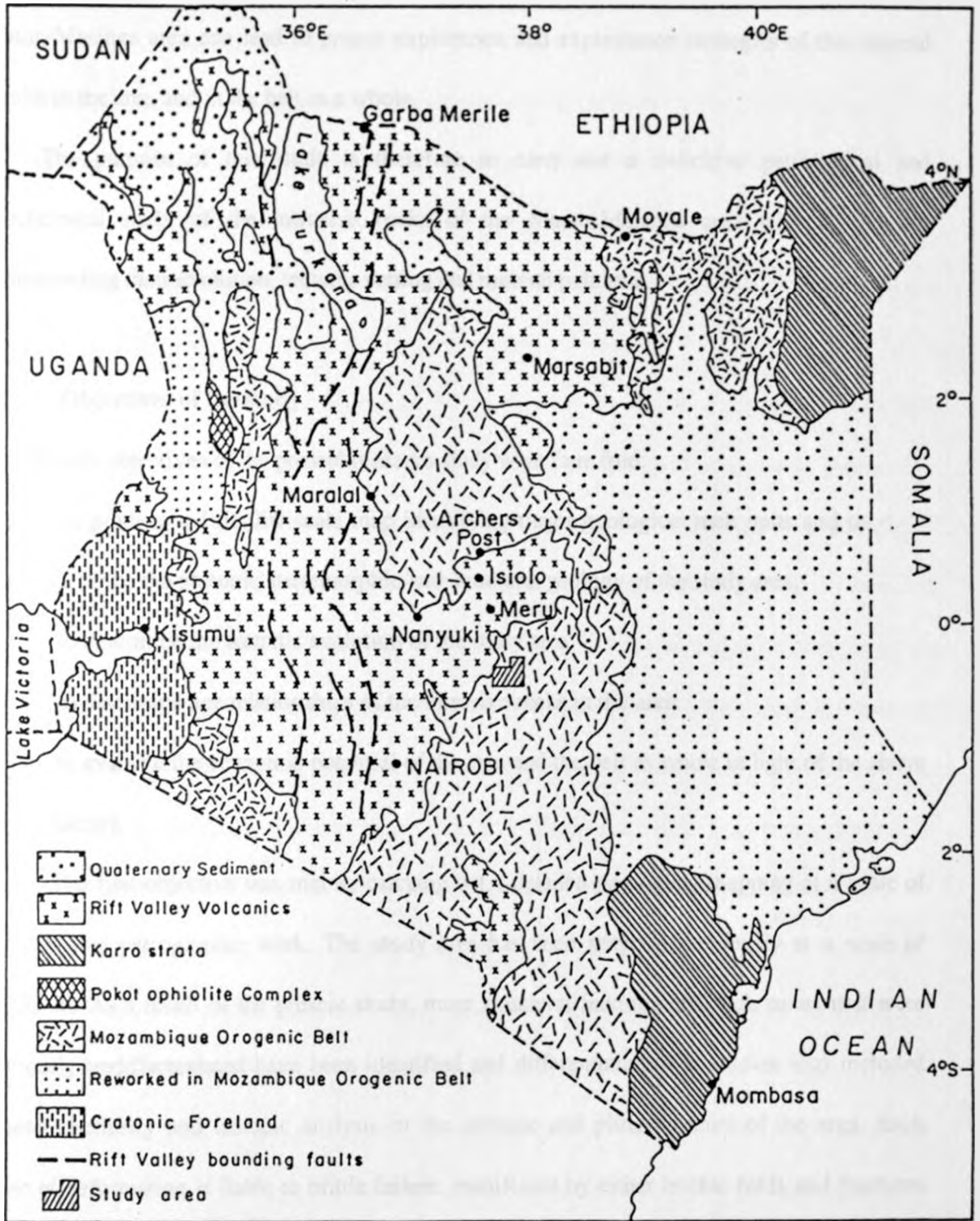


Fig. 1.1. The study area superimposed on the geological map of Kenya (after Key et al., 1989.)

Matuu-Masinga area can lead to proper exploration and exploitation strategies of the mineral wealth in the area and in the belt as a whole.

The purpose of this study is therefore to carry out a definitive petrological and geochemical study of the intrusive rocks of the Matuu-Masinga area with a view to understanding their evolution, tectonic setting and mineral potential.

1.2 Objectives of the study

The primary objectives of the present research study were four-fold:

- i) to produce a 1:50,000 scale map identifying major geological rock units and to describe the plutonic, metamorphic and structural geology of the study area;
- ii) to determine the tectonic evolution of the study area;
- iii) to determine age relationships of the intrusive rocks in the area;
- iv) to evaluate the economic potential of the area and the belt as whole in light of the above factors.

The first objective was met by carrying out a detailed geological mapping at a scale of 1:50,000 and petrographic work. The study area has been mapped previously at a scale of 1:125,000. As a result of the present study, more structural features and rock suites that were previously undifferentiated have been identified and differentiated. The studies also included mineral chemistry and isotopic analysis of the gneissic and plutonic units of the area. Each phase of deformation is liable to brittle failure, manifested by either buckle folds and fractures or ductile deformation, manifested by cleavage or foliation, stretching lineation, folds, oriented minerals, shear zones, microfolds and boudinage. Petrological studies and characteristic mineral compositions have given vital data on the textural, mineralogical and thermobarometric

conditions that prevailed in the study area. Determination of the precise P/T conditions of metamorphism has an important bearing on elucidating the economic potential of the belt. Such P/T values, among other factors, are known to control the conditions at which gemstones are formed. Gemstones of high quality form part of the mineral wealth in the Kenyan segment of the Mozambique belt (Nyamai et al., 1993) and in the adjoining terranes (Malisa and Muhongo, 1990; Pohl, 1988).

The second objective was obtained by drawing evidence from magmatism and mafic/ultramafic rock suites of the study area. The commonest magmatic rocks are "granitoids". These rocks can give crucial evidence on the tectonic evolution of the region, especially in enabling to distinguish those originating above subduction zone, in an island arc or a continental (Andean type) arc, in a collision zone or in a within-plate tectonic setting. The most effective and reliable method is based on trace element analyses (Pearce et al., 1984), partly because the trace elements used are relatively insensitive to alteration during weathering, metamorphism or metasomatism. Evidence of subduction-generated and collisional granitoids is very important as is the transition from collisional to within-plate magmatism. Many of the older granitoids in the belt, now granitic gneisses, were formerly misinterpreted as granitised sediments (Shackleton, 1991). The available results from the present study contribute new information in forming a basis for determining the sequence of tectonic events within the central part of the belt.

The third objective was realized by carrying out geochemical and isotopic studies on the plutonic suites with a view of elucidating their nature, age and genesis. The Mozambique belt is itself polycyclic, consisting, in different regions, of components with very different ages (Key et al., 1989). One of the major problems in the Kenyan Mozambique belt is that there is little comparable geochronological data to establish the age relationship of the various superimposed

tectonic events. The present research study seeks to bridge this gap by providing some data from the Matuu-Masinga area.

The fourth objective has been realized by firstly identifying the major economic mineral deposits in the Kenyan segment of the Mozambique Belt, and secondly by evaluating the data on mineral occurrences in the study area. Based on the research results obtained from the present study, future mineral exploration strategies in the belt is proposed.

1.3 Laboratory methods

Petrographic studies of the rock specimens were carried out by use of an optical microscope at the Institute of Advanced Materials, Tohoku University, Japan. For identification of mineral grains and where necessary determination of certain structural properties, the X-ray diffraction method was employed using a Reigaku Geiger Flex X-ray diffractometer equipped with a copper anode CuK_α ($\lambda = 1.5405$), an accelerating voltage of 35 kV, a current of 26 mA, and a scanning speed of 20 degrees per second. Electron microprobe analyses of minerals were performed by the wavelength dispersive technique using a CAMECA SX 50 electron probe microanalyser (EPMA) at the Geological Survey of Finland (GSF) and a Hitachi X-650S with KEVEX 7000 Q microprobe at the Institute of Advanced Materials, Tohoku University, Japan. Analytical conditions for silicate minerals were an accelerating potential of 15 keV, a sample current of 25 nA, and a beam diameter of 10 μm . Details of the analytical method and a table of simple mineral and metal standards have been published by Alpieti and Sivonen (1983). Results were corrected using the PAP data correction method (Pouchou and Pichoir, 1994) with enhanced light element analysis. The analytical results of the two laboratories are comparable.

Whole rock chemical analysis of the rock samples for the major and trace elements were determined by applying the conventional X-ray fluorescence analysis (XRF) using Philips PW 1400 spectrometers at the Department of Geochemistry, Tohoku University, Japan and the atomic absorption spectrometric (AAS) method at the Mines and Geological Department, Nairobi. Isotopic studies were done using a JEOL-05RB mass spectrometer at the Department of Geochemistry, Tohoku University. The pressure and temperature conditions of the characteristic mineral assemblages were determined by the use of the PTMAFIC software computer program after Soto (1993).

1.4 Sampling

Collection of field samples from Matuu-Masinga area was done with an aim of acquiring a sets of representative fresh specimens. On both petrographical and geochemical grounds, analyses from the best preserved samples were selected for geochemical analyses and computation of average values. Samples were taken from the middle parts of outcrops wherever the exposure conditions allowed this.

1.5 LOCAL GEOLOGICAL SETTING

1.5.1 Local Framework

a) Location

The study area, which lies about 70 km north-east of Nairobi, is situated in Machakos District, central Kenya (Fig. 1.2). It is bounded by the latitudes $1^{\circ} 3'S$ to $1^{\circ} 9'S$ and longitudes $37^{\circ} 25'$ to $37^{\circ} 33'E$. It covers an approximate area of 125 sq.km. Administratively, the area lies mainly in the Matuu and Ol Donyo Sabuk divisions of Machakos District. The road transport to

the study area is provided by the major Thika - Garissa road. Junctions from this major road give access to the hinterland of the study area.

b) Physiography and climate

The study area is characterised by a fairly lowland of basement rocks that consist mainly of granitoids, migmatitic gneisses, biotite gneisses, amphibolites, meta-dolerites, gabbro and anorthosites. The basement rocks give rise to some prominent hills in the area reaching an altitude of 1500m at Mavoloni, 1440m at Ithanga and 1450m at Nzukini the Needles (Plate 1.1).

The study area has an average altitude of about 1200 m above sea level with a gentle topography characterized by small hills and ridges. The main seasonal rivers are the Ndalani to the NW of Matuu town, Kithendu, Kathuleni and Kikwa in the central part, and Mathauta in the eastern part of the survey area respectively. The major rivers in the regional study area are the Tana and Thika. Both rivers are fed by three distinct drainage systems, viz.:

- (i) temporary streams that arise from the Neoproterozoic basement hills
- (ii) permanent streams arising from Mt. Kenya and
- (iii) permanent streams which flow from the Aberdares.

The drainage pattern over the whole study area appears to have been determined by various features. These features include the direction of slope of the Mt. Kenya volcanics, faulting, the relative hardness of the rock types, position of intrusives and dip of the joints. The aforementioned features are particularly noticeable along the Tana river, which for greater part of its course flows across the strike of the formations and is characterized by several sharp right-angled bends. Rapids and small waterfalls are common. Some deep sided gorges along the Tana have been cut giving rise to suitable conditions for dam constructions such as the ones at



Plate 1.1. Field photograph showing the prominent Nzukini the Needles granite hills. Matuu-Masinga area, central Kenya.

Masinga, Kamburu and Kiambere. Elsewhere, within the area, the tributaries form dendritic pattern largely controlled by regional surface gradients and strikes.

Temperatures in the regional survey area vary with altitude. The climate on the higher volcanic landscape to the north of the study area is generally cooler than the lower lying basement system of the Tana and Thika valleys. Rainfall over much of the area is again controlled by altitude, being lowest to the south and east of Tana river and increasing northwards towards the slopes of Mt. Kenya and Aberdares. Total amount of rainfall annually in the Matuu-Masinga study area is between 840 - 890 mm with a mean temperature of 23 °C.

c) **Previous Geological Work**

The Matuu-Masinga study area lies within the predominantly metamorphic rocks of the Mozambique belt in central Kenya (see Figs. 1.1 and 1.2). The Mozambique belt is a Pan-African Neoproterozoic mobile belt that experienced a series of strong deformation, metamorphic and magmatic events about 950 to 450 Ma ago (Kröner, 1984; Shackleton, 1986).

Geological maps on a scale of 1:125,000 with accompanying reports of the Kenya Mines and Geological Department covered the present study area (Bear, 1952; Fairburn, 1958, 1963). Fairburn's (1958) report showed that the basement rocks had suffered high grade metamorphism that included granitoids of replacement origin. Although Fairburn's (1958) report did not indicate economic mineral deposits within the basement system apart from small deposits of Magnetite and Kaolin, it identified considerable reserves of building stone and groundwater within the volcanic succession in the area.

The geology of Ithanga hills area, which borders the north-western section of the present study area, was shown by Mathu and Tole (1984) to be structurally heterogeneous and to have

suffered deformation and high grade regional metamorphism in the upper conditions of the amphibolite facies. According to Mathu and Tole (1984), the degree of granitization in the area is envisaged to have increased south-eastwards culminating in the formation of granitoid gneisses. The granitoid gneisses, interpreted as post-tectonic to the main regional folding and metamorphism, are identified to be of the type: magnetite-bearing magnetite series. By virtue of their occurrence, Mathu and Tole (1984) suggest exploration for sulphide ore deposits and ores of Zn, Mn, Ag, Hg and Cu as these metal ores have been associated with this type of granitoid series (Ishihara, 1980).

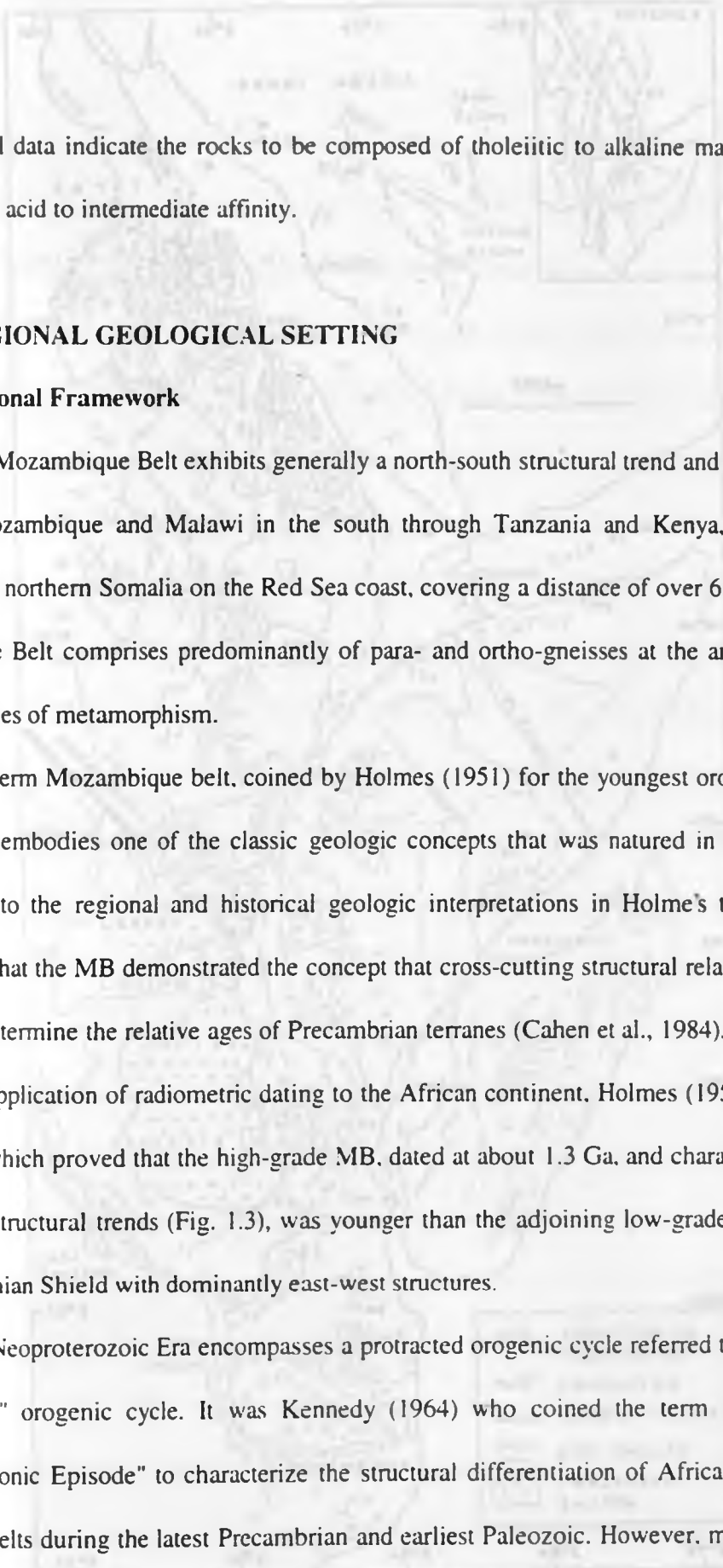
A field mapping exercise carried out in an area located about 30 kms to the west of the present survey area was shown to have suffered a complex structural deformation that includes several shear zones formed in the high grade metamorphism, various foliation surfaces and linear structures, complex super-posed folds as well as strike-slip faults (Mathu et al., 1991). These structures were interpreted to suggest a complex tectonic history of the region with at least three phases of deformation. Based on petrological and structural evidence, Mathu et al. (1991) proposed that the region could have existed as an island arc tectonic environment prior to the final tectonic evolution of the Mozambique belt.

About 40 kms south of the present survey area, a geochronological study by Shibata and Suwa (1979) on the granitoid gneiss occurring in the Mbooni Hills, Machakos area gave a Rb-Sr whole rock age of 766 Ma and low initial $^{87}\text{Sr}/^{86}\text{Sr}$ ratio of 0.7041. Considering the low initial ratio, the age was interpreted to indicate the time of original emplacement for magma derived from the mantle. There is no possibility of a long crustal history for these rocks before this event, and the rocks cannot be reworked material of Archaean age.

Recent geological works undertaken by the Tana and Athi Development Authority in the site investigations of the Masinga and Kamburu dams gave details of the subsurface geology. The report for Masinga dam described the rocks of the area to comprise of granitoid and hornblende gneisses, amphibolite, metamorphosed quartzo-feldspathic gneisses and occasional intrusive pegmatites and dolerites. Structurally, the area is shown to have undergone extensive warping and folding but with minor faulting. At the river level, the metamorphosed basement rocks are covered by alluvial deposits and riverine sediments. The thick loam soils which cover the valley sides represent the older sub-Miocene surface, while the younger black cotton soils have developed over the poorly drained crests of low hills in the area.

Experimental work on the distribution of elements in mineral-pairs from the Mozambique belt rocks of Matuu area has been reported by Gaciri et al. (1993). Gaciri et al. (op.cit) showed the mineral pairs (garnet-biotite, garnet-clinopyroxene, amphibole-clinopyroxene and amphibole-biotite) to be consistent with amphibolite facies, and estimated the temperatures and pressures that affected the area to be between 550° to 880°C and 2 to 10 kbars respectively.

Structural data from recent geological mapping exercise in the present study area (Nyamai, 1995) show the structural trend to vary from NNW-SSE to NW-SE direction, with westerly dips ranging from 50° to the vertical. On outcrop scale, isoclinal, open and overturned folds are a common feature in the area. Competent mafic lensoidal layers that have been rotated and boudinized, and displaced microfaults define a dextral sense of shear. Medium to high-grade (i.e. amphibolite to granulite) mineralogical assemblages of the meta-igneous rocks of the area are represented by quartz, plagioclase, orthopyroxene, clinopyroxene, garnet, actinolite and Mg-hornblende. Accessories include zircon, titanite, apatite, magnetite, ilmenite and pyrite.



Geochemical data indicate the rocks to be composed of tholeiitic to alkaline mafic rocks and calc-alkaline acid to intermediate affinity.

1.6 REGIONAL GEOLOGICAL SETTING

1.6.1 Regional Framework

The Mozambique Belt exhibits generally a north-south structural trend and extends from northern Mozambique and Malawi in the south through Tanzania and Kenya, into Sudan, Ethiopia and northern Somalia on the Red Sea coast, covering a distance of over 6,000 km. The Mozambique Belt comprises predominantly of para- and ortho-gneisses at the amphibolite to granulite facies of metamorphism.

The term Mozambique belt, coined by Holmes (1951) for the youngest orogenic belt in East Africa, embodies one of the classic geologic concepts that was natured in Africa. With significance to the regional and historical geologic interpretations in Holme's time was his observation that the MB demonstrated the concept that cross-cutting structural relationships can be used to determine the relative ages of Precambrian terranes (Cahen et al., 1984). In what was the earliest application of radiometric dating to the African continent, Holmes (1951) furnished actual ages which proved that the high-grade MB, dated at about 1.3 Ga, and characterized by a north-south structural trends (Fig. 1.3), was younger than the adjoining low-grade greenstones of the Tanzanian Shield with dominantly east-west structures.

The Neoproterozoic Era encompasses a protracted orogenic cycle referred to here as the "Pan-African" orogenic cycle. It was Kennedy (1964) who coined the term "Pan-African Thermo-Tectonic Episode" to characterize the structural differentiation of Africa into cratons and mobile belts during the latest Precambrian and earliest Paleozoic. However, more recently,

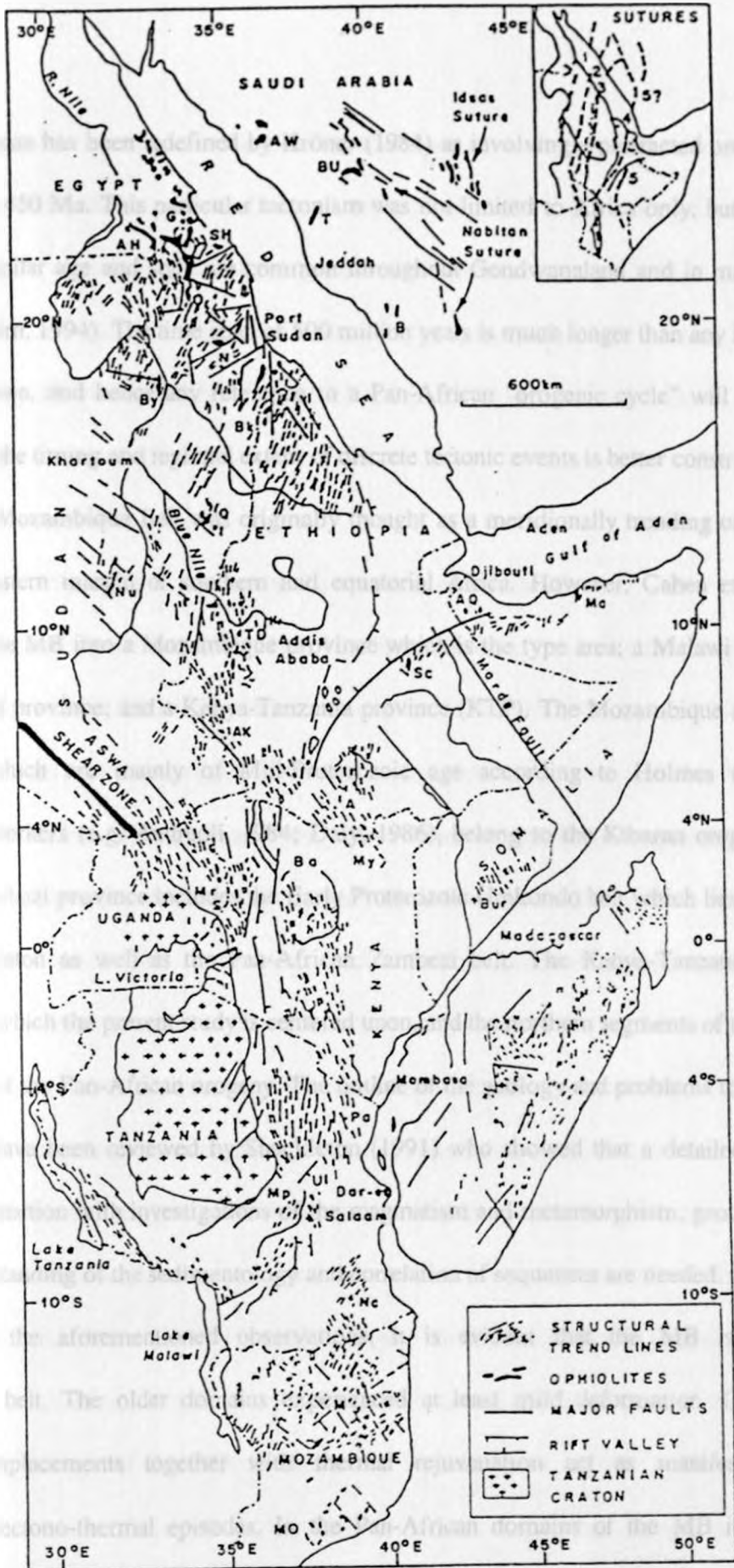


Fig. 1.3. Structural trends in the Mozambique belt (Redrawn from Behre, 1990.)

the Pan African has been redefined by Kröner (1984) as involving a protracted orogenic cycle from 950 to 450 Ma. This particular tectonism was not limited to Africa only, but diastrophic events of similar age and style are common throughout Gondwanaland and in many parts of Laurasia (Stem, 1994). The time span of 500 million years is much longer than any Phanerozoic orogeny known, and hence any reference to a Pan-African "orogenic cycle" will continue to suffice until the timing and regional extent of discrete tectonic events is better constrained.

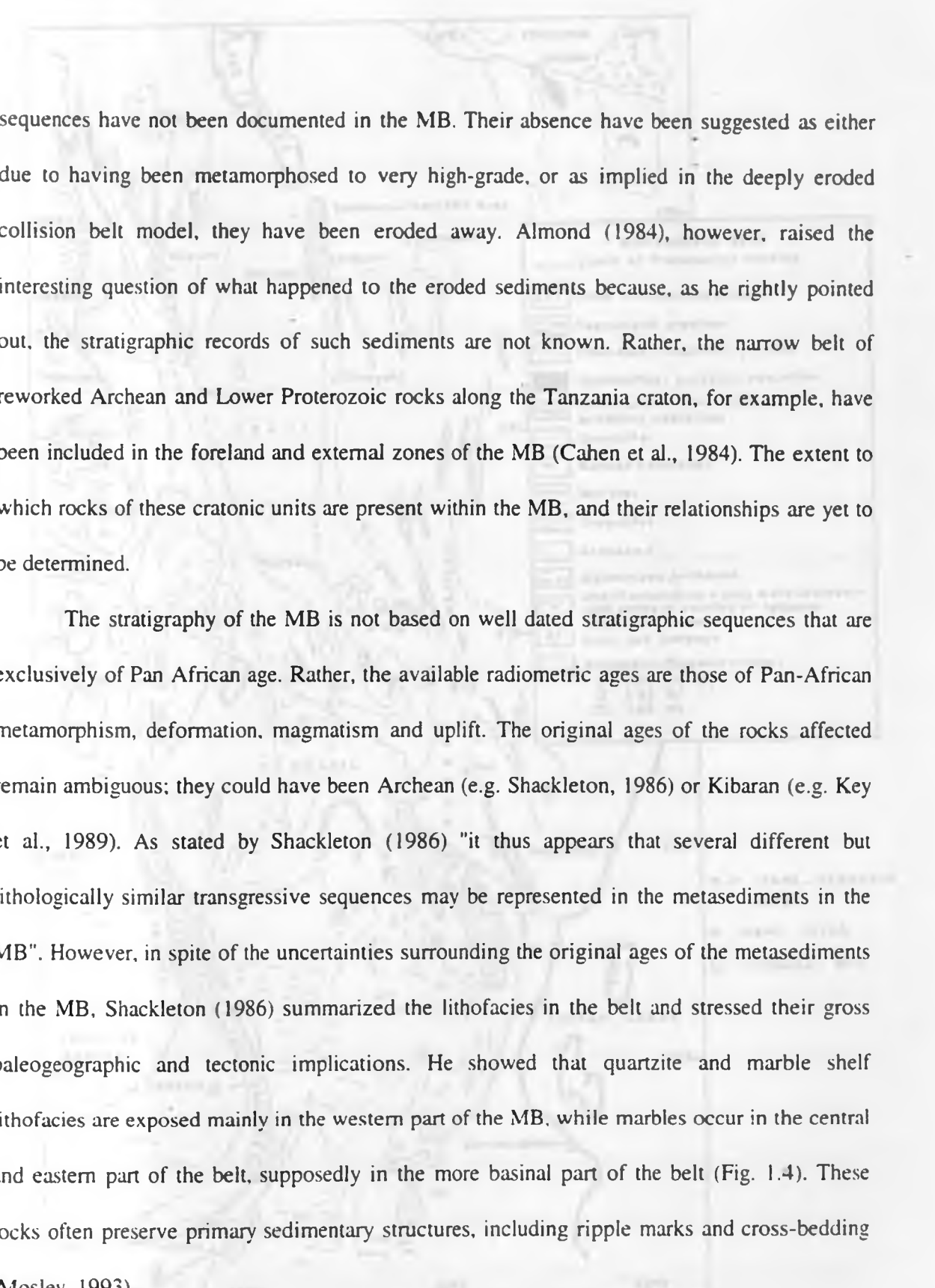
The Mozambique Belt was originally thought as a meridionally trending orogenic belt along the eastern margin of southern and equatorial Africa. However, Cahen et al. (1984) subdivided the MB into a Mozambique province which is the type area; a Malawi province; a Mid-Zambezi province; and a Kenya-Tanzania province (KTP). The Mozambique and Malawi provinces, which are mainly of Mid-Proterozoic age according to Holmes (1951) and subsequent workers (e.g. Andreoli, 1984; Daly, 1986), belong to the Kibaran orogenic cycle. The Mid-Zambezi province includes the Early Proterozoic Umkondo belt which lies east of the Zimbabwe craton as well as the Pan-African Zambezi belt. The Kenya-Tanzania province (KTP), from which the present study is centered upon, and the northern segments of the MB, are the products of the Pan-African orogeny. The outline of the geology and problems to be tackled in the KTP have been reviewed by Shackleton (1991) who showed that a detailed structural study in conjunction with investigations of the magmatism and metamorphism, geochronology, and an understanding of the sedimentology and correlation of sequences are needed.

From the aforementioned observations, it is evident that the MB is indeed a polyorogenic belt. The older domains experienced at least mild deformation. Granite and pegmatite emplacements together with thermal rejuvenation act as manifestations of Pan-African tectono-thermal episodes. In the Pan-African domains of the MB it has been

suggested that older rocks of Archaean to Kibaran age were overprinted by Pan-African events (Almond, 1984; Shackleton, 1986; Key et al., 1989). An overall study of the Mozambique belt must address the characteristics of these provinces and evaluate the significance of common or unique features recognized therein. In pursuit of this goal, a review of the main elements of the Kenya-Tanzania Province (KTP) - from which the present study is centered upon - is presented here below:

1.6.2 Tectonic Features of the Kenya-Tanzania Province (KTP)

The Kenya- Tanzania province (KTP), which constitutes the Pan African segment of the MB in East Africa, is defined with certain salient geologic features. Shackleton (1979) and Pohl (1988) summarized the main features of the MB as: the ubiquitous presence of Pan-African ages of about 600 Ma; the high grade and polyphase metamorphism which is generally of upper amphibolite facies with ubiquitous incipient migmatization; the occurrence of granulites, charnockites and anorthosites representing deep crustal environments; polyphase deformation; the easterly dipping thrusts along the western orogenic front adjacent to the Tanzania craton; and the general rarity of granitic intrusives in this belt. These characteristics are believed to represent the tectonic signatures in the exposed deep crustal levels of a Precambrian orogen that had suffered continent-continent collision. An examination of the Kenya-Tanzania province from the cratonic foreland in the west across the internal or mobile zone shows that the rock assemblages and the thrust and fold structures display the characteristics of a gigantic east-west collisional suture (Berhe, 1990; Key et al., 1989; Muhongo, 1989; Shackleton, 1986). A review paper on the geology of the MB in Kenya by Nyamai et al. (1993) outlines the main lithostratigraphic units of the MB in the Kenyan domain. Large Pan- African stratigraphic



sequences have not been documented in the MB. Their absence have been suggested as either due to having been metamorphosed to very high-grade, or as implied in the deeply eroded collision belt model, they have been eroded away. Almond (1984), however, raised the interesting question of what happened to the eroded sediments because, as he rightly pointed out, the stratigraphic records of such sediments are not known. Rather, the narrow belt of reworked Archean and Lower Proterozoic rocks along the Tanzania craton, for example, have been included in the foreland and external zones of the MB (Cahen et al., 1984). The extent to which rocks of these cratonic units are present within the MB, and their relationships are yet to be determined.

The stratigraphy of the MB is not based on well dated stratigraphic sequences that are exclusively of Pan African age. Rather, the available radiometric ages are those of Pan-African metamorphism, deformation, magmatism and uplift. The original ages of the rocks affected remain ambiguous; they could have been Archean (e.g. Shackleton, 1986) or Kibaran (e.g. Key et al., 1989). As stated by Shackleton (1986) "it thus appears that several different but lithologically similar transgressive sequences may be represented in the metasediments in the MB". However, in spite of the uncertainties surrounding the original ages of the metasediments in the MB, Shackleton (1986) summarized the lithofacies in the belt and stressed their gross paleogeographic and tectonic implications. He showed that quartzite and marble shelf lithofacies are exposed mainly in the western part of the MB, while marbles occur in the central and eastern part of the belt, supposedly in the more basinal part of the belt (Fig. 1.4). These rocks often preserve primary sedimentary structures, including ripple marks and cross-bedding (Mosley, 1993).

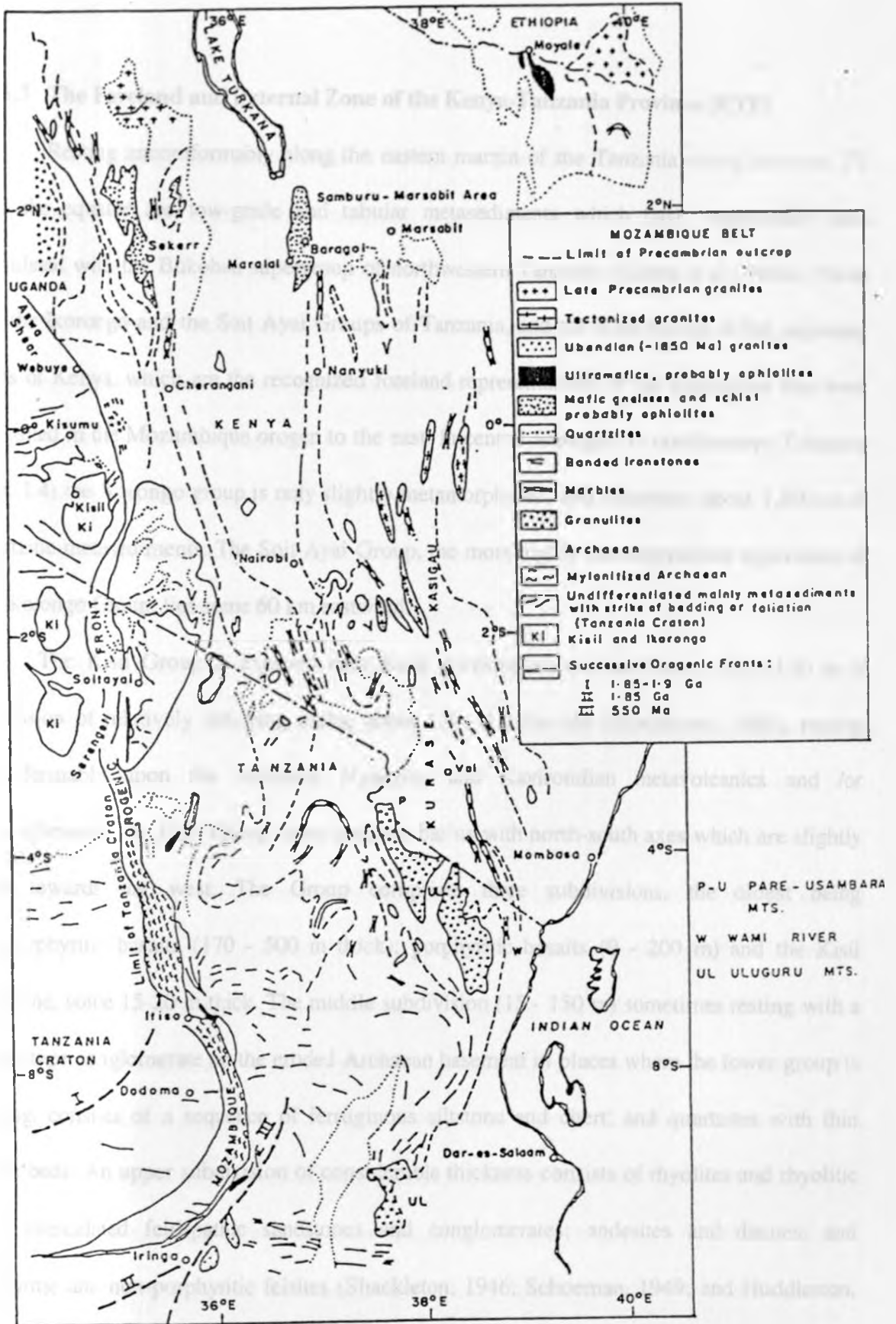


Fig. 1.4. Structural and stratigraphic sketch map of the Mozambique belt (Redrawn from Shackleton, 1986.)

1.6.3 The Foreland and External Zone of the Kenya-Tanzania Province (KTP)

Resting unconformably along the eastern margin of the Tanzania craton between 3°S and the equator are low-grade and tabular metasediments which have traditionally been correlated with the Bukoban supergroup of northwestern Tanzania (Cahen et al., 1984). These are the Ikorongo and the Soit Ayai Groups of Tanzania, and the Kisii Group of the adjoining parts of Kenya, which are the recognized foreland representatives of the formations that were deposited in the Mozambique orogen to the east. In central Serengeti in northwestern Tanzania (Fig. 1.4) the Ikorongo group is only slightly metamorphosed, and comprises about 1,500 m of quartzitic metasediments. The Soit Ayai Group, the more highly metamorphosed equivalent of the Ikorongo Group, lies some 60 km eastward.

The Kisii Group is exposed near Kisii township in western Kenya (Fig. 1.4) as a succession of relatively flat-lying rocks, about 1.3 - 1.0 Ga old (Shackleton, 1986), resting unconformably upon the Archaean Nyanzian and Kavirondian metavolcanics and /or metasediments. The Kisii Group forms shallow basins with north-south axes which are slightly tilted towards the west. The Group comprises three subdivisions, the oldest being non-porphyrific basalts (170 - 500 m thick); porphyritic basalts (0 - 200 m) and the Kisii soapstone, some 15-20 m thick. The middle subdivision (15 - 150 m) sometimes resting with a blanket-type conglomerate on the eroded Archaean basement in places where the lower group is missing, consists of a sequence of ferruginous siltstone and chert; and quartzites with thin pebble beds. An upper subdivision of considerable thickness consists of rhyolites and rhyolitic tuffs; intercalated feldspathic sandstones and conglomerates; andesites and dacites; and porphyritic and non-porphyrific felsites (Shackleton, 1946; Schoeman, 1949; and Huddleston, 1951).

1.6.4 The Internal (or Mobile) Zone of the Kenya-Tanzania Province

Predominantly high-grade metamorphic assemblages (granulite- and amphibolite-facies) and minor but tectonically significant ophiolitic rocks characterize the internal or mobile zone of the MB in the Kenya-Tanzania Province. Both the granulite and ophiolitic complexes are discussed below in areas where they are best known:

1.6.4.1 Granulite Complexes

(a) North-Central Kenya Granulite Complex

The North-Central Kenya granulite complex constitutes a vast exposure of the MB south of Lake Turkana in the Samburu-Marsabit area of north-central Kenya (Fig. 1.5). The complex geology of this region was unraveled by Key et al. (1989) in such a detail that it warrants a close examination of its tectonic features in order to gain more insight into the polyphase evolution of the MB as a whole.

The lithostratigraphy of the Samburu-Marsabit area (Fig. 1.5) consists of the basal Mukogodo Migmatites which are unconformably overlain by metasediments such as banded gneisses, into which the migmatites have been thrust as subconcordant sheets. Continental clastic units (e.g. Ndura, Loroki, Kotim gneisses) comprising meta-arkoses, meta-quartzites and manganese sandstones, with locally preserved sedimentary structures, are among the banded gneisses. These continental units show facies change into more pelitic metasediments, the Don Dol Gneisses, in the center of the Samburu-Marsabit area. The basal metasediments are overlain by a sequence of marbles, meta-pelites and vanadiferous graphitic gneisses (Ol Doinyo Ng'iro, Lolkoitoi, Makoni and Il Busi Gneisses). Meta-volcanic slices, some of which are ophiolitic

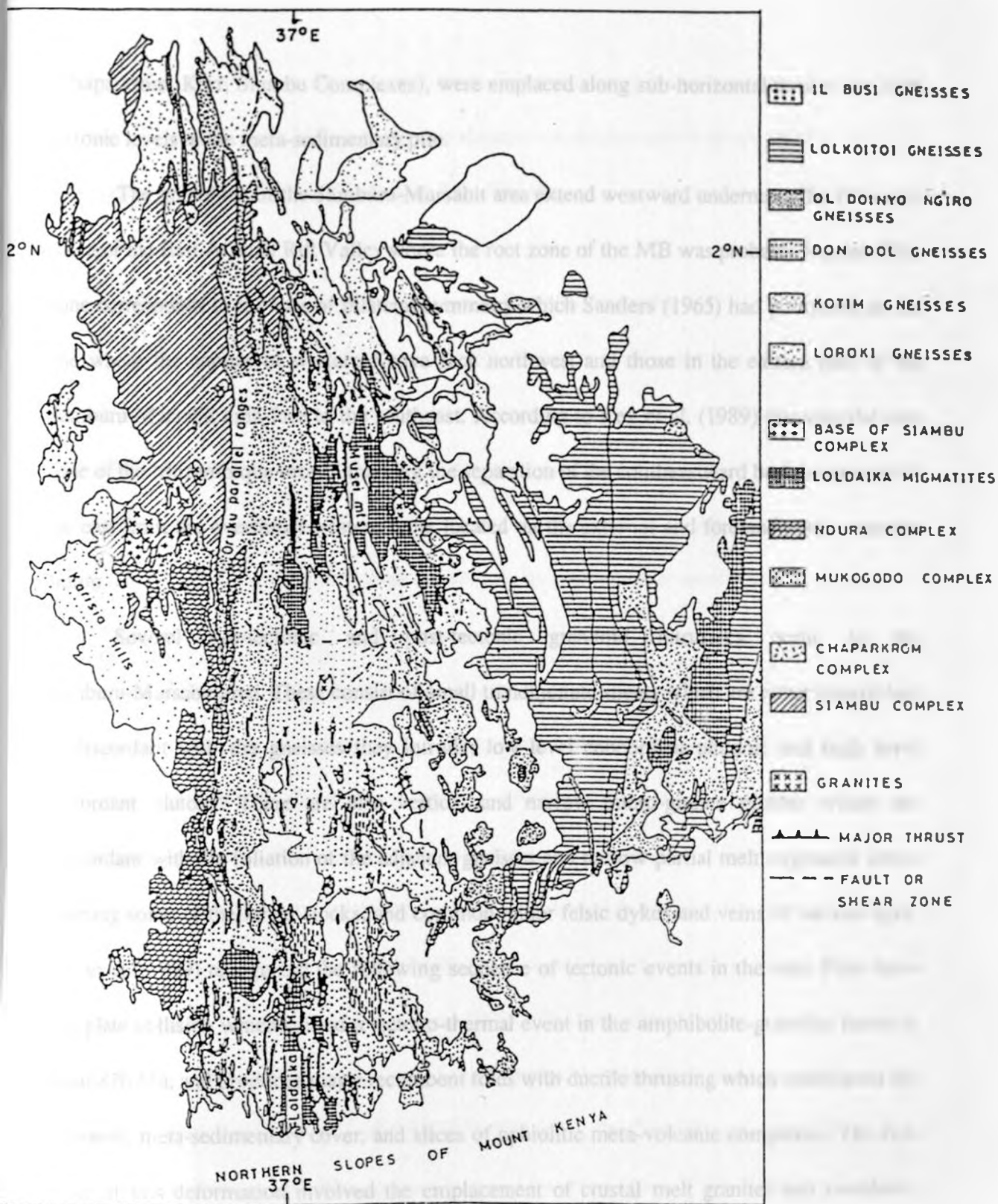


Fig. 1.5. Geological Map of Northern Kenya (Samburu-Marsabit area). (Redrawn from Key et al., 1989.)

(Chaparkrom, Korr, Siambu Complexes), were emplaced along sub-horizontal thrusts into high tectonic levels in the meta-sedimentary pile.

The granulites of the Samburu-Marsabit area extend westward underneath the Cenozoic strata of the East African Rift Valley where the root zone of the MB was probably located. This zone corresponds to the axis of bilateral symmetry which Sanders (1965) had postulated as the one where the nappes of western Kenya face northwest and those in the eastern part of the Samburu-Marsabit area face to the southeast. According to Key et al. (1989) this was the root zone of the Mozambique orogen marking the separation of the southeastward backthrust units in the east from the overthrust western units located on the external and foreland zones near the craton.

Several syn-tectonic and post-tectonic granitoid intrusives occur in the Samburu-Marsabit area. These consist of small trondhjemite sheets which are either concordant or discordant with the gneisses they intrude; low level concordant plutons; and high level discordant plutons. There are also vertical and narrow micro-granite plutons which are concordant with the foliation of the adjacent gneisses and narrow partial melt migmatite zones rimming some of the larger stocks; and common minor felsic dykes and veins of various ages. Key et al. (1989) recognized the following sequence of tectonic events in the area: First there was plate collision which caused a tectono-thermal event in the amphibolite-granulite facies at about 820 Ma. and produced major recumbent folds with ductile thrusting which interleaved the basement, meta-sedimentary cover, and slices of ophiolitic meta-volcanic complexes. The first phase of this deformation involved the emplacement of crustal melt granites and metabasic dykes. Between 620 Ma and 570 Ma there was post-collisional greenschist-amphibolite facies deformation which produced regional upright folds and vertical ductile strike-slip shear zones

which strike subparallel to the orogenic strike. This culminated in the intrusion of syntectonic granites. High level open folding and brittle shears mark the terminal orogenic events. The final uplift and cooling has been dated at about 500 - 480 Ma.

(b) The Proterozoic Granulite Terranes in Eastern Tanzania.

In Tanzania, the Proterozoic Granulite Terranes (PGT) form north-south trending discontinuous domains. Based on tectonic domains, Hepworth (1972) had grouped the granulites into 3 major groups (the Western granulites which lie on the craton and do not exhibit Pan-African ages (Muhongo, 1989); Central granulite complexes which are characterized by quartzitic lithofacies; and Eastern granulite complexes which lack or seldom contain quartzites, but contain mostly marbles).

In the framework of plate tectonics, the three major Proterozoic granulite terrains (PGT) are now interpreted as indicating shelf- (Western granulites), fore-deep - (Central granulites) and suture (Eastern granulites) zones (Muhongo, 1994). The distinctive major rock associations in the Western (shelf) PGT are gneisses - charnokites - migmatites - quartzites - schists - amphibolites - eclogites - metagabbros - mylonites, whereas in the Eastern (suture) PGT are granulites - meta-anorthosites - amphibolites - gneisses - marbles and scattered mafic and ultramafic bodies (Malisa and Muhongo, 1990). The granulites in the suture zone are predominantly composed of clino- and orthopyroxene, hornblende, quartz, plagioclase, K-feldspar and garnets (enderbites) and contain 50-75% SiO₂. The ⁸⁷Sr/⁸⁶Sr ratios of 0.705 - 0.707 recorded from dolomitic marbles in the Uluguru Mountains (part of the Eastern granulites) could signify deposition in the "Mozambique Sea-water". Calc-alkaline characteristics of the

Eastern meta-igneous granulites suggest a subduction-zone environment for their formation (Muhongo, 1991).

Metamorphic ages recorded from the PGT using Rb-Sr whole-rock and zircon U-Pb dating techniques put the PGT into two major groups, those in the Usagaran tectonic domain (originally used as the local term for the Mozambique Belt in Tanzania, Quennell et al. (1955) with the last metamorphism occurring at ca. 1900 Ma ago (Gabert and Wendt, 1974). The second group of the PGT is now defined as the Pan-African Mozambique Belt with diachronous granulite-facies metamorphism occurring in the period between 645-715 Ma. This diachronism is interpreted to be due to the different times required to attain peak P-T granulite-facies conditions in different localities in the same orogen (e.g. probably due to episodic magmatic underplating, crustal thickening, or irregular leading edges of the colliding fragments).

Memories of older ages (>950 Ma; Cahen et al., 1984) have been reported from some PGT in the Mozambique Belt. Isotopic studies on the granulites in the foreland terrane (part of the Western granulites), reworked during the Mozambiquan orogeny, gave a Rb-Sr whole-rock errorchron age of 2750 Ma ($^{87}\text{Sr}/^{86}\text{Sr} = 0.7204\text{-}0.7361$; Spooner et al., 1970). Evidence for the presence of older zircons (>2000 Ma) in Eastern granulites has been reported from the U-Pb data that yielded upper intercept ages (between 2000-3000 Ma; Coolen et al., 1982). Traces of older reworked crustal materials in the Eastern Granulites are indicated by their higher $^{87}\text{Sr}/^{86}\text{Sr}$ ratios (.0.720), e.g. from pyroxene granulites in the Pare Mountains (Spooner et al., 1970).

Inference drawn from the aforementioned isotopic memories in the shelf (Western granulites- in the Usagaran tectonic domain) and in the fore-deep (Central granulites- in the transition zone between the Usagaran and the Pan-African Mozambique Belt), is that an

Archaen basement, which acted as a floor to these granulites, was deformed and metamorphosed in the Pan-African orogeny (ca. 950- ca. 550 Ma).

(c) **Central Granulite Complexes of Tanzania**

According to Malisa and Muhongo (1990), the central granulite complexes of Tanzania, represented by the Loliondo, Longido, Ifakara, Fura and Songea complexes, have fault-bounded structures, and consists lithologically of pelitic and psammitic metasediments and their migmatized equivalents. They are predominantly biotite-hornblende and garnet-pyroxene granulites; feldspathic micaceous quartzites; and chlorite schists. Metamorphosed equivalents of igneous rocks include meta-gabbros, meta-pyroxenites, meta-dolerites, and amphibolite lenses. Pegmatites are abundant. Commonly occurring quartzites suggest sedimentation of the granulite protoliths under the influence of granitic and gneissic source areas which lay on the Tanzania craton.

The central granulites have been metamorphosed at the almandine-amphibolite grade, with granulite-facies reached in certain areas. The complexes occur as synformal and antiformal structures. Their general east-west trending axes swing towards the southeast; and mineral stretching lineations dominantly plunge to the southeast and northeast, suggesting the refolding of earlier folds in the MB. Faulting was predominantly in the NE-SW direction. The original ages of the rocks of the central granulite complexes are not known, but they have yielded only Pan-African ages (Malisa and Muhongo, 1990).

(d) The Kurase and Kasigau Groups of Kenya

Key et al. (1989) outlined the main features of the internal zone in Kenya. Throughout this region a migmatite basement to the metasediments has been recognized. Part of the basement (Turbo migmatites of Sanders, 1965) in western Kenya represents the reworked Archean of the Tanzania craton, which has been traced for about 100 km eastwards into the MB (Vearncombe, 1983):

Elsewhere in Kenya mid-Proterozoic ages have been obtained from the migmatite basement. In southeastern Kenya the overlying Kurase-Kasigau group of metasediments shows facies change from shallow water shelf lithofacies eastward into deeper water sediments. The uppermost shelf metasediments to the east of Nairobi contain an evaporite component in the form of scapolite-bearing gneisses.

The Kurase-Kasigau Group of metasediments occurs in the Voi-Tsavo area of southeastern Kenya (Fig. 1.4) as a continuation of the Pare-Usambara mountain terrane. The Kurase Group comprises miogeosynclinal lithologies such as marble and quartzite; and graphite, sillimanite and kyanite-gneiss and schists; biotite-hornblende gneiss; and amphibolite (Gabert, 1984). The overlying Kasigau Group represents the eugeosynclinal facies, and consists mostly of greywackes which have been metamorphosed to quartz-feldspar-biotite-hornblende gneiss, with intercalations of ortho-amphibolites. Facies transitions occur between the Kurase and Kasigau Groups; and basic and ultrabasic rocks were emplaced along regional faults or thrust zones. Three phases of deformation have been recognized in the Kurase and Kasigau Groups, the last of which controlled the emplacement of late pegmatites and the joint pattern in this region (Gabert, 1984). Isoclinal and open folds with NNE and NNW striking axes are prevalent in the Kurase and Kasigau Groups.

Although the succession of geologic events was not clearly defined, Gabert (1984) outlined the late phases of the geological history of the Kurase-Kasigau area as comprising: Barrovian medium- to high-grade metamorphism; hydrothermal activity leading to syngenetic base metal mineralization; pegmatite emplacement; and widespread resetting of radiometric ages during Pan-African tectonism at about 550 Ma.

1.6.4.2 Ophiolitic Rocks

The internal zone of the Mozambique belt contains imbricate slices of mafic and ultramafic rocks whose ophiolitic nature has survived the high grades metamorphism and intense deformation in the mobile zone. Although these ophiolitic rocks have been widely reported by several previous authors (e.g. Kazmin et al., 1978; Prochaska and Pohl, 1984; Shackleton, 1986; Vearncombe, 1983), Berhe (1990) has added more geochemical and structural data which have further elucidated their geodynamic significance. Berhe (1990) also traced these ophiolitic rocks northward which defines cryptic sutures in the MB, and linked them with the extensive ophiolites of the Arabian-Nubian Shield (Fig. 1.3). He therefore demonstrated that the MB and northeast Africa were affected by the same regional collision events. The Sekerr, Baragoi and Moyale ophiolites of northern Kenya (Fig. 1.4) provide the links between the MB and the Arabian-Nubian Shield (ANS) ophiolites.

(a) Sekerr and Itiso Ophiolite

As aforementioned, there is a complicated imbricate zone of ophiolites which rests upon the metasediments of the Sekerr area (Vearncombe, 1983) which has been followed northwards into the Karamoja District of southern Sudan (Vail, 1988) where there is strong thrusting of the

ophiolites onto the meta-sedimentary units. According to Vail (1988) the Sekerr-Karamoja ophiolites are a sequence of andesitic meta-volcanic rocks; pillow lavas; gabbros with preserved layering; hornblende schists; serpentinites with podiform chromite; basic dykes which probably represent a sheeted dyke complex; marble lenses; and narrow bands of quartzites which are believed to have been original chert layers; psammites and mica schists which were probably tuffs; and pyroclastics and turbiditic sediments. All of the above lithofacies are believed to belong to an island-arc ophiolite sequence.

The Sekerr ophiolite represents a regional ophiolite belt that extends all the way through western Ethiopia where it is exposed in the Akabo region. This ophiolite belt probably continues south of Sekerr into Itiso along the eastern Mozambique front in Tanzania (Fig 1.4) where in the Itiso area mafic-ultramafic complex, pillow lavas are associated with the ultramafic rocks (Berhe, 1990; Shackleton, 1986). Trace element data suggest the origin of the Sekerr ophiolite in a back-arc basin between 1000 Ma and 663 Ma ago (Berhe, 1990).

(b) Baragoi Ophiolite

Several ophiolitic complexes occur in the high-grade rocks of the Samburu-Marsabit area in north-central Kenya, including the Siambu complex at Baragoi. The Baragoi ophiolite includes metamorphosed mantle derived dunites and sheeted dykes with trace elements showing a transition between mid-ocean ridge basalts and island-arc tholeiites. Two separate suites of ophiolitic gabbroic rocks in the Baragoi area have yielded ages of 796 Ma and 609 Ma. The Samburu-Marsabit ophiolites occur as thrust slices, which at Marsabit have been transported up to a distance of about 100 km, thus reflecting severe crustal shortening (Key et al., 1989).

Evidence presented by Berhe (1990) as indications of an ophiolitic origin for the Baragoi complex includes high chrome/low titanium values, and a MORB-normalized spidergram (Fig.1.6) for the Baragoi amphibolites similar to an average Marianas island-arc lava (boninitic), with low abundance's of incompatible elements and depletion in HFSE and REE, but with much higher Cr values than the Marianas lava. Discriminant diagrams such as Zr/Y-Zr (Pearce and Norry, 1979) (Fig. 1.7) and Ti-Zr-Y plots (Fig. 1.8) show the Baragoi amphibolite data overlapping the fields of mid-ocean ridge basalt (MORB) and island-arc tholeiites (IAT) defined by Pearce and Cann (1973) and Pearce (1982). Modern analogues of these volcanic rocks are situated near destructive plate margins in an island arc setting (Pearce, 1982).

(c) Moyale Ophiolite

At Moyale in northernmost Kenya (Fig. 1.4) a low-grade ophiolite occurs which extend into the Adola fold and thrust belt of southern Ethiopia. The Moyale ophiolite includes serpentinitized harzburgite and gabbros which occur as thrust slices among continental shelf meta-pelites. Behre (1990) assigned this ophiolite (see Fig's. 1.7 & 1.8) to a back-arc tectonic setting.

(d) Pare Mountains Ophiolite

A highly dismembered and scattered ophiolite occurs in Pare Mountains, NE Tanzania, comprising of serpentinites, meta-pyroxenites, meta-gabbros and amphibolites. Ophiolites also occur in the neighbouring Taita Hills of southeast Kenya in what probably represents the continuation of a suture zone which Berhe (1990) extrapolated northward into the Adola-Moyale belt (Fig. 1.3).

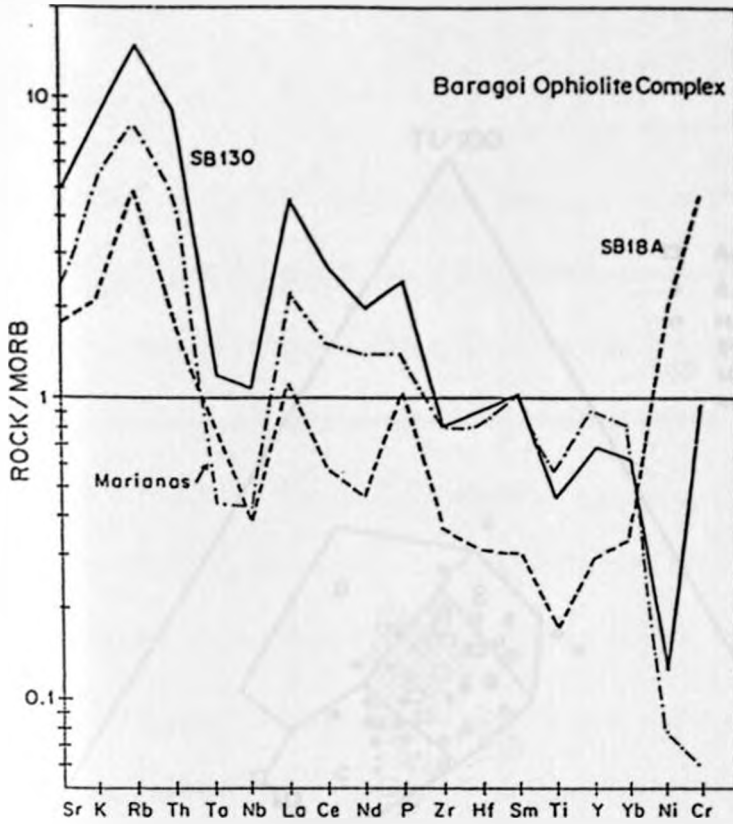


Fig. 1.6. Representative geochemical patterns for the Baragoi lavas. Hornblende plagioclase gneiss (SB 130); amphibolite (SB 18A). Normalising values taken from Pearce (1982). The Baragoi lavas are compared with an average Marianas island arc lava (Hole et al., 1984). (Redrawn from Berhe, 1990.)

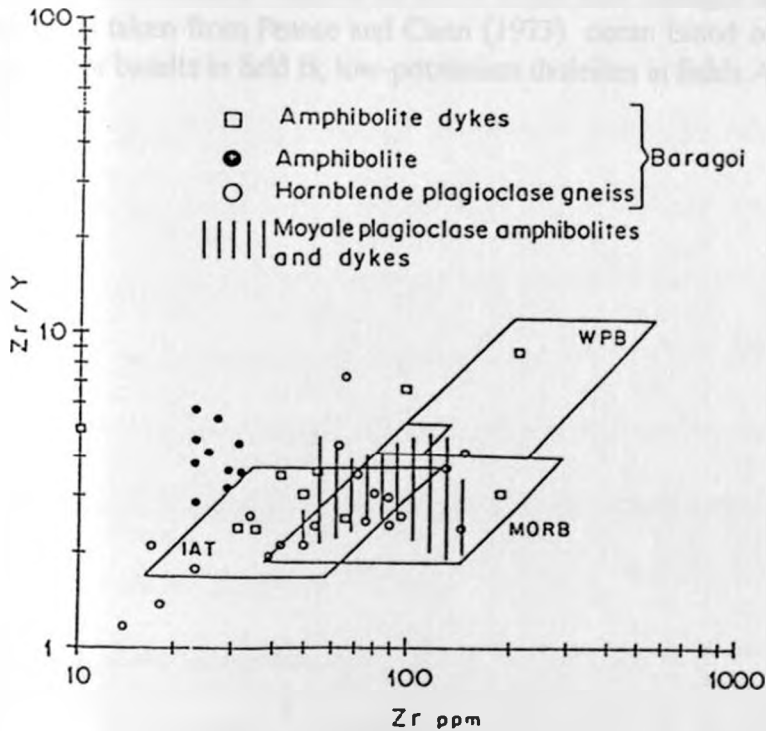


Fig. 1.7. Zr/Y versus Zr discrimination diagram for basic rocks of Baragoi and Moyale ophiolite zones. Discriminant fields taken from Pearce and Norry (1979). (Modified after Berhe, 1990).

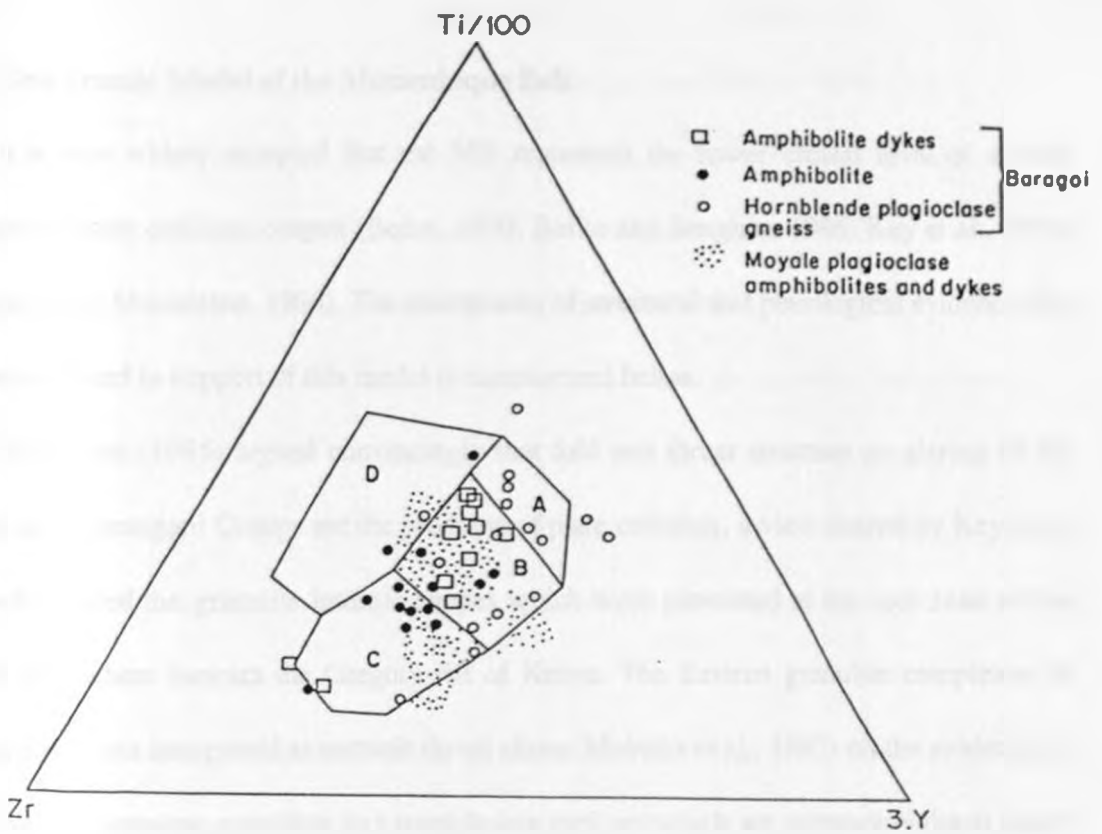


Fig. 1.8. Ti-Zr-Y discriminant diagram for basic rocks from Baragoi and Moyale ophiolite belts. Discriminant fields taken from Pearce and Cann (1973). ocean island or continental basalt plot in field D; ocean-floor basalts in field B; low-potassium tholeiites in fields A & B; calc-alkali basalts in fields C & B.

1.6.5 Geodynamic Model of the Mozambique Belt

It is now widely accepted that the MB represents the lower crustal level of a huge continent-continent collision orogen (Berhe, 1990; Burke and Senghor, 1986; Key et al., 1989; Muhongo, 1989; Shackleton, 1986). The multiplicity of structural and petrological evidence that have been adduced in support of this model is summarized below.

Shackleton (1986) argued convincingly that fold and thrust structure so glaring in the Kurasuk and Cherangani Groups are the products of plate collision, a view shared by Key et al. (1989) who placed the granulite internal nappes which were generated at the root zone of the collision somewhere beneath the Gregory rift of Kenya. The Eastern granulite complexes of Tanzania have been interpreted as tectonic thrust slices (Maboko et al., 1985) on the evidence of the hornblende-pyroxene granulites and amphibolite gneisses which are commonly thrust under the graphitic marbles (Muhongo and Lenoir, 1993).

Although the actual number of sutures and the age of suturing have not been precisely determined. (e.g. Berhe (1990) suggested two suture zones), the position of some of these sutures is roughly known based on the dismembered ophiolites which decorate them. The stretching lineations in the western part of the MB commonly plunge to the southeast and trend NW-SE, like the brittle shear zones and the Aswa wrench fault (Fig. 1.3), thus implying approximately NW-SE plate motion. However, the stretching lineations in the central zones show a rather persistent roughly north-south trend which probably resulted from a late orogenic relative motion of plates parallel to the plate boundaries (Shackleton, 1986). Whether or not there is enough evidence for the operation of a complete Wilson Cycle, and what plates collided, are pertinent questions raised by this model. A possible Wilson Cycle scenario for the

MB was proposed by Berhe (1990) who suggested an early stage of rifting, followed by a phase of subduction and island-arc accretion, ending with continent-continent collision.

Although the stratigraphic record of early rifting in the MB is quite tenuous and circumstantial compared with the other coeval Pan-African mobile belts, the rifting of a Kibaran continent along East Africa would account for the presence of Archaean to Kibaran rocks in central Kenya and in Madagascar, east of the suture zones, and also explain the existence of passive continental margin sediments (Kisii, Ikorongo, Soit Ayai Groups) along the foreland of the MB. Subduction and island-arc accretion are evident from the ophiolites of the MB, while continent-continent collision, as already mentioned, generated nappe-type folds and thrusts on a regional scale.

Paleomagnetic evidence (McWilliams, 1981) in the form of a large misfit between East and West Gondwana suggest that a large ocean separated both regions and that Madagascar and parts of eastern Tanzania, Kenya, Ethiopia and Somalia belonged to East Gondwana, whereas the Tanzania craton lay in West Gondwana (Fig. 1.9).

1.7 MINERALIZATION WITHIN THE KENYAN SEGMENT OF THE MOZAMBIQUE OROGENIC BELT

1.7.1 Ores Related to Intermediate Magmatic Rocks

Copper occurrences associated with diorite-rhyolite gneiss in subduction related arcs are found in Voi area (Frisch and Pohl, 1986), west Pokot, Baragoi and Kapenguria. Magnetite/ilmenite occurrences in charnockites, gneisses, anorthosites and associated pegmatites are known to occur in Marimanti, central Kenya, and natural concentrations of these

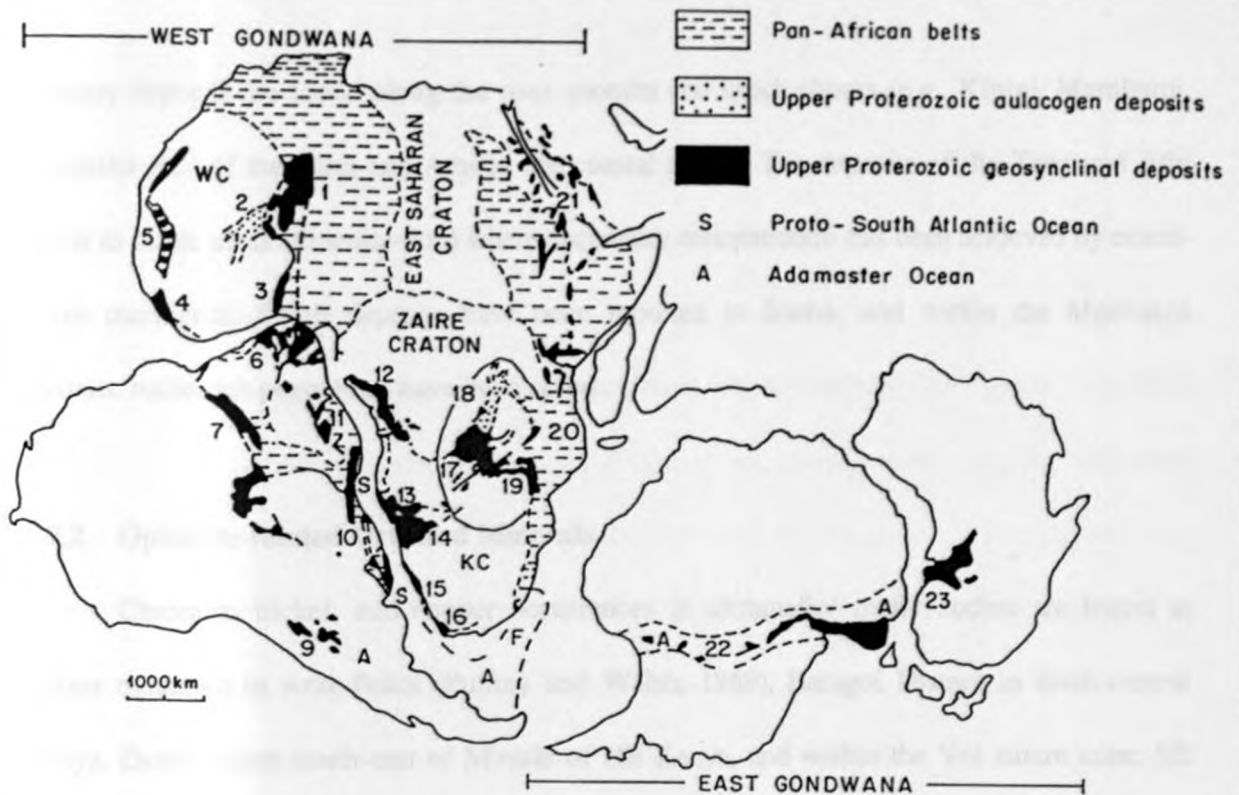


Fig. 1.9. Pre-drift reconstruction of Gondwana showing Pan-African belts. 1, Pharosian belt; 2, Gourma aulacogen; 3, Daho-meyan belt; 4, Rokelide belt; 5, Maritanide belt; 6, Northeastern fold belt (Borborema province); 7, Araguaia belt; 8, Paraguay belt; 9, Sierras Pampeanas; 10, Ribeira belt; 11, Mantqueira belt; 12, West Congolian belt; 13, Kaoko belt; 14, Damara belt; 15, Gariep belt; 16, Saldanhia belt; 17, Lufilian arc; 18, Shaba aulacogen; 19, Zambezi belt; 20, Mozambique belt; 21, Red Sea fold belt; 22, Transantarctic belt; 23, Adelaide belt. (Redrawn from Porada, 1989.)

primary deposits are found along the river mouths and beach shores (e.g., Kipini, Mamburui, Fundisha etc.) of the Tana and Athi in the coastal region. The deposits of the Tana and Athi occur as black sands (ilmenite-rich) where secondary concentration has been achieved by ocean-wave mechanics. Small deposits have been reported in Ikutha, and within the Machakos District, rutile-rich pegmatites have been noted.

1.7.2 Ophiolite-related Ores and Minerals

Chromite, nickel, and copper occurrences in ultramafic/ mafic bodies are found at Sekerr mountain in west Pokot (Pulfrey and Walsh, 1969), Baragoi District in north-central Kenya, Debel region south-east of Moyale of NE Kenya, and within the Voi suture zone, SE Kenya. Magnesite veinlets and stockwork bodies in dunites have been reported to occur e.g., at Kinyiki Hill and Mtito-Andei area in SE Kenya (Pohl et al., 1980), Baragoi District, south Kapoponi Hill in Kitui District and in the Embu District.

1.7.3 Metamorphogenic Minerals

Major metamorphogenic minerals of the Kenyan Mozambique belt can be summarised as follows:

(a) *Kyanite and graphite in meta-sediments*

Deposits of kyanite occur at Murka hill in the NE of Taveta District and at Sultan Hamud in Machakos District. Graphite is known to occur at Mtito Andei - Tsavo area, Taita hills, north Kitui and Machakos District, and extensively in north-central Kenya (Pulfrey and Walsh, 1969).

(b). *Anthophyllite asbestos in metamorphosed ultramafics*

Deposits of asbestos are reported to occur at Kinyiki hill, Taita Hills, southern Kitui District, west Pokot and Baragoi area (Pulfrey and Walsh, 1969).

(c). *Gemstones*

Reported gemstones of metamorphogenic origin include the green vanadium grossularite in calc-silicate graphite schists (Pohl et al., 1980) within highly variegated metasediments in a possible paleo- evaporitic environment (Suwa et al., 1979), the red ruby (corundum), the pink and red garnets in metamorphic rocks and the blue zoisite (tanzanite) in impure marbles which largely occur in the Taita-Taveta area.

(d). *Wollastonite in calc-silicate metasediments*

Economic deposits of wollastonite have been found to occur at Lolkidongai in Kajiado District, southern Kenya (Pulfrey and Walsh, 1969). Assessment of the Lolkidongai Wollastonite deposit in Kajiado District (Saltikoff et al., 1991) has revealed one continuous ore body of wollastonite-rich rock about 4-6 m thick, plus several other minor parallel lenses. The deposit has average grade of 38% pure wollastonite and approximately 670,000 tonnes of probable ore.

1.7.4 Pegmatite Ores and Minerals

Coloured gemstones, mainly tourmaline, aquamarine, morganite, hiddenite, kunzite, rose quartz, amazonite, emerald and, in plumasitic pegmatites within ultramafics, ruby and sapphire have been reported to occur mainly in the Embu and Meru District, Baragoi, Taita-Taveta, and at Cherangani Hills in west Pokot (Pulfrey and Walsh, 1969; Pohl et al., 1980). Whereas quartz, feldspar and kaolin are almost available everywhere within the Kenyan MB.

muscovite and vermiculite deposits have been reported in Sultan Hamud, Kinyiki Hill, west Pokot (Du Bois and Walsh, 1970) and recently in the Kajiado District.

1.7.5 Syngenetic Stratiform Ores

Ores of syngenetic stratiform origin reported within the Kenyan Mozambique Belt include :

- (a). Ubiquitous Fe-quartzites
- (b). Magnetite beds associated with ortho-amphibolites (e.g., Wanjala, SE Kenya)
- (c). The banded iron formations in the Ablun group, NE Kenya
- (d). Spessartine-(kyanite) quartzites, which may either be potential Mn-deposits when oxidised and enriched by weathering or which may be guides to possible base metal deposits (SE Kenya: Pohl and Niedermayr, 1979).
- (e). Small gossans with high grade metal values in association with sulphide quartzites, carbonates, calc silicate-graphite schists and metamorphosed ultramafics at Mikeli, SE Kenya (Pohl and Niedermayr, 1979).

1.7.6 Industrial raw Materials

Large economic deposits of marble (limestone) occur in the Mozambique belt terrane of the Kajiado District, southern Kenya. These deposits are currently the major source of limestone for the cement production at the East African Portland Cement Factory situated in Athi River town. Other economic deposits of marble have been discovered in West Pokot District, western Kenya. Potential economic deposits of graphite (3-12% graphite) and Manganese (33.55 -

61.47% Mn₂O) in the Ol Doinyo Ng'iro and Kotim gneisses Formations respectively, occur in the Samburu-Marsabit area (Key et al., 1989).

1.7.7 Potential Mineralization

The role of metallogenic heritage in the Mozambique belt of Kenya is shown by the following evidence:

Copper mineralisation

- (a). Reported copper occurrences (Pulfrey and Walsh, 1969) in Tsavo East and south of Voi being contained in biotite gneiss (up to 1.5 wt.% Cu), quartzofeldspathic granulite (up to 1.8 wt.% Cu), and microline-rich granitoid gneiss (up to 2.21 wt.% Cu) makes this a target area for metal exploration.
- (b). The Siambu Complex, with its wealth of altered basic and ultrabasic rocks have been proposed as a good setting for copper mineralisation (Key, 1987).

Tin mineralisation

In the Kaisut desert, Laisamis area, located in the Marsabit and Samburu district, Sn mineralisation anomalies (up to 1.54 wt. % Sn) have been reported by Charsley, 1987.

Chromite mineralisation

Chromite pods in ultrabasic rocks in Cherangani hills, west Pokot (Vearncombe, 1983), Kangura (Baker, 1963), Boji hill (Du Bois, 1970), and Noljushin Hill, Maralal area (up to 27.7 wt.% Cr₂O₃) reported by Key et al. (1989) warrant further detailed exploration.

Nickel mineralisation

The nickeliferous serpenitised dunite intrusives south of Ol Doinyo Sabachi, Isiolo area, with the possibility of a surrounding mantle of nickeliferous laterite (Hackman et al., 1989), justify further investigation. Anomalous values for Ni recorded from analysis of rock samples from the intrusiveness range from 900 to 2215 ppm (Hackman et al., op.ct.).

Manganese mineralisation

A complex zone of manganese mineralisation 8 km north-east of Archer's Post stretching for 3 km along strike. The economic potential of this deposit has not been evaluated. The initial laboratory analysis of this deposit gave MnO₂ values of 39.55 and 61.47 per cent (Jennings, 1967). As manganese acts as a scavenger of base metals in the lacustrine environment, it would be worthwhile to test for these elements and for gold.

1.7.8 Conclusion

Evidence based on the aforementioned studies show the Kenyan segment of the Mozambique belt to be endowed with numerous minerals. The full economic potential of these minerals have not been fully realized. This has been partly due to lack of adequate knowledge concerning the tectonic evolution of this belt and indirectly the parameters that control the ore genesis of these minerals. It is envisaged that with a better understanding of the tectonic setting of this belt, proper mineral exploration strategies can be put into practice.

* * * *

CHAPTER TWO

PETROGRAPHY, MINERAL CHEMISTRY AND THERMOBAROMETRY OF THE MOZAMBIQUE BELT INTRUSIVE ROCKS OF MATUU-MASINGA AREA, CENTRAL KENYA.

2.0 INTRODUCTION

Previous studies on the metamorphism of the Kenyan Mozambique belt have largely been based on petrography of the mineral phases. Quantification of the more precise original metamorphic conditions of this belt based on probe analyses of its thermobarometers is lacking. Suwa et al. (1979) obtained temperatures of about 500 to 700 °C in the Mbooni-Uvete area of Machakos district through petrographic studies. According to Inoue and Suwa (1979), the Mozambiquan metamorphic rocks south of Machakos are considered to have been deformed in the major period of regional metamorphism at a temperature of 570 to 590 °C and a hydrostatic pressure of 6.8 kbars (corresponding to 24 km in depth). Later Miyake and Suwa (1981) carried out probe analyses on the metamorphic conditions of these Mozambique belt rocks in the Mbooni-Uvete area and obtained more precise temperature (T °C) and pressure (P kbars) values of 540 +/- 40 and 6.5 +/- 0.5 respectively. The Mbooni-Uvete area lies approximately along the same longitude and metamorphic isograd as the Matuu-Masinga area and it is of interest therefore to compare the unknown metamorphic variations along this isograd.

In spite of several researchers working in the regional survey area, no systematic scientific study of the Mozambique belt intrusive rocks of Matuu-Masinga area has been done. The present work seeks to fill that gap. The main objective is to have a systematic investigation of the petrology and mineral chemistry of the rocks of the survey area, and to estimate, on the basis of the results obtained, the P/T conditions of metamorphism that affected the area.

2.1 PETROGRAPHY AND MINERAL CHEMISTRY

The major geological rock units identified in the study area (see Fig. 1.2 or appendix 1) are the biotite gneisses, amphibolite gneisses, granitoids, migmatites, anorthosites, meta diorite, meta gabbro and granites. The high-grade mineralogical assemblages of the meta-igneous rocks of Matuu area is represented by quartz, plagioclase, K-feldspar, orthopyroxene, clinopyroxene, garnet, actinolite, hornblende and spinel. The accessory minerals are zircon, sphene, apatite, muscovite, epidote, magnetite, ilmenite, and pyrite. Representative samples for all the major outcrops encountered in the survey area ranging from gabbroic to granitic in composition are plotted in Fig. 2.1. The diagram (Fig. 2.1), which is consistent with the QAPF classification of Streckeisen (1976), represents their overall nomenclature based on the $(\text{Na}_2\text{O} + \text{K}_2\text{O})$ wt.% versus SiO_2 wt.% (after Cox et al., 1979). Full chemical analyses of the rock samples is presented in appendix 3.

2.1.1 The Mafic Rocks

Mafic rocks in the study area are represented by the meta diorites, anorthosites, meta gabbros, hornblende gneiss, biotite gneiss and granulites. Surface outcrops of meta-diorites and gabbroic rock intrusions were relatively few and these rock units were mapped largely by inferences based on soil types. Field evidence showed that the black-cotton soils were underlain by the gabbroic rock type. Good exposures of gabbroic intrusions extending for about 50 m on the surface were observed about 1/2 km north of Matuu town and south of Kathuleni river (Fig. 1.2).

Despite the ubiquitous presence of anorthositic layers in the area, there is nowhere a mappable anorthositic body and overall the anorthositic gabbros form a sequence of metamorphosed mafic and ultramafic intrusions. Individual anorthositic bodies may or may not be continuous due to extensive shearing and boudinage. In the northwest of Ikaatini school (Fig. 1.2), small bodies that have not been differentiated are mapped as amphibolites. The close association of net veining from a felsic differentiate in these gabbroic bodies appears to suggest that they are late-stage co-magmatic differentiates.

One outcrop of anorthositic gabbro shows presence of relict igneous layering with coarse grained mafic cumulates. The relict igneous layering is recognized by the characteristic equigranular pyroxenes up to a centimeter across, arranged in cumulate layers 30-70 cm thick usually with sharp basal margins. Characteristically the pyroxene is completely replaced by green amphibole which tends to pick out and enhance the coarse-grained nature of the old pyroxenitic cumulates. Locally the layered anorthositic gabbros are highly sheared and tectonised preventing the recognition of the relict layering. Along the Mathauta river in the Masinga-Nzukini road, a group of streaky hornblende gneisses (mafic orthogneisses) locally show evidence of relict igneous cumulate layering and contains disrupted layers and pods of amphibolitised pyroxenite.

2.1.1.1 Petrography of the meta-diorite

Petrographically the meta-diorite rock, which has been subjected to granulite-facies metamorphism, consists essentially of hypersthene, clinopyroxene, calcic plagioclase, hornblende, biotite and apatite (Plate 2.1 (a) & (b)) with minor quartz, spinel, chlorite, epidote, sphene, magnetite, ilmenite and pyrite. The modal composition of representative dioritic rocks is presented in Table 2A.

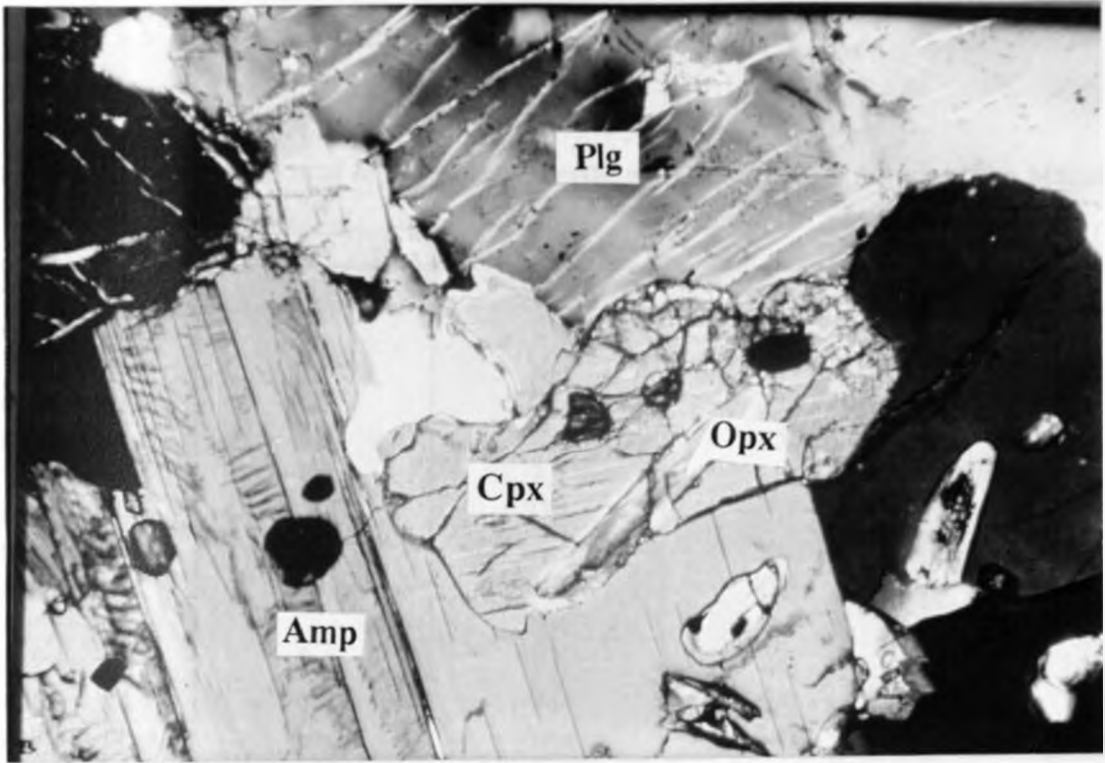


Plate 2.1 (a). Photomicrograph of clinopyroxene (Cpx) with exsolved orthopyroxene (Opx), amphibole (Amp) and zoned plagioclase (Plg). Meta diorite rock (MU-7), crossed polars, X 100.

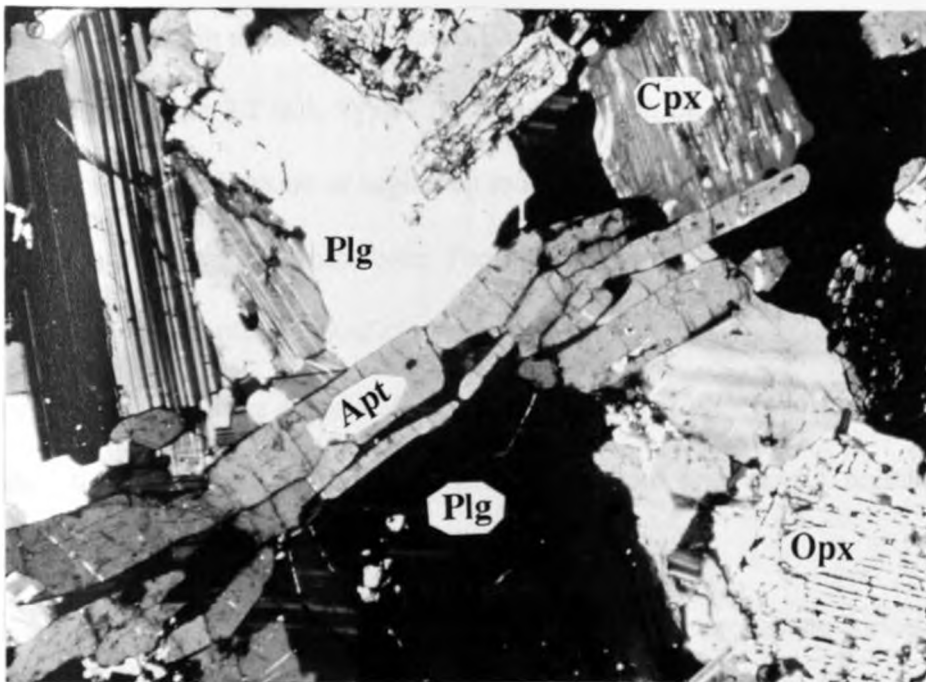


Plate 2.1 (b). Photomicrograph of elongated crystals of apatite (Apt) occurring within interstices of plagioclase (Plg), clinopyroxene (Cpx), and orthopyroxene (Opx). Meta diorite rock (MU-7), crossed polars, X 50.

Table 2A. Modal composition of representative dioritic and gabbroic rock samples from Matuu-Masinga area, central Kenya.

Specimen No.	MU-7	MU-16	MU-3	MU-28
Quartz	-	2.1	-	-
K-feldspar	5.35	11.7	0.4	1.6
Plagioclase	32.8	27.3	20.6	17.9
Clinopyroxene	5.0	6.6	20.3	14.8
Orthopyroxene	2.1	3.1	11.2	11.1
Amphibole	25.1	23.4	5.1	11.2
Biotite	26.5	21.5	38.3	34.3
Sphene	2.32	1.7	0.5	2.6
Epidote	-	0.4	0.6	1.8
Apatite	0.4	1.5	2.3	2.8
Opaques	0.8	0.6	0.6	1.7
Plagioclase Comp.	An ₃₅	An ₃₈	An ₅₁	An ₆₂

Index to Table 2A:

MU-7	Medium grained diorite	MU-3	Medium grained gabbro
MU-16	Coarse grained diorite	MU-28	Medium grained gabbro

In the clinopyroxene, tiny inclusions of translucent reddish-brown mineral, probably iron oxide have been noted in some of the crystals. Well developed reaction rims occur in some of the clinopyroxenes (Plate 2.2 (a)). Typically three zones can be made out; a core of pale greenish-yellow or colorless diopside or augite, an intermediate zone of pale green hornblende and an outer zone of darker green amphibole. The intensity of coloration increased markedly towards the periphery. The replacement of clinopyroxene by amphibole results in the release of free silica and droplets of quartz are usually found in the altered clinopyroxene. Microprobe analysis of the clinopyroxenes were only taken from the core and margin regions of the unaltered crystals.

There are several conditions under which reaction rims or coronas are formed. Shand (1945) suggests that they are formed under regional metamorphic conditions of the granulite facies. Ellis and Green (1979) think that thermal metamorphism induces directed stress resulting

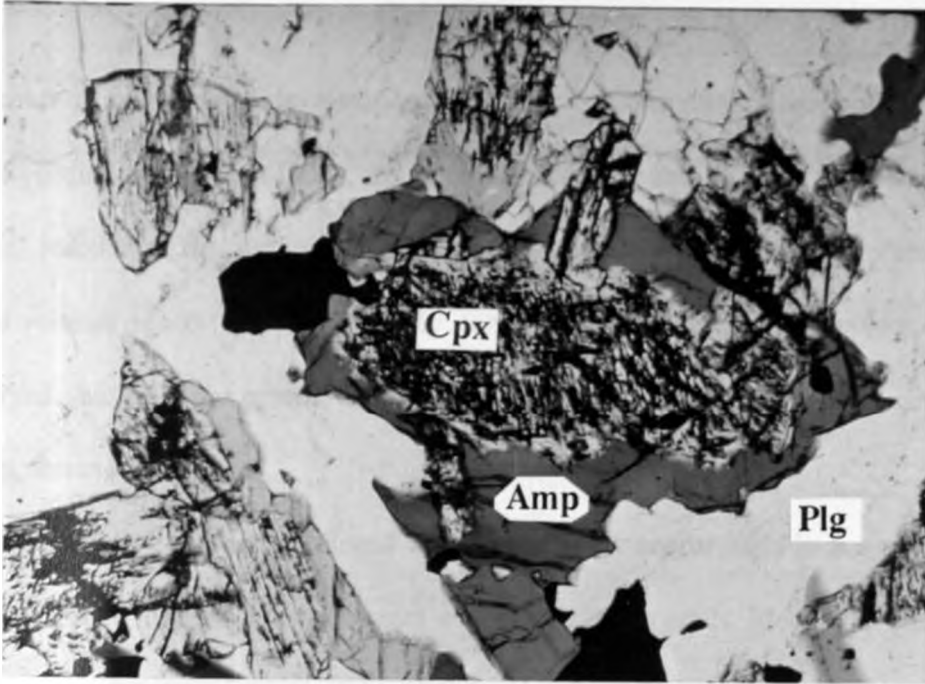


Plate 2.2 (a). Photomicrograph of clinopyroxene - with tiny inclusions of iron oxide - being replaced by a corona of amphibole (Amp) and in contact with plagioclase (Plg). Meta diorite rock (MU-7), Plane polarized light, X 50.

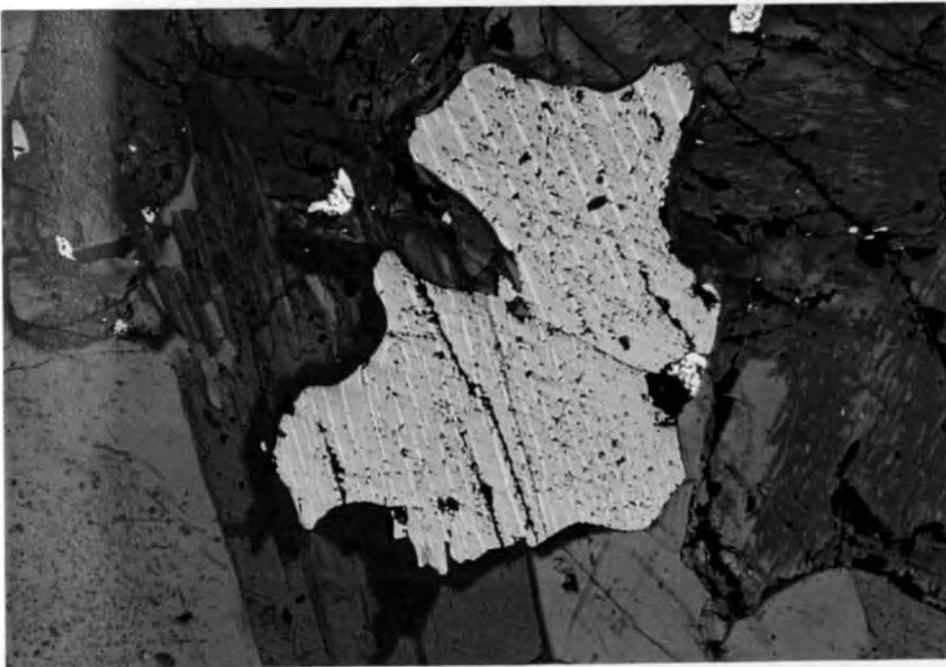
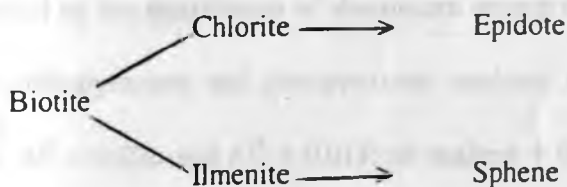


Plate 2.2. (b) Magnetite with exsolved ilmenite lamellae. Meta diorite rock (MU-7), Reflected light, X 100.

in the migration of ions and the development of different corona minerals around olivine and pyroxene. According to Bowen (1956), the formation of a corona of a mineral lower in the discontinuous reaction series around another higher in the series is to be expected if the early-formed mineral reacts with the melt. In coronites formed by metamorphism, Murphy (1958) observed that the outer corona was developed by replacement of plagioclase in contact with ferromagnesian minerals.

Petrographically, coronas developed around clinopyroxene crystals in the meta-diorite rock of Matuu area are in most cases in contact with plagioclase crystals. More over, the textural and the mineral association envisaged by the development of spinel and the clouding of plagioclase seem to attest that the coronas were developed under metamorphic conditions.

The hornblende grains are commonly twinned parallel to the prismatic outline. Pleochroism is very pronounced, X and Y = yellowish green; Z = dark green. Prismatic crystals have an average extinction of 21° . Biotite is usually found intergrown with the hornblende. Apatite and zircon occur occasionally as inclusions in the mafic minerals. Magnetite with ilmenite ex-solution lamellae (Plate 2.2(b)) and pyrite are sparsely distributed throughout the rock. Retrogression of the granulite-facies metamorphism in the meta diorite is documented by petrographic features such as alterations of hornblende and biotite to chlorite, saussuritization in plagioclases, symplectization of pyroxene and growth of minerals such as epidote and sphene. The trend of alterations in the biotite are as follows:



The intergrowing nature of the hornblende and plagioclase suggests that they have crystallized at about the same time, though hornblende crystals have been found as inclusions in plagioclase. The mineralogical diffraction pattern of the meta diorite, presented in Fig. 2.2, confirms some of the mineral components (i.e. plagioclase, biotite and quartz) in the rock identified earlier by petrographic study.

2.1.1.2 Mineral chemistry of the meta-diorite rock

Probe analyses of the major minerals occurring in the Matuu meta diorite rocks are presented in Appendices 2.1, 2.2, 2.3, 2.5 and 2.8. Representative mineral analyses are presented in Table 2.1. Its characteristic mineral chemistry is discussed as follows:

Pyroxene: Both the orthopyroxene crystals of hypersthene composition ($\text{Ca}_{2.36} \text{Mg}_{57.19} \text{Fe}_{40.45}$) and clinopyroxene grains of augite composition ($\text{Ca}_{43.04} \text{Mg}_{37.78} \text{Fe}_{19.18}$) were noted to occur in the meta-diorite rock (Table 2.1, analysis 2 & 4). Clinopyroxene is enriched in Al, Ti, Cr, and Na relative to the coexisting orthopyroxene, and the reverse is true for Mn. A composition plot of representative clinopyroxenes in the Ca-Mg-Fe triangular diagram (Fig. 2.3) show the grains to be of typical alkaline rocks affinity. This is in agreement with the chemistry and mineralogy of the rocks from which these clinopyroxenes were extracted.

According to Le Bas (1962), high load pressure during crystallization produce relatively small Al^{IV} values and large Al^{VI} values; low pressure should give the reverse. In this respect, the evidence provided by the distribution of aluminium among the tetrahedral and octahedral sites in the present orthopyroxene and clinopyroxene analyses (e.g., in Table 2.1 analysis 2 for orthopyroxene, $\text{Al}^{\text{IV}} = 0.036$ and $\text{Al}^{\text{VI}} = 0.013$; in analysis 4 for clinopyroxene, $\text{Al}^{\text{IV}} = 0.033$ and

Diorite Rock from Matuu Area, Central Kenya.

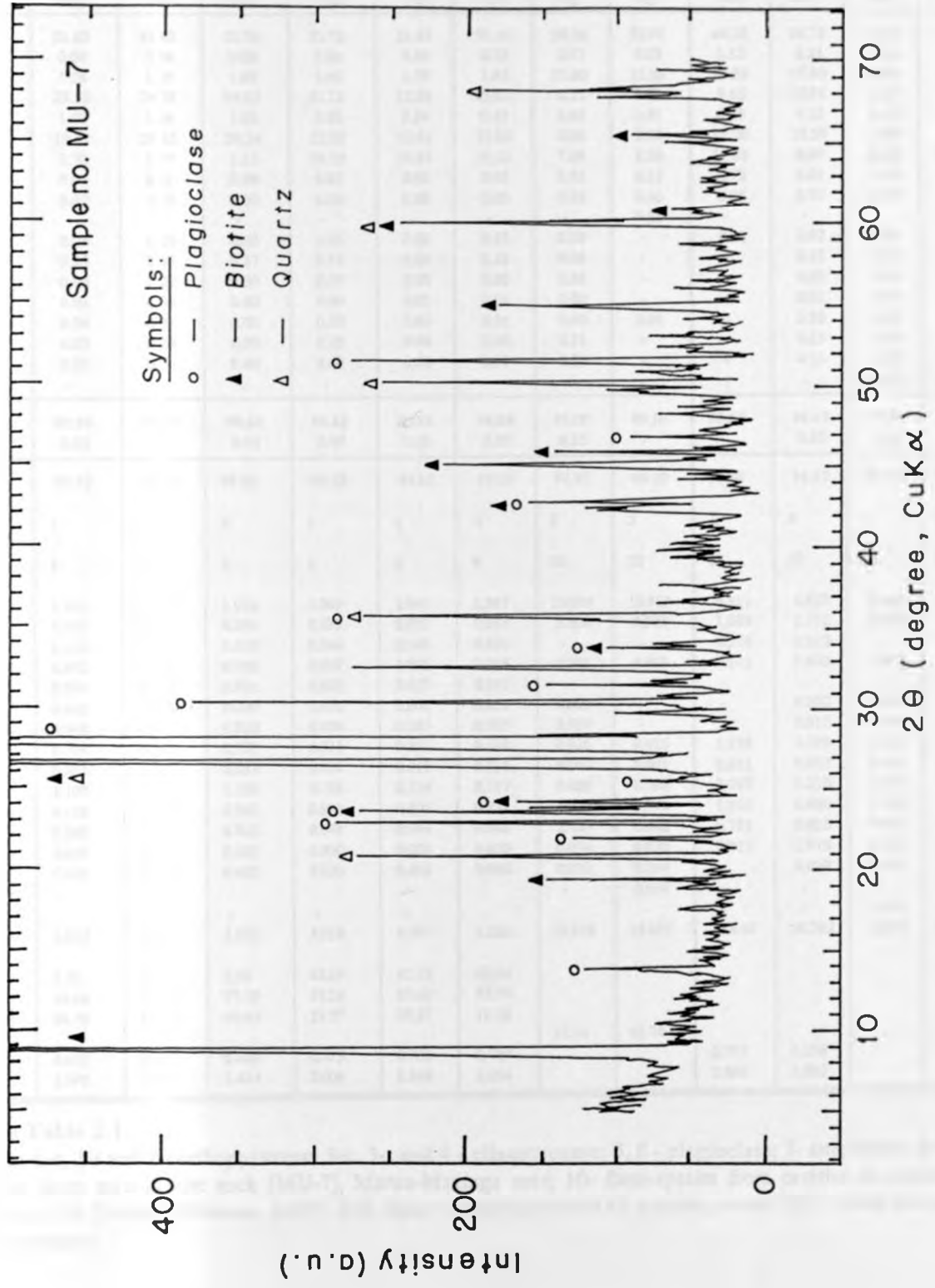


Fig 2.2 X-ray diffraction pattern for diorite rock from Matuu-Masinga area, central Kenya.

Table 2.1. Microprobe analyses of orthopyroxene (Opx), clinopyroxene (Cpx), plagioclase (Plg), biotite (Bio) and Apatite (Apt) from meta-diorite rock, Matuu-Masinga area, central Kenya. n = number of analysis.

Analy.	1-c	1-r	2	3-c	3-r	4	5	6	7	8	9	10
Mineral	Opx	Opx	Opx	Opx	Cpx	Cpx	Plg	Plg	Amp	Bio	Apt	Apt
SiO ₂	51.63	51.93	51.78	51.71	51.83	51.86	59.36	59.99	44.30	36.78	0.19	-
TiO ₂	0.06	0.09	0.08	0.24	0.19	0.22	0.01	0.02	1.32	5.21	0.01	-
Al ₂ O ₃	1.18	1.00	1.09	1.92	1.75	1.85	25.00	25.06	13.50	13.80	0.01	-
FeO*	23.30	24.78	24.35	11.11	11.58	11.01	0.11	0.10	9.45	15.91	0.14	0.17
MnO	1.03	1.08	1.03	0.58	0.54	0.47	0.02	0.01	0.09	0.13	0.12	0.28
MgO	19.59	20.35	20.14	12.51	12.61	12.68	0.00	0.00	15.20	13.59	0.00	-
CaO	2.70	0.49	1.15	20.19	19.66	20.11	7.06	6.90	11.80	0.00	53.63	55.16
Na ₂ O	0.07	0.01	0.03	0.65	0.60	0.63	6.93	0.12	2.72	0.03	0.10	0.09
K ₂ O	0.00	0.00	0.00	0.00	0.00	0.00	0.32	0.30	0.06	9.76	0.00	-
SrO	-	-	-	-	-	-	-	6.51	-	-	-	-
Cr ₂ O ₃	0.03	0.00	0.03	0.05	0.02	0.03	0.00	-	0.12	0.02	0.04	-
V ₂ O ₅	0.25	0.00	0.17	0.14	0.24	0.18	0.06	-	-	0.12	0.00	-
CoO	0.00	0.00	0.00	0.00	0.00	0.00	0.00	-	-	0.03	0.01	-
NiO	0.01	0.00	0.00	0.00	0.01	0.01	0.00	-	-	0.01	0.00	-
BaO	0.04	0.02	0.03	0.00	0.00	0.01	0.00	0.06	-	0.30	0.00	-
F	0.05	0.00	0.00	0.22	0.00	0.00	0.11	-	-	0.65	2.19	3.63
Cl	0.00	0.00	0.00	0.00	0.00	0.00	0.00	-	-	0.13	0.38	tr
P ₂ O ₅	-	-	-	-	-	-	-	-	-	-	42.72	41.87
O=F,Cl	99.94	99.75	99.88	99.32	99.03	99.04	99.00	99.10	98.56	96.47	99.54	101.20
	0.02	-	0.00	0.09	0.00	0.00	0.05	-	-	0.30	1.01	1.53
Total	99.92	99.75	99.88	99.23	99.03	99.04	98.95	99.10	98.56	96.17	98.53	99.67
n	1	1	4	1	1	4	6	5	2	4	4	1
Ox	6	6	6	6	6	6	32	32	23	22	26	26
Si	1.957	1.969	1.964	1.963	1.969	1.967	10.695	10.913	6.311	5.829	0.036	-
Al ⁴	0.043	0.031	0.036	0.037	0.031	0.033	5.308	5.373	1.689	2.171	0.002	-
Al ³	0.010	0.014	0.013	0.049	0.048	0.050	-	-	0.578	0.312	-	-
Ti	0.002	0.003	0.002	0.007	0.005	0.006	0.001	0.003	0.141	0.621	0.002	-
Fe ³	0.034	0.012	0.021	0.022	0.017	0.017	-	-	-	-	-	-
Cr	0.001	0.000	0.000	0.001	0.001	0.001	0.000	-	-	0.002	0.002	-
V	0.008	0.000	0.002	0.004	0.007	0.005	0.039	-	-	0.015	0.000	-
Fe ²	0.704	0.774	0.751	0.331	0.351	0.332	0.016	0.015	1.126	2.108	0.014	0.023
Mn	0.033	0.035	0.033	0.019	0.017	0.015	0.001	0.001	0.011	0.017	0.016	0.040
Mg	1.107	1.150	1.138	0.708	0.714	0.717	0.000	0.000	3.227	3.210	0.000	-
Ca	0.110	0.020	0.047	0.821	0.800	0.817	1.363	1.344	1.801	0.000	9.788	9.966
Na	0.005	0.001	0.002	0.048	0.044	0.046	2.420	0.042	0.751	0.010	0.013	0.029
K	0.000	0.000	0.000	0.000	0.000	0.000	0.074	0.070	0.011	1.973	0.000	-
Ba	0.001	0.000	0.001	0.000	0.000	0.000	0.000	0.004	-	0.019	0.001	-
Sr	-	-	-	-	-	-	-	0.686	-	-	-	-
P	-	-	-	-	-	-	-	-	-	-	6.181	5.977
Total	4.015	4.009	4.010	4.010	4.004	4.006	19.918	18.455	15.646	16.292	16.055	16.035
Wo	5.53	1.00	2.36	43.19	42.13	43.04						
En	55.68	57.78	57.19	37.24	37.60	37.78						
Fs	38.78	41.22	40.45	19.57	20.27	19.18						
An							35.34	62.74				
X _{Mg}	0.652	0.647	0.648	0.715	0.708	0.719			0.782	0.656		
Mg/Fe	1.500	1.463	1.474	2.006	1.940	2.054			2.866	1.523		

Index to Table 2.1

Analysis: 1-c, 1-r and 2 - orthopyroxene; 3-c, 3-r and 4 - clinopyroxene; 5, 6 - plagioclase; 7- amphibole; 8- biotite; 9- apatite from meta-diorite rock (MU-7), Matuu-Masinga area; 10- fluor-apatite from cavities in cleavelandite pegmatite, S.W. Finland (Pehrman, 1939). NB. X_{Mg} = Mg/(Mg+Fe x 0.8); c-centre, r-rim; FeO* = total iron as FeO; - not determined.

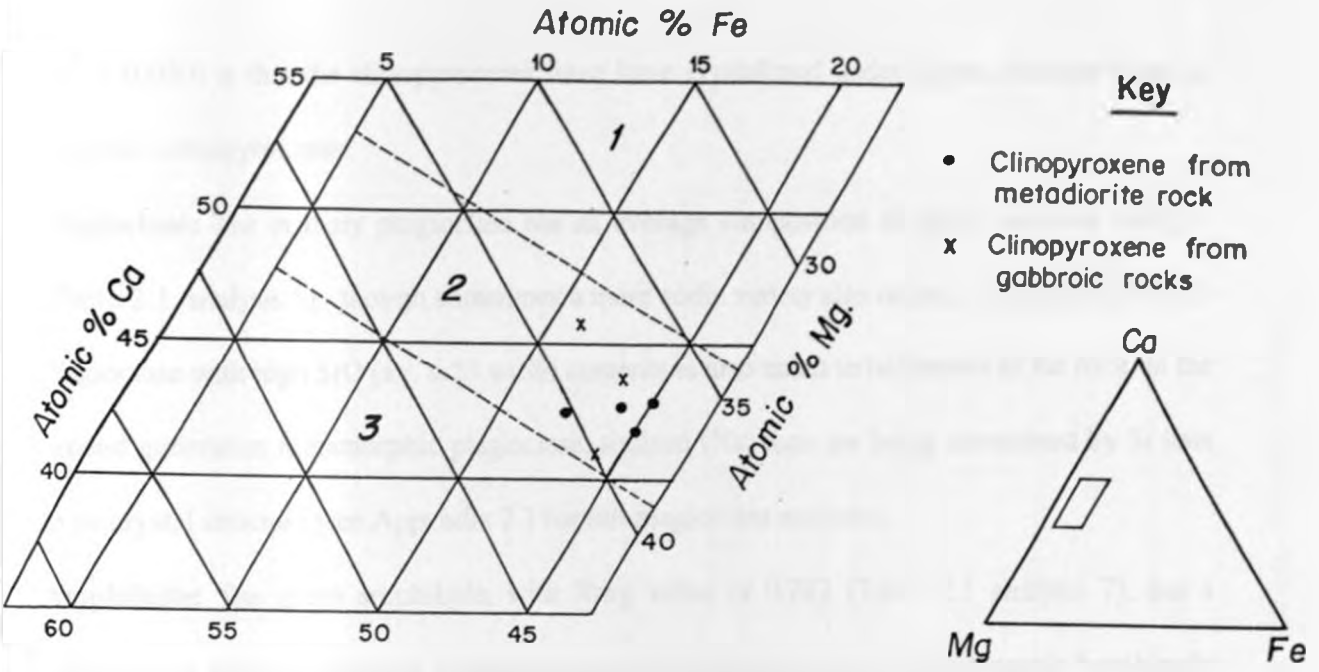


Fig. 2.3 Plot of clinopyroxenes given in Tables 2.1 & 2.2 on part of triangular diagram in terms of Ca:Mg:Fe atomic percent. The dashed lines separate the pyroxenes into three fields, : 1) per - alkaline rocks, 2) alkaline rocks and 3) from non-alkaline rocks. The smaller diagram gives the position of the main diagram within the triangle (modified from M.J. Le Bas, 1962.)

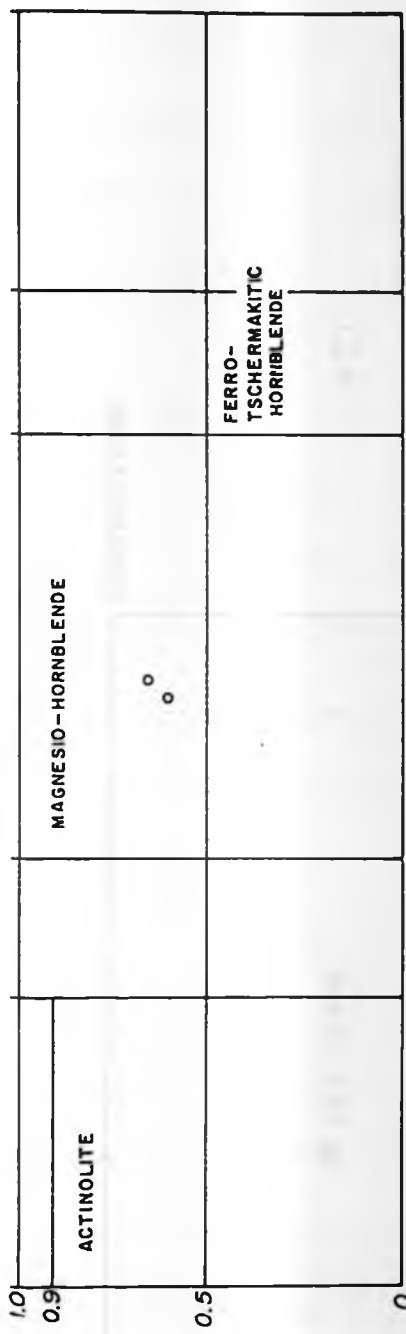
$Al^6 = 0.050$) is that the clinopyroxenes must have crystallized under higher pressure than the iron rich orthopyroxenes.

Plagioclase: The primary plagioclase has an average composition of calcic andesine (An_{35}) - (Table 2.1, analysis 5) - though sometimes a more sodic variety also occurs. A secondary Sr-rich plagioclase with high SrO (av. 6.51 wt.%) contents is also noted to be present in the rock. In the second generation metamorphic plagioclase, sodium (Na) ions are being substituted by Sr ions in its crystal structure (see Appendix 2.3 for full plagioclase analyses).

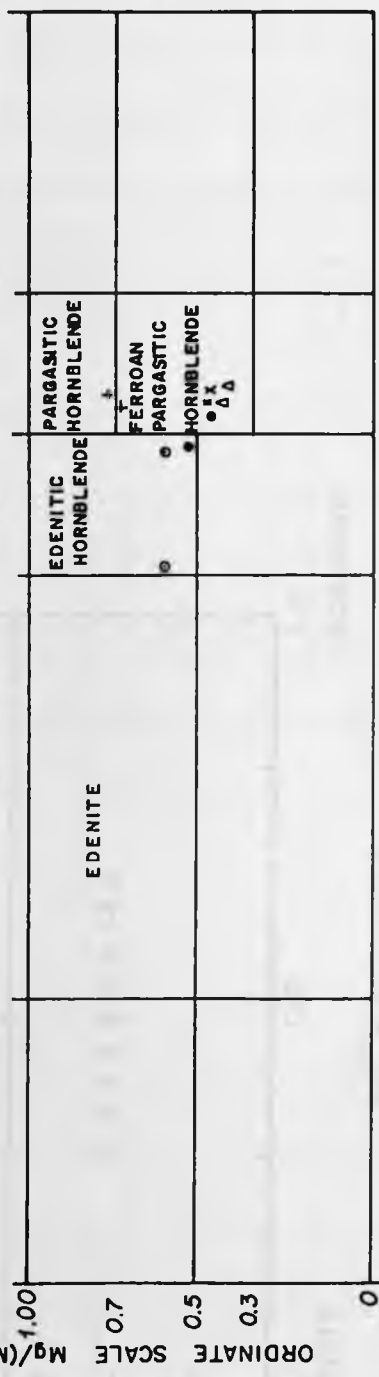
Amphibole: The green amphibole, with X_{Mg} value of 0.782 (Table 2.1 analysis 7), has a composition that straddles the boundary between ferroan pargasitic- and pargasitic hornblende (Fig. 2.4) following the classification of Leake (1978). Within these groups amphiboles are classified using the number of Si atoms and $Mg/(Mg + Fe^{2+})$. Some inaccuracy is inevitable however, because the Fe^{2+}/Fe_{total} ratio cannot be determined by electron microprobe. A ratio of 0.8 is nevertheless considered as a reasonable estimation: in the vein-type Con and Giant Mines in the Yellowknife district, Canada, the whole-rock ratio for unmineralized metabasaltic background samples is 0.7, compared with 0.9 for reduced carbonate-muscovite schists enveloping Au-bearing quartz veins (Kerrick & Fyfe, 1981).

Biotite: The biotite contains characteristically high TiO_2 (av. 5.21 wt.%) content and low Al_2O_3 (av. 13.80 wt.%). It is chemically homogeneous from one grain to another, and has the X_{Mg} atomic ratio of 0.656 and Mg/Fe value of 1.523 (Table 2.1, analysis 8). CaO was not detected in the biotite. A plot of the biotites in the $Fe/(Fe+Mg)$ vs $Al^{IV}-2$ composition diagram (Fig. 2.5) discriminating between biotite and phlogopite (after Azzouni-Sekkal and Boissonnas, 1987), show the Matuu dioritic biotites plotting in the biotite affinity zone.

A. $(Na+K)_A < 0.5$; $Ti < 0.50$



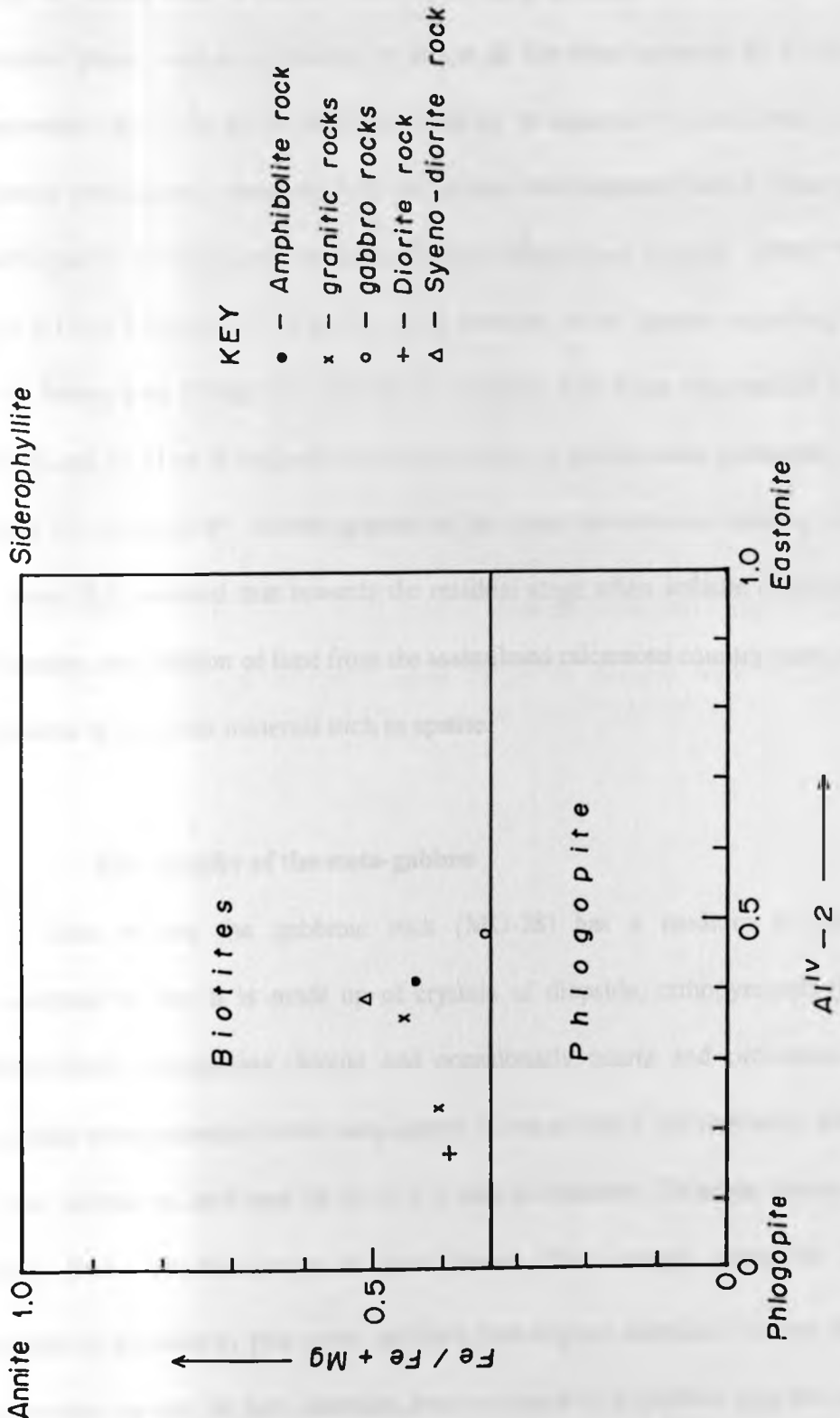
B. $(Na+K)_A \geq 0.50$; $Ti < 0.50$; $Fe^3 \leq Al^6$



KEY

- Amphibolite
- ; ◦ Gabbro
- x Granite
- Δ Syeno-diorite
- + Diorite

Fig 2.4. Nomenclature of calcic amphiboles from Matuu-Masinga area. Fields after Leake (1978).



- KEY
- - Amphibolite rock
 - x - granitic rocks
 - - gabbro rocks
 - + - Diorite rock
 - △ - Syeno-diorite rock

Fig. 2.5. Biotites in the diagram Fe/(Fe+Mg) vs Al^{IV} - 2. Diagram after Azzouni-Sekkal and Boissonnas (1987).

Apatite: Apatite is the commonest accessory mineral in many alkaline rocks such as the dioritic intrusives of Matuu area. It occurs both as elongate prismatic crystals (Plate 2.1 (b)) - an intercumulus phase - and as inclusions in almost all the other minerals. Its F and Cl contents range between 1.91 - 2.36 wt. % and 0.30 - 0.38 wt. % respectively (see Table 2.1 & appendix 2.8). Apatite with higher F contents (3.05 wt.%) have been reported from a gabbro-pegmatite in the middle part of the Pilgugarvi intrusion, Finland (Hanski and Smolkin, 1990). The CaO (av. 53.63 wt.%) and P₂O₅ (av. 42.72 wt.%) mean contents of the apatites occurring in the meta-diorite of Matuu area (Table 2.1, analysis 8) compare with those reported for fluor-apatite (55.16 wt.% and 41.87 wt.% respectively) from cavities in cleavalandite pegmatite, S.W. Finland (see Table 2.1, analysis 9). Apatite appears as the main phosphorous-bearing mineral in the dioritic rock. It is believed that towards the residual stage when volatile constituents become more abundant, the addition of lime from the assimilated calcareous country rocks, enhances the crystallization of lime-rich minerals such as apatite.

2.1.1.3 Petrography of the meta-gabbro

In thin section, the gabbroic rock (MU-28) has a medium to coarse grained hypidiomorphic texture. It is made up of crystals of diopside, orthopyroxene (hypersthene), green hornblende, plagioclase, biotite and occasionally quartz and orthoclase (Plate 2.3). Metamorphic orthopyroxene in the meta-gabbro is occasionally poikiloblastic with occasional plagioclase inclusions, and may be up to 3-4 mm in diameter. Diopside crystals are weakly pleochroic from yellowish-brown to pale brown. The average extinction $Z_{\wedge c} = 41^{\circ}$. Replacement of diopside by pale green and deep bluish-green amphibole occurs in the margins of the pyroxene crystals. In fact, alteration from pyroxene to amphibole and then to biotite can

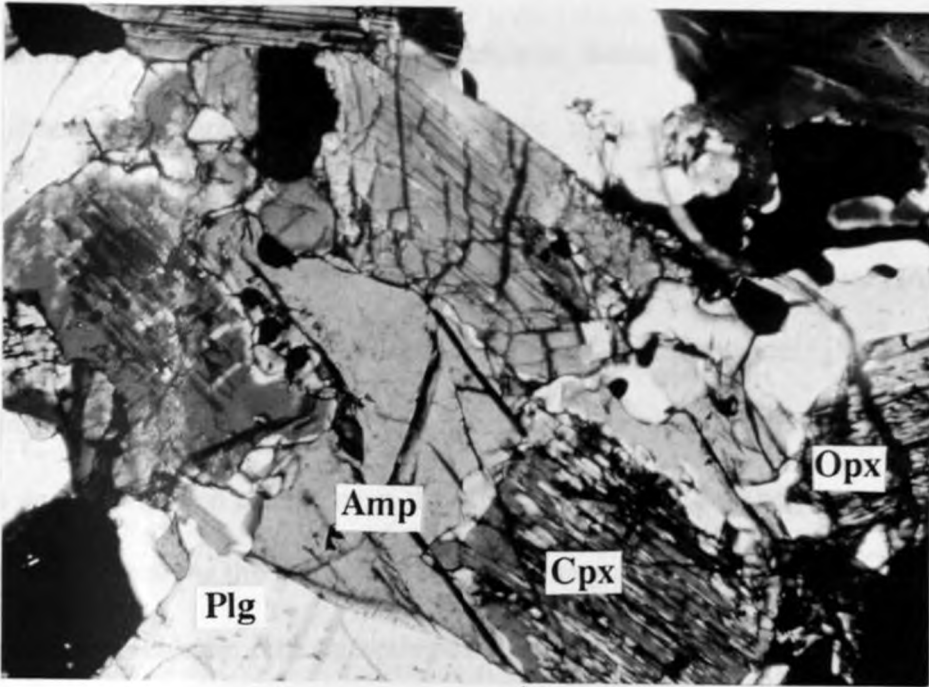


Plate 2.3. Photomicrograph of plagioclase (Plg) in contact with clinopyroxene (Cpx), orthopyroxene (Opx) and amphibole (Amp). Gabbro rock (MU-28), Crossed polars, X 50.

be observed in one and the same crystal in successive rims. Primary hornblende usually forms parallel intergrowth with diopside. In other instances (e.g. sample MU-20), diopside shows an optical continuity while being replaced by amphibole. Biotite plates are commonly altered to granular ilmenite and sphene along the cleavage traces and ragged edges. The modal composition of representative gabbroic rocks is presented in Table 2A.

The plagioclase of the meta-gabbro (MU-28) is mainly labradoritic (An_{62-67}) in composition. Besides the combined carlsbad-albite twins, pericline twinning is not uncommon in the plagioclase crystals. Quartz and orthoclase make their appearance usually in the interstices and they seldom exceed more than 10 % of the rock. Apatite, magnetite and pyrite are common accessories in the gabbroic rock. Magnetite grains are sometimes found in clusters inside secondary hornblende. The mineralogical diffraction pattern of the bulk groundmass for gabbroic rock (MU-28) is presented in Fig. 2.6. The pattern gives characteristic peaks of plagioclase, a strong reflection at 3.17 \AA being recognized as the (002) reflection, and also peaks at 2.45 and 1.77 \AA corresponding to the reflection of (112) and (204) respectively. The groundmass of the rock consists also of biotite with strong peaks at 10.1 and 3.37 \AA that correspond to the reflection (001) and (003) respectively. The orthopyroxene grains shows their presence with strong reflection peaks at 3.18 and 1.75 \AA . The groundmass pattern further show minor presence of amphibole and K-feldspar. The relatively high intensities of biotite, plagioclase and pyroxene are an indication of their degree of crystallinity and relative abundance in the rock.

Fig. 2.6. X-ray diffraction pattern for gabbroic rock from MU-28. The x-axis is labeled '2θ (degrees)' and the y-axis is labeled 'Intensity (counts)'. The pattern shows several sharp peaks, with the most prominent ones at approximately 3.17, 2.45, 1.77, 10.1, and 3.37 Å.

Gabbro Rock from Matuu Area, Central Kenya .

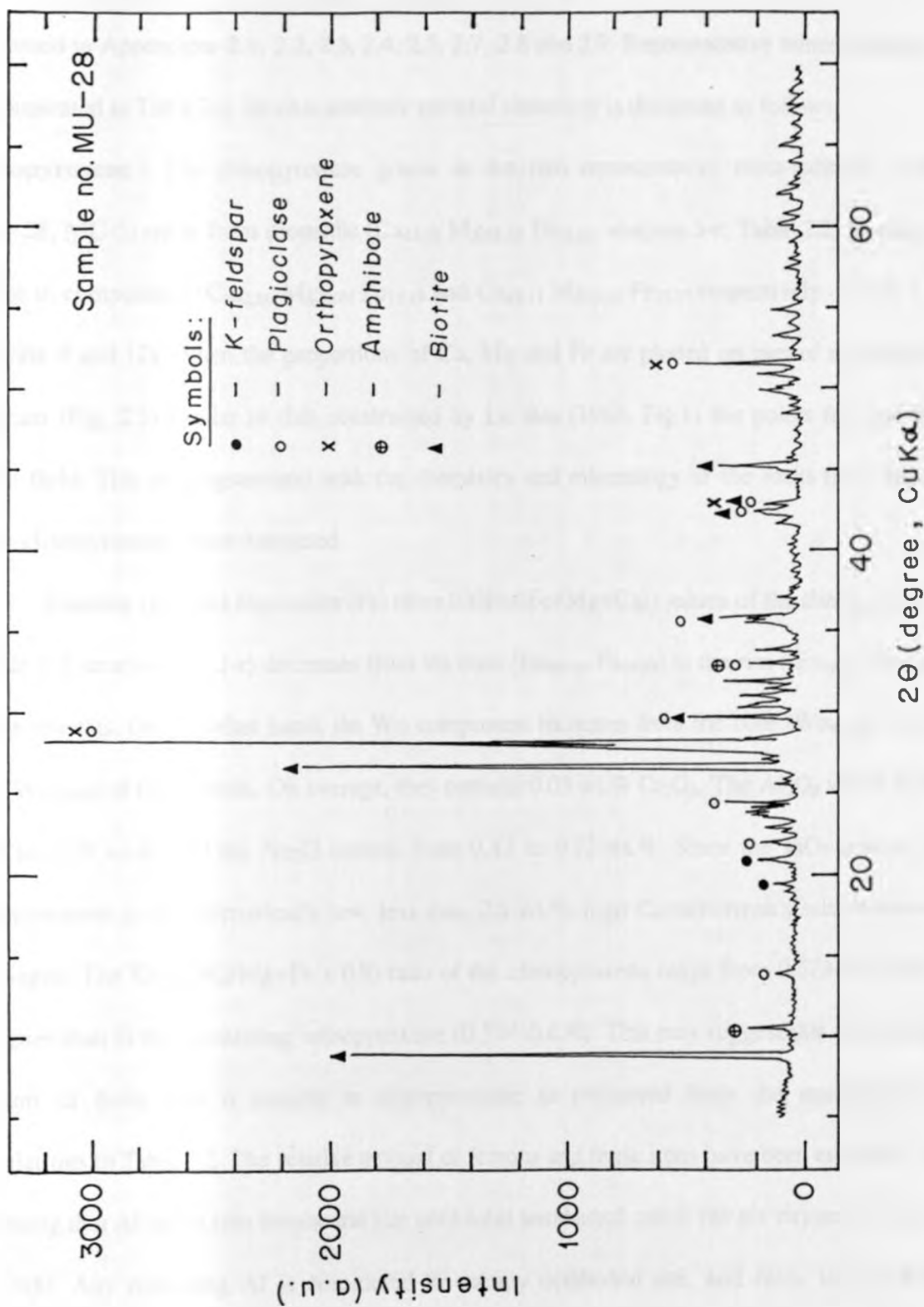


Fig. 2.6. X-ray diffraction pattern for gabbroic rock from Matuu-Masinga area, central Kenya.

2.1.1.4 Mineral chemistry of the meta-gabbro

Probe analyses of the major minerals occurring in the Matuu gabbroic rocks are presented in Appendices 2.1, 2.2, 2.3, 2.4, 2.5, 2.7, 2.8 and 2.9. Representative mineral analyses are presented in Table 2.2. Its characteristic mineral chemistry is discussed as follows:

Clinopyroxene : The clinopyroxene grains in the two representative meta-gabbroic rocks (MU-28, MU-5) range from diopsidic ($\text{Ca}_{45.98} \text{Mg}_{38.40} \text{Fe}_{15.62}$, analysis 3-r, Table 2.2) to mainly augite in composition ($\text{Ca}_{42.80} \text{Mg}_{38.01} \text{Fe}_{19.19}$ and $\text{Ca}_{42.11} \text{Mg}_{39.12} \text{Fe}_{18.77}$ respectively - Table 2.2, analysis 4 and 12). When the proportions of Ca, Mg and Fe are plotted on part of a triangular diagram (Fig. 2.3) similar to that constructed by Le Bas (1962, Fig.1) the points fall into the alkali field. This is in agreement with the chemistry and mineralogy of the rocks from which these clinopyroxenes were extracted.

Enstatite (En) and Ferrosilite (Fs) ($\text{Fs} = 100\text{Fe}/(\text{Fe}+\text{Mg}+\text{Ca})$) values of the clinopyroxene (Table 2.2, analysis 3-c, 3-r) decreases from the core ($\text{En}_{40.16}$, $\text{Fs}_{19.25}$) to the rim ($\text{En}_{38.40}$, $\text{Fs}_{15.62}$) of the crystals. On the other hand, the Wo component increases from the core ($\text{Wo}_{40.59}$) to the rim ($\text{Wo}_{45.98}$) of the crystals. On average, they contain 0.03 wt.% Cr_2O_3 . The Al_2O_3 varies from 1.75 to 3.38 wt.%, and the Na_2O content from 0.42 to 0.72 wt.%. Since the TiO_2 content in clinopyroxene is characteristically low, less than 0.5 wt.%, high Ca-tschermak's substitution is envisaged. The X_{mg} ($\text{Mg}/\text{Mg}+\text{Fe} \times 0.8$) ratio of the clinopyroxene range from 0.673-0.728 and is higher than in the co-existing orthopyroxene (0.594-0.656). This may suggest that substantial amount of ferric iron is present in clinopyroxene as evidenced from the stoichiometric calculations in Table 2.2. The relative amount of ferrous and ferric irons have been estimated by assuming that Al enters into tetrahedral site until total tetrahedral cation per six oxygens is equal to 2.000. Any remaining Al is considered to occupy octahedral site, and ferric iron is then

Table 2.2. Microprobe analyses for orthopyroxene (opx), clinopyroxene (cpx), plagioclase (plg), amphibole (amp) and biotite (bio) minerals occurring in representative gabbroic rocks from Matuu-Masinga area, central Kenya. Analysis 1-c, 1-r, 2, 3-c, 3-r, 4, 5-c, 5-r & 8 from coarse grained gabbro (MU-28); 7, 9- from Gabbro (MX-21); 6, 10- from Gabbro (MU-20); 11, 12, & 13 from fine grained gabbro (MU-5); 14- from gabbro sill, Radnitsohkka area, Finland (Pekka,1992). n = number of analyses.

Analysis	1-c	1-r	2	3-c	3-r	4	5-c	5-r
Mineral	Opx	Opx	Opx	Cpx	Cpx	Cpx	Plg	Plg
SiO ₂	51.76	51.79	51.66	50.63	52.06	51.16	58.58	59.48
TiO ₂	0.10	0.20	0.11	0.42	0.22	0.32	0.02	0.02
Al ₂ O ₃	1.19	1.11	1.23	3.38	1.95	2.68	25.98	25.21
FeO	23.93	24.41	24.50	11.13	9.27	11.12	0.13	0.17
MnO	0.84	0.79	0.76	0.27	0.31	0.41	0.01	0.03
MgO	20.03	20.04	20.10	13.35	13.20	12.81	-	-
CaO	1.26	1.43	1.11	18.78	22.02	20.07	7.69	7.05
Na ₂ O	0.03	0.02	0.03	0.67	0.52	0.60	0.07	0.16
K ₂ O	0.00	0.01	0.01	0.23	0.01	0.01	0.40	0.44
Cs ₂ O	-	-	-	-	-	-	0.06	0.04
Cr ₂ O ₃	0.00	0.06	0.04	0.09	0.02	0.06	-	-
V ₂ O ₃	0.36	0.21	0.26	0.58	0.07	0.32	-	-
CoO	0.05	0.00	0.02	0.00	0.01	0.00	-	-
NiO	0.02	0.08	0.01	0.00	0.01	0.00	-	-
BaO	0.00	0.00	0.00	0.00	0.05	0.00	0.06	0.07
SrO	-	-	-	-	-	-	5.86	6.28
F	0.20	0.10	0.06	0.13	0.27	0.12	-	-
Cl	0.00	0.01	0.00	0.00	0.00	0.00	-	-
O=F,Cl	99.77 0.04	100.26 0.08	99.90 0.02	99.66 0.06	99.99 0.11	99.68 0.05	98.86 -	98.95 -
Total	99.73	100.18	99.88	99.60	99.88	99.63	98.86	98.95
n	1	1	6	1	1	4	1	1
Ox	6	6	6	6	6	6	32	32
Si	1.963	1.958	1.958	1.910	1.955	1.933	10.697	10.851
Al ⁴	0.037	0.042	0.042	0.090	0.045	0.067	5.591	5.421
Al ⁶	0.016	0.007	0.013	0.061	0.041	0.052	-	-
Ti	0.003	0.006	0.003	0.012	0.006	0.009	0.003	0.003
Fe ⁺³	0.017	0.024	0.025	0.054	0.030	0.041	-	-
Cr	0.000	0.002	0.001	0.003	0.000	0.002	-	-
V	0.005	0.006	0.010	0.018	0.001	0.008	-	-
Fe ⁺²	0.742	0.747	0.751	0.297	0.261	0.310	0.020	0.026
Mn	0.027	0.025	0.024	0.009	0.010	0.013	0.001	0.004
Mg	1.132	1.129	1.135	0.751	0.740	0.721	-	-
Ca	0.051	0.058	0.045	0.759	0.886	0.812	1.504	1.378
Ba	0.000	0.000	0.000	0.000	0.003	0.000	0.004	0.006
Sr	-	-	-	-	-	-	0.621	0.664
Na	0.002	0.001	0.002	0.049	0.038	0.044	0.024	0.057
K	0.000	0.000	0.000	0.011	0.000	0.000	0.094	0.103
Cs	-	-	-	-	-	-	0.004	0.002
Co	0.003	0.000	0.001	0.000	0.001	0.000	-	-
Ni	0.003	0.009	0.002	0.000	0.002	0.000	-	-
Total	4.004	4.017	4.010	4.024	4.019	4.014	18.563	18.515
En	57.49	56.93	57.32	40.16	38.40	38.01	-	-
Wo	2.59	2.93	2.27	40.59	45.98	42.80	-	-
Fs	39.92	40.14	40.40	19.25	15.62	19.19	-	-
An	-	-	-	-	-	-	67.05	62.58
X _{Mg}	0.656	0.594	0.646	0.728	0.718	0.673	-	-
Mg/Fe	1.491	1.464	1.463	2.140	2.543	2.054	-	-

Index to Table 2.2

Analysis 1-c, 1-r and 2 - orthopyroxene; 3-c, 3-r and 4 - clinopyroxene; 5-c and 5-r plagioclase;

Table 2.2. cont.../2

Analys.	6	7	8	9	10	11	12	13	14
Mineral	Plg	Plg	Amp	Amp	Amp	Opx	Cpx	Bio	Bio
SiO ₂	44.75	46.04	43.13	45.93	46.58	51.21	50.64	36.26	36.25
TiO ₂	0.02	0.01	2.30	0.39	0.63	0.18	0.30	4.81	4.57
Al ₂ O ₃	34.84	33.72	9.90	8.06	9.10	1.67	2.83	14.13	16.27
FeO ⁺	0.07	0.02	14.98	15.46	11.49	22.83	10.80	13.55	14.80
MnO	0.03	0.01	0.21	0.27	-	0.77	0.36	0.05	-
MgO	0.00	0.00	11.71	11.54	14.38	20.60	13.08	14.69	13.75
CaO	18.44	17.11	10.99	12.01	11.81	1.07	19.60	0.01	-
Na ₂ O	0.79	1.51	1.42	0.84	0.91	0.06	0.49	0.02	-
K ₂ O	0.01	0.02	1.61	0.50	0.40	0.00	0.00	9.39	9.41
Cs ₂ O	0.06	0.03	-	-	-	-	-	-	-
Cr ₂ O ₃	-	-	0.04	0.02	-	0.01	0.03	0.05	-
V ₂ O ₅	-	-	0.39	0.03	-	0.08	0.08	0.02	-
CoO	-	-	0.00	0.00	-	0.00	0.00	0.00	-
NiO	-	-	0.00	0.02	-	0.00	0.00	0.00	-
BaO	0.05	0.06	0.00	0.05	-	0.00	0.07	0.90	-
SrO	0.00	0.00	-	-	-	-	-	-	-
F	-	-	0.36	0.12	-	0.15	0.27	0.54	-
Cl	-	-	0.12	0.04	-	0.01	0.00	0.11	-
O=F,Cl	99.06	98.53	97.16	95.28	95.30	98.64	98.55	94.53	95.06
	-	-	0.18	0.06	-	0.06	0.11	0.25	-
Total	99.06	98.53	96.98	95.22	95.30	98.58	98.44	94.28	95.06
n	4	4	1	3	1	3	3	3	1
Ox	32	32	23	23	23	6	6	22	22
Si	8.336	8.587	6.523	6.979	6.914	1.952	1.933	5.522	5.433
Al ⁴	7.649	7.412	1.477	1.021	1.086	0.048	0.067	2.478	2.567
Al ⁶	-	-	0.288	0.423	0.507	0.027	0.060	0.059	0.291
Ti	0.003	0.001	0.262	0.045	0.071	0.005	0.009	0.551	0.515
Fe ³⁺	-	-	-	-	-	0.015	0.025	-	-
Cr	-	-	0.006	0.003	-	0.001	0.001	0.005	-
V	-	-	0.047	0.001	-	0.002	0.002	0.002	-
Fe ²⁺	0.011	0.003	1.894	1.965	1.426	0.713	0.320	1.726	1.852
Mn	0.005	0.001	0.027	0.035	-	0.025	0.012	0.006	-
Mg	0.000	0.000	2.639	2.614	3.181	1.170	0.744	3.335	3.066
Ca	3.680	3.419	1.781	1.956	1.878	0.044	0.801	0.002	-
Ba	0.003	0.005	0.000	0.003	-	0.000	0.001	0.054	-
Sr	0.000	0.000	-	-	-	-	-	-	-
Na	0.284	0.547	0.416	0.246	0.262	0.004	0.036	0.005	-
K	0.002	0.004	0.311	0.097	0.075	0.000	0.000	1.825	1.796
Cs	0.009	0.004	-	-	-	-	-	-	-
Co	-	-	0.000	0.000	-	0.000	0.000	0.000	-
Ni	-	-	0.000	0.003	-	0.000	0.000	0.000	-
Total	19.982	19.983	15.671	15.391	15.400	4.006	4.011	15.570	15.521
En						59.48	39.12		
Wo						2.24	42.11		
Fs						38.28	18.77		
An	92.80	86.12							
X _{Mg}			0.635	0.624	0.736	0.668	0.729	0.707	0.674
Mg/Fe			1.393	1.330	2.231	1.607	2.157	1.932	1.656

Analysis: 6, 7- plagioclase; 8, 9, 10 - amphibole; 11- orthopyroxene, 12- clinopyroxene; 13 and 14 - biotite.

NB. X_{Mg} = Mg/(Mg+Fe x 0.8) ; c-centre, r-rim ; FeO⁺ - total iron as FeO ; - not determined.

calculated as $Fe^{3+} = (Al^{IV} + Na) - (Al^{VI} + 2Ti)$. This provides an estimate of the Fe^{3+} content which is sensitive to small errors in SiO_2 and Al_2O_3 analyses. However, this is believed to be the best arbitrary method for calculating trivalent iron in pyroxene (McLelland and Whitney, 1977). The estimated $Fe^{3+}/(Fe^{2+}+Fe^{3+})$ ratio range from 0.10 to 0.15 in clinopyroxene as compared to orthopyroxene which range from 0.02 to 0.03. In general, probe analysis of the crystals (analysis 3-c, 3-r, Table 2.2) show that SiO_2 , MnO, CaO, BaO and F are relatively more enriched in the rim than in the core of the crystals.

Comparing the clino- and ortho-pyroxene crystals in the meta-gabbro rock, MU-28, (analysis 2 & 4 in Table 2.2), the clinopyroxenes are relatively more enriched in TiO_2 (av. 0.32 wt.%), Al_2O_3 (av. 2.68 wt.%), Na_2O (av. 0.60 wt.%), Cr_2O_3 (av. 0.06 wt.%), V_2O_5 (av. 0.32 wt.%) and F (av. 0.12 wt.%) contents than in the orthopyroxene crystals with TiO_2 (av. 0.11 wt.%), Al_2O_3 (av. 1.23 wt.%), Na_2O (av. 0.03 wt.%), Cr_2O_3 (av. 0.04 wt.%), V_2O_5 (av. 0.26 wt.%) and F (av. 0.06 wt.%). Conversely the orthopyroxene crystals show a relatively higher enrichment in MnO (av. 0.76 wt.%) than in the clinopyroxenes (av. 0.41 wt.% MnO). This overall composition pattern of the clinopyroxenes in the gabbro rock MU-28 is similar to that observed in the gabbro rock MU-5 (Table 2.2, analysis 11 & 12).

The almost equal amounts of jadeite (Al^{VI}) and Ca-Tschermak (Al^{IV}) in the clinopyroxenes of the representative specimens (MU-28, MU-5, Table 2.2) could have resulted from the combined effects of high pressure and high temperature. Compared to pyroxene trends in some continental stratiform gabbros the pyroxene of Matuu-Masinga area show a high iron enrichment, a less pronounced decrease in calcium content with enrichment for the clinopyroxene, and a greater compositional gap.

Orthopyroxene: The orthopyroxene grains occurring in the representative gabbroic rocks (MU-28 & MU-5) are mainly hypersthene ($\text{Ca}_{2.27} \text{Mg}_{57.32} \text{Fe}_{40.40}$ and $\text{Ca}_{2.24} \text{Mg}_{59.48} \text{Fe}_{38.28}$) in composition (Table 2.2, analysis 2 & 11). The Al_2O_3 content varies from 1.00 to 1.88 wt.% (av. 1.24 wt.%), and the CaO content from 0.5 to 2.70 wt.% (av. 0.98 wt.%). Whereas the En values show a decrease from the core to the rim of the crystals (Table 2.2, analysis 1-c, & 1-r), the Wo and Fs components show an increment from the core to the rim. They have a mean En value ($\text{En} = 100\text{Mg}/\text{Mg}+\text{Fe}+\text{Ca}$) of 57.32 and 59.48 for samples MU-28 and MU-5 respectively. Calcium contents, measured by the wollastonite component ($\text{Wo} = 100\text{Ca}/\text{Ca}+\text{Mg}+\text{Fe}$) have a mean value of 2.27 and 2.24 respectively for the two representative gabbroic samples MU-28 and MU-5 (Table 2.2, analysis 2 & 11).

Probe analysis of the rim and core of the orthopyroxene grain (MU-28) (Table 2.2, analysis 1-c & 1-r) show that SiO_2 , CaO, TiO_2 , FeO, Cr_2O_3 and NiO contents are relatively more enriched in the rim than in the core of the crystal. The reverse is true for Al_2O_3 , MnO, V_2O_3 , and CoO contents. The orthopyroxene contains appreciable amounts of aluminium (av. 1.18 wt.%). In the orthopyroxene (as well as the clinopyroxenes) Al^{IV} is higher than Al^{VI} (e.g., In Table 2.2 analysis 2 for orthopyroxene $\text{Al}^{\text{IV}} = 0.042$ and $\text{Al}^{\text{VI}} = 0.013$). If according to Le Bas (1962) high P_{load} during crystallization results in small Al^{IV} and large Al^{VI} , the orthopyroxene (and clinopyroxene) in the gabbroic rocks must have crystallized at relatively low pressures as opposed to those occurring in the meta diorite rock.

Plagioclase: The plagioclase in the meta-gabbro rock (MU-28) of Matuu area is mainly of labradolitic in composition with high anorthite contents ($\text{An}_{62.58-67.05}$) as exemplified by its core and rim analysis in Table 2.2, analysis 5-c & 5-r. The anorthite contents increases from bytownitic composition (An_{86}) in gabbroic sample MX-21 to anorthite (An_{93}) in gabbroic

sample MU-20. Sample MU-20 and MX-21 are representatives of small intrusive gabbroic bodies in Matuu area.

Amphibole: According to the amphibole classification of Leake (1978), probe analysis of the amphiboles occurring in representative Matuu gabbroic rocks (e.g., MU-28, -20, & -21) were identified to be mainly of two varieties: the calcic edenitic hornblende (e.g. Table 2.2, analysis 8) and magnesio-hornblende (e.g., Table 2.2, analysis 9 and 10) as shown in Fig. 2.4. The magnesio-hornblendes has characteristically low total (Na+K) cations (i.e < 0.5) as compared to the edenitic hornblendes with (Na+K) cations > 0.5.

Biotite: The biotite occurring in the meta-gabbroic rock (MU-5) (Table 2.2, analysis 13) is chemically homogeneous from grain to grain (see Appendix 2.5), and has the $X_{mg} = (Mg/Mg+Fe*0.8)$ atomic ratio of 0.707 and Mg/Fe ratio of 1.932. The biotite contains characteristically high TiO_2 (av. 4.81 wt.%) and low Al_2O_3 (14.13 wt.%). These values compare relatively well with the biotite reported from a similar gabbroic rock from Ridnitsohkka area, Finland (Table 2.2, analysis 14) which has a X_{mg} value of 0.674 and Mg/Fe ratio of 1.656. The gabbroic biotite straddle in the boundary between biotite-phlogopite according to the discriminant diagram after Azzouni-Sekkal and Boissonnas (1987) in Fig. 2.5.

2.1.1.5 Petrography of the Anorthositic gabbros

Despite exhibiting wide macroscopic lithological variations within the anorthositic gabbro units, there are a number of similarities in thin section. In one specimen MU-30, original equant pyroxene grains, often coarse, ranging from 4-10 mm in grain size, are partially and sometimes completely replaced by medium to dark green pleochroic amphibole crystals. The

Photomicrograph in Plate 2.4 shows an original clinopyroxene in optical continuity while undergoing replacement by amphibole.

In another sample MU-33, the thin section shows a relict igneous texture, large plagioclase feldspars with orthopyroxene inclusions (hypersthene) (Plate 2.5) and fresh metamorphic brown amphibole occupying an interstitial position (Plate 2.6). In paragenetic terms, this texture suggests that plagioclase is older than hornblende; hornblende obviously being late magmatic or deuteric in origin. In the leucocratic layers, the large igneous plagioclases have subsequently been recrystallized into fine-grained optically oriented aggregates (Plate 2.7 (a) & (b)) that give a clear evidence of extensive metamorphic overprint in the central parts and the more massive anorthositic gabbro units. The common occurrence of hypersthene indicates that the gabbros were originally noritic. A distinctive dark brown fibrous rims of spinel-hornblende symplectites in contact with plagioclase (Plate 2.8) define a corona texture that elsewhere has been interpreted to be as a result of sub-solidus reactions during lower temperature re-equilibration on cooling (Emslie, 1983).

2.1.1.6 Petrography of the Hornblende gneiss

The mafic hornblende gneiss is a minor but widespread component, with the largest mass occurring at the NE section of the study area. The rock consists essentially of hornblende, plagioclase (andesine) and quartz. Diopside, hypersthene, biotite and K-feldspar constitute the minor minerals. Secondary and accessory minerals are chlorite, sphene, epidote, apatite, garnet, sericite, carbonate, opaque and prehnite. A microphotograph of a representative hornblende gneiss (sample MU-19) illustrating the texture and mineralogy common to amphibolite grade of metamorphism is shown in Plate 2.9

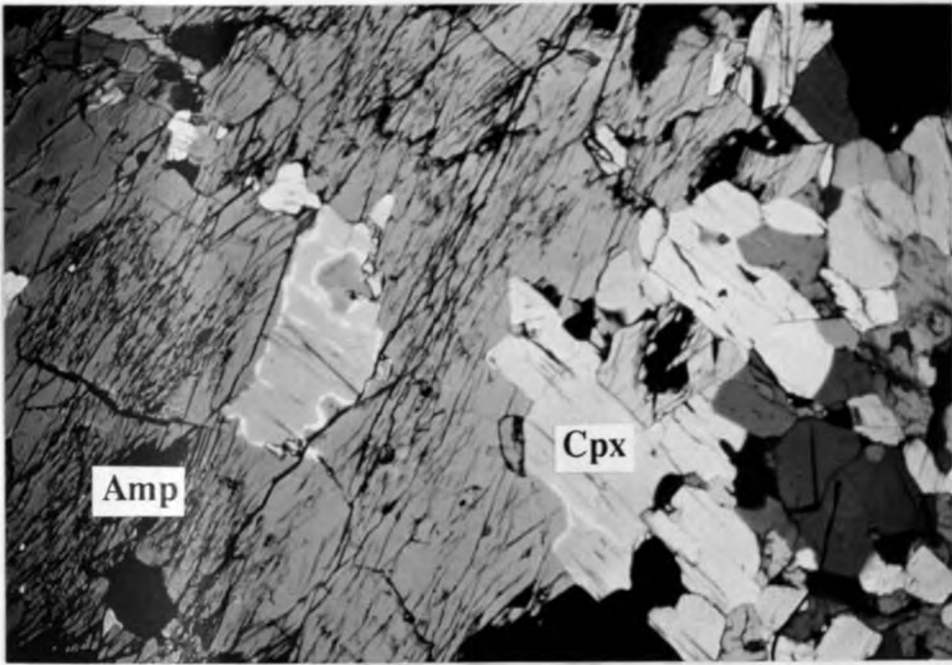


Plate 2.4. Photomicrograph of clinopyroxene (Cpx) in optical continuity and being replaced by amphibole (Amp). Anorthositic gabbro (MU-30), Crossed polars, X 100.

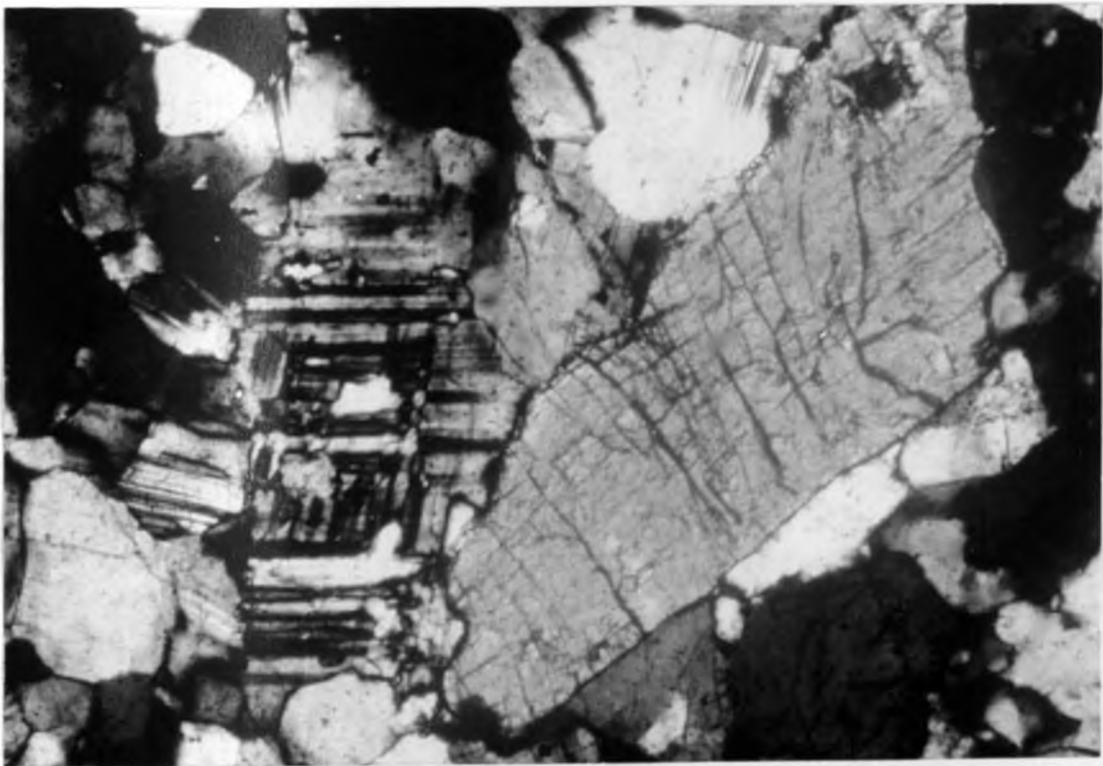


Plate 2.5. Photomicrograph of hypersthene inclusion in plagioclase. Anorthositic gabbro (MU-33), Crossed polars, X 100.

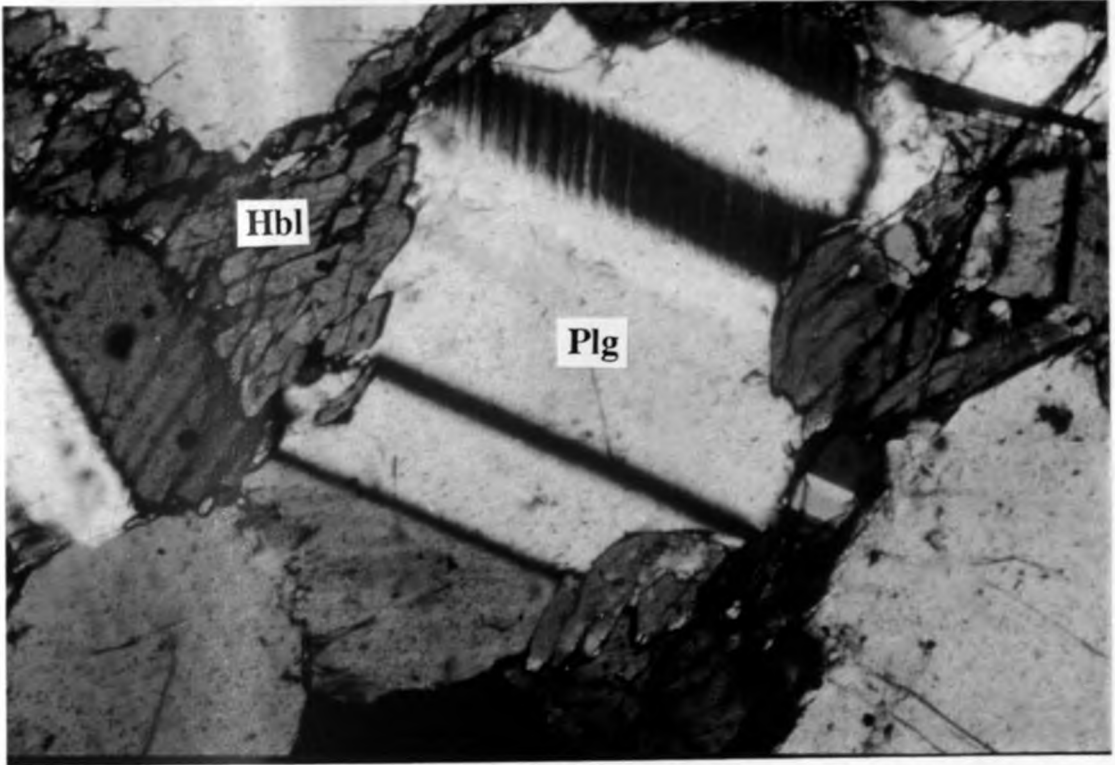


Plate 2.6. Photomicrograph of secondary hornblende (Hbl) in plagioclase (Plg) crystal crevices. Anorthositic gabbro (MU-33), Crossed polars, X 100.

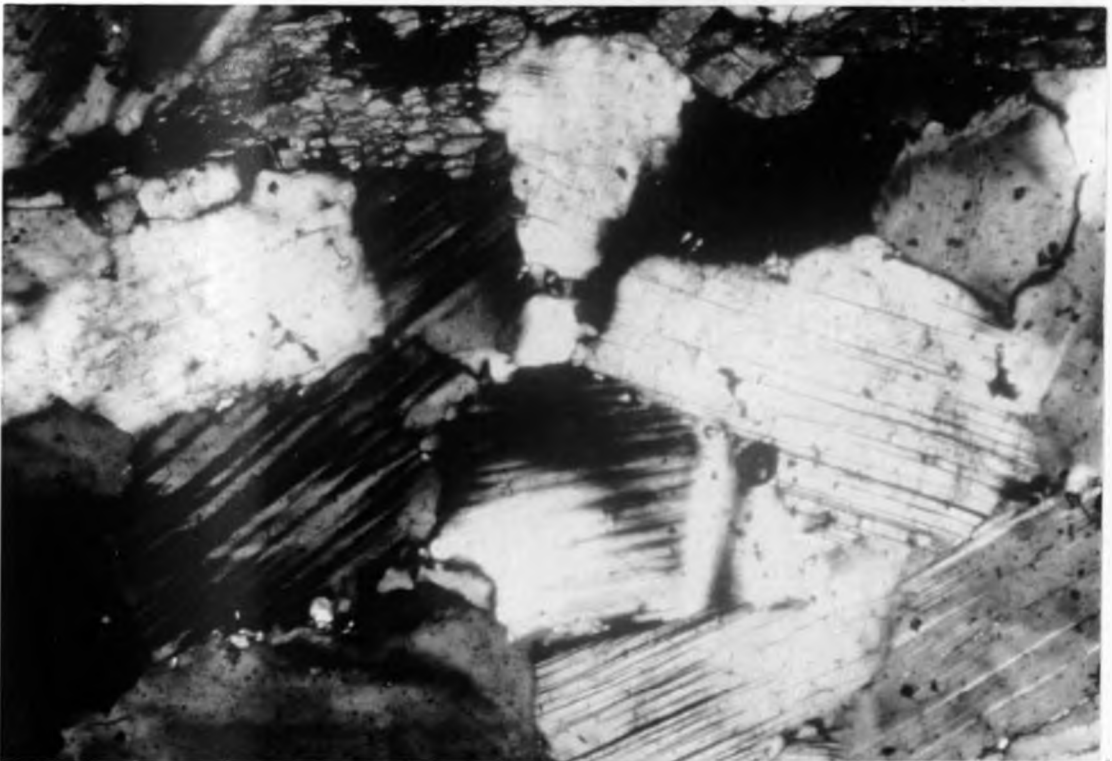


Plate 2.7. (a) Photomicrograph of optically oriented recrystallized plagioclase (light) and amphibole (yellowish-brown). Anorthositic gabbro (MU-33), Crossed polars, X 100.



Plate 2.7. (b) Photomicrograph of secondary fine grained aggregates of plagioclase crystals from the leucocratic layer. Note the diffuse crystal-grain boundaries. Anorthositic gabbro, (MU-33), Crossed polars, X 50.

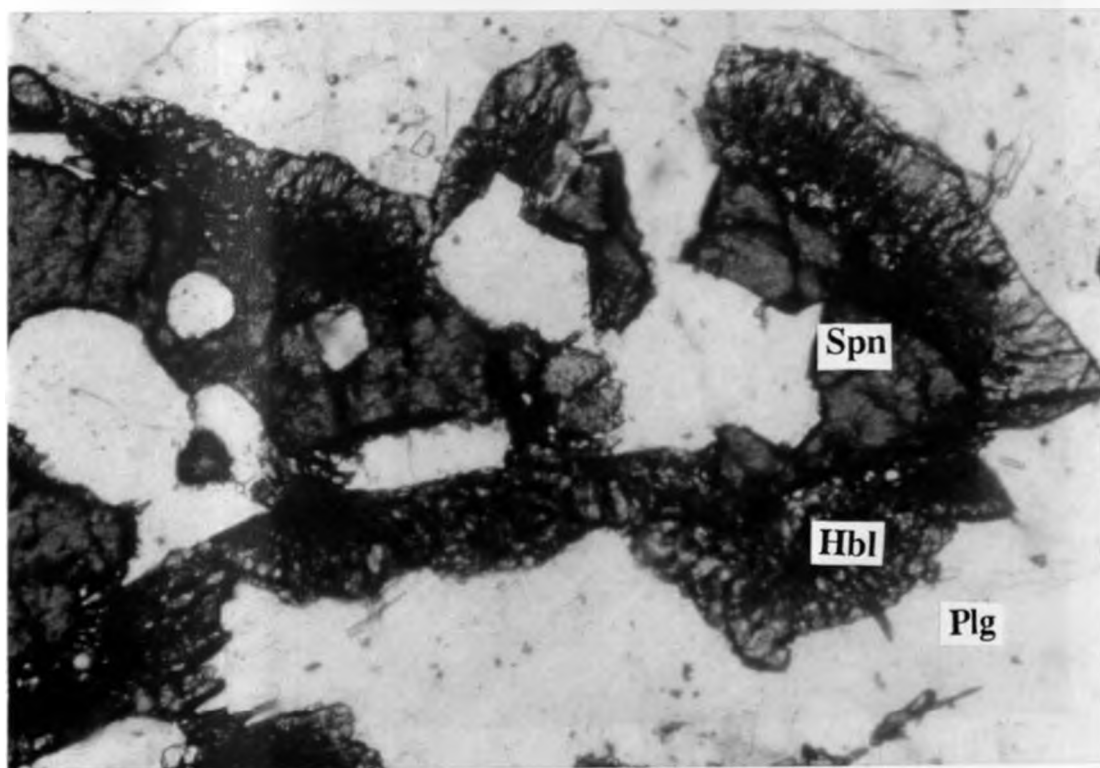


Plate 2.8. Photomicrograph of spinel-hornblende-plagioclase reaction zoning. Spinel (Spn)-hornblende (Hbl) symplectite between plagioclase (Plg). Anorthositic gabbro, (MU-34), X 100.

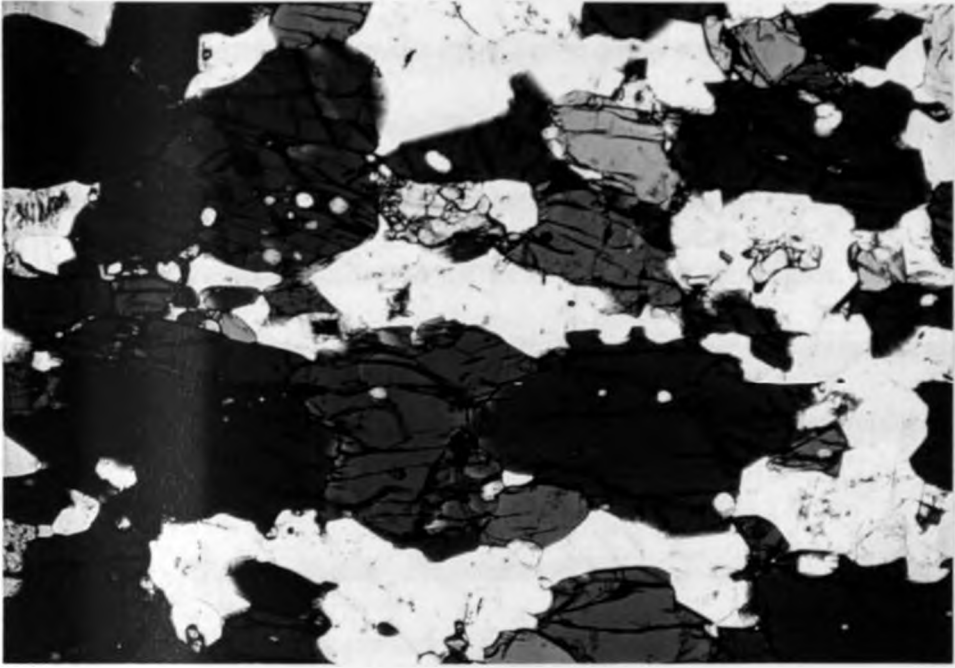


Plate 2.9. Photomicrograph of amphibole (dark green) alternating with plagioclase (light) showing lineation texture. Hornblende gneiss (MU-19), Plane Polarised light, X 50.



Plate 2.10. Field photograph of foliated biotite gneiss, Matuu-Masinga area.

In other instances, granoblastic mafic amphibolite gneiss occurs as narrow discontinuous bands and intercalations within quartzo-feldspathic gneisses. The bands probably represent metamorphosed and deformed mafic dykes. The amphibolite rocks weather to a greenish gray color and are thus readily distinguished in the field from other lithologies. Hornblende and plagioclase are the major minerals within these bands. Minor and accessory minerals are quartz, biotite, augite, hypersthene, epidote and garnet. The characteristic mineral assemblages noted in the amphibolite gneisses are:

1. *Hornblende - Epidote - Biotite - Plagioclase - Quartz +/- sphene*
2. *Hornblende - Epidote - Plagioclase - Quartz + sphene*
3. *Garnet - Hornblende - Epidote - Biotite - Plagioclase - Quartz + sphene*

Considering the presence of accessory hypersthene in this rock and its occurrence as a major mineral in the bordering meta-gabbro and dioritic rocks of the study area, it can be inferred that the metamorphic grade is that of the regional hypersthene zone. Thus it can be concluded that the hornblende-epidote-plagioclase assemblage in the present case is not that of the epidote amphibolite facies but that of the amphibolite facies. Such characteristic mineral assemblages from this area may be correlated with those from the Machakos and the Uvete areas (Biyajima et al., 1975; Nureki et al., 1977; Inoue and Suwa, 1979; Miyake and Suwa, 1981) which approximately lie in the same longitude and metamorphic isograd as the Matuu area.

2.1.1.7 Mineral chemistry of the Hornblende gneiss

The composition of the major minerals occurring in the amphibolite rocks of Matuu-Masinga area are presented in appendices 2.3, 2.4, 2.5, 2.7, 2.8 and 2.9. Representative mineral analyses are tabulated in Table 2.3

Amphibole: The composition of the amphiboles occurring in the amphibolite rocks (MU-16, MU-19) straddle between the calcic edenitic hornblende and ferroan pargasitic hornblende (Fig. 2.4) according to the nomenclature classification of Leake (1978). The hornblende exhibits the Z-axial colour of bluish green to green. The $X_{Mg} = Mg / (Mg + Fe \times 0.8)$ ratio of the primary amphiboles ranges from 0.52 - 0.56.

Plagioclase: Composition of plagioclase in the amphibolite rocks is variable and ranges from andesine (An_{38}) in sample MU-16 to bytownite (An_{75}) in sample MU-19 (Table 2.3, analysis 3 and 4). The strontium-rich plagioclase (av. Sr 5.36 wt.%, Table 2.3, analysis 4) in sample MU-19 is interpreted to be of secondary metamorphic origin, where through ionic substitution, the strontium replaced the Na cations in its crystal structure.

Comparing the plagioclase composition in the two amphibolite samples (MU-16 & MU-19), plagioclase grains occurring in sample MU-19 (Table 2.3, analysis 4) are more enriched in immobile elements (i.e SrO (av. 5.36), wt.% BaO (av. 0.11 wt.%), Cs_2O (av. 0.16 wt.%), K_2O (av. 0.16 wt.%), relative to that in sample MU-16 (i.e. SrO (av. 0.00 wt.%), BaO (av. 0.01 wt.%), Cs_2O (av.0.07 wt.%), K_2O (av. 0.09 wt.%). The relative enrichment of the these highly mobile elements (K, Ba, Sr, and Cs) in the plagioclase crystal structure in sample MU-19 compared to that in sample MU-16 (Table 2.3) suggest the plagioclase grains in sample MU-19 to have crystallized from a more fractionated magmatic source and / or metasomatic medium.

Table 2.3. Microprobe analysis of amphibole (Amp), plagioclase (Plg) and biotite (Bio) occurring in amphibolite rocks, Matuu-Masinga area, central Kenya. Analysis 1, 3-c, 3-r, and 5 from amphibolite gneiss (MU-16); analysis 2 and 4 from amphibolite gneiss (MU-19); analysis 6 from gneiss interlayer between gabbro sills, Ridnitsohkka area, Finland (Pekka, 1992 - Geol. Surv. Fin. Bull., 362). n = number of analyses.

Analysis Mineral	1 (Amp)	2 (Amp)	3-c (Plg)	3-r (Plg)	4 (Plg)	5 (Bio)	6 (Bio)
SiO ₂	41.97	41.55	59.29	59.09	56.76	35.82	35.52
TiO ₂	0.78	0.85	0.01	0.02	0.00	2.08	4.29
Al ₂ O ₃	11.36	12.37	25.54	25.70	27.13	15.77	15.43
FeO*	16.52	18.29	0.07	0.07	0.10	16.90	14.08
MnO	0.42	0.38	0.03	0.01	0.07	0.22	-
MgO	9.36	8.84	0.03	0.00	0.00	11.94	13.88
CaO	11.59	11.54	7.30	7.31	9.16	0.07	-
Na ₂ O	1.19	1.26	6.44	6.49	0.00	0.10	-
K ₂ O	1.09	1.09	0.09	0.08	0.16	9.31	10.00
Cs ₂ O	-	-	0.03	0.07	0.16	-	-
Cr ₂ O ₃	0.03	0.02	-	-	-	0.03	-
V ₂ O ₅	0.22	0.10	-	-	-	0.00	-
CoO	0.00	0.00	-	-	-	0.00	-
NiO	0.02	0.02	-	-	-	0.00	-
BaO	0.01	0.02	0.01	0.01	0.11	0.01	-
SrO	-	-	0.00	0.00	5.36	-	-
F	0.11	0.10	-	-	-	0.08	-
Cl	0.10	0.03	-	-	-	0.10	-
O=F,Cl	94.77 0.07	96.46 0.05	98.84 -	98.85 -	99.01 -	92.78 0.06	93.20 -
Total	94.70	96.41	98.84	98.85	99.01	92.72	93.20
n	3	3	3	3	3	1	1
Ox	23	23	32	32	32	22	22
Si	6.527	6.385	10.659	10.627	10.395	5.587	5.449
Al ^t	1.473	1.615	5.411	5.448	5.856	2.413	2.551
Al ^f	0.609	0.625	-	-	-	0.486	0.224
Ti	0.092	0.098	0.001	0.003	0.000	0.244	0.495
Cr	0.004	0.002	-	-	-	0.004	0.000
V	0.028	0.013	-	-	-	0.000	-
Fe	2.148	2.351	0.011	0.011	0.015	2.204	1.804
Mn	0.055	0.049	0.004	0.001	0.011	0.029	0.000
Mg	2.169	2.025	0.008	0.000	0.000	2.776	3.168
Ca	1.931	1.900	1.406	1.409	1.797	0.011	-
Na	0.359	0.375	2.244	2.263	0.000	0.030	0.000
K	0.217	0.214	0.022	0.019	0.037	1.852	1.953
Cs	-	-	0.002	0.006	0.007	-	-
Ba	0.000	0.001	0.000	0.000	0.008	0.000	-
Sr	-	-	0.000	0.000	0.569	-	-
Co	0.000	0.000	-	-	-	0.000	-
Ni	0.003	0.003	-	-	-	0.000	-
Total	15.615	15.659	19.778	19.788	18.695	15.659	15.645
An			38.29	38.17	74.78		
X _{Mg}	0.558	0.519				0.612	0.687
Mg/Fe	1.010	0.861				1.260	1.756

Index to Table 2.3

Analysis 1 and 2 - amphibole; 3c, 3-r and 4 - plagioclase; 5 and 6 - biotite.

NB. X_{Mg} = Mg/(Mg + Fe x 0.8); c-centre, r-rim; * - total iron as FeO; - not determined.

Biotite: According to Deer et al. (1967), biotite is defined as a Fe-rich mica which is arbitrarily distinguished from phlogopite in having a Mg/Fe ratio, expressed in atomic proportions, of less than two to one. The biotite in the amphibolite rock (MU-16) falls within the composition range defined by Deer et al. (1967) with Mg/Fe ratio of 1.26 and a $Mg/(Mg + Fe \times 0.8)$ ratio of 0.61 (Table 2.3, analysis 5). Its mineral composition compares rather well with the biotite reported from a similar mafic gneiss from Ridnitsohka area, Finland (Table 2.3, analysis 6) which has a Mg/Fe ratio of 1.76 and a $Mg/(Mg + Fe \times 0.8)$ ratio of 0.687. The amphibolite biotite plot in the characteristic zone of the biotites according to the discriminant diagram after Azzouni-Sekkal and Boissonnas (1987) in Fig. 2.5.

2.1.1.8 Petrography of the biotite gneiss

The biotite gneisses are the most widespread rocks in the study area. They are medium to coarse grained, mesocratic and well foliated (Plate 2.10) with colour banding or mineralogical layering of feldspar and opaque minerals. There are localized occurrence of garnet and/or sillimanite bearing biotite gneisses particularly along the shear zones. Petrographically, the rock consists of plagioclase (An_{22-30}), orthoclase, microcline, quartz, biotite, sillimanite and garnet with accessory magnetite, ilmenite and muscovite. Also noted to occur within this rock unit are amphibole-bearing mafic enclaves (disrupted dykes) which have biotite-rich margins, suggesting that small-scale mobility of alkalis and fluid phases took place during metamorphism to account for the formation of these hydroxyl-bearing minerals. The modal composition of representative biotite gneisses occurring in the study area are presented in Table 2B.

Table 2B. Modal composition of representative biotite gneisses occurring in Matuu-Masinga area, central Kenya.

Specimen No.	MU-9	MU-11	MU-18
Quartz	26.3	22.05	39.38
K-feldspar	28.7	35.24	28.34
Plagioclase	28.4	26.41	19.86
Biotite	10.2	11.79	9.21
Hornblende	2.0	-	-
Zircon	-	-	0.02
Epidote	-	0.58	1.72
Apatite	1.2	-	0.40
Sillimanite	-	1.10	-
Garnet	-	2.21	-
Opagues	3.2	0.62	1.07
Plagioclase Comp.	An ₃₀	An ₂₂	An ₂₄

2.1.1.9 Petrography and mineral chemistry of the minor mafic intrusives

(a) Syeno-diorite rock.

The rare syeno-diorite rock, which commonly occurs on the margins of the larger batholithic intrusives, was noted to be grading into the dioritic rocks of Matuu-Masinga area. Due to its nature of occurrence (i.e. limited aerial extent), this rock body was mapped under the dominant diorite rock unit. In thin section the rock consists of subhedral intermediate plagioclase (oligoclase and andesine) and orthoclase which appears to be partially replaced by albite and accompanied by greenish brown hornblende (with altered borders) and biotite. Magnetite and apatite occur as accessory minerals. The amphibole is generally brown: textural relations indicate that it is postcumulus or metamorphic. In other instances, crystals of andesine are enclosed in poikilitic plates of perthite. Plagioclase commonly shows alteration to saussurite and sericite.

The compositions and structural formulae of the major minerals occurring in the syenodiorite rock are presented in Table 2.4. The alkali feldspar has a high orthoclase (Or₉₆) composition with an average BaO content of 0.99 wt.%. Plagioclase has an average composition of approximately An₄₉. Although alteration precluded the study of plagioclase compositional zoning in various samples, in samples where this investigation was possible such zoning is generally absent. However, two samples show grain margins that are enriched in the anorthite component by approximately 2 to 4 percent. Significant strontium (av. 7.75 wt.% SrO) is present in all analyzed plagioclase. A stoichiometric analysis suggests that the Sr is substituting for Na.

All the amphibole analyses are principally ferroan pargasitic hornblende (Fig. 2.4). The iron enrichment trend of the amphibole parallels that of the associated biotite (Table 2.4, analysis 3 & 4), but the amphibole has a lower $X_{Mg} = (Mg/Mg + Fe \times 0.8)$ ratio. TiO₂ is relatively high (1.25 - 1.39 per cent, Table 2.4 & appendix 2.4) but below the value suggested by Leake (1968) (>0.25 Ti ions per 23 oxygens) to be called titaniferous pargasite.

(b) Mafic granulite (plagioclase-pyroxene-garnet) gneiss.

These were minor but widespread granulite mafic bodies that were noted to occur as competent tectonised enclaves within quartzo-feldspathic gneisses. Petrographically, these bodies essentially consist of clinopyroxene, plagioclase (An₉₀) and garnet. Epidote, sphene and quartz occur as accessory minerals. A microphotograph presented in Plate 2.11 (a) & (b) illustrates its characteristic textural and mineralogical composition. Representative probe analyses of its constituent minerals are presented in Table 2.5.

Table 2.4. Mean microprobe analyses of K-feldspar (Kfd), plagioclase (Plg), amphibole (Amp) and biotite (Bio) from syeno-diorite rock, Matuu-Masinga area, central Kenya. (Analyst Bo Johanson). n = number of analysis.

Analysis	1	2	3	4
Mineral	Kfd	Plg	Amp	Bio
SiO ₂	63.89	62.85	41.26	36.62
TiO ₂	0.00	0.01	1.33	3.01
Al ₂ O ₃	18.76	23.22	10.10	13.79
FeO ⁺	0.04	0.06	20.83	20.54
MnO	0.03	0.01	0.58	0.29
MgO	0.01	0.00	8.08	10.96
CaO	0.02	4.52	10.74	0.03
Na ₂ O	0.41	0.16	1.55	0.06
K ₂ O	14.24	0.20	1.61	9.57
Cr ₂ O ₃	-	-	0.02	0.02
V ₂ O ₃	-	-	0.08	0.07
CoO	-	-	0.00	0.00
NiO	-	-	0.03	0.00
BaO	0.99	0.05	0.02	0.02
SrO	0.15	7.75	-	-
Cs ₂ O	0.00	0.01	-	-
F	-	-	0.37	0.75
Cl	-	-	0.19	0.20
O=F,Cl	99.54	98.84	96.79	95.93
	-	-	0.20	0.36
Total	99.54	98.84	96.59	95.57
n	3	7	8	4
Ox	32	32	23	22
Si	11.916	11.375	6.444	5.611
Al ⁴	4.084	4.625	1.556	2.389
Al ⁶	0.038	0.338	0.304	0.100
Ti	0.000	0.001	0.156	0.347
Cr	-	-	0.002	0.002
V	-	-	0.009	0.009
Fe	0.007	0.009	2.721	2.633
Mn	0.005	0.001	0.077	0.038
Mg	0.002	0.000	1.881	2.504
Ca	0.005	0.878	1.797	0.005
Na	0.148	0.057	0.469	0.017
K	3.389	0.046	0.321	1.871
Ba	0.073	0.003	0.001	0.001
Sr	0.124	0.817	-	-
Ni	-	-	0.004	0.000
Cs	0.000	0.000	-	-
Total	19.791	18.150	15.742	15.527
Or	95.68	2.56		
Ab	4.18	48.61		
An	0.14	48.83		
Xmg			0.464	0.543
Mg/Fe			0.691	0.951

Index to Table 2.4

Analysis: 1- K-feldspar, 2- plagioclase, 3- amphibole, 4- biotite from syeno-diorite (MU-10).

NB. Xmg = Mg/(Mg+Fe x 0.8); FeO⁺ = total iron as FeO; - not determined.

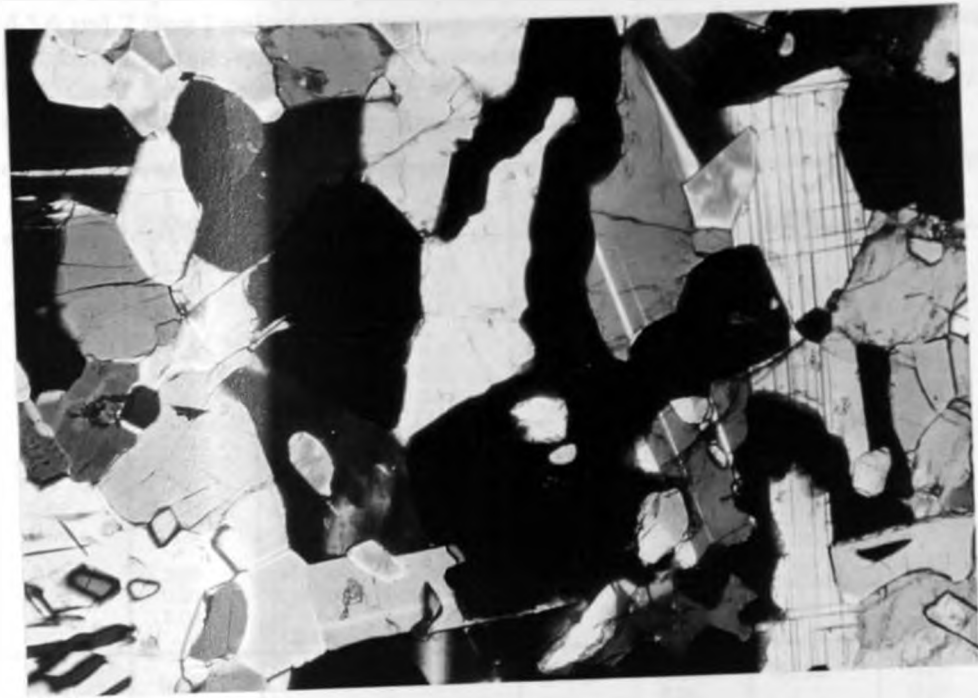


Plate 2.11. (a) Photomicrograph of mafic granulite showing recrystallized garnet (dark) traversing plagioclase and in contact with pyroxene and epidote. Mafic granulite (MU-23), Crossed polars, X 50.

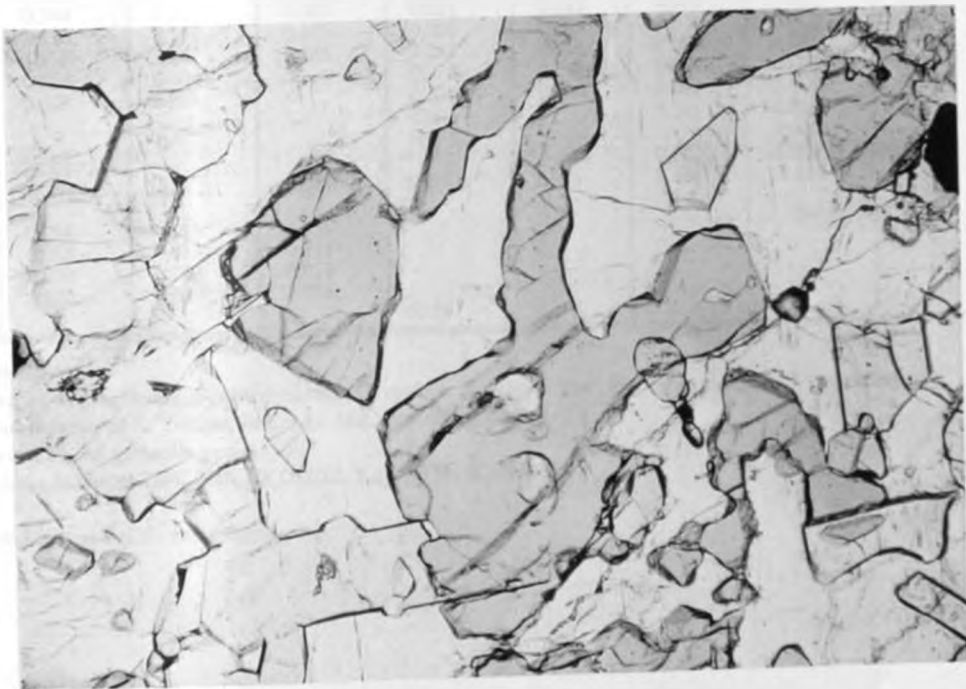


Plate 2.11. (b) Photomicrograph of mafic granulite showing garnet (light brown) in contact with plagioclase. Plane polarised light, X 50.

Table 2.5. Electron microprobe analysis of garnet (Grt), plagioclase (Plg), clinopyroxene (Cpx) and sphene (Spn). Analysis 1,2,4,5,6 and 7 from Plagioclase-pyroxene-garnet granulite gneiss (MU-23), Matuu-Masinga area, central Kenya; 3- garnet: from Anorthite-clinozoisite-corundum-garnet gneiss, Sittampundi complex, Madras (Subramanica, A.P., 1956, Bull. Geol. Soc. Amer., 67, p 317); 8- sphene: from beach sand, Waimu inlet, N.W. Nelson, New Zealand (Hutton, C.O., 1950, Bull. Geol. Soc. Amer., vol 61, p 635).

Analysis Mineral	1 (Grt)	2 (Grt)	3 (Grt)	4 (Plg)	5 (Cpx)	6 (Epd)	7 (Spn)	8 (Spn)
SiO ₂	37.58	36.26	38.69	45.28	47.95	37.24	31.98	30.35
TiO ₂	0.36	0.56	0.55	0.01	0.38	0.16	35.53	35.44
Al ₂ O ₃	16.19	10.69	18.17	34.64	4.71	23.55	1.47	2.15
Fe ₂ O ₃	9.72	-	5.70	-	5.45	-	-	2.50
FeO	4.26	18.43	3.78	0.17	7.79	12.47	1.01	-
MnO	2.59	1.02	0.64	0.01	0.69	0.03	0.03	0.25
MgO	0.51	0.45	0.76	0.00	9.10	0.00	0.00	0.10
CaO	29.18	28.95	31.76	17.84	23.74	22.92	28.44	26.46
Na ₂ O	0.01	0.01	-	1.05	0.56	0.01	0.01	-
K ₂ O	0.01	0.02	-	0.04	0.01	0.02	0.00	0.02
BaO	-	0.00	-	0.05	-	0.03	0.32	0.00
Cr ₂ O ₃	0.02	0.00	-	-	0.02	0.00	0.00	-
V ₂ O ₅	0.04	0.00	-	-	-	0.04	0.00	-
Cs ₂ O	-	-	-	0.05	-	-	0.00	-
NiO	0.01	0.00	-	-	-	0.02	0.01	-
F	0.38	0.20	-	-	-	0.37	0.00	0.67
Cl	0.01	0.00	-	-	-	0.00	0.00	-
H ₂ O	-	-	0.19	-	-	-	-	1.10
O=F,Cl	100.87 0.16	96.52 0.08	100.24 -	99.14 -	100.40 -	96.86 0.16	98.82 -	99.04 0.28
Total	100.71	96.44	100.24	99.14	100.40	96.70	98.82	98.76
n	2	2	1	2	2	2	1	1
Ox	24	24	24	32	6	13	20	20
Si	5.890	6.191	5.966	8.418	1.826	3.185	4.188	3.936
Al ⁴	0.110	-	0.034	7.588	0.174	-	0.230	0.329
Al ⁶	2.882	2.151	3.268	-	0.037	2.373	-	-
Fe ³	1.134	-	0.662	-	0.156	-	-	0.245
Ti	0.042	0.072	0.064	0.001	0.011	0.010	3.548	3.457
Cr	0.002	-	-	-	0.000	0.000	0.000	-
V	0.006	-	-	-	-	0.001	0.000	-
Fe ²	0.558	2.632	0.487	0.027	0.248	0.892	0.113	-
Mn	0.344	0.148	0.083	0.001	0.022	0.002	0.003	0.027
Mg	0.118	0.113	0.175	0.000	0.515	0.000	0.000	0.020
Ca	4.900	5.297	5.248	3.553	0.968	2.100	4.046	3.677
Na	0.004	0.004	-	0.378	0.041	0.001	0.003	-
K	0.002	0.004	-	0.009	0.000	0.001	0.000	0.003
Ba	-	-	-	0.003	-	0.001	0.017	0.000
Cs	-	-	-	0.004	-	-	0.000	-
Ni	0.001	-	-	-	-	0.002	0.001	-
Total	15.993	16.612	15.980	19.982	3.998	8.668	12.153	11.674
Alm	0.094	0.321	0.081	-	-	-	-	-
Sps	0.058	0.018	0.041	-	-	-	-	-
Fsp	0.020	0.014	0.029	-	-	-	-	-
Grs	0.820	0.647	0.876	-	-	-	-	-
An	-	-	-	90.38	-	-	-	-

Index to Table 2.5.

Analysis 1- Garnet, 4- plagioclase, 5- clinopyroxene, 6- epidote, 7- sphene (analyst: B. Johanson, Geol. Surv. Finland).

Analysis 2- Garnet (analyst: S. Yorkou, Inst. Adv. Mat. Processing, Japan).

Analysis 3- Brownish red grossular garnet.

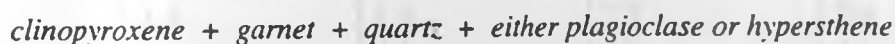
Analysis 8- sphene (includes ThO₂ 0.28, Ce₂O₃ 0.03, La₂O₃ 0.85, Y₂O₃ 0.18).

NB. FeO* = total iron as FeO; - not determined.

The Matuu granulite enclaves are characterized by the high grade clinopyroxene-plagioclase-garnet mineral assemblage that have subsequently been retrogressed as evidenced by the presence of epidote and sphene (Table 2.5, analysis 6 & 7). Epidote, besides being a characteristic mineral of metasomatic rocks, it is considered to be a stress mineral, its formation being favoured by shearing stress and low temperatures (Deer et al., 1963). Its presence in the Matuu tectonised mafic enclaves is in conformity with the interpretation of Deer et al. (op.cit) and concurs with the observed field relations. According to the petrographic observations of De Waard in Winkler (1979), the assemblage orthopyroxene + plagioclase becomes unstable if load pressure exceeds a particular value at constant temperature. The two minerals react to produce clinopyroxene + (almandine-pyrope-grossularite) garnet + quartz as illustrated below:



The previous reaction, which is continuous over a certain range of physical conditions, may have both the reactants and products coexisting during a transitional stage. Eventually, with gradual increase of metamorphism, the new mineral assemblages:



becomes stable phases. The Matuu mafic granulite enclaves, which show a dominance of the stable clinopyroxene-plagioclase-garnet mineral assemblage, represent the higher pressure clinopyroxene-almandine-quartz granulite subzone of the regional hypersthene zone.

It is worth noting that in mafic rocks, as in the present case, the grossularite content of almandine-rich garnets is consistently high, ranging between 65 - 82 molecular per cent (Table 2.5, analysis 1 & 2). The widespread occurrence of garnets in Matuu-Masinga area, particularly

along the shear zones (see Fig. 1.2), calls for a detailed study to evaluate their economic potential. A review paper on the geology of the Mozambique belt in Kenya (Nyamai et al., 1993), has outlined the occurrence of garnets and related gemstones in the belt.

2.1.2 The Granitic Rocks

Granitic plutons in the study area are represented by the granitoid gneisses and granites, which as a whole, cover aerially about 30 % of the total survey area (Fig. 1.2). Their relative voluminous occurrence in this area demonstrate the importance of crustal accretion (or anatexis) during the Mozambiquan orogeny as demonstrated earlier by Suwa et al. (1979) in Machakos area, central Kenya. The modal analyses of representative granitic rocks from the study area are presented in Table 2C.

Table 2C. Modal composition of representative granitic rock samples from Matuu-Masinga area, central Kenya.

Specimen No.	MU-6A	MU-8	MU-12	MU-29
Quartz	20.5	25.3	30.6	25.3
K-feldspar	44.3	50.5	38.6	36.2
Plagioclase	24.3	18.5	23.7	27.4
Biotite	4.9	1.9	2.7	2.4
Hornblende	1.6	2.1	2.2	4.1
Zircon	0.4	0.7	0.1	0.2
Epidote	0.7	-	0.2	0.6
Apatite	1.0	0.1	0.6	1.5
Sphene	-	-	0.4	0.5
Chlorite	0.6	0.4	-	1.2
Opagues	1.7	0.5	0.8	0.4
Plagioclase Comp.	An ₂₈	An ₂₄	An ₂₃	An ₂₈

Index to Table 2C.

MU-6A : Coarse grained grey granite.

MU-8 : Coarse grained pink granite.

MU-12 : Coarse grained granitoid gneiss.

MU-29 : Coarse grained porphyritic granite.

2.1.2.1 Petrography of the granitoid gneiss

In outcrop, the granitoid gneiss is an equigranular, medium to coarse grained rock with faint foliation nature. It consists essentially of quartz, microcline, plagioclase (An_{23}), biotite, and sometimes muscovite and pargasitic amphibole, with minor amounts of apatite, epidote, sphene, zircon and iron ore minerals (see Table 2C for modal analysis). Antiperthite and perthite textures are common. According to Edelman (1985), most granitoid rocks were formed through a number of processes, such as metamorphism, metasomatism, anatexis and/or intrusion.

2.1.2.2 Petrography of the porphyritic granite

Coarse grained porphyritic granite (e.g. sample MU-29) is common and form most of the topographic hills south-east of the survey area. In particular the porphyritic granite unit (Plate 2.12) bordering south of Matuu town (Fig. 1.2) is coarse grained and consists of potassium-feldspar porphyroblasts (Plate 2.13) studded in a medium grained matrix of quartz, plagioclase (An_{28}), microcline, hornblende, biotite, epidote and muscovite with minor amounts of apatite, sphene, zircon, calcite and iron ores. Grain size of the phenocryst ranges from 0.5 cm to 1.5 cm. Mesoperthite phenocryst is commonly mantled with a cloudy albite. Hornblende is subhedral, prismatic, and strongly pleochroic (X = light greenish yellow, Y = olive green, Z = bluish green). Aggregate of flaky biotite with epidote sometimes replaces the hornblende.

2.1.2.3 Petrography of the pink granite

On the other hand, at Ndalani area, a different intrusion of a medium to coarse grained, pink colored alkali granite (MU-8), currently being mined as a dimension stone by Athi River mining company, was noted to contain mainly microcline, plagioclase (An_{36}) and quartz (Plate

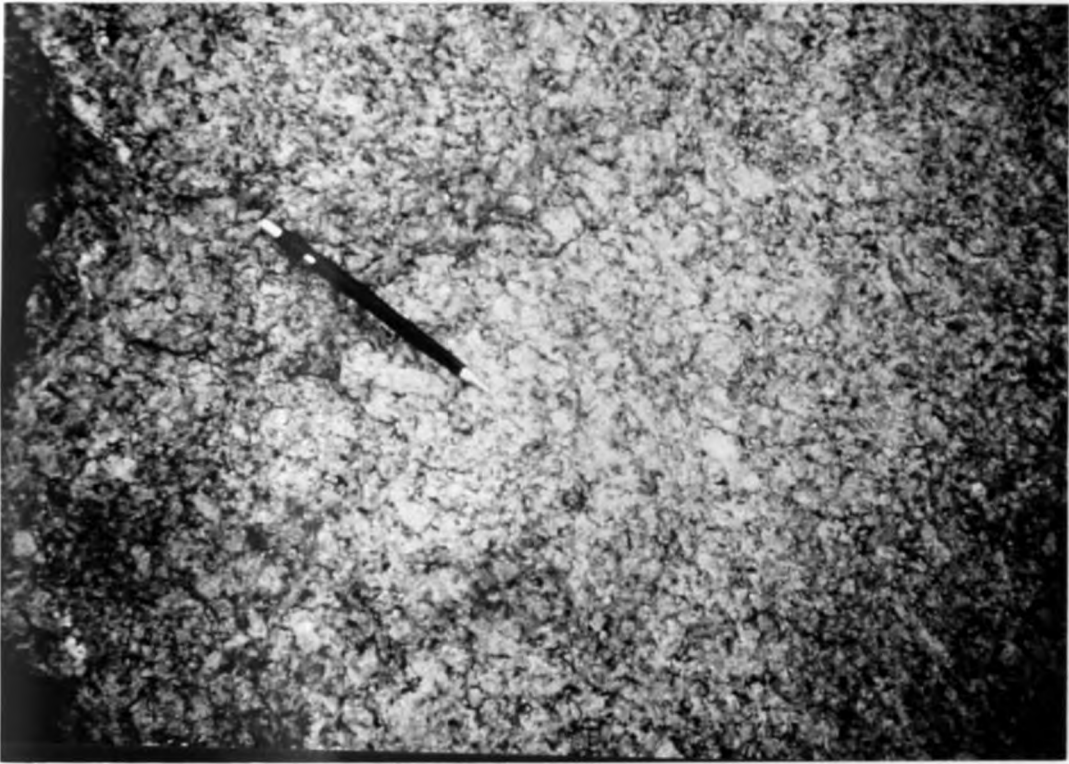


Plate 2.12. Field photograph of outcrops of Matuu area porphyritic granite.



Plate 2.13 Photomicrograph of microcline (Mce) porphyroblast with exsolved plagioclase (Plg) and in contact with quartz (Qtz). Porphyritic granite (MU-29), Crossed polars, X 50.

2.1.4). Accessories are biotite, apatite, sphene, zircon and iron oxides. This rock exhibits an equigranular texture with a grain size of less than 5 mm. Anhedral to subhedral crystals of perthite, quartz and plagioclase occupy large volume of the rock. Biotite flakes commonly makes an intergrowth with chlorite. A comparative diffraction pattern between the pink and porphyritic granite is presented in Fig. 2.7. The X-ray pattern of the bulk groundmass gives characteristic peaks of microcline, a strong reflection at 3.29 Å being recognized as the (220) reflection, and also peaks at 3.24, 3.35 and 6.49 Å corresponding to the reflection of (040), (220) and (020) respectively. The groundmass of both granitic rocks contains small grains of quartz and biotite with strong reflection at 3.34 and 10.1 Å respectively.

2.1.2.4 Petrography of the grey granite

The grey granite (MU-6) constitutes mainly the Mavoloni and Nzukini the Needles hills in the north-western part of the survey area. It is an equigranular rock with a grain size of 2 mm to 7 mm. It consists essentially of K-feldspar, plagioclase (An₂₃), mesoperthite and quartz with minor amphibole and biotite. Allanite, apatite, zircon and iron oxides are also contained as accessories. K-feldspar is mainly microcline as shown by XRD identification. Mesoperthite and quartz are subhedral to anhedral and the mesoperthite crystal is often surrounded by grains of microcline and quartz. Plagioclase occurs mainly as exsolution lamella in the mesoperthite. The amphibole, which exhibits a strong pleochroism (X = pale green, Y = grayish green, Z = bluish green) and an abnormal interference color, is partly altered to carbonate minerals. Small flakes of biotite occur around the amphibole, along the grain boundary and along the shear plane. The biotite is pleochroic with X = pale brownish yellow, Y = Z dark brown.

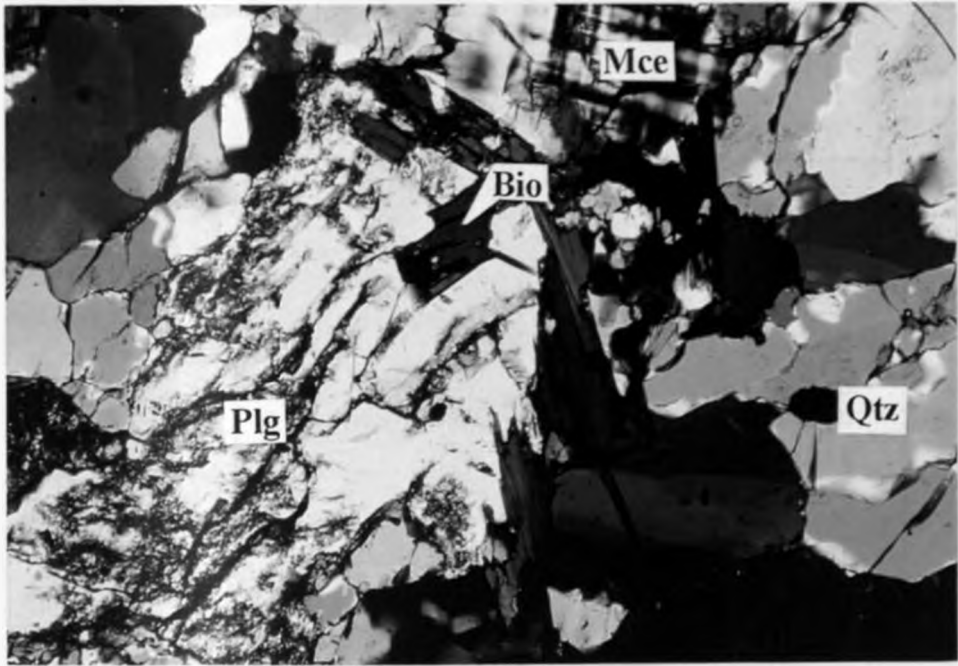


Plate 2.14 Photomicrograph of partially sericitized plagioclase (Plg), biotite (Bio), microcline (Mce) and quartz (Qtz). Pink alkali granite (MU-8), Crossed polars, X 50.

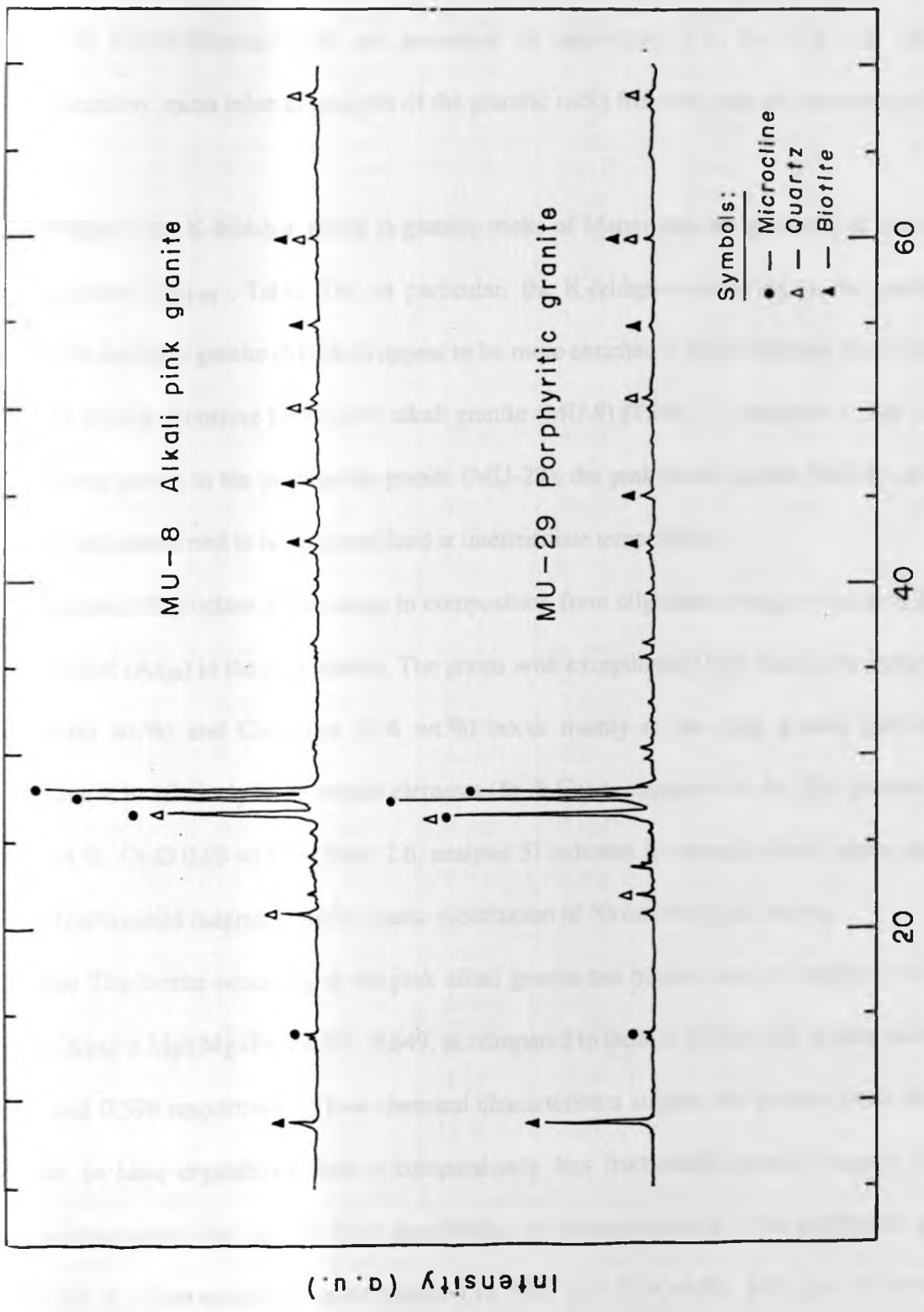


Fig. 2.7. Comparative diffraction pattern between alkali pink granite and porphyritic granite, Matuu-Masinga area, central Kenya.

2.1.2.5 Mineral chemistry of the granitic rocks

Full microprobe analyses of the main minerals occurring in the representative granitic rocks of Matuu-Masinga area are presented in appendices 2.3, 2.4, 2.5, 2.6 and 2.9. Representative mean mineral analyses of the granitic rocks from the area are presented in Table 2.6.

K-feldspar: The K-feldspar grains in granitic rocks of Matuu area are generally of microcline composition (Or_{90-95} , Table 2.6). In particular, the K-feldspars occurring in the porphyritic (MU-29) and grey granite (MU-6A) appear to be more enriched in BaO, SrO and Cs_2O contents relative to that occurring in the pink alkali granite (MU-8) (Table 2.6, analysis 1, 2 & 3). The K-feldspar grains in the porphyritic granite (MU-29), the pink alkali granite (MU-8) and grey granite are interpreted to have crystallized at intermediate temperatures.

Plagioclase: Plagioclase grains range in composition from oligoclase (An_{23}) in the grey granite to andesitic (An_{36}) in the pink granite. The grains with exceptionally high strontium content SrO (av. 8.60 wt.%) and Cs_2O (av. 0.08 wt.%) occur mainly in the pink granite (MU-8). Its enrichment in relatively large mobile elements (Sr & Cs) as compared to the grey granite - SrO 0.00 wt.%, Cs_2O 0.03 wt.% - (Table 2.6, analysis 5) indicates its crystallization from a possibly more fractionated magma or metasomatic substitution of Na cations by Sr cations.

Biotite: The biotite occurring in the pink alkali granite has higher ratios of Mg/Fe (1.48) and X_{mg} ($X_{mg} = Mg/(Mg+Fe \times 0.8)$) - 0.649, as compared to those in porphyritic granite which are 1.19 and 0.598 respectively. These chemical characteristics suggest the biotites from the pink granite to have crystallized from a comparatively less fractionated granitic magma to that making the porphyritic granite. More specifically, the biotite occurring in the porphyritic granite (MU-29) is characteristically more enriched in TiO_2 (av. 3.14 wt.%), FeO (av. 18.32 wt.%).

Table 2.6. Microprobe analyses of K-feldspar (Kfd), plagioclase (Plg) biotite (Bio), amphibole (Amp) and chlorite (Chl) occurring in granitic rocks of Matuu-Masinga area, central Kenya. Analysis 1, 6, and 8 from porphyritic granite (MU-29); 2, 4, 7 and 9 from pink alkali granite (MU-8); 3 and 5 from grey alkali granite (MU-6A). n = number of analyses.

Analysis Mineral	1 Kfd	2 Kfd	3 Kfd	4 Plg	5 Plg	6 Bio	7 Bio	8 Amp	9 (Chl)
SiO ₂	64.44	64.78	64.43	65.07	63.36	36.65	38.08	41.65	28.57
TiO ₂	0.00	0.03	0.01	0.00	0.02	3.14	2.13	1.52	0.05
Al ₂ O ₃	18.72	18.35	18.57	21.75	23.26	13.80	14.26	10.52	16.62
FeO*	0.07	0.07	0.03	0.10	0.09	18.32	16.31	19.21	33.93
MnO	0.00	0.01	0.01	0.02	0.04	0.36	0.21	0.61	0.08
MgO	0.01	0.02	0.01	0.00	0.00	12.26	13.57	8.93	7.36
CaO	0.01	0.01	0.00	2.92	4.35	0.00	0.01	10.86	0.19
Na ₂ O	0.32	0.35	1.11	0.21	8.12	0.05	0.06	1.58	0.06
K ₂ O	14.74	15.35	14.41	0.17	0.18	9.65	9.81	1.54	0.12
BaO	0.46	0.29	0.68	0.03	0.01	0.14	0.06	0.00	0.02
SrO	1.03	0.65	0.00	8.60	0.00	-	-	-	-
Cs ₂ O	0.09	0.00	0.09	0.08	0.03	-	-	-	-
Cr ₂ O ₃	-	-	-	-	-	0.02	0.01	0.04	0.01
V ₂ O ₃	-	-	-	-	-	0.26	0.17	0.07	0.06
F	-	-	-	-	-	0.91	1.12	0.24	0.09
Cl	-	-	-	-	-	0.15	0.07	0.15	0.01
O= F,Cl	99.89	99.91	99.35	98.95	99.36	95.71	95.90	96.79	87.19
	-	-	-	-	-	0.42	0.49	0.13	0.04
Total	99.89	99.91	99.35	98.95	99.36	95.29	95.41	96.79	87.15
n	4	4	3	2	2	2	2	2	7
Ox	32	32	32	32	32	22	22	23	28
Si	11.949	11.998	11.965	11.754	11.223	5.642	5.769	6.456	6.319
Al ⁴	4.051	4.002	4.035	4.246	4.777	2.358	2.231	1.544	1.681
Al ⁶	0.040	0.004	0.029	0.384	0.079	0.147	0.316	0.378	2.651
Ti	0.000	0.005	0.001	0.000	0.003	0.364	0.243	0.177	0.008
Fe	0.011	0.011	0.005	0.015	0.014	2.359	2.066	2.491	6.275
Cr	-	-	-	-	-	0.002	0.002	0.006	0.003
V	-	-	-	-	-	0.032	0.020	0.009	0.011
Mn	0.000	0.001	0.001	0.003	0.006	0.047	0.026	0.080	0.146
Mg	0.003	0.006	0.003	0.000	0.000	2.813	3.064	2.063	2.427
Ca	0.002	0.002	0.000	0.565	0.826	0.000	0.002	1.804	0.044
Na	0.116	0.125	0.399	0.074	2.787	0.015	0.018	0.475	0.024
K	3.487	3.625	3.415	0.039	0.040	1.894	1.895	0.305	0.035
Ba	0.033	0.021	0.049	0.002	0.001	0.008	0.004	-	0.001
Sr	0.111	0.070	0.000	0.901	0.000	-	-	-	-
Cs	0.007	0.000	0.013	0.006	0.004	-	-	-	-
Total	19.810	19.870	19.915	17.989	19.760	15.681	15.658	15.788	19.625
Or	93.84	94.85	89.54	2.47	1.09				
Ab	6.10	5.10	10.46	61.75	76.29				
An	0.05	0.05	0.00	35.78	22.61				
X _{mg}						0.598	0.649	0.509	0.326
Mg/Fe						1.192	1.483	0.828	0.387

Index to Table 2.6

Analysis 1, 2 and 3 - K-feldspar; 4 - strontium-rich plagioclase, 5-plagioclase; 6 and 7 - biotite; 8- amphibole; 9- chlorite.

NB. X_{mg} = Mg/(Mg + Fe x 0.8); FeO* - total iron as FeO; - not determined.

MnO (av. 0.36 wt.%), BaO (av. 0.14 wt.%), and V₂O₃ (av. 0.26 wt.%) (Table 2.6, analysis 6) relative to that occurring in the pink granite (MU-8) with TiO₂ (av. 2.13 wt.%), FeO (av. 16.31 wt.%), MnO (av. 0.21 wt.%), BaO (av. 0.06 wt.%), and V₂O₃ (av. 0.17 wt.%) (Table 2.6, analysis 7). The relative enrichment of mobile elements in the biotites of the porphyritic granite further suggests their crystallization from a more fractionated magma. The granitic biotites plot in the characteristic zone of the biotites according to the discriminant diagram after Azzouni-Sekkal and Boissonnas (1987) in Fig. 2.5.

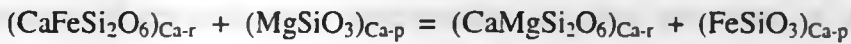
Amphibole: The amphibole occurring in the porphyritic granite (Table 2.6, analysis 8) with X_{mg} (X_{mg} = Mg/Mg + Fe x 0.8) value of 0.509 is ferroan pargasitic hornblende in composition (Fig. 2.4) according to the classification of Leake (1978).

Sample	Chemical composition				Elementary analysis			Sp
	Ca	Mg	Al ^{IV}	Ti ^{IV}	Mn	Fe ²⁺	Fe ³⁺	
101-1	0.00	0.00	0.00	0.00	0.00	0.00	0.00	1.00
101-2	0.00	0.00	0.00	0.00	0.00	0.00	0.00	1.00
101-3	0.00	0.00	0.00	0.00	0.00	0.00	0.00	1.00
101-4	0.00	0.00	0.00	0.00	0.00	0.00	0.00	1.00
101-5	0.00	0.00	0.00	0.00	0.00	0.00	0.00	1.00
101-6	0.00	0.00	0.00	0.00	0.00	0.00	0.00	1.00
101-7	0.00	0.00	0.00	0.00	0.00	0.00	0.00	1.00
101-8	0.00	0.00	0.00	0.00	0.00	0.00	0.00	1.00

2.2 ESTIMATIONS OF THE METAMORPHIC CONDITIONS

2.2.1 Conditions of pyroxene crystallization

Studies of the magnesium / iron distribution between coexisting minerals of ultramafic nodules has been used as a measure of the temperature of crystallization for the ferromagnesian phases. Kretz (1961) has examined this method on a thermodynamic basis with chemical equilibrium between calcium-rich (Ca-r) and calcium poor (Ca-p) pyroxene expressed as:



Average values for an equilibrium constant, $K_p(T)$, of this reaction for igneous and metamorphic pyroxenes are respectively 1.4 and 1.8, and a K_p value of 1.6 occurs only rarely (Kretz, 1963)). Ratios of $\text{Fe}^{2+}:\text{Mg}$ in seven coexisting pyroxene pairs from Matuu-Masinga mafic rocks are given in Table 2.7.

Table 2.7. K_p values for seven co-existing pyroxene pairs from Matuu-Masinga mafic rocks. Compositions determined by microprobe analysis.

Sample no.	Clinopyroxene				Orthopyroxene			K_p
	Ca	Mg	Fe^{2+}	Fe^{2+}/Mg	Mg	Fe^{2+}	Fe^{2+}/Mg	
MU-7	44.14	38.06	17.80	0.47	61.13	38.87	0.64	1.36
MU-7	42.80	38.28	18.82	0.49	59.77	40.23	0.67	1.37
MU-7	43.78	38.42	17.80	0.46	60.24	39.76	0.66	1.43
MU-28	42.00	41.56	16.44	0.39	60.41	39.59	0.66	1.69
MU-28	46.95	39.22	13.83	0.35	60.18	39.82	0.66	1.88
MU-28	44.06	39.12	16.82	0.43	60.18	39.82	0.66	1.54
MU-5	42.95	39.89	17.16	0.43	62.13	37.87	0.61	1.42

NB. MU-7 - Meta diorite rock; MU-28, MU-5 - Gabbroic rocks.

The range in K_p for the meta diorite rock MU-7 range from 1.36 - 1.43 with an average of 1.39. Since the equilibrium constant decreases with increasing temperature, the notably low K_p values of the meta diorite pyroxenes correspond to those of igneous in origin, and points to a higher temperature than that required by the K_p values for other pyroxenes of similar bulk composition of metamorphic origin.

On the other hand, the K_p values of the gabbroic rock (MU-28) range from 1.54 to 1.88 with an average of 1.7. The notably high values of K_p in the gabbroic rock point to a lower temperature of crystallization, corresponding to other pyroxenes of similar bulk composition of metamorphic origin (Kretz, 1963). Comparatively, the relatively low K_p values of the pyroxenes in the gabbroic rock MU-5 (i.e 1.43) point to a higher temperature corresponding to those of magmatic origin.

2.2.2 Thermobarometric conditions of formation of the mafic rocks

There is now an abundance of thermobarometric calibrations applicable to mafic and ultramafic rocks. The P/T conditions of mafic rocks have added advantage in that they can elucidate the predominant P/T conditions of the initial metamorphic stages of an orogeny (Brodie and Rutter, 1985). Different calibrations of clinopyroxene-orthopyroxene, garnet-clinopyroxene, and amphibole-plagioclase were used as thermometers. The garnet-orthopyroxene, clinopyroxene-plagioclase-quartz, garnet-clinopyroxene and Al in amphibole calibrations were used as barometers.

In this study, geothermometric and geobarometric methods based on the composition of co-existing minerals were used to estimate the conditions of metamorphism of the rocks in Matuu-Masinga area. The thin sections of the analyzed samples were examined for any sign

of disequilibrium such as mineral zonation, symplectites, coronas, exsolution or obvious alteration. The mineral homogeneity was carefully examined by analyzing at least three grains of one mineral. It is important to note that careful textural analysis and sufficient analytical data from a single thin section is necessary to obtain meaningful results. Minor heterogeneity of minerals noted in Matuu-Masinga rock samples could variably be attributed to simple retrograde cation exchange during cooling or paragenetic changes during cooling which produces a variety of exsolution textures in pyroxenes and ilmenite, and growth of retrograde minerals. Table 2.8 gives a summary of the thermobarometric data obtained for rocks from the Matuu-Masinga study area.

2.2.2.1 Amphibolitic rocks

Using the Al-in-amphibole geobarometer method after Hollister et al. (1987) and that of Hammarstrom and Zen (1986), the Matuu amphibolite (MU-16) yields a pressure of 6.98 +/- 1 and 6.55 kbars respectively. Using the amphibole-plagioclase geothermometer after Blundy and Holland (1990), the same specimen (MU-16) yields a temperature of 750 °C (using analysis 1 and 3-r in Table 2.3). For amphibolite sample MU-19, the equilibrium pressure was estimated at 6.55 kbars (using analysis 2 & 4 in Table 2.3), by applying the Al-in-amphibole geobarometer experimental calibrations after Johnson and Rutherford (1989).

2.2.2.2 The gabbroic and meta-dioritic rocks.

(a) Gabbroic rocks

The equilibrium temperature for the coarse grained gabbro rock MU-28 range from 904 +/- 15 °C (for mineral core composition: Table 2.2. analysis 3-c & 1-c) to 719 +/- 15 °C

Table 2.8. Thermobarometric data for rocks from Matuu-Masinga area, central Kenya. c-ore, r-rim, T: orthopyroxene-clinopyroxene (Brey and Kohler, 1990); Amphibole-plagioclase (Blundy and Holland, 1990); Garnet-Clinopyroxene (Krogh, 1988; Pattison and Newton, 1989) and Al-in-Amphibole (Blundy and Holland, 1990). P:clinopyroxene-plagioclase-quartz (Ellis, 1980); Al-in-Amphibole (Hammarstrom and Zen, 1986; Johnson and Rutherford, 1989; Hollister et al., 1987) and Garnet-clinopyroxene-plagioclase-quartz (Eckert et al., 1991; Powell and Holland, 1988).

ROCK TYPE	THERMOMETER	T(°C)	BAROMETER	P (kbars)
Diorite	Opx-Cpx	854(c) - 843(r)	Cpx-Plg-Qtz	15.01
Gabbro - 1	Opx-Cpx	904 +/- 15(c)	Cpx-Plg-Qtz	5.89 - 6.31
Gabbro - 2	Opx-Cpx	879 +/- 15(c)	-	-
Amphibolite - 1	Amp-plg	750	Al-in-amphibole	6.55 - 6.98 +/- 1
Amphibolite - 2	-	-	Al-in-amphibole	6.55
Mafic granulite	Grt-Cpx	603	Grt-Cpx-Plg-Qtz	6.95 - 7.12 +/- 1.9
Granite	Al-in-Amphibole	750	Al-in amphibole	5.7 - 6.14

for mineral rim composition, Table 4, analysis 3-r & 1-r) according to the miscibility gap and the distribution of Ca and Na between both pyroxenes (Brey and Kohler, 1990). Using the obtained temperature, the equilibrium pressure is estimated between 5.89 and 6.31 kbar using the clinopyroxene-plagioclase-quartz (cpx-plg-qtz) geobarometer after Ellis (1980). The temperature and pressure is in good agreement with those estimated by the enstatite - diopside solvus and the Al_2O_3 content in the orthopyroxene (Mori and Green, 1976), and correspond to granulite facies metamorphism and a depth of about 20 km. Using the orthopyroxene and clinopyroxene mineral compositions from the fine grained gabbro rock MU-5 (Table 2.2, analysis 11 & 12), the sample gives an equilibrium temperature of 879 ± 15 °C using the mixed calibration by Brey and Kohler (1990).

(b) Dioritic rock

Using the same Opx-Cpx geothermometer by Brey and Kohler (1990), the Matuu meta-diorite rock, MU-7, gave an equilibrium temperature ranging from 854 °C (for mineral rim composition: Table 2.2, analysis 1-r & 3-r) to 843 °C (for mineral core composition: Table 5, analysis 1-c & 3-c) respectively. Using the obtained temperature, the equilibrium pressure is estimated at 15.09 kbars using the Cpx-Plg geobarometer after Ellis (1980). The high pressure and temperature parameters of this dioritic rock correspond to upper eclogite facies metamorphism, and is comparable to the granulite facies rocks of eastern Uluguru Mountain Ranges of Tanzania that gave an equilibrium temperature from 915-960 °C and 12.9-14.5 kbar to 800-880 °C and 10.5-12.5 kbar (Muhongo and Tuisku, 1995).

2.2.2.3 Mafic granulite (plagioclase-pyroxene-garnet) gneiss

The rare granulitic mafic enclaves that have been partially retrogressed, gave an equilibrium temperature of 603 °C based on the garnet-clinopyroxene geothermometer (Pattison and Newton, 1989 ; Krogh, 1988) using the experimental calibration of Fe-Mg exchange between garnet and clinopyroxene phases. Using the obtained temperature, the equilibrium pressure is estimated to range between 6.95 +/- 1.9 and 7.12 kbar using the garnet-clinopyroxene-plagioclase-quartz geobarometer after Eckert et al. (1991) and Powell and Holland (1988) respectively.

2.2.3 Thermobarometric conditions of formation of the granitic rocks.

Considering the porphyritic granite (MU-29) as a representative sample of the granites in Matuu area, the Al-in-amphibole geothermometer after Blundy and Holland (1990) gave an equilibrium temperature of 750 °C. Three calibrations using the total Al in hornblende as a barometer in granitic rocks has been published in the literature:

$$P = 5.03 \text{ Al}^{\text{Tot}} - 3.92 \text{ kbar} \quad \text{Hammarstrom and Zen (1986)}$$

$$P = 5.64 \text{ Al}^{\text{Tot}} - 4.76 \text{ kbar} \quad \text{Hollister et al. (1987)}$$

$$P = 5.03 \text{ Al}^{\text{Tot}} - 3.53 \text{ kbar at } 700 \text{ }^{\circ}\text{C} \quad \text{Blundy and Holland (1990)}$$

Applying the above empirical calibrations to the porphyritic granite (MU-29) it yields pressures of 5.75, 6.08 and 6.14 kbar with an average of 5.97 kbar respectively. Within experimental errors, all the three calibrations yield reasonable results that are consistent with field relations and the aforementioned temperature estimate considering that the solidus of granitic rock is approximately 700°C +/- 20 °C (Piwinskii, 1975).

2.3 DISCUSSION AND CONCLUSION

2.3.1 Mafic rocks

Based on field evidence, the Matuu-Masinga anorthositic rocks are interpreted as moderate to thick sheets that have been intruded into the gneisses and boudinaged on a large scale during the last phases of the regional metamorphism. This observation is in agreement with that reported by Ochieng (1993) on a research study carried out on similar gabbroic rock suite occurring south east of Mt. Kenya.

In the regional context, the mafic bodies of Matuu-Masinga area are tentatively correlated with the large meta-gabbro / mafic orthogneiss bodies mapped to the north of the present survey area, in particular those to the east of Chuka around the Ntungi, Kiero and Engakuni hills, and Chanler's Falls (Williams, 1966) and Barchuma-Kom areas (Dodson, 1991). There are, however, marked differences between the Matuu area anorthositic gabbros and those in the Ishiara and Mituguu areas. The Ishiara and Mituguu anorthositic gabbros notably have olivine with subsequent metamorphic coronas around the olivines. This contrasts strongly with the lack of olivine and the ubiquitous replacement of the original pyroxene by green amphibole in the Matuu-Masinga area.

On the wider regional scale, Andreoli (1991) describes a series of anorthositic and gabbro-norite suites with similar mineralogy and featuring granulite facies assemblages that occur in a roughly N-S linear belt from Mozambique to northern Tanzania. Comparatively, the anorthositic suites in Matuu-Masinga area are interpreted to be a continuation of these series along the same longitudinal strike. Many of the gneisses and migmatitic formations

enveloping the present intrusives are granulitic in appearance: where hypersthene, spinel, diopside, plagioclase and garnets form common assemblages (Nyamai et al., 1999).

Petrographical, mineralogical and mineral chemistry studies on the mafic rocks have shown that :

1. Diopside, hypersthene, hornblende, plagioclase and biotite occur as essential minerals in the dioritic and gabbroic rocks. Spinel, apatite, quartz, chlorite, magnetite, ilmenite and pyrite occur as minor or secondary minerals.
2. Coronas developed around clinopyroxenes in the diorite and gabbroic rocks are in most cases in contact with plagioclase crystals. The textural and mineral association envisaged by the development of spinel and the clouding of the plagioclase suggest the coronas to have developed under metamorphic conditions.
3. The clinopyroxenes range in composition from diopsidic to mainly in Augite in composition. The clinopyroxenes are in general enriched in Al, Ti, Cr and Na relative to the co-existing orthopyroxene, and the reverse is true for Mn. The orthopyroxene crystals are mainly of hypersthene composition. On the Ca-Mg-Fe triangular composition plot, representative clinopyroxene grains are shown to be of typical alkaline rocks affinity.
4. The distribution of aluminium among the tetrahedral and octahedral sites in the pyroxene analyses from the dioritic rock shows the grains to have crystallized under higher pressure than their corresponding iron rich pyroxenes. On the other hand, the almost equal amounts of jadeite (Alvi) and Ca-Tschermak (Al) in the clinopyroxenes of the gabbroic rocks could have resulted from the combined effects of high pressure and temperature.
5. The amphibole occurring in the dioritic rock has a composition that straddles the boundary between ferroan pargasitic- and pargasitic hornblende, while those occurring in the gabbroic rocks are mainly calcic edenitic- and magnesio-hornblende. In the amphibolite

rocks, the amphiboles straddle between calcic edenitic hornblende and ferroan pargasitic hornblende.

6. The plagioclase in the gabbro rocks range in composition from labradolite ($An_{62-58-67.05}$) through bytownite (An_{86}) to anorthite (An_{93}). The primary plagioclase in the dioritic rock has an average composition of calcic andesine (An_{35}). A secondary Sr-rich plagioclase (av. 7.05 wt.% SrO) was noted to occur in the diorite, amphibolite and syeno-diorite rocks.
7. Studies on the conditions of pyroxene crystallization using the magnesium-iron distribution between coexisting calcium-rich and calcium-poor pyroxene minerals suggest that in the meta diorite rock they point to a temperature of crystallization corresponding to those of igneous in origin, while in the gabbroic rocks they point to a temperature of crystallization corresponding to those of metamorphic and igneous in origin.
8. The thermobarometric P-T calibrations obtained from various mineral pairs occurring in the major mafic rocks show: (a) a temperature of 750°C and pressures between 6.55 to 6.98 kbars for the amphibolite rocks; (b) temperatures between 879-904°C and pressures between 5.89 to 6.31 kbars for the gabbroic rocks; (c) temperatures between 843-854°C and a pressure of 15 kbar for the dioritic rock; (d) a temperature of 603°C and pressures between 6.95 to 7.12 kbars for the granulitic mafic plagioclase-pyroxene-garnet gneiss.

It is important to note that the presented PT conditions are average values and that there is considerable difference between different calibrations and end member models. For example, barometric calibrations involving Mg-end members tend to give more isobaric cooling than Fe-end member models.

2.3.2 Granitic Rocks

Petrographical, mineralogical and thermobarometric features of the Matuu-Masinga granitic rocks can be summarized as follows:

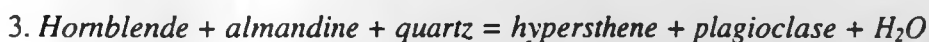
- 1) The pink granite contains two feldspars, alkali-feldspar and Sr rich (av. 8.6 wt.% SrO) plagioclase (andesine), biotite and chlorite.
- 2) The porphyritic granite has one feldspar (alkali-feldspar), Fe⁺² rich pargasitic hornblende, and biotite.
- 3) The grey granite contains two feldspars, alkali-feldspar and plagioclase (oligoclase).
- 4) The mineral chemistry of the K-feldspar, plagioclase and biotite occurring in the granitic rocks from Matuu area suggest a paragenetic sequence of the order : grey granite < pink granite < porphyritic granite.
- 5) The use of Al-in-amphibole geothermometric data for the granite rocks gave an average equilibrium temperature of 750 °C and a pressure of 5.97 kbar.

2.3.3 Metamorphic grade

Field and petrographic studies suggest that the Matuu area firstly experienced regional prograde granulite facies metamorphism which was later downgraded to the amphibolite- and greenschist-facies. Evidence for the high grade granulite metamorphism is obtained from the hypersthene-clinopyroxene-plagioclase mineral associations of the mafic gabbroic and dioritic rocks. Retrogression of the granulite-facies metamorphism into amphibolite- and greenschist-facies is documented by petrographic features such as sericitization of feldspars, the partial break-down of clinopyroxene into clinopyroxene-hornblende-biotite reaction rims, symplectization of pyroxene by biotite and quartz, development of myrmekites and growth of minerals such as muscovite, chlorite, epidote and sphene.

In agreement with De Waard in Winkler (1979), the best boundary between common high-grade metamorphism (high-grade almandine-amphibolite facies) and granulite facies

metamorphism is the hypersthene isograd, based upon the first appearance of hypersthene regardless of rock type and nature of the hypersthene-producing reaction. A number of reactions have been suggested by De Waard in Winkler (1979) to account for the diagnostic appearance of orthopyroxene (mostly hypersthene), the formation of additional almandine-rich garnet, and the decrease or disappearance of hornblende and biotite. In mafic rocks these are:



(N.B. It is important to note that all reactions involving hornblende and/or biotite are continuous over a certain range of physical conditions and, during a transitional stage, reactants and products co-exist).

With reference to the observed diagnostic mineral assemblage of the mafic rocks of Matuu-Masinga area, (i.e. hypersthene + clinopyroxene + plagioclase +/- quartz), which is consistent with reaction 1 & 2 above, the assemblage falls into the field of hypersthene-pyroxene granulite according to the nomenclature of hypersthene-bearing granulites proposed by Winkler (1979).

The temperature in granulite terrains is estimated to range from 650° to 800 °C. This temperature range, which is substantiated by the work of Bohlen and Essene (1977) in Winkler (1979), falls within the range of the estimated range of equilibrium temperatures (i.e., 603 - 904 °C) reported for the granulitic mafic rocks of Matuu-Masinga area.

The obtained pressure estimates for Matuu-Masinga amphibolite and gabbroic gneisses (i.e., average 6.43 kbars) - corresponding to 22 km in depth - compare with those

CHAPTER THREE

PROGNOSE AND TECTONOMETRIC EVOLUTION OF THE
MATUU-MASINGA BELT: STRUCTURAL TECTONICS OF MATUU-MASINGA
AREA, CENTRAL KENYA

reported by other workers for regional metamorphism in the Mbooni-Uvete area (Suwa et al., 1979; Inoue and Suwa, 1979; Miyake and Suwa, 1981). The deformation under the aforementioned physical conditions is relatively ductile. It is worthy noting that Mbooni-Uvete area, occurring to the south of the survey area, lies in the same longitude and metamorphic isograd as Matuu-Masinga area

The Matuu-Masinga area is geographically situated between the Mbooni-Uvete area and the Matuu-Masinga area. The area is a tectonic zone composed of various tectonic units and the evolution of the geotectonic environment is complex. The field occurrence of these rocks in the survey area is a clear evidence of contact with the Mbooni-Uvete area. These rocks are of greater extent than the surrounding area and are composed of various tectonic units.



In the present study, the rocks are studied from their structural evolution and metamorphism. The area is a tectonic zone composed of various tectonic units and the evolution of the geotectonic environment is complex. The field occurrence of these rocks in the survey area is a clear evidence of contact with the Mbooni-Uvete area.

STRUCTURAL OF TTECTONIC

The general structure of the area is the tectonic zone composed of various tectonic units and the evolution of the geotectonic environment is complex. The field occurrence of these rocks in the survey area is a clear evidence of contact with the Mbooni-Uvete area.

CHAPTER THREE

GEOCHEMISTRY AND TECTONOMAGMATIC AFFINITIES OF THE MOZAMBIQUE BELT INTRUSIVE ROCKS IN MATUU-MASINGA AREA, CENTRAL KENYA.

3.0 INTRODUCTION

The Matuu- Masinga area is predominantly underlain by rocks of the Mozambique orogenic belt in central Kenya. The area offers a striking geological region composed of granitoids, ultramafic/mafic intrusive rocks and the field association of the granulite-(meta)-anorthosite-amphibolite rocks. The field association of these rocks in the study area is a rare phenomenon/ occurrence in the Mozambique belt as a whole. These rocks are of greater importance insofar as the understanding of the tectonic evolution of the belt and petrogenesis of the deep continental crust is concerned.

In the present study area, little or no studies have been done to determine its crustal and tectonic evolution. The aim of the present study is to bridge this gap and offer new geochemical information that can lead to understanding their evolution, tectonic setting, and proper exploration strategies of the mineral wealth in this region and the belt as a whole.

3.1 STRUCTURAL SETTING

The general structural trend in the surveyed area varies from NNW-SSE to NW-SE direction with localized concentric trends around granitoid intrusions. The dip is predominantly to the west with angles varying from 50° to the vertical. The mineral lineations are mostly parallel to the regional structural trend. The foliations are well pronounced in the hornblende

and biotite gneisses and vary in degrees on an outcrop scale with mafic and felsic bands of 3 to 5 cm thickness to small scale segregational banding in hand specimen.

On an outcrop scale, isoclinal, open, overturned and migmatitic folds (Plate 3.1) are a common feature in the survey area. Several shear zones formed in the high grade metamorphism and associated with the growth of almandine porphyroblasts were noted mainly in the central and eastern section of the study area (see Fig. 1.2). Competent mafic lensoidal layers that have undergone ductile deformation and associated with rotated boudins and displaced micro-faults define a sinistral sense of shear. The observed cleavage patterns and boudins along with thinning of incompetent layers suggest severe strains to have affected the area.

Mafic dykes mainly of doleritic composition (Plate 3.2) occur sporadically in the study area. Highly compressed leucocratic microfolds within the dykes suggest their intrusion occurred during a strong stress regime. The contacts with the host rock are normally sharp except in those shear zones where the margins have been highly deformed and mylonitization of the host rock has occurred. Joints formed due to stress release and later filled by leucocratic veins are apparent in some of the dykes.

3.2 PETROGRAPHY

The rocks in this area vary from medium to high grade gneisses and granulites, to granites, anorthosites, diorites and gabbros. The characteristic mineral assemblages of the meta-igneous rocks of the study area are quartz, plagioclase, hypersthene, diopside, garnet, biotite, actinolite and Mg-hornblende. The accessory minerals are zircon, sphene, apatite, magnetite, hematite, ilmenite and pyrite.

The Matuu-Masinga mafic samples show typical intrusive magmatic textures. The main mineralogical components are plagioclase, clinopyroxene and orthopyroxene. Brown hornblende, biotite, apatite, Ti-Fe oxides and sulfide minerals are present as accessories.



Plate 3.1. Field photograph showing migmatitic folds. Note the alternating mafic and felsic layers with accompanied ductile thinning of the leucosomes. Matuu- Masinga area, central Kenya.



Plate 3.2. Field photograph showing mafic dykes of doleritic composition intruding the basement. Matuu-Masinga area, central Kenya.

Plagioclase occurs as coarse xenomorphic andesine grains (An_{35-40}) and small subhedral labradorite crystals (An_{62-67}). Pyroxene occurs in two modes: coarse subhedral grains of orthopyroxene and clinopyroxene, containing (100) lamellae and blebs of clinopyroxene and vice-versa, and clinopyroxenes with symplectites of biotite and quartz. In sample MU-7, augite is surrounded and/or partially replaced by two types of amphibole. Commonly, an inner zone of pale green hornblende is surrounded by an outer zone of deep green tremolite-actinolite. The calcic amphiboles, which occur both as Mg- and Fe-rich varieties, vary in composition from edenitic- to magnesio- hornblende in the gabbroic rocks to Fe-pargasite in the dioritic rocks. The hornblende in samples MU-20A & MU-20B occurs as large, optically continuous pseudomorphs after clino-pyroxene. Biotite forms interstitial lamellae with yellow to brown pleochroism. Magnetite and ilmenite occur either in large clustered grains or as symplectites in the orthopyroxene.

The granitic rocks, which are represented by the alkali granites, porphyritic granites and granitoid gneisses, are generally medium to coarse grained. The alkali granites exhibit an equigranular texture with anhedral to subhedral crystals of perthite, quartz and plagioclase (An_{28}) occupying the larger volume of the rock. Biotite flakes commonly make an intergrowth with chlorite. The porphyritic granites, which form most of the topographic hills in the survey area, are coarse grained and essentially consist of potassium-feldspar porphyroblasts studded in a medium grained matrix of quartz, plagioclase, microcline, hornblende, biotite and epidote with minor apatite, sphene, calcite and Fe ores. The granitoid gneisses consist essentially of quartz, microcline, plagioclase (An_{23}), biotite and sometimes muscovite with minor amounts of apatite, epidote, sphene and Ti-Fe oxides.

3.3 GEOCHEMISTRY AND TECTONOMAGMATIC AFFINITIES

3.3.1 Alteration effects

Effects due to the possible alteration of rocks can be avoided to some extent by selecting the samples carefully and by using "immobile" elements in the classification (e.g. Pearce and Cann, 1973). The geochemical alteration of magmatic rocks can be examined by a ternary diagram proposed by Davies et al. (1978). Practically all the Matuu-Masinga rock suite plot in the field of unaltered rocks (Fig. 3.1).

Close observations reveal that although the gneissic intrusive rocks of Matuu area have undergone regional metamorphism, features of their magmatic origin have been retained. This magmatic affinity is further exemplified in the major element discriminant diagram (Fig. 3.2) distinguishing between ortho- and para-gneiss rocks in high grade metamorphic terrains (Passchier et al., 1990). The three samples in Figure 3.2 with para-gneissic affinity are interpreted to be high grade metamorphosed rocks of sedimentary origin.

3.3.2 Geochemical Characteristics

Geochemical analyses of 24 representative rock samples of the Mozambique belt rocks of the Matuu-Masinga area are presented in appendix 3.1. The Mg^* ($Mg^* = 100MgO/(MgO+FeO')$) number of the Matuu mafic rocks ranges in composition from 23 - 51 with a mean of 32; the granitic Mg^* value range from 14 - 21 with an average of 17. The mafic rocks have relatively high contents in TiO_2 (0.42-4.51, av. 2.14 wt.%), Cu (188-5810, av. 1960 ppm), Ni (31-93, av. 55 ppm), Cr (15-274, av. 160 ppm) and V (111-380, av. 223 ppm). The mean content of copper (i.e, 1960 ppm) and Zn (i.e, 155 ppm) in the mafic rocks of the study area is high compared with the average for ultramafic rocks of 30 ppm and 50 ppm reported by Goles (1967) and Turekian and Wedepohl in Scotford and Williams (1983) respectively. Although in part dispersed, the increase in K content with increasing Si content as well as the

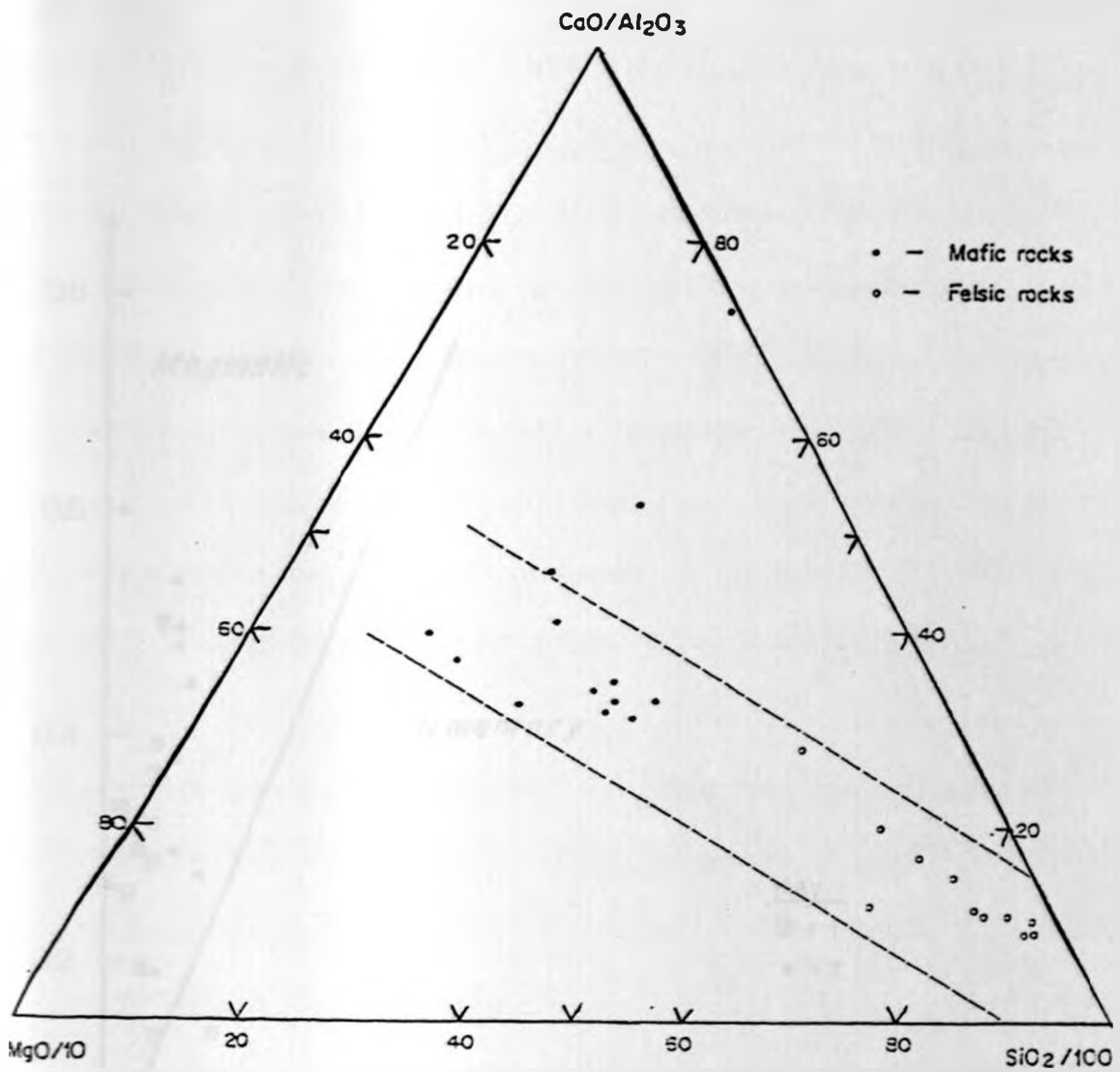


Fig. 3.1 Diagram for assessing alteration of magmatic rocks of the Matuu-Masinga area. Unaltered rocks plot between the lines (Davies et al., 1978.) Symbols : filled circles = mafic rocks, open circles = granitic rocks.

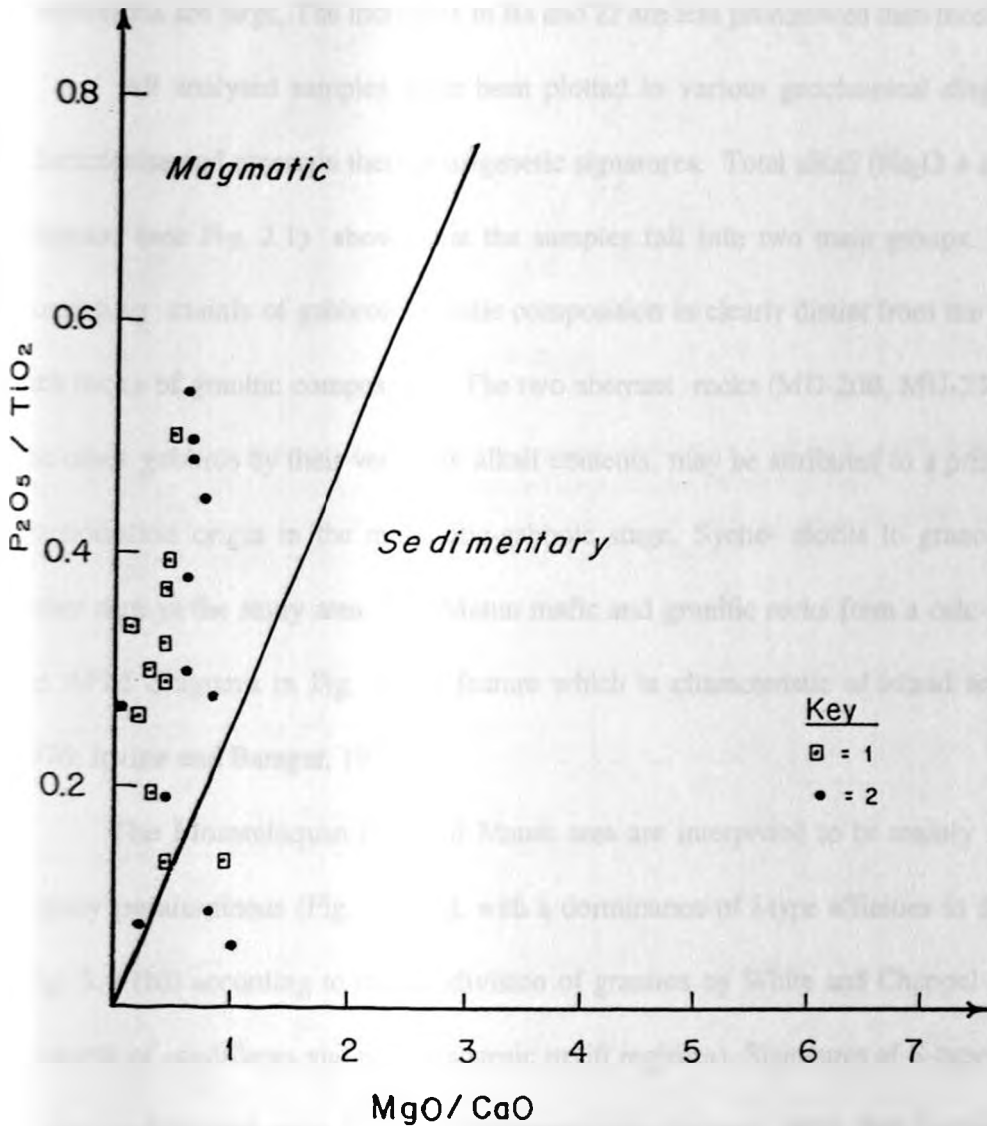


Fig. 3.2. Major element discrimination diagram distinguishing ortho- and para-gneiss in high grade metamorphic terrain in Matuu-Masinga area, central Kenya (Diagram after Werner in Passchier et al, 1990). 1 = granitic rocks, 2 = mafic rocks.

decrease in Ti, Fe, Mn, Mg, Ca, Cu, Zn, Ni, Co, Cr and V with increasing Si are quite coherent. The P contents are higher in the mafic rocks than in the granitic rocks. In general, the Rb, Th, Ba, Zr, Sr and Pb contents increase with the increasing Si content, but in the granitic rocks the dispersions are large. The increases in Ba and Zr are less pronounced than those in Rb and Th.

All analysed samples have been plotted in various geochemical diagrams in order to characterise and ascertain their petrogenetic signatures. Total alkali ($\text{Na}_2\text{O} + \text{K}_2\text{O}$) versus silica diagram (see Fig. 2.1) shows that the samples fall into two main groups. The mafic group consisting mainly of gabbroic/dioritic composition is clearly distinct from the felsic and alkali-rich rocks of granitic composition. The two aberrant rocks (MU-20B, MU-23) that differ from the other gabbros by their very low alkali contents, may be attributed to a primary cumulation-fractionation origin in the magmatic-gabbroic stage. Syeno-diorite to granodiorite rocks are rather rare in the study area. The Matuu mafic and granitic rocks form a calc-alkaline trend on the AFM diagrams in Fig. 3.3, a feature which is characteristic of island arc suites (Jensen, 1976; Irvine and Baragar, 1971).

The Mozambiquan rocks of Matuu area are interpreted to be mainly metaluminous to slightly peraluminous (Fig. 3.4 (a)), with a dominance of I-type affinities in the granitic rocks (Fig. 3.4 (b)) according to the subdivision of granites by White and Chappel (1977) - (i.e., as products of cordilleran and post-orogenic uplift regimes). Signatures of S-type granites, typical of post-collisional stage like the Himalayan-type orogenic belts, that formed as a result of partial melting of a tectonically thickened lower continental crust, show some imprint in the study area.

Considering the granitic rocks of the study area, trace element (Y, Nb and Rb) versus SiO_2 discriminant diagrams in Fig. 3.5 shows an apparent bias for volcanic arc affinities of these rocks. On the other hand, the Rb versus (Y+Nb) discriminant diagram in Fig. 3.6 show a characteristic tendency from calc-alkaline volcanic arc to within-plate affinities.

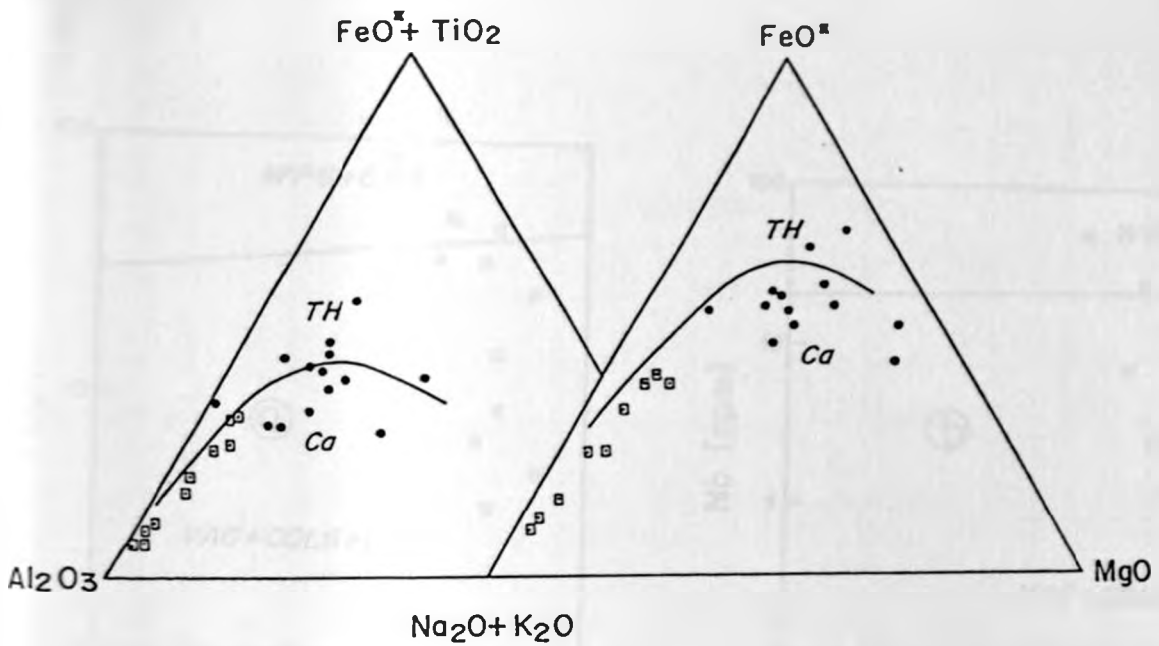


Fig. 3.3 Composition of the mafic and granitic rock suite from Matuu-Masinga area projected onto $(\text{FeO}^* + \text{TiO}_2) - \text{Al}_2\text{O}_3 - \text{MgO}$ diagram (after Jensen, 1976) and $\text{FeO}^* - (\text{Na}_2\text{O} + \text{K}_2\text{O}) - \text{MgO}$ diagram (after Irvine and Baragar, 1971) discriminating between volcanic rocks of tholeiitic (TH) and calc-alkaline (Ca) affinity. Symbols as in Figure 3.2.

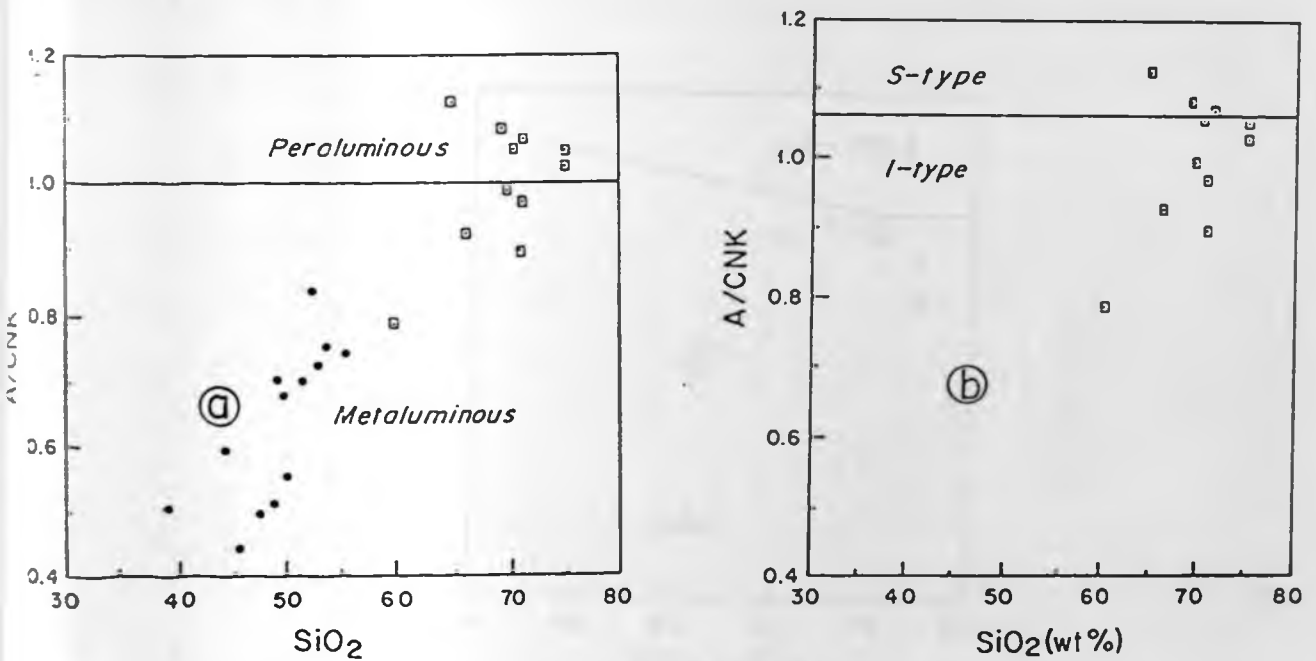


Fig. 3.4 (a). Plot of SiO_2 versus A/CNK molar ratio for mafic and granitic rocks of Matuu area. A, C, N and K are the molar values of Al_2O_3 , CaO , Na_2O and K_2O respectively; (b). Alumina saturation-silica diagram of the granitic rocks of Matuu area. I-S line after White & Chappel (1977). Symbols as in Figure 3.2

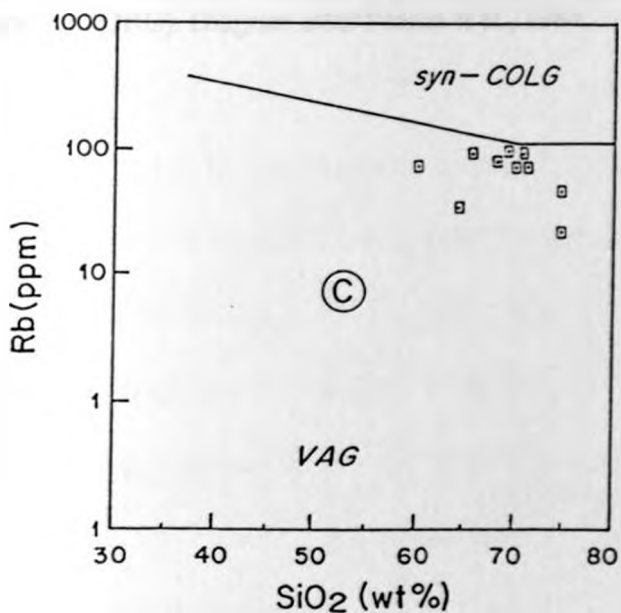
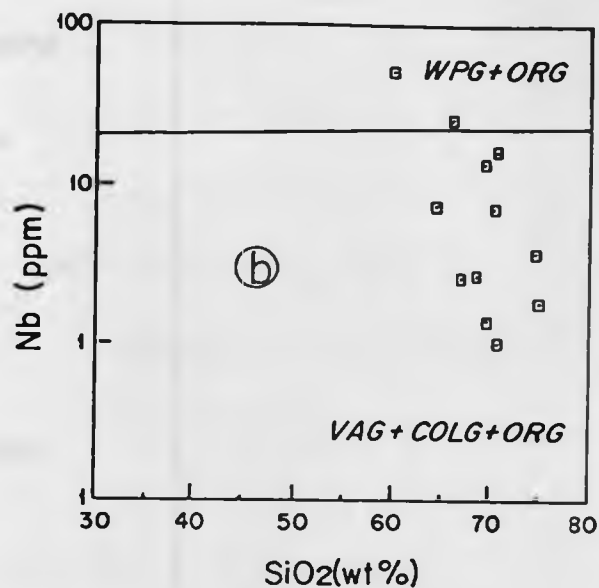
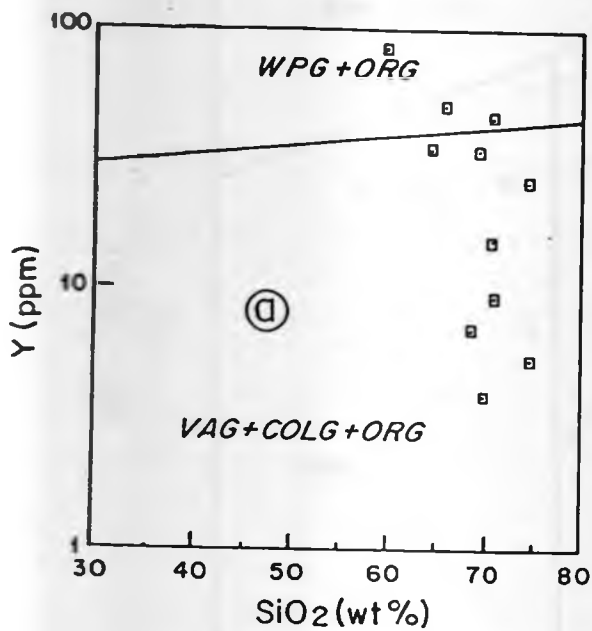


Fig 3.5. SiO₂ variation diagrams for Rb, Nb and Y on the Matuu-Masinga area granitic rocks discriminating between syn-collision granites (syn-COLG), volcanic arc granites (VAG), within plate granites (WPG), and ocean ridge granites (ORG). Diagrams after Pearce et al. 1984). Symbols as in Figure 3.2

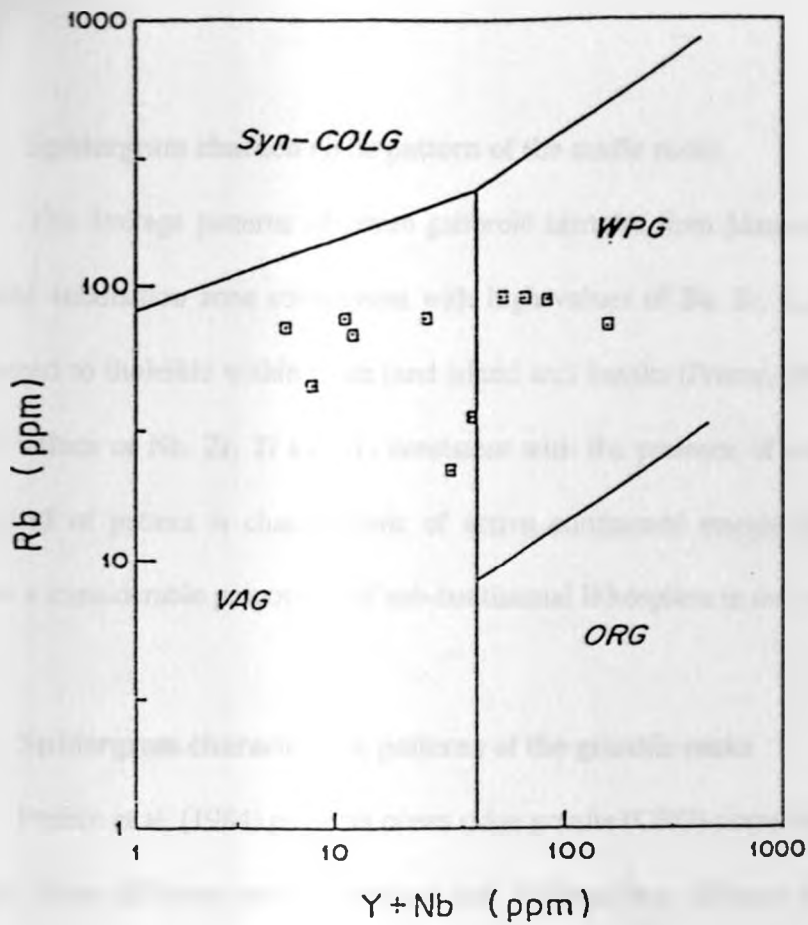


Fig. 3.6. Rb-(Y+Nb) variation diagram for the Matuu-Masinga area granitic rocks discriminating between syn-collision granites (syn-COLG), volcanic arc granites (VAG), within-plate granites (WPG), and ocean ridge granites (ORG). Diagram after Pearce et al., 1984.

3.3.3 Spidergram characteristic pattern of the mafic rocks

The average patterns of seven gabbroic samples from Matuu area (Fig. 3.7) show an apparent subduction zone component with high values of Ba, Sr, K, Rb, Th, Ce, Nb and P. Compared to tholeiitic within-plate (and island arc) basalts (Pearce, 1982), the pattern also has higher values of Nb, Zr, Ti and Y, consistent with the presence of a within-plate component. This kind of pattern is characteristic of active continental margin calc-alkaline basalts that contain a considerable proportion of sub-continental lithosphere in their source (Pearce, 1983).

3.3.4 Spidergram characteristic patterns of the granitic rocks

Pearce et al. (1984) presents ocean ridge granite (ORG)-normalized element patterns for granites from different tectonic settings and distinguishes different source components that affect the level and shape of the patterns. The patterns of five granitic rocks from Matuu area (Fig. 3.8) with silica values close to 70 per cent (appendix 3.1) demonstrates that there is a relative enrichment in large ion lithophile (LIL) elements (Rb, Sr, Ba and K) over the other incompatible elements (Nb, P, Zr, Ti and Y). This feature is commonly apparent in volcanic arc granites that are normally characterised by enrichments in K, Rb, Ba, Th (typical in calc-alkaline series) and Ce relative to Nb, Zr and Y (Pearce et al., 1984). Nb shows a marked depletion characteristic pattern - which may be attributed to an effect of incorporation of Ti-phases in subduction environments. Depletion of Nb and other high field strength elements (HFSE) (P, Zr, Ti, Y), relative to LIL elements, is a characteristic feature of all subduction-related magma (Saunders et al., 1980). This has been attributed to:

- a) partitioning of HFSE into residual Ti phases (e.g. ilmenite, rutile and sphene) which stabilized during hydrous partial melting conditions; and

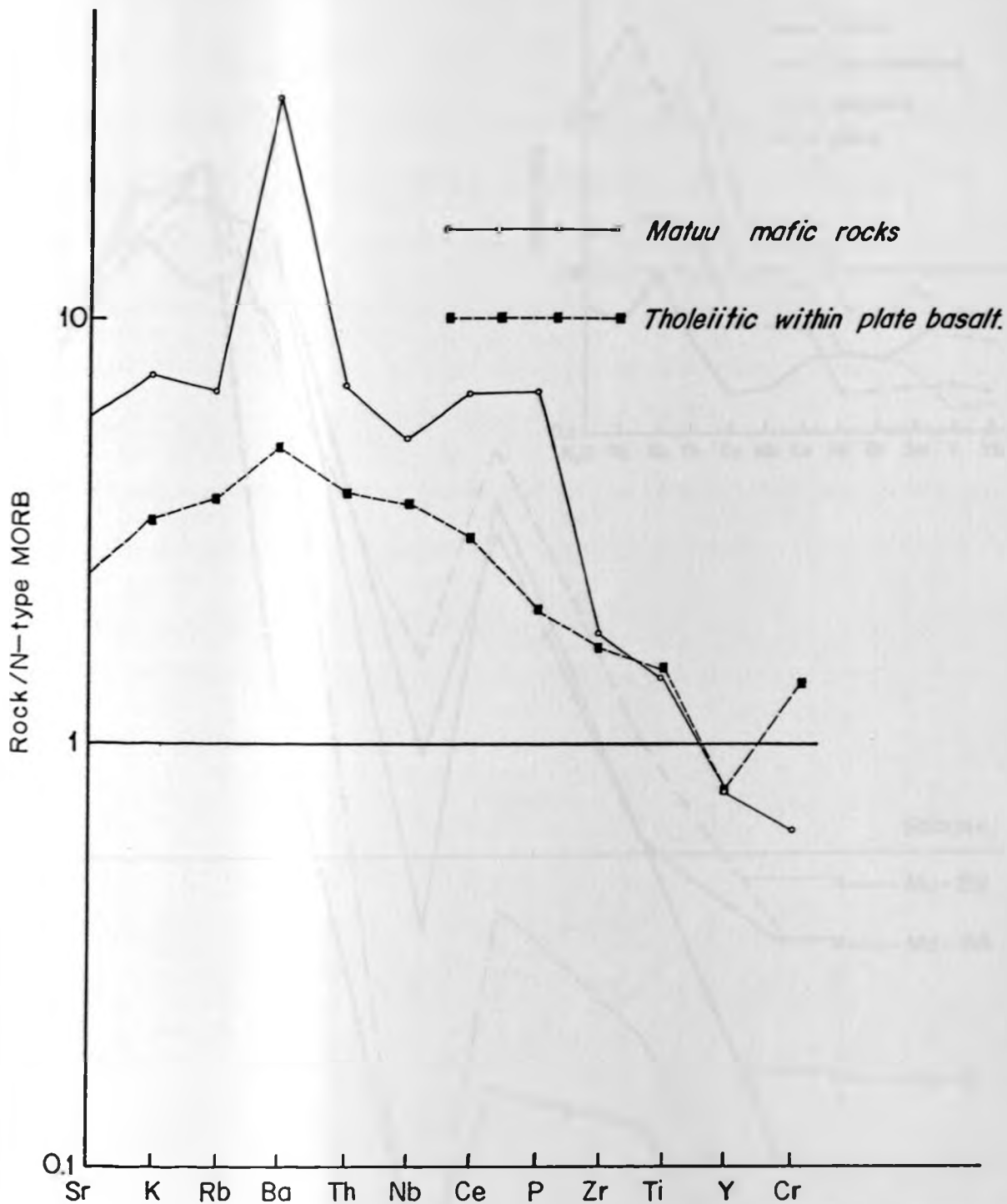


Fig 3.7 Spidergrams of the averages of some mafic rocks from Matuu-Masinga area. Normalised data after Pearce (1982).

VOLCANIC ARC GRANITES

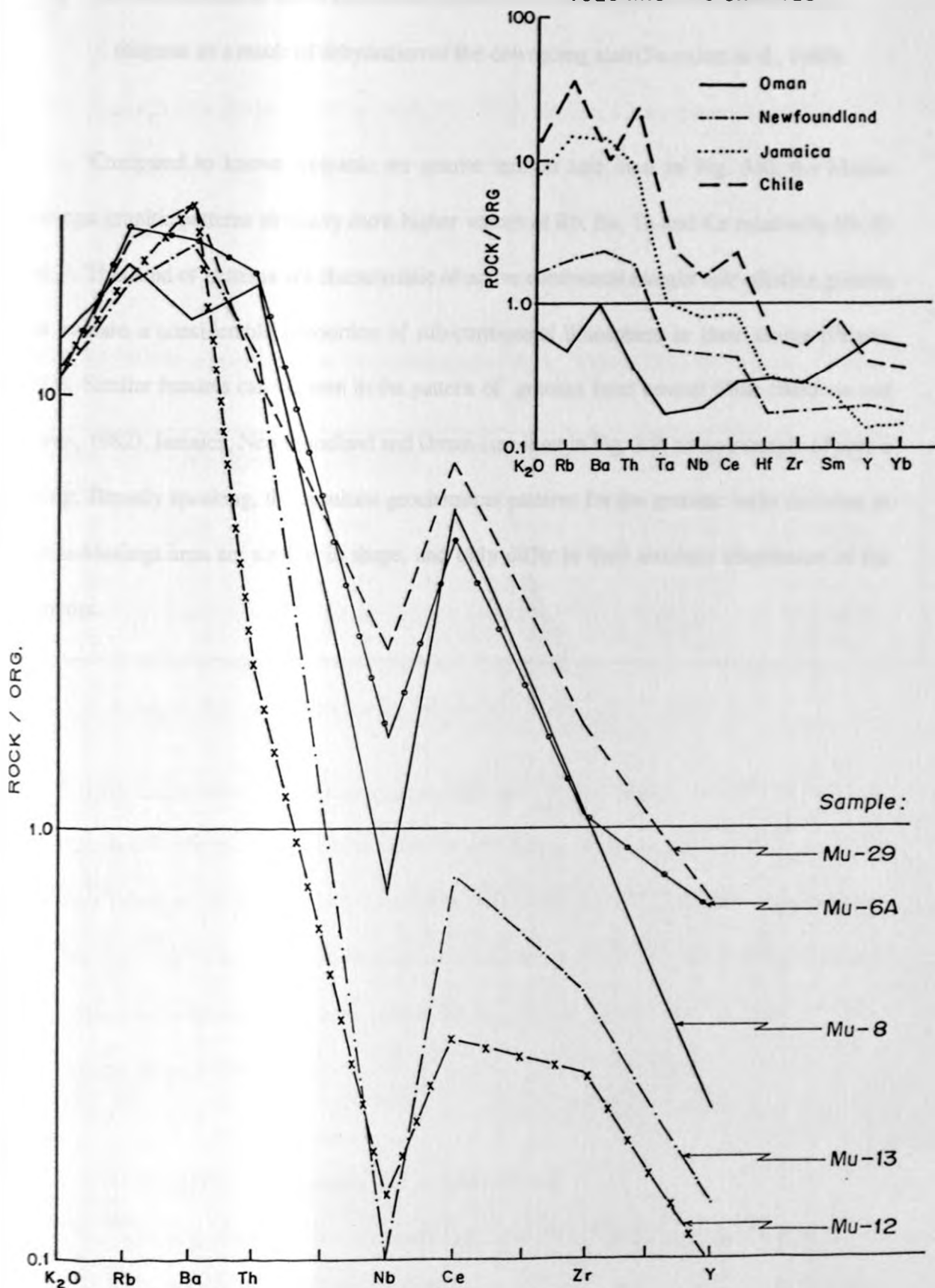


Fig 3.8 Ocean ridge granite (ORG) normalised patterns for some granitic rocks from Matuu-Masinga area, central Kenya. Inset shows some representative volcanic arc granite patterns (after Pearce et al., 1984.)

b) the transportation of the LIL elements into the source regions of the calc-alkaline magmas as a result of dehydration of the downgoing slab (Saunders et al., 1980).

Compared to known volcanic arc granite terrains (see inset in Fig. 3.8), the Matuu-Masinga granitic patterns similarly show higher values of Rb, Ba, Th and Ce relative to Nb, Zr and Y. This kind of patterns are characteristic of active continental margin calc-alkaline granites that contain a considerable proportion of sub-continental lithosphere in their source (Pearce, 1983). Similar features can be seen in the pattern of granites from central Chile (Baldwin and Pearce, 1982), Jamaica, Newfoundland and Oman (see inset in Fig. 3.8) as an example of such a setting. Broadly speaking, the resultant geochemical patterns for the granitic rocks occurring in Matuu-Masinga area are similar in shape, and only differ in their absolute abundances of the elements.

Sample	100000	10000	1000	100	10
11-75	13	197	110000	1100000	1100000
11-29	92	480	110000	1100000	1100000
11-31	81	318	110000	1100000	1100000
11-18	72	274	110000	1100000	1100000

Fig. 3.8. Matuu-Masinga granitic patterns (Rb, Ba, Th, Ce, Nb, Zr, Y) (Pearce, 1983)

The characteristic geochemical patterns of the Matuu-Masinga granites, which appear to be similar to those of the active continental margin granites, indicate that the source region of the Matuu-Masinga granites was a sub-continental lithosphere. The geochemical patterns of the Matuu-Masinga granites are similar to those of the active continental margin granites, which are characteristic of active continental margin calc-alkaline granites. This is consistent with the view that the Matuu-Masinga granites were derived from a sub-continental lithosphere.

THE MATUU-MASINGA GRANITIC TERRAIN

The Matuu-Masinga granitic terrain is a large area of granitic rocks, which is situated in the Matuu-Masinga area. The granitic rocks are characterized by their high Rb, Ba, Th and Ce relative to Nb, Zr and Y.

3.4 ISOTOPE GEOCHEMISTRY

Analysis of initial $^{87}\text{Sr}/^{86}\text{Sr}$ ratios from some of the mafic and granitic rocks from Matuu-Masinga area are presented in Table 3.1. Evidence drawn from the relatively low range of the $^{87}\text{Sr}/^{86}\text{Sr}$ ratios for the representative mafic rocks (0.7043 - 0.7046) and granitic rocks (0.7066 - 0.7091) of the study area is that, the rocks had a high proportion of juvenile mantle-derived material, or they were derived from young crustal precursors.

Table 3.1. Rb-Sr analytical data for representative rocks from Matuu-Masinga area, central Kenya.

Sample Number	Rb (ppm)	Sr (ppm)	$^{87}\text{Rb}/^{86}\text{Sr}$	$^{87}\text{Sr}/^{86}\text{Sr}$	2 sigma mean
MU - 7	32	992	0.09385	0.704367	0.000028
MU - 16	23	469	0.14382	0.704551	0.000018
MU - 29	92	410	0.64440	0.709059	0.000024
MU - 8	81	518	0.45382	0.707539	0.000015
MU - 10	75	676	0.31863	0.706622	0.000025

N.B. MU-7, MU-16 - Mafic rocks; MU-8, MU-10, MU-29 - Granitic rocks.

This characteristic isotopic geology exemplifies a similar pattern observed by Key et al. (1989) in the Samburu-Marsabit area, north-central Kenya, which reported a small spread of strontium initial ratios from 0.7045 +/- 0.0006 to 0.7030 +/- 0.003. The low range of initial $^{87}\text{Sr}/^{86}\text{Sr}$ ratios for rocks of Matuu-Masinga area also concurs with that reported for a gneiss along strike in Machakos area, central Kenya, with an initial $^{87}\text{Sr}/^{86}\text{Sr}$ ratio of 0.7041 (Shibata and Suwa, 1979).

3.5 DISCUSSION : Petrogenesis and tectonic setting

The Matuu mafic rocks have relatively high contents of Cr (av. 160 ppm) and Ni (av. 55 ppm) compared with averages for ultramafic rocks (Goles, 1967). Thus, if they are derived from

mafic melts of the mantle (i.e., as inferred from their analysed low $^{87}\text{Sr}/^{86}\text{Sr}$ ratios of 0.7039-0.7045) little fractionation of the mafic phases is implied. The general decrease in Cr, V and Ti in the felsic granitic rocks suggests fractionation of mafic silicates (olivine, pyroxene, Ca-plagioclase, amphibole etc.) and magnetite, and the low P content is an indication of fractionation of apatite. Petrographically, apatite was found to occur as an essential mineral in the mafic rocks. The relatively high content of P in the mafic rocks is exemplified in their general rock chemistry where P_2O_5 ranges from 0.09 - 2.15 wt% with an average of 1.37 wt% (e.g. samples MU-2, MU-5B and MU-28 in appendix 3.1).

The behaviour of Zr and Ba suggest the mineral assemblage of the rocks in Matuu-Masinga area to have contained hornblende and biotite. These features agree with the mineral relics and pseudomorphs of phenocrysts of plagioclase, pyroxene, hornblende and biotite observed in the mafic and granitic rocks. The mineral assemblages of the rocks are interpreted to have contained phases with relatively high distribution coefficients for Ba and Zr. The distribution coefficients of Zr for hornblende and biotite ($D_{\text{Zr}}^{\text{hbl}}$ and $D_{\text{Zr}}^{\text{bt}}$) are notably higher than those for olivine, plagioclase and pyroxenes (Pearce & Norry, 1979). Further, the distribution coefficients of Ba for biotite ($D_{\text{Ba}}^{\text{bt}}$) is higher than those for clinopyroxene, plagioclase and hornblende (Arth, 1976; Hanski, 1983). It is apparent therefore, hornblende and/or biotite, which petrographically were noted to occur as essential minerals, to be responsible for partitioning of Ba and Zr in their magmatic phases.

The major- and trace-element signatures of the rocks in the Matuu-Masinga area facilitate definition of their tectonic setting. Geochemical data and field studies suggest that calc-alkaline granites (Fig. 3.3) abound in Matuu-Masinga area. The low $^{87}\text{Sr}/^{86}\text{Sr}$ ratios of 0.703 - 0.709 recorded from some of the representative rocks in the study area suggest that their source magma is of deep crustal or mantle origin. This magma did not have a long crustal

history and hence cannot be reworked material of Archean age. The calc-alkaline affinity of these rocks further indicates a subduction zone environment for their formation.

Considering the whole Matuu-Masinga rock suite in total, rocks plotting in arc fields in the discrimination diagrams are more common. This geochemical evidence appears to substantiate the work done in the proximity of the study area by Mathu et al. (1991) in which they inferred the presence of island arc tectonism in the central part of the Mozambique belt. Leeman (1983) postulated a connection between the thickness of the crust and the composition of volcanic rocks erupted in the volcanic arc. Tholeiitic basalts and basaltic andesites are common in volcanic arcs overlying thin, oceanic crust, whereas more acid calc-alkaline volcanics are dominant in mature island arcs and active continental margins overlying thick, continental crust. In Matuu-Masinga area, where calc-alkaline granitic plutons constitute about 30% of the total survey area, it suggests that in their accretion, the island arc palaeo-tectonic environment was underlain by a thick crust during the intrusion of these rocks. Their relative voluminous occurrence in this area further demonstrates the importance of crustal accretion during the Mozambique Belt orogeny as demonstrated earlier by Suwa et al. (1979) in the Machakos area, central Kenya. The effect of a within-plate component in the trace elements (i.e., Figs 3.6 & 3.7) suggests the influence of the sub-continental lithosphere in magma genesis.

3.6 CONCLUSION

Based on the tectonomagmatic diagrams as well as other structural and petrographical evidence presented in this chapter it is concluded that:

- (i) The rocks of Matuu-Masinga area, mainly of magmatic origin, are mainly metaluminous to slightly peraluminous. The granitic rocks, which show signatures of dominantly I-type with subordinate S-types, are mainly of calc-alkaline affinity.
- (ii) The rocks of Matuu-Masinga area are dominantly of island arc-tectonic setting with subordinate within plate affinities.
- (iii) The relatively low range of strontium initial ratios (0.7039-0.7091) for the rocks in the study area suggest that the rocks had a high proportion of juvenile mantle-derived material, or they were derived from young crustal precursors.
- (iv) The rocks in Matuu-Masinga area, with high Ba (av. 1331 ppm) and Zr (av. 370 ppm) contents, are petrographically interpreted to have contained hornblende and biotite mineral assemblage phases that had a relatively high distribution coefficients for Ba and Zr.
- (v) the relatively high concentration of Cu (188-5810 ppm, av. 1960 ppm) and Zn (88-264 ppm, av. 155 ppm) in the mafic rocks of the study area compared with averages for ultramafic rocks of 30 ppm and 50 ppm reported by (Goles, 1967) and Turekian and Wedepohl in Scotford and Williams (1983) warrant further exploration of their ore minerals.

CHAPTER FOUR
STRUCTURES, METAMORPHISM AND GEOCHRONOLOGY OF THE
MOZAMBIQUE BELT INTRUSIVE ROCKS IN MATUU-MASINGA AREA,
CENTRAL KENYA.

4.0 INTRODUCTION

The study area has an average altitude of about 1500 m above sea level with a gentle topography characterized by small hills and ridges (Plate 4.1). Reconstruction of the structural evolution of the study area has relied on the documentation of the geometry of different ages of structural elements developed in various rock units. The relative age of these features is established from structural overprinting relations, which records a relative sequence of deformational events, and forms crosscutting igneous intrusions, which provide temporal markers recording (or separating) orogenic events. Structural features are considered to result from discontinuous deformation if they are temporally separated by, for example, an intrusive event. Matuu-Masinga plutonic rocks, which intrude the gneissic complex, are potentially used to distinguish the relative ages of the structures.

The Mozambique belt itself has a complex history of superimposed deformation and metamorphism which consists of high grade reworked or reactivated basement (Muhongo, 1991). The belt has been inferred to mark the sites for several superimposed Proterozoic subduction zones and collisional sutures (Muhongo, 1998, and references therein). Geochronological studies with a view of unraveling this tectonism on the Kenyan segment of the Mozambique belt is very scanty (Nyamai et al. 1993; Mosley, 1993). Important high-grade tectonothermal events in the belt took place between about 845 and 715 Ma B.P. (Cahen et al., 1984; Andriessen et al., 1985; Key et al., 1989). The subsequent cooling and uplift of the basement has been traced by K-Ar dates on biotites, which range between 438 and 528 Ma (Shibata and Suwa, 1979; Cahen et al., 1984; Frisch and Pohl, 1986). The fact that these dates show some systematic regional variation points to regionally different cooling histories. Fission-track ages between 479 and 572 Ma on sphene and zircon from the basement in northeast Kenya (Gleadow, 1980) indicate that the presently exposed basement had cooled to temperatures



Plate 4.1. Field photograph showing the general topography of Matuu-Masinga area.



Plate 4.2. Field photograph of foliated biotite gneiss, Matuu-Masinga area.

between 300 and 200°C at about 500 Ma B.P. A reconnaissance study on apatite fission-track analysis of Kenyan basement rocks by Wagner et al., 1992 showed that the tectonothermal evolution of the basement in Kenya was not uniform but regionally variable, with a clear relationship to Mesozoic-Recent rifting.

There is still a lack of adequate geochronological data to fully understand the tectonic and characteristic metamorphic evolution in different segments of the belt. The present study aims to bridge this gap by providing more structural, metamorphic and geochronological data. This data is envisaged to give more light on the tectonic and metamorphic evolution of the Mozambique belt rocks in Matuu-Masinga area.

4.1 STRUCTURAL SETTING OF MATUU-MASINGA AREA

4.1.1 Structures

Although contact relations are generally not observed due to thick soil cover in some areas, it is apparent that the Matuu-Masinga granitic plutons postdate gneissic fabrics in the country rock. Evidence for this is provided by the absence of high grade mineral assemblages and of gneissic fabrics in the granitic plutons, and from the observation that the granites are enveloped by regionally conformable fabrics that are locally discordant. The main granite mass at Mavoloni, which occurs on the western part of the study area (Fig. 1.2), has the long axis parallel to the regional fold axes. On its east and west sides, the surrounding rocks are generally concordant with its margin, and are near vertical and associated with minor folds. The general structure suggests that the granite is an intrusive body whose bulk has been partly compensated by folding on the east and west.

The general structural trend in the survey area varies from NNW-SSE to NW-SE direction with localized concentric trends around granitoid intrusions. The dip is predominantly to the west with angles varying from 50° to the vertical. The mineral lineations are mostly parallel to the regional structural trend. The foliations are well pronounced in the schistose

hornblende and biotite gneisses (Plate 4.2) and vary in degrees on an outcrop scale with mafic and felsic bands of 3 to 5 cm thickness to small scale segregational banding in hand specimen. When the poles to foliation are plotted on a stereographic projection (Fig. 4.1), they exhibit an imperfect monoclinic symmetry with a fairly high degree of homogeneity for a fold axis in a direction of 291° . The plot illustrates folds with more prominent westerly limbs.

On an outcrop scale, isoclinal, open, tight, overturned and migmatitic folds (Plate 4.3) are a common feature in the survey area. The observed cleavage patterns and boudins along with thinning of incompetent layers suggest severe strains to have affected the area. The orientations of the isoclinal fold axial planes suggest compressive forces acting on a south westerly direction. Three generations of northeast-trending, northwest- overturned microfolds (termed here F_1 , F_2 , and F_3) were noted to occur in the study area with F_2 being more prominent. The first (NW-SE) F_1 generation microfolds consisting of tight to isoclinal folds (Plate 4.4) are associated with shallow north-plunging linear structures. The second generation (NE-SW) F_2 microfolds, which gently affects the whole area are related to the foliation within granitoid rocks. These are inferred to have been accompanied by amphibolite facies metamorphism. The late open F_3 folds (Plate 4.5), which mildly deform the basement rocks of the study area, are postulated to involve the last phase of deformation in the study area. These structures suggest a complex tectonic history of the region with at least three phases of deformation.

Mafic dykes mainly of doleritic composition (Plate 4.6), occur sporadically in the area. In particular, a dyke swarm around Kilango school (see Fig. 1.2) average about 200 m in width with individual dyke thickness ranging from 0.3-3.0 m and trends in $N 20^{\circ} W$ direction with a vertical dip. Highly compressed leucocratic microfolds within the dykes suggest their intrusion

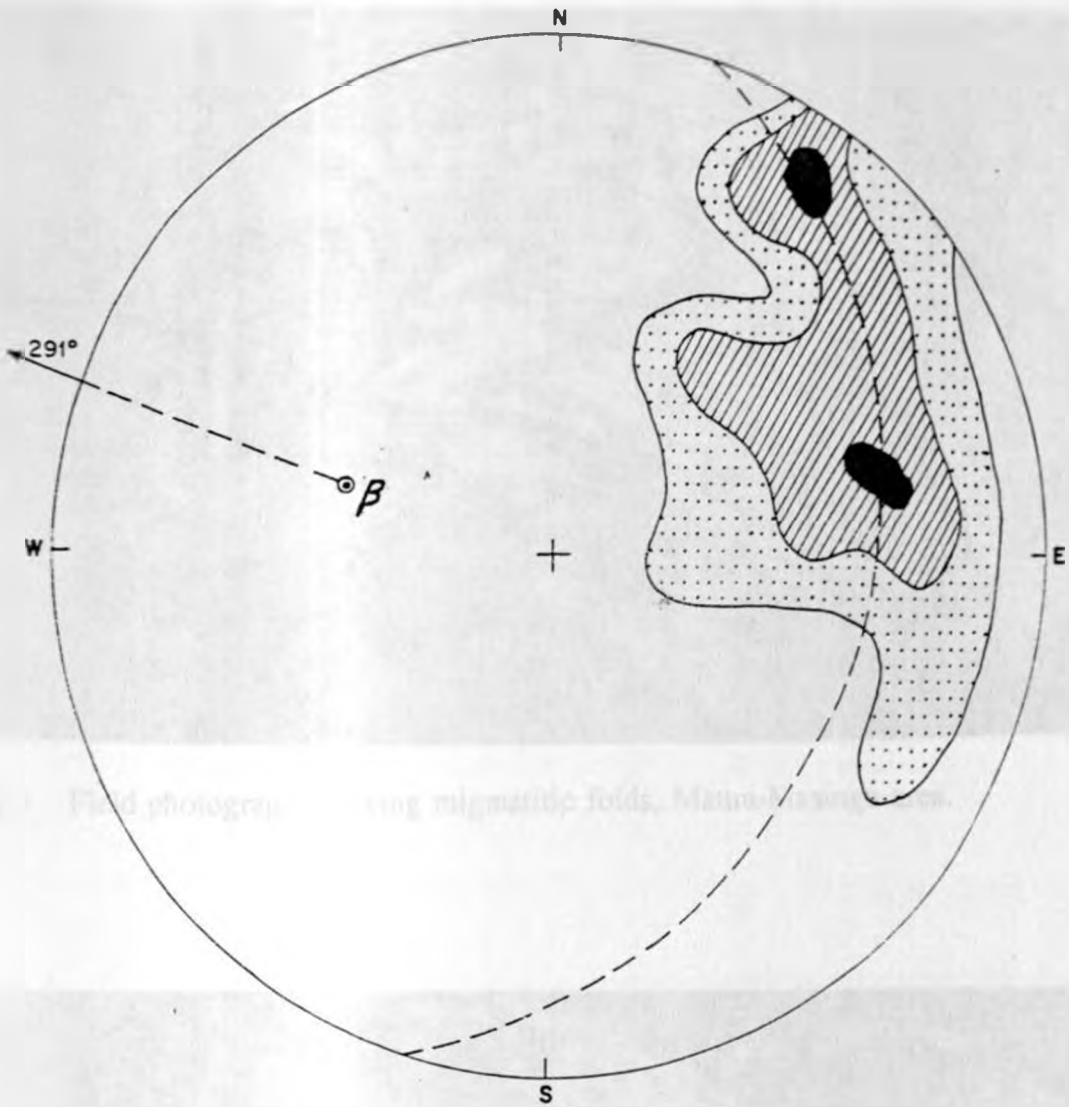


Fig. 4.1 : Orientation diagram of foliation poles in the Matuu-Masinga area (125 readings) projected from the lower hemisphere. β is the statistical fold-axis. Density contours are at 3% , 2% and 1% per 1% area .

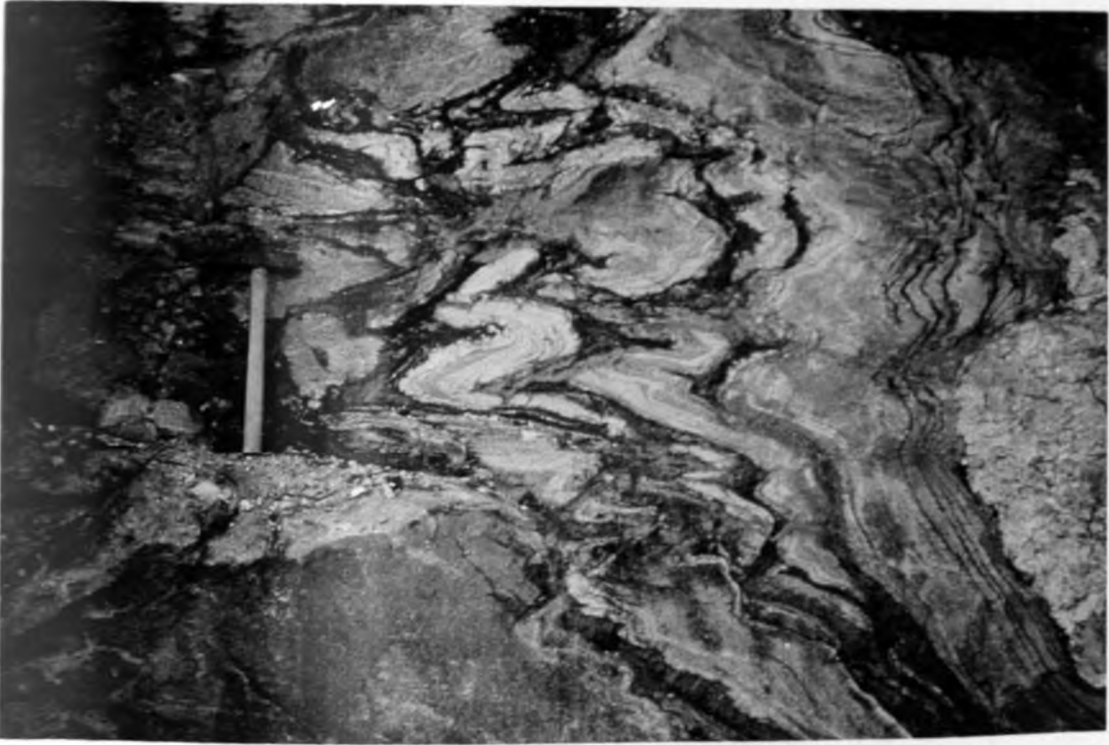


Plate 4.3. Field photograph showing migmatitic folds, Matuu-Masinga area.



Plate 4.4. Field photograph showing an isoclinally folded leucosome within a gabbroic intrusive, Matuu-Masinga area. The pen is 10 cm long.



Plate 4.5. Field photograph showing open folds, Matuu-Masinga area.



Plate 4.6. Field photograph showing mafic dykes of doleritic composition intruding the basement, Matuu-Masinga area, central Kenya.

to have occurred during a strong stress regime. The contacts with the host rock are normally sharp except in those shear zones where the margins have been highly deformed and mylonitization of the host rock has occurred. Joints formed due to stress release and later filled by leucocratic vein materials are apparent in some of the dykes.

Several shear zones formed in the high grade metamorphism were noted mainly in the central and eastern sections of the study area (Fig. 1.2). A major characteristic feature of these shear zones is the intimate occurrence of the almandine garnet porphyroblasts with growth concentrated along the biotite rich layers. The occurrence of these garnets give an insight into the metamorphic conditions operating at the time of deformation. Competent mafic lensoidal layers that have undergone ductile deformation and associated with rotated boudins (Plate 4.7) and displaced micro-faults define a sinistral sense of shear.

Faults were not a common feature in the survey area. However, strike-slip faults which owe their origin to mechanical failure of the rocks, were noted east of Kathuleni hills and along the major shear zones. Though no regional joint pattern was apparent in the area, the granitoid and psammitic gneisses around Kilango school showed five joint sets which include longitudinal and a-c joints (Plate 4.8). Pegmatites and aplites in Matuu area, dominantly of quartz and feldspathic composition, are variably intrusive (Plate 4.9) or segregational. The intrusive pegmatites are mainly confined to areas of more intense granitization. Since some of the pegmatites are deformed (Plate 4.10) in the shear zones, while others are not deformed, these pegmatites may potentially be used to bracket the age of the minor faults occurring in the shear zones.



Plate 4.7. Field photograph showing a rotated hornblende boudin in psammitic gneiss affected by a sinistral shear zone. Note the quartz-filled tensional gash developed in the boudin. Ndalani River, Matuu-Masinga area. Hammer is 25 cm long.



Plate 4.8. Field photograph showing longitudinal and a-c joints within a psammitic gneiss, Matuu-Masinga area, central Kenya.



Plate 4.9. Field photograph showing a zoned and faintly deformed feldspathic pegmatite. Note the chilled margins (5 cm in width) and coarsening of the grains as you move towards the core of the pegmatite. Pen-knife is 7 cm long.

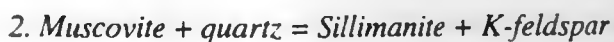


Plate 4.10 Field photograph showing deformed pegmatitic vein with a marked fracture cleavage conformable to the regional foliation planes. Mathauta River, south of Kilango, Matuu-Masinga area. Pencil is 13 cm long.

4.1.2 Metamorphism

The occurrence of the mineral assemblages quartz-muscovite-sillimanite-biotite-garnet and the hornblende-plagioclase-two pyroxene-garnet within some of the gneisses and dioritic intrusions of the study area give an insight of the P/T conditions that affected the area. In the shear zones for example, localized outcrops of garnetiferous biotite gneiss and muscovite schists 2 km east of Ndalani school (see Fig. 1.2) contained fibrous sillimanite along with minor apatite, microcline, carbonates and micas which are mostly of secondary derivation. The constituent minerals exhibit various features reflecting the effect of dynamic metamorphism. These include non-extinction patches, distorted cleavages, irregular or dislocated twin lamellae (especially in plagioclase), bent, fractured and abraded or kinked crystals, and strong undulose or anomalous extinction. The non-extinction patches possibly denote crushed particles or very large lattice strains, whereas the irregular twins may have formed from deformation and nucleation in areas of stress concentration (Marshall and McLaren, 1977).

With increase of metamorphic grade, the mineralogical breakdown of biotite and muscovite to form garnet and sillimanite respectively is governed by the reactions 1 & 2 below:



Clearly the high grade amphibolite and locally granulite facies appears to have had their imprints in the survey area. This observation concurs with that of Mathu and Tole (1984) and Suwa et al. (1979) from the regional survey area. This high grade metamorphism is further alluded to by the poor preservation of relict structures, abundant microfolds and the intensity of the shear zones.

There appears to exist a relationship between the intrusive bodies, the growth of the garnet metacrysts and the shear zones in the survey area. This relationship is exemplified by the observation that:

(a) the high temperature exomorphic zones of the emplaced intrusives appear to have provided the required energy and driving force of the necessary chemical constituents to account for the growth of large crystals of garnet along their margins. The garnet growth was noted to decrease in crystal size and abundance as one moves further away from the contact of the intrusive bodies. This phenomenon suggests a gradual drop in the grade of metamorphism with decreasing temperature.

(b) the elevated temperature along the exomorphic zones of the intrusives is envisaged to have made the contact rocks more susceptible to ductile deformation. With the onset of deformational forces, shear zones presently occurring adjacent to these intrusive bodies (Fig. 1.2) were formed.

Structures such as the shear zones, various foliation surfaces and linear structures, complex folds as well as strike-slip faults noted in the study area, all suggest a complex tectonic history of the region with at least three phases of deformation.

4.2 GEOCHRONOLOGICAL STUDIES

4.2.1 Nature of samples

Five co-magmatic samples of granitic composition from Mavoloni hill in Matuu area were used for dating. The five granitic rocks (MU-6A, -6B, -8, -10A, & -29) variably consists essentially of quartz, microcline and plagioclase with minor amounts of biotite and amphibole. Accessories are composed of apatite, epidote, sphene, magnetite, magnetite exhibiting exsolution with ilmenite and secondary hematite. Chemical compositions of these five samples are shown in Table 4.1.

Table 4.1. Chemical analyses of granite rock samples from Mavoloni hill, Matuu-Masinga area, central Kenya. Major elements in weight %.

Sample	MU-6A	MU-6B	MU-29	MU-8	MU-10
SiO ₂	70.44	69.04	65.54	70.43	66.76
TiO ₂	0.75	0.62	1.02	0.50	1.63
Al ₂ O ₃	13.43	13.80	14.02	13.79	13.33
Fe ₂ O ₃	5.95	4.70	6.31	3.34	4.45
MnO	0.06	0.06	0.09	0.04	0.18
MgO	0.99	0.79	1.16	0.58	1.75
CaO	2.24	1.80	2.62	1.35	2.96
Na ₂ O	3.79	3.49	3.40	3.57	3.46
K ₂ O	4.38	4.51	4.45	5.37	3.70
P ₂ O ₃	0.24	0.23	0.45	0.15	0.83
Total	102.27	99.04	99.01	99.12	99.05

4.2.2 Analytical method

Powdered samples for Rb-Sr whole-rock analysis were carefully prepared from 1-2 kg of rock. The procedure involved crushing the rocks into small chips. The rock chips were then ground in an agate mortar into powders after cleaning with dilute HCL solution and distilled

water. Rb and Sr contents were determined at first with X-ray fluorescence method and then determined with the conventional isotopic dilution method. Relative errors of $^{87}\text{Rb}/^{86}\text{Sr}$ ratios were estimated to be less than 2%. $^{87}\text{Sr}/^{86}\text{Sr}$ ratios were determined on unspiked samples using the JEOL-O5RB mass spectrometer. All errors associated with isotopic ratios are listed in Table 4.2 at 2 sigma level. Decay and other constants used in the age calculations are as recommended in Steiger and Jager (1977). The isochron age was calculated by the least-square method of York (1966) with least square residual of 2.54% and MSWD of 0.85.

Table 4.2. Rb-Sr analytical data for granite samples from Matuu area, central Kenya.

Sample	Rb (ppm)	Sr (ppm)	$^{87}\text{Rb}/^{86}\text{Sr}$	$^{87}\text{Sr}/^{86}\text{Sr}$	2 sigma mean
MU - 6A	96	336	0.01048	0.703957	0.000015
MU - 6B	94	257	0.05489	0.704487	0.000021
MU - 29	92	410	0.64440	0.709059	0.000024
MU - 8	81	518	0.45382	0.707539	0.000015
MU - 10	75	676	0.31863	0.706622	0.000025

4.2.3 Results

With reference to Fig. 4.2, five data points define an isochron of 558 +/- 16.5 Ma with initial $^{87}\text{Sr}/^{86}\text{Sr}$ ratio of 0.70398 +/- 0.00008. The Rb/Sr ratios of the rocks are well spread and hence a reasonably good isochron was obtained. This age compares with Rb/Sr whole rock ages and initial isotope ratios of 566 +/- 30 Ma and 0.7042 +/- 0.0004 and 572 +/- 20 Ma and 0.7045 +/- 0.0006 reported on Lolmungi (G4) and Moruposi (G3) granite series respectively along strike in the Mozambique belt of North-central Kenya (Key et al., 1989).

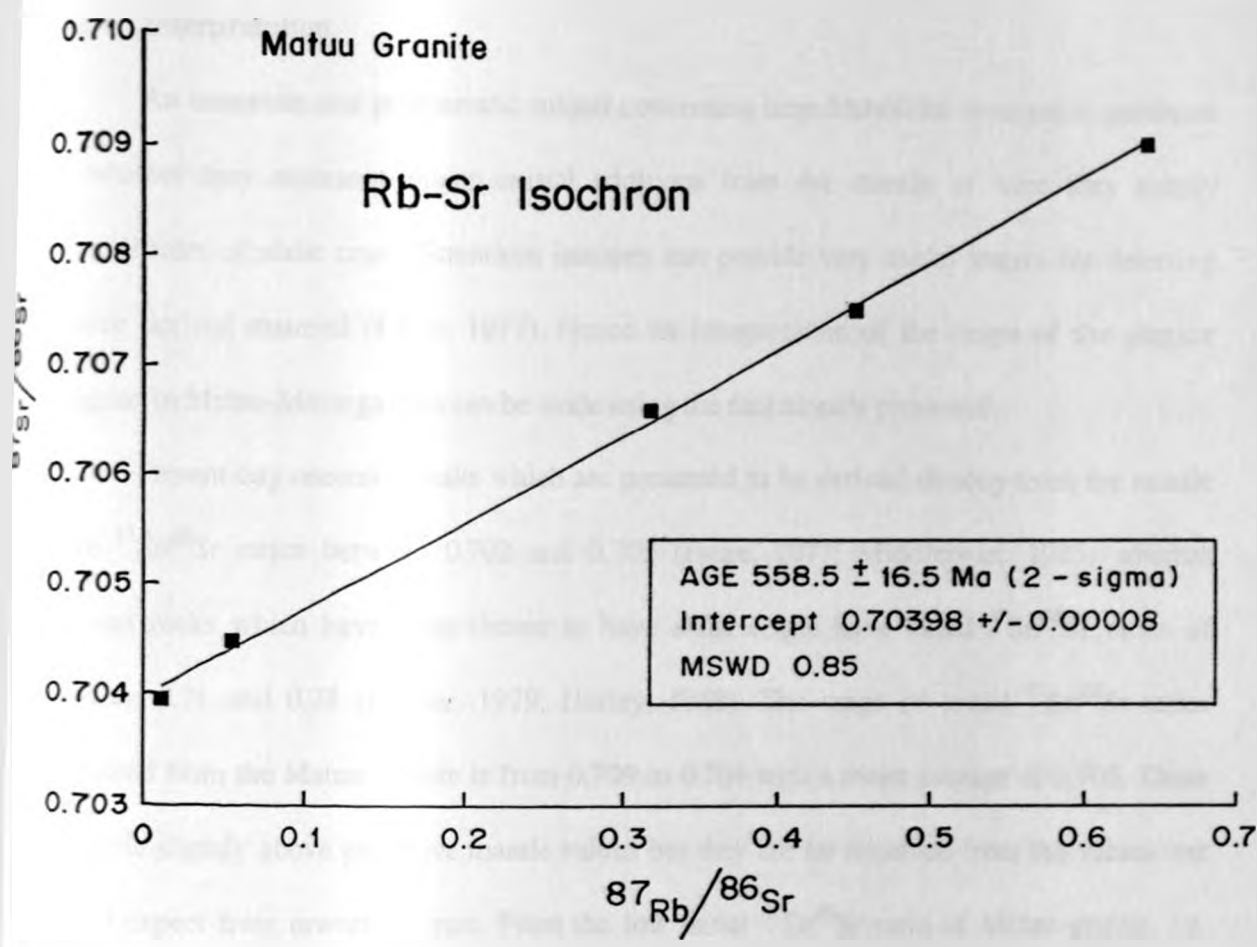


Figure 4.2 . Isochron diagram for granite from Matuu area, central Kenya.

4.2.4 Interpretation

An important and problematic subject concerning large batholiths in orogenic provinces is whether they represent major crustal additions from the mantle or were they simply remobilisates of sialic crust. Strontium isotopes can provide very useful tracers for detecting mantle derived material (Faure, 1977). Hence an interpretation of the origin of the granitic magmas in Matuu-Masinga area can be made using the data already presented.

Present day oceanic basalts which are presumed to be derived directly from the mantle have $^{87}\text{Sr}/^{86}\text{Sr}$ ratios between 0.702 and 0.705 (Faure, 1977; Middlemost, 1985) whereas igneous rocks which have been shown to have sialic origin have initial $^{87}\text{Sr}/^{86}\text{Sr}$ ratios of between 0.71 and 0.78 (Pitcher, 1979; Hurley, 1968). The range of initial $^{87}\text{Sr}/^{86}\text{Sr}$ ratios measured from the Matuu granite is from 0.709 to 0.704 with a mean average of 0.705. These ratios lie slightly above primitive mantle values but they are far removed from the values one would expect from reworked crust. From the low initial $^{87}\text{Sr}/^{86}\text{Sr}$ ratio of Matuu granite, i.e. 0.70398, the age is interpreted to indicate the time of original emplacement for granitic magma formed from a juvenile mantle-derived material or if a significant amount of pre-existing continental crust was reworked during this period, it was either very young crust, or it had low Rb/Sr ratios comparable to those in some parts of the lower crust or in the upper mantle. In any case there is no possibility of a long crustal history for these rocks (i.e. recycled material) before this event, and the rocks therefore cannot be reworked material of Archaean age.

4.3 CONCLUSION

Evidence obtained from the structural, metamorphic and geochronological studies of Matuu-Masinga area have shown that:

- (a) The structural trend of the area varies from NNW-SSE to NW-SE with westerly dips ranging from 50° to the vertical. On stereographic projection, the poles to foliation exhibit imperfect monoclinic symmetry with a high degree of homogeneity for a fold axis in a direction of 291° .
- (b) That the area suffered a complex tectonic history with at least three phases of deformation that are documented by various shear zones, foliation surfaces and linear structures, complex folds as well as strike-slip faults.
- (c) High grade amphibolite and locally granulite facies metamorphism had their imprint in the study area. This is evidenced by the presence of the hornblende- plagioclase-two pyroxene-garnet and quartz-muscovite-sillimanite-biotite-garnet mineral assemblages in the rock units of the study area.
- (d) The whole-rock age of 558 ± 16 Ma for granite rock from the area with the low initial $^{87}\text{Sr}/^{86}\text{Sr}$ ratio of 0.70398 ± 0.00008 is interpreted to indicate the time of original emplacement for granitic magma formed from a juvenile mantle-derived material or if a significant amount of pre-existing continental crust was reworked during this period, it was either very young crust, or it had low Rb/Sr ratios comparable to those in some parts of the lower crust or in the upper mantle.

CHAPTER FIVE

CONCLUSIONS

Based on the objectives of the present study, many interesting features concerning the crustal evolution of the Mozambique Belt rocks in Matuu-Masinga area have been recognized. The conclusions listed below, except for those asterisked, are entirely new data produced during this study. The asterisked ones are, in part, the result of previous work; they are relevant to this study and must be included in this chapter.

5.1 PETROGRAPHY

Evidence obtained from the field, petrographical and mineralogical features of the Matuu-Masinga rock suites were as follows:

- 1) As a result of the present study, a new detailed geological map at a scale of 1:50,000 with more structural features and rock suites that were previously undifferentiated have been identified and differentiated respectively. Previous geological map of the study area have been mapped at a scale of 1:125,000.
- 2) The characteristic mineral assemblages are quartz, plagioclase, K-feldspar, hypersthene, diopside, augite, garnet, spinel, biotite and hornblende with accessory sphene, chlorite, epidote, apatite and Fe-Ti oxides.
- 3) The anorthositic gabbros of Matuu-Masinga area are marked by an ubiquitous replacement of the original pyroxene by a corona of green amphibole. This contrasts strongly with the anorthosites occurring along strike from the Ishiara and Mituguu areas that are notably associated with olivine and subsequent metamorphic coronas around the olivines.

5.2 STRUCTURAL EVOLUTION

- 1) The structural trend of the area varies from NNW-SSE to NW-SE with westerly dips ranging from about 50° to the vertical. On stereographic projection, the poles to foliation exhibit imperfect monoclinic symmetry with a high degree of homogeneity for a fold axis in a direction of 310° .
- 2) The study area suffered a complex tectonic history with at least three phases of deformation that are documented by various shear zones, foliation surfaces and linear structures, complex folds as well as strike-slip faults.
- 3) Based on field evidence, the Matuu-Masinga anorthositic rocks are interpreted as moderate to thick sheets that have been intruded into the gneisses and boudinaged on a large scale during the last phases of the regional metamorphism.
- * 4) In the regional context, the mafic bodies of Matuu-Masinga area are tentatively correlated with:
 - (a) the large meta-gabbro / mafic orthogneiss bodies mapped to the north of the present survey area, in particular those to the east of Chuka around the Ntungi, Kiero and Engakuni hills, and Chanlers Falls (Williams, 1966) and Barchuma-Kom areas (Dodson, 1991).
 - (b) the occurrence of the roughly N-S linear belt of a series of anorthositic and gabbro-norite suites from Mozambique to northern Tanzania that have similar mineralogy and featuring granulite facies assemblages (Andreoli, 1991).

5.3 METAMORPHISM

- 1) Field and petrographic studies suggest that the Matuu-Masinga area firstly experienced regional prograde granulite metamorphism which was later downgraded to the amphibolite- and greenschist-facies. Evidence for the high grade granulite metamorphism is obtained from the hypersthene-clinopyroxene-plagioclase mineral associations of the mafic gabbroic and dioritic rocks.
- 2) Retrogression of the granulite-facies metamorphism into amphibolite- and greenschist-facies is documented by petrographic features such as sericitization of feldspars, the partial break-down of clinopyroxene into clinopyroxene-hornblende-biotite reaction rims, symplectization of pyroxene by biotite and quartz, development of myrmekites and growth of minerals such as muscovite, chlorite, epidote and sphene.
- 3) Based on textural and mineral associations, the coronas developed around clinopyroxene crystals in the meta-diorite and gabbroic rocks of Matuu-Masinga area are interpreted to have developed under metamorphic conditions.
- 4) Disposition of the metamorphic facies with respect to the thermobarometric conditions and major structures suggests that metamorphism was related to tectonic thickening.
- 5) The scarcity of granulitic material in the cratonic areas and in the Arabian-Nubian Shield compared with their comparative abundance in the Mozambique belt of East Africa supports interpretation of continent-continent collision model which caused crustal thickening.
- 6) Superimposed on the regional metamorphism was a late high T contact metamorphism associated with granitic intrusions.

5.4 MINERAL CHEMISTRY

- 1) The clinopyroxene grains in the dioritic and gabbroic rocks range from diopsidic ($\text{Ca}_{45.98} \text{Mg}_{38.40} \text{Fe}_{15.62}$) to mainly augite in composition ($\text{Ca}_{42.80} \text{Mg}_{38.01} \text{Fe}_{19.19}$). The orthopyroxene crystals are mainly of hypersthene composition ($\text{Ca}_{2.36} \text{Mg}_{57.19} \text{Fe}_{40.45}$). Clinopyroxenes of Matuu area are in general enriched in Al, Ti, Cr, and Na relative to the coexisting orthopyroxene, and the reverse is true for Mn.
- 2) A composition plot of representative clinopyroxenes in the Ca-Mg-Fe triangular diagram show the grains to be of typical alkaline rocks affinity. This is in agreement with the chemistry and mineralogy of the rocks from which these clinopyroxenes were extracted.
- 3) Evidence provided by the distribution of aluminium among the tetrahedral and octahedral sites in the orthopyroxene and clinopyroxene analyses in the dioritic rock is that the clinopyroxenes must have crystallized under higher pressure than their corresponding iron rich orthopyroxenes. On the other hand, the almost equal amounts of jadeite (Al^{VI}) and Ca-Tschermak (Al^{IV}) in the clinopyroxenes of the gabbroic rocks indicate that they could have resulted from the combined effects of high pressure and high temperature.
- 4) The amphibole occurring in the dioritic rock have a composition that straddles the boundary between ferroan pargasitic- and pargasitic hornblende; while those occurring in the gabbroic rocks are mainly the calcic edenitic hornblende and magnesio-hornblende. The composition of the amphiboles occurring in the amphibolite rocks straddle between the calcic edenitic hornblende and ferroan pargasitic hornblende.

- 5) The plagioclase in the gabbro rocks range in composition from labradolite ($An_{62.58 - 67.05}$) through bytownite (An_{86}) to anorthite (An_{93}). The primary plagioclase in the dioritic rock has an average composition of calcic andesine (An_{35}). A secondary Sr-rich plagioclase was noted to have a common occurrence in the diorite (av. 6.51 wt.% SrO), amphibolite (av. 5.36 wt.% SrO), syeno-diorite (av. 7.75 wt.% SrO) and in the pink granite (av. 8.60 wt. % SrO) rocks.
- 6) The mineral chemistry of the K-feldspar, plagioclase and biotite occurring in the granitic rocks from Matuu area suggest a paragenetic sequence of the order : grey granite < pink granite < porphyritic granite.
- 7) The grossularite content of the almadine-rich garnets occurring in Matuu area is consistently high, ranging between 65 - 82 molecular percent.

5.5 THERMOBAROMETRIC CONDITIONS

- 1) Studies of the magnesium /iron distribution between coexisting calcium-rich and calcium poor pyroxene minerals in the meta diorite rock point to a temperature of crystallization corresponding to igneous in origin than that required by other pyroxenes of similar bulk composition of metamorphic origin.
- 2) The thermobarometric PT calibrations obtained from various mineral pairs occurring in the major mafic rocks is as follows: a temperature of 750 °C and pressures between 6.55 to 6.98 kbars for the amphibolite rocks, to temperatures between 879-904 °C and pressures between 5.89 to 6.31 kbars for the gabbroic rocks, to temperatures between 843-854 °C and a pressure of 15 kbar for the dioritic rock.
- 3) The use of Al-in-amphibole geothermometric data for the granite rocks gave an average equilibrium temperature of 750 °C and a pressure of 5.97 kbar.

5.6 GEOCHRONOLOGY

- 1) A Rb-Sr whole rock age of 558 +/- 16 Ma is given on the Mavoloni hills granite from Matuu area.
- 2) From the low initial $^{87}\text{Sr}/^{86}\text{Sr}$ ratio of 0.70398 recorded from the Matuu granite, the age is interpreted to indicate the time of original emplacement for granite magma from a juvenile mantle-derived material. However, if a significant amount of pre-existing continental crust was involved during this period, it was either a very young crust or it had low Rb/Sr ratios comparable to those in some parts of the lower crust or in the upper mantle.
- 3) The new whole rock Rb-Sr data presented here confirm the existence of the Neoproterozoic (Pan-African) tectonothermal event in the Mozambique Belt of Kenya. The data from the Matuu-Masinga area granite rocks show no evidence for the presence of older reworked (thermally overprinted) late Archean to mid-Proterozoic crustal precursors, a possibility suggested also from the Rb-Sr data of Shibata and Suwa (1979) for the Mbooni hills granitoids and gneisses.
- 4) Large volume of granitic magma derived from the mantle and intruded into the upper crust lead to the conclusion that the Pan African belt in Matuu area was a site of major crustal accretion event.

5.7 GEOCHEMISTRY

- 1) The rocks of Matuu-Masinga area, mainly of magmatic origin, are mainly metaluminous to slightly peraluminous.
- 2) The granitic rocks, which show signatures of dominantly I-type with subordinate S-type affinities, are mainly of calc-alkaline origin.
- 3) The rocks of Matuu-Masinga area have a dominantly island arc-tectonic setting with subordinate within-plate affinities. The effect of a within-plate component in the trace elements suggests the influence of the sub-continental lithosphere in magma genesis.
- 4) The relatively low range of strontium initial ratios (0.7039-0.7091) for the granitic and mafic rocks in the study area implies that their protoliths were probably of juvenile Pan-African origin.
- 5) The rocks in Matuu-Masinga area, with high Ba (av. 1331 ppm) and Zr (av. 370 ppm) contents, are petrographically interpreted to have contained hornblende and biotite mineral assemblage phases that had a relatively high distribution coefficients for Ba and Zr.
- 6) The relatively high concentration of Cu (188-5810 ppm, av. 1960 ppm) and Zn (88-264 ppm, av. 155 ppm) in the mafic rocks of the study area compared with the average for ultramafic rocks of 30 ppm and 50 ppm reported by Goles (1967) and Turekian and Wedepohl in Scotford and Williams (1983) respectively invokes further exploration of these ore minerals.
- 7) The mafic rocks have a relatively high contents of Cr (av. 160 ppm) and Ni (av. 55 ppm). Thus, if these rocks are derived from mafic melts of the mantle (i.e. as

inferred from their low initial $^{87}\text{Sr}/^{86}\text{Sr}$ ratios), little fractionation of the mafic phases is implied.

5.8 ECONOMIC MINERAL POTENTIAL

The role of metallogenic heritage in the Mozambique belt of Kenya is shown by the following evidence:

- 1). The determined Cu (188-5810 ppm, av. 1960 ppm) and Zn (88-264 ppm, av. 155 ppm) occurrences in the gabbroic rocks of Matuu-Masinga area from this study, make this region a target area for subduction related mineralization.
- 2). Reported copper, chromite and nickel occurrences in Tsavo East and south of Voi (up to 2.21 wt.% Cu) (Pulfrey and Walsh, 1969; Frisch and Pohl, 1986); in the ultramafic/ mafic bodies found at Sekerr mountain in west Pokot Baragoi District, north-central Kenya (Pulfrey and Walsh, 1969; Key, 1987) and the nickeliferous serpenitised dunite intrusives in Isiolo area (Hackman et al., 1989) make these target areas for metal exploration.
- 3). Magnetite/ilmenite occurrences in charnockites, gneisses, anorthosites and associated pegmatites are known to occur in Marimanti, central Kenya, Ikutha, Kitui District, and Wanjala, SE Kenya. Natural concentrations of these primary deposits are found along the river mouths and beach shores (e.g., Kipini, Mamburui, Fundisha etc.) of the Tana and Athi in the coastal region.
- 4). Magnesite veinlets and stockwork bodies in dunites have been reported to occur e.g., at Kinyiki Hill and Mtito-Andei area in SE Kenya (Pohl et al., 1980), Baragoi District, south Kapoponi Hill in Kitui District and in the Embu District.

- 5). Economic deposits of wollastonite (with an average grade of 38% pure wollastonite and approximately 670,000 tonnes) and limestone have been found to occur at Lolkidongai in Kajiado District, southern Kenya (Saltikoff et al., 1991) and in Kajiado and West Pokot Districts respectively.
- 6). Coloured gemstones mainly tourmaline, green vanadium grossularite, red garnet, aquamarine, rose quartz, amazonite, emerald, the blue zoisite (tanzanite), the red ruby (corundum) and sapphire have been reported to occur mainly in the Embu and Meru District, Baragoi, Taita-Taveta, and at Cherangani Hills in west Pokot (Pulfrey and Walsh, 1969; Pohl et al., 1980).

5.9 RECOMMENDATIONS FOR FURTHER WORK

The recommendation for further research work is as follows:

- 1). To extend the mapping and related research to adjacent segments of the Mozambique belt with the aim of quantifying the P-T conditions for the essentially amphibolite and locally granulite facies metamorphism of the belt that have not been precisely determined.
- 2). The age of the gabbro and diorite rocks in Matuu area remain undated. A geochronological study (e.g., using Rb/Sr, Nd/Sm and U-Pb methods) of these rocks will further constrain the tectonic evolution of this segment of the belt.
- 3). Further investigations of the tectonic setting of the regional area is required.
- 4). For resource-oriented surveys, the Matuu area mafic rocks potential for subduction related mineralization is inferred. The determined Cu-occurrences in the gabbroic rocks makes this a new target area for metal exploration.

5). Given the good road network and the proximity of the study area to the developing cities of Thika and Nairobi, the occurrence of granites in Matuu-Masinga area should be further evaluated to establish their economic potential in the construction and building industry. Presently, the Athi River Mining company is carrying out a small-scale mining of the pink granite in the survey area as a dimension stone for the construction Industry.

* * * *

REFERENCES

- Almond, D.C. 1984. The concept of "Pan-African Episode" and "Mozambique Belt" in relation to the geology of east and north-east Africa. *Bulletin of the Faculty of Earth Sciences, King Abdulaziz University*, **6**, 71-78.
- Alpieti, T. and Sivonen, S.J. 1983. Use of the electron microprobe in the investigation of the Early Proterozoic Koillismaa igneous complex, NE Finland. Geological Survey of Finland, *Investigation Report*, **61**, 22pp.
- Andreoli, M.A. 1984. Petrochemistry, tectonic evolution and metasomatic mineralisations of Mozambique belt granulites from S. Malawi and Tete (Mozambique). *Precambrian Research*, **25**: 161-186.
- Andreoli, M.A. 1991. Petrological markers in terrane analysis: massif anorthosites, high pressure granulites and scapolitized rocks from the Mozambique Belt, Southern Malawi. In: UNESCO, Geology for Economic Development, *Bulletin/Newsletter*, **8**, pp 43-55.
- Andriessen, P.A.M., Coolen, J.J.M.M.M. and Hebeda, E.H. 1985. K-Ar hornblende dating of late Pan-African metamorphism in the Furua granulite complex of southern Tanzania. *Precambrian Research*, **30**: 351-360.
- Arth, J.G. 1976. Behaviour of trace elements during magmatic processes - A summary of theoretical models and their application. U.S. Geological Survey, *Journal of Research*, **4**, 41-47.
- Azzouni-Sekkal, A. and Boissonnas, J. 1987. Geochemistry of the Tioueine Pan-African granite complex, Hoggar, Algeria. *Geological Journal*, **22**. Thematic issue, 213-224.
- Baldwin, A.J. and Pearce, J.A. 1982. Discrimination of productive and non-productive porphyritic intrusions in the Chilean Andes. *Economic Geology*, **77**, 664-674.

- Baker, B.H. 1963. Geology of the Baragoi area. *Report of the Geological Survey of Kenya*, No. 53.
- Bear, L.M. 1952. The Geology of the area south-east of Embu. Geological Survey of Kenya. *Report No. 23*, 45 pp.
- Berhe, S.M. 1990. Ophiolites in North-East and East Africa: implications for the Proterozoic crustal growth. *Journal of Geological Society, London*, **147**, 41-57.
- Biyajima, K., Suwa, K. and Miyakawa, K. 1975. Mantled gneiss dome in the Mozambique belt around the Machakos area, Kenya. *1st Preliminary Report on African Studies*, pp 6-13. Nagoya University, Japan.
- Blundy, J.D. and Holland, T.J.B. 1990. Calcic amphibole equilibria and a new amphibole-plagioclase geothermometer. *Contributions to Mineralogy and Petrology*, **104**, 208-224.
- Bohlen, S.R. and Essene, E.J. 1977. *Contributions to Mineralogy and Petrology*, **62**, 153-169.
- Bowen, N.L. 1956. *The evolution of igneous rocks*. Dover Publication, New York.
- Brey, G.P. and Kohler, T. 1990. Geothermobarometry in four-phase lherzolites. II. New thermobarometers, and practical assessment of existing thermobarometers. *Journal of Petrology*, **31**, 1353-1378.
- Brodie, K.H. and Rutter, E.H. 1985. On the relationships between deformation and metamorphism with special reference to the behavior of basic rocks. In A.B. Thompson and D.C. Rubie, (eds.), *Metamorphic reactions, kinetics, textures and deformation*, pp 138-179. Springer-verlag, New York.
- Burke, K.C. and Sengor, C. 1986. Tectonic escape in the evolution of continental crust. In M. Barazangi and L. Brown (eds.), *Reflection seismology: The continental crust*, pp 41-53. Washington, D.C. : American Geophysical Union.

- Cohen, L., Snelling, N.J., Delhal, T. and Vail, J.R. 1984. *The Geochronology and Evolution of Africa*. 512 pp. Clarendon Press, Oxford.
- Charsley, T.J. 1987. Geology of the Laisamis area. *Report of the Mines and Geological Department, Kenya*, 106, 70 pp.
- Coolen, J.J., Priem, H.N., Verdürmen, E.A. and Verschure, R.H. 1982. Possible zircon U-Pb evidence for Pan-African granulite-facies metamorphism in the Mozambique belt of southern Tanzania. *Precambrian Research*, 17, 31-40.
- Cox, K.G., Bell, J.D. and Pankhurst, R.J. 1979. *The Interpretation of Igneous Rocks*. London: Allen & Unwin, 450 pp.
- Daly, M.C. 1986. The intercratonic Irumide belt of Zambia and its bearing on collision orogeny during the Proterozoic of Africa. In: M.P. Coward and A.C. Ries (eds.), *Collision tectonics*, pp 321-328. Geological Society Special Publication. 19.
- Davies, A., Blackburn, W.H., Brown, W.R. and Ehmann, W.D. 1978. Trace element geochemistry and origin of late Precambrian-early Cambrian Catoclin greenstones of the Appalachian Mountains. University of California at Davies, *Report (unpublished)*.
- Deer, W.A., Howie, R.A. and Zussman, J. 1967. Rock-forming minerals. Vol. 2. Chain Silicates. Longmans, London, 379 pp.
- Deer, W.A., Howie, R.A. and Zussman, J. 1963. Rock-forming minerals. Vol. 3, Sheet Silicates. Longmans, Green and Co Ltd., London, 265 p.
- Dodson, R.G. 1991. Geology of the Barchuma-Kom area. *Mines and Geological Department Report*, 93, 72 pp.
- Du Bois, C.G.B. and Walsh, J. 1970. Minerals of Kenya. *Geological Survey of Kenya Bulletin*. 11, 82 pp.

- Eckert, J.O., Jr., Newton, R.C. and Kleppa, O.J. 1991. The ΔH of reaction and recalibration of garnet-pyroxene-plagioclase-quartz geobarometers in the CMAS system by solution calorimetry. *American Mineralogist*, **76**, 148-160.
- Edelman, N. 1985. Explanation to the maps of Pre- Quaternary rocks. Sheet 1034. Summary in English on Pre-Quaternary rocks of the Nauvo map sheet area. *Geological Survey of Finland, Espoo*. 47pp.
- Ellis, D.J. and Green, D.H. 1979. An experimental study of the effect of Ca upon garnet-clinopyroxene Fe-Mg exchange equilibria. *Contributions to Mineralogy and Petrology*, **71**, 13-22.
- Ellis, D.J. 1980. Osumilite-sapphirine-quartz granulites from Enderby Land, Antarctica: P-T conditions of metamorphism, implications for garnet-cordierite equilibria and the evolution of the deep crust. *Contributions to Mineralogy and Petrology*, **74**, 201-210.
- Emslie, R.F. 1983. The coronitic Michael gabbros, Labrador: assessment of Grenvillian metamorphism in northeastern Grenville Province. *Current Research, Part A, Geological Survey of Canada, Paper 83-1A*, 139-145.
- Fairburn, W.A. 1958. Geology of the Fort Hall area. Geological survey of Kenya, *Report No. 73*, 47 pp.
- Fairburn, W.S., 1963. Geology of the North Machakos-Thika area. Geological Survey of Kenya. *Report No. 59*. 43 pp.
- Faure, G. 1977. *Principles of Isotope Geology*. New York: Wiley, 266pp.
- Frisch, W. and Pohl, W. 1986. Petrochemistry of some mafic and ultramafic rocks from the Mozambique Belt, SE Kenya. *Mitteilungen Osterreichischen Geologischen Gesellschaft*, **78**, 97-114.

- Gabert, G. and Wendt, I. 1974.** Datierung von granitische Gesteinen im Dodoman- und Usagaran-system und in der Ndembera series (Tanzania). *Geologie Jahrbuch*, **B 11**, 3-55.
- Gabert, G. 1984.** Structural-lithological units of Proterozoic rocks in East Africa, their base, cover and mineralisation. In: J. Klerkx and J. Michot (eds.), *African Geology*, pp 11-21. Tervuren.
- Gaciri, S.J., Altherr, R., Nyamai, C.M. and Mathu, E.M. 1993.** Distribution of elements in mineral pairs from Mozambique belt rocks of Matuu area, central Kenya. In Opiyo-Akech, N., Ed., *Proceedings of the 5th Conference on the Geology of Kenya - Geology for sustainable Development*, pp 57-62. UNEP/ UNESCO, Nairobi.
- Gleadow, A.J.W. 1980.** Fission track age of the KBS Tuff and associated hominid remains in northern Kenya. *Nature*, **284**, 225-230.
- Goles, G.G. 19677.** Trace elements in ultramafic rocks. In P.J. Wyllie, Ed., *Ultramafic and related rocks*, pp. 352-362. John Wiley and Sons, Inc.
- Hackman, B.D., Charsley, T.J., Kagasi, J., Key, R.M., Siambi, W.S. and Wilkinson, A.F. 1989.** Geology of the Isiolo area. *Report of the Mines and Geological Department, Kenya*. 103,88 pp.
- Hammarstrom, J.M. and Zen, E-an. 1986.** Aluminium in hornblende: an empirical igneous geobarometer. *American Mineralogist*, **71**. 1297-1313.
- Hanski, E. 1983.** Alkuaineiden jakaantuminen mineraalien ja silikattien kesken: Jakaantumiskertoimet. Arkeisten alueiden malmiprojekti. *Raportti 15*. 179p. University of Oulu, Finland.

- Hanski, E. and Smolkin, V.F. 1990.** Thick, layered ferropicrites flows in the Pechenga area. Kola Peninsula and their relation to associated Ni-Cu deposits. International Volcanology Congress, 3-8 Sept. 1990, Mainz (FGR), *Abstracts*.
- Hepworth, J.V. 1972.** The Mozambique orogenic belt and its foreland in north-east Tanzania : a photogeologically-based study, *Journal of Geological Society, London*, **128**, 461-500.
- Hole, M.J., Saunders, A.D., Marriner, G.F. and Tarney, J. 1984.** Subduction of pelagic sediments: implications for the origin of Ce-anomalous basalts from the Marianas Islands. *Journal of Geological Society, London*, **141**, 453-472.
- Hollister, L.S., Grissom, G.C., Peters, E.K., Stowell, H.H. and Sisson, V.B. 1987.** Confirmation of the empirical correlation of Al in hornblende with pressure of solidification of calc-alkaline plutons. *American Mineralogist*, **72**, 231-239.
- Holmes, A. 1951.** The sequence of Pre-Cambrian orogenic belts in south and central Africa. *18th International Geological Congress, London (1948)* **14**, 254-269.
- Huddleston, A. 1951.** Geology of the Kisii District. Degree sheet 41, S.E. Quadrant. *Geological Survey Report*, **18**, 64 pp.
- Hutton, C.O. 1950.** Studies of heavy detrital minerals. *Bulletin of the Geological Society of America*, **61**, p.635.
- Hurley, P.M. 1968.** The confirmation of continental drift. *Scientific America*, **218**, 52-64.
- Inoue, H. and Suwa, K. 1979.** Petrographical note on Staurolite-Kyanite-almandine pelitic gneiss occurring at the western foot of the Mbooni Hills. Machakos area. Kenya - with special reference to the ZnO content in Staurolite. *4th Preliminary Report on African Studies*, pp 97-111. Nagoya University, Japan.

- Irvine, T.N. and Baragar, W.R.A. 1971. A guide to the chemical classification of common volcanic rocks. *Canadian Journal of Earth Science*, **8**, 523-548.
- Ishihara, S. 1980. The granitoid series and mineralization. In: Economic Geology. *Economic Geology Anniversary vol.*, **75**, 484-558. Lancaster, Pennsylvania.
- Jensen, L.S. 1976. A new cation plot for classifying subalkalic volcanic rocks. *Ont. Dep. Min. Misc. Pap.* **66**, 1-22.
- Jennings, D.J. 1967. Geology of the Archer's Post area. Report of the Geological Survey of Kenya, No.77.
- Johnson, M.C. and Rutherford, M.J. 1989. Experimental calibration of the aluminum-in-hornblende geobarometer with application to Long Valley Caldera (California) volcanic rocks. *Journal of Geology*, **17**, 837-841.
- Kazmin, V., Shifferaw, A. and Balcha, T. 1978. The Ethiopian basement: Stratigraphy and possible manner of evolution. *Geologische Rundschau*, **67**, 531-546.
- Kennedy, W.Q. 1964. The structural differentiation of Africa in the Pan-African (+/- 500 m.y) tectonic episode. *Annual Report of the Research Institute of African Geology, University of Leeds*, **8**, 28-49.
- Kerrick, R. and Fyfe, W.S. 1981. The gold-carbonate association: source of CO₂ and CO₂ fixation reactions in Archaean lode deposits. *Chemical Geology*, **33**, 265-294.
- Key, R.M., Charsley, T.J., Hackman, B.D., Wilkinson, A.F. and Rundie, C.C. 1989. Superimposed upper Proterozoic collision-controlled orogenises in the Mozambique orogenic belt of Kenya. *Precambrian Research*, **44**, 197-225.
- Key, R.M. 1987. Geology of the Maralal area. *Report of the Mines and Geological Department, Kenya*, **105**. 93 pp.

- Kretz, R. 1961.** Some applications of thermodynamics to coexisting minerals of variable composition. Examples, orthopyroxene-clinopyroxene and orthopyroxene-garnet. *Journal of Geology*, **69**, 361-387.
- Kretz, R. 1963.** Distribution of magnesium and iron between orthopyroxene and calcic pyroxene in natural mineral assemblages. *Journal of Geology*, **71**, 773-785.
- Krogh, E.J. 1988.** The garnet-clinopyroxene Fe-Mg geothermometer: A re-interpretation of existing experimental data. *Contributions to Mineralogy and Petrology*, **99**, 44-48.
- Kröner, A. 1984.** Late Precambrian plate tectonics and orogeny: a need to re-define the term Pan-African. In: J. Klerkx and J. Michot (eds.), *African Geology*, pp 23-28, Tervuren.
- Leake, B.A. 1978.** Nomenclature of amphiboles. *American Mineralogist*, **63**, pp 1023- 1052.
- Leake, B.A. 1968.** A catalog of analyzed calciferous and sub-calciferous amphiboles together with their nomenclature and associated minerals. *Geological Society of America Special Paper*, **98**, 210 pp.
- Le Bas, M.J. 1962.** The role of aluminium in igneous clinopyroxene with relation to their parentage. *American Journal of Science*, **260**, 267-288.
- Leeman, W.P. 1983.** The influence of crustal structure on compositions of subduction-related magmas. *Journal of Volcanology and Geothermal Research*, **18**, 561-588.
- Maboko, M.A.H., Boelrijk, N.A.I.M., Priem, H.N.A. and Verdurmen, E.A.Th. 1985.** Zircon U-Pb and biotite Rb-Sr dating of the Wami River granulites, eastern granulites, Tanzania: evidence for approximately 715 Ma old granulite facies metamorphism and final Pan-African cooling approximately 475 Ma ago. *Precambrian Research*, **30**, 361-378.

- Malisa, E. and Muhongo, S. 1990.** Tectonic setting of gemstone mineralization in the Proterozoic metamorphic terrane of the Mozambique belt in Tanzania. *Precambrian Research*, **46**, 167-176.
- Marshall, D.B. and McLaren, A.C. 1977.** Deformation mechanisms in experimentally deformed plagioclase feldspars. *Physical Chemistry of Minerals*, **1**, 351-370.
- Mathu, E.M. and Tole, M.P. 1984.** Geology of Ithanga hills area in Kenya. *Journal of African Earth Sciences*, **2**, 1-16.
- Mathu, E.M., Ngecu, W.M., Nyamai, C.M. and Davies, T.C. 1991.** Proterozoic Island Arc Tectonism in the Kenyan Mozambique belt east of Nairobi. International Fieldworkshop on the crustal Evolution of the Mozambique belt of Eastern Africa (continent), Tanzania, 1991. *Extended Abstracts & Abstracts*, p. 59.
- McLelland, J.M. and Whitney, P.R. 1977.** The origin of garnet in the anorthosite-chamokite suite of the Adirondacks. *Contributions to Mineralogy and Petrology*, **60**, 161-181.
- McWilliams, O. 1981.** Palaeomagnetic and Precambrian tectonic evolution of Gondwana. In: A.Kröner (ed.), *Precambrian plate tectonics*, pp. 649-687. Amsterdam: Elsevier.
- Middlemost, E.A.K. 1985.** *Magmas and Magmatic rocks*. New York. Wiley. 266 pp.
- Miyake, A. and Suwa, K. 1981.** Geological structure of the Uvete dome, Kenya. *6th Preliminary Report on African Studies*, pp 33-41. Nagoya University, Japan.
- Miyashiro, A. 1978.** Nature of alkalic volcanic rock series. *Contributions to Mineralogy and Petrology*, **66**, 91-104.
- Mori, T. and Green, D.H. 1976.** Sub-solidus equilibria between pyroxenes in the CaO-MgO-SiO₂ systems at high pressures and temperatures. *American Mineralogist*, **61**, 616-625.

- Mosley, P.N. 1993. Geological Evolution of the Late Proterozoic "Mozambique Belt" of Kenya. *Tectonophysics*, 221, 223-50.
- Muhongo, S. 1989. Tectonic setting of the Proterozoic metamorphic terrains in eastern Tanzania and their bearing on the evolution of the Mozambique belt. UNESCO. IGCP Project 255. *Bulletin/Newsletter*, 2, 43- 50.
- Muhongo, S. 1991. The Mozambique Belt: a polyorogenic mobile belt. UNESCO. Geology for Economic Development. *Newsletter/Bulletin*, 8, 5-14.
- Muhongo, S. and Lenoir, J.L. 1993. Pan-African granulite-facies metamorphism in the Mozambique Belt of Tanzania: evidence from U-Pb on zircon geochronology. *Journal of the Geological Society, London*, 151, 343-347.
- Muhongo, S. 1994. Neoproterozoic collision tectonics in the Mozambique belt of East Africa: evidence from the Uluguru Mountains, Tanzania. *Journal of African Earth Sciences*, 19, 153-168.
- Muhongo, S. and Tuisku, P. 1995. Thermo-barometry of the Uluguru Mountain Ranges, eastern Tanzania: Evidence for Pan-African isobaric cooling and rapid exhumation. International earth-science congress to commemorate the centennial of the Geological Society of South Africa. *Extended Abstracts*, pp 394-397.
- Muhongo, S. 1998. Anatomy of the Mozambique Orogenic Belt of eastern and southern Africa. *Journal of African Earth Sciences*, 27, No. 1A p 142.
- Murphy, M.V.N. 1958. Coronites from India and their bearing on the origin of coronas. *Bulletin of Geological Society of America*, 69, 23-38.

- Nureki, T., Suwa, K., Biyajima, K., Saka, Y. and Yusa, Y. 1977.** Tectonic evolution of the Mozambique belt in area south-east of Machakos, Kenya. *2nd Preliminary Report on African Studies*, pp 33-41. Nagoya University, Japan.
- Nyamai, C.M., Mathu, E.M. and Ngecu, W.M. 1993.** A review of the geology of the Mozambique Belt in Kenya. In: Peters, J.W., Kesse, G.O. and Acquah, P.C., (Eds.), *Proceedings of the 9th International Geological Conference of the Geological Society of Africa - Regional Trends in African Geology*, pp 334-347. Accra, Ghana.
- Nyamai, C.M. 1995.** Petrography and Geochemistry of Mozambique Belt rocks of the Matuu area, central Kenya. In: UNESCO, Geology for Sustainable Development. *Newsletter/Bulletin*, **10**, 154-155.
- Nyamai, C.M., Opiyo-Akech, N., Gaciri, S.J. and Johanson, BO. 1999.** Mineral chemistry and thermobarometry of the Neoproterozoic Mozambique Belt intrusive rocks of the Matuu-Masinga area, central Kenya. *Journal of African Earth Sciences*, **28**, 58-59.
- Ochieng, J.O. 1993.** Petrology of the gabbroic suite of rocks occurring south east of Mt. Kenya. In: Geology for Sustainable Development. In: Opiyo-Akech, N., Ed., *Proceedings of the 5th Conference on the Geology of Kenya- Geology for Sustainable Development*, pp 33-36. UNEP/ UNESCO, Nairobi.
- Passchier, C., Myers, J. and Kröner, A. 1990.** *Field Geology of High Grade Gneiss Terrains*. Elsevier, Amsterdam, 257pp.
- Pattison, D.R.M. and Newton, R.C. 1989.** Reversed experimental calibration of the garnet-clinopyroxene Fe-Mg exchange thermometer. *Contributions to Mineralogy and Petrology*, **101**, 87-103.

- Pearce, J.A. and Cann, J.R. 1973. Tectonic setting of basic volcanic rocks determined using trace element analyses. *Earth Planetary Science Letters*, **19**, 290-300.
- Pearce, J.A. and Norry, M.J. 1979. Petrogenetic implications of Ti, Zr, Y and Nb variations in volcanic rocks. *Contributions to Mineralogy and Petrology*, **69**, 33-47.
- Pearce, J.A. 1982. Trace element characteristics of lavas from destructive plate boundaries. In: Thorpe, R.S (ed.) *Andesites, Orogenic Andesites and Related Rocks*. Chichester: Wiley. pp. 525-548.
- Pearce, J.A. 1983. Role of sub-continental lithosphere in magma genesis at active continental margins. In: Hawkesworth, C.J. and Norry, M.J., (Eds.) *Continental Basalts and Mantle Xenoliths*, pp 230-249. Shiva, Cheshire.
- Pearce, J.A., Harris, N.B.W. and Tindle, A.G. 1984. Trace element discrimination for the tectonic interpretation of granitic rocks. *Journal of Petrology*, **25**, 956-983.
- Pehrman, G. 1939. Über Phosphate aus dem Pegmatit von Lemnäs (Kimito, S.W. Finland). *Acta Acad. Aboensis, Math. et Physica*, **12**, No.6 (M.A. 7-417).
- Pekka, S. 1992. The Caledonian Halti-Ridnitsohkka igneous complex in Lapland. *Geological Society of Finland Bulletin* **362**. 75 pp.
- Pitcher, W.S. 1979. Comments on the geological environment of granites: pp 1-8 in Atherton, M.P. and Tarney, J. (eds), *Origin of Granite Batholiths: Geochemical Evidence*. Shiva Pub. Ltd., Orpington, Kent.
- Piwinskii, A.J. 1975. Experimental studies of granitoid rocks near the San Andreas Fault zone in the Coast and Transverse Ranges and Mojave Desert, California. *Tectonophysics*, **25**, 217-231.

- Pohl, W. 1979.** Metallogenic/Minerogenic analysis - contribution to the differentiation between Mozambiquian basement and Pan-African superstructure in the Red Sea region. *Annals of the Geological Survey of Egypt*, **9**, 32-44.
- Pohl, W. and Niedermayr, G. 1979.** Geology of the Mwatate quadrangle and the vanadium grossularite deposits of the area (with a geological map 1:50,000 by W. Pohl). *Geological Survey of Kenya, Report No. 101*, 55 pp.
- Pohl, W. 1988.** Precambrian metallogeny of NE Africa. In S. El Gaby and R.O. Greiling (eds.), *The Pan-African belt of north-east Africa and adjacent areas*, pp 319-341. Freidr. Vieweg & Sohns. Braunschweig, Wiesbaden.
- Pohl, W., Horkel, A., Neubauer, W., Niedermayr, G., Okelo, R.E., Wachira, J.K. and Werneck, W. 1980.** Notes on the geology and mineral resources of the Mtito-Andei - Taita Hills area (southern Kenya). *Mitteilungen Osterreichischen Geologischen Gesellschaft*, **73**, 135-152.
- Porada, H. 1989.** Pan-African rifting and orogenesis in southern to equatorial Africa and eastern Brazil. *Precambrian Research*, **44**, 103-136.
- Pouchou, J.L. and Pichoir, F. 1994.** A new model for advanced X-ray microanalysis. *La Recherche'Aerospatiale*, **3**, 167-192
- Powell, R. and Holland, T.J.B. 1988.** An internally consistent dataset with uncertainties and correlation's. III. Applications to geobarometry, worked examples and a computer program. *Journal of Metamorphic Geology*, **6**, 173-204.
- Prochaska, W. and Pohl, W. 1984.** Petrochemistry of some mafic and ultramafic rocks from the Mozambique Belt, Northern Tanzania. *Journal of African Earth Sciences*, **1**, 183-191.

- Pulfrey, W. and Walsh, J. 1969.** The geology and mineral resources of Kenya. *Geological Survey of Kenya Bulletin*, 9, 34 pp.
- Quennell, A.M., McKinlay, A.C.M. and Aitiken, W.G. 1955.** Summary of the Geology of Tanganyika. Part I; Introduction and stratigraphy. *Geological Survey of Tanganyika Bulletin*, 37, 69pp.
- Saltikoff, W., Githinji, J.K., Ombasa, L.K. and Rask, M. 1991.** Assessment of Lolkidongai Wollastonite Deposit in Kajiado District, Kenya. Republic of Kenya. Ministry of Environment and Natural Resources, Mines and Geological Department. *Geological Memoir*, 12, 21pp.
- Sanders, L.D. 1965.** Geology of the contact between the Nyanza Shield and the Mozambique belt in western Kenya. *Geological Survey of Kenya Bulletin*, 7.
- Saunders, A.D., Tarney, J. and Weaver, S.D. 1980.** Transverse geochemical variations across the Antarctic peninsula: implications for the genesis of calc-alkaline magmas. *Earth planetary Science Letters*, 46, 344-360.
- Scotford, D.M and Williams, R.J. 1983.** Petrology and geochemistry of metamorphised ultramafic bodies in a portion of the Blue Ridge of North Carolina and Virginia. *American Mineralogist*, volume 68, pp 78-94.
- Schoeman, J.J. 1949.** Geology of the Sotik District. Degree sheet 42. S.W. Quadrant. *Geological Survey of Kenya Report*, 16, 39 pp.
- Shackleton, R.M. 1946.** Geology of the Migori Belt and adjoining areas. *Geological Survey of Kenya Report*, 10, 60 pp.
- Shackleton, R.M. 1977.** Possible late-Precambrian ophiolites in Africa and Brazil. *Research Report for the Institute of African Geology*, University of Leeds. 20. 3-7.

- Shackleton, R.M. 1979. Precambrian tectonics of northeast Africa. In, A.M.S. Shanti (ed.), *Evolution and Mineralisation of the Arabian-Nubian Shield*, 2. pp. 1-6, Oxford: Pergamon.
- Shackleton, R.M. 1986. Precambrian Collision Tectonics in Africa. In: Coward, M.P. and Ries, A.C. (eds.) *Collision Tectonics*. Geological Society of London Special Publication, 19. pp 329-349.
- Shackleton, R.M. 1991. Problems with Mozambique Belt of Tanzania. UNESCO, Geology for Economic Development, *Newsletter/Bulletin*, 8, 23-30.
- Shand, S.J. 1945. The present status of Daly's hypothesis of the alkaline rocks. *American Journal of Science*, 243(a), 495-507.
- Shibata, K. and Suwa, K. 1979. A geochronological study on granitoid gneiss from the Mbooni Hills, Machakos Area, Kenya. *4th Preliminary Report on African Studies*, pp 163-167. Nagoya University, Japan.
- Soto, J.I. 1993. PTMAFIC: Software for thermo-barometry and activity calculations with mafic and ultramafic assemblages. *American Mineralogist*, 78, 840-844.
- Spooner, C.M., Hepworth, J.V. and Fairbairn, H.W. 1970. Whole-rock Rb-Sr isotopic investigations of some East African granulites. *Geological Magazine*, 107, 511-521.
- Steiger, R. and Jager, E. 1977. Subcommittee on geochronology: convention on the use of decay constants in geo- and cosmochronology. *Earth Planetary Science Letters*, 36, 359-362.
- Stern, J.R. 1994. Arc assembly and continental collision in the Neoproterozoic East African Orogeny: Implications for the Consolidation of Gondwanaland. *Annual Reviews of Earth Planetary Science*, 22, 319-351.
- Streckeisen, A.L. 1976. To each plutonic rock its proper name. *Earth Science Reviews*, 12, 1-33.

- Subramanica, A.P. 1956.** Mineralogy and petrology of the Sittampundi Complex, Salem District, Madras State, India. *Bulletin of Geological Society of America*, **67**, p.317
- Suwa, K., Nureki, T., Inoue, H., Biyajima, K. and Miyakawa, K. 1979.** Geology and Petrology of the Machakos area, Kenya. *4th Preliminary Report on African Studies*, pp 3-20. Nagoya University, Japan.
- Vail, J.R. 1988.** Tectonics and evolution of the Proterozoic basement of northeastern Africa. In S. El Gaby and R.O. Greiling (eds.), *The Pan-African belt of northeast Africa and adjacent areas*, pp 195-226. Friedr. Vieweg & Sohns, Braunschweig, Weisbaden.
- Vearncombe, J.R. 1983.** A dismembered ophiolite from the Mozambique belt, West Pokot. *Journal on African Earth Sciences*, **1**, 133-143.
- Wagner, M., Altherr, R. and Van den haute, P. 1992.** Apatite fission-track analysis of Kenyan basement rocks: constraints on the thermo-tectonic evolution of the Kenya dome. A reconnaissance study. *Tectonophysics*, **204**, 93-110.
- White, A.J.R. and Chappel, B.W. 1977.** Ultrametamorphism and granitoid genesis. *Tectonophysics*, **43**, 7-22.
- Williams, L.A.J. 1966.** Geology of the Chanler's Falls area. *Geological Survey of Kenya Report*, **75**.
- Winkler, H.G.F. 1979.** *Petrogenesis of Metamorphic Rocks*. 5th Ed. Springer-Verlag, New York. 348pp.
- York, D. 1966.** Least-squares fitting of a straight line. *Canadian Journal of Physics*, **44**, 1079-1086.

* * * *

APPENDIX 2: MICROPROBE MINERAL ANALYSES

Sample ID	Mineral	Analysis 1	Analysis 2
1-1-1001	Quartz	12000000000	12000000000
1-1-1002	Quartz	12000000000	12000000000
1-1-1003	Quartz	12000000000	12000000000
1-1-1004	Quartz	12000000000	12000000000
1-1-1005	Quartz	12000000000	12000000000
1-1-1006	Quartz	12000000000	12000000000
1-1-1007	Quartz	12000000000	12000000000
1-1-1008	Quartz	12000000000	12000000000
1-1-1009	Quartz	12000000000	12000000000
1-1-1010	Quartz	12000000000	12000000000
1-1-1011	Quartz	12000000000	12000000000
1-1-1012	Quartz	12000000000	12000000000
1-1-1013	Quartz	12000000000	12000000000
1-1-1014	Quartz	12000000000	12000000000
1-1-1015	Quartz	12000000000	12000000000
1-1-1016	Quartz	12000000000	12000000000
1-1-1017	Quartz	12000000000	12000000000
1-1-1018	Quartz	12000000000	12000000000
1-1-1019	Quartz	12000000000	12000000000
1-1-1020	Quartz	12000000000	12000000000

Appendix 2.1 Clinopyroxene compositions in the gabbroic and dioritic rocks of Matuu-Masinga area. Lith. = lithologies: GAB = gabbro, DRT = diorite.

Sample Lith.	MU-5		MU-7		MU-7		MU-7		MU-7		MU-7		MU-28		MU-28		MU-28		MU-28		
	GAB.	GAB.	DRT.	DRT.	DRT.	DRT.	DRT.	DRT.	DRT.	DRT.	DRT.	DRT.	GAB.	GAB.	GAB.	GAB.	GAB.	GAB.	GAB.	GAB.	
SiO ₂	50.59	50.69	52.14	51.71	51.83	51.75	51.73	51.74	51.52	52.10	52.40	51.47	52.06	51.74	51.52	52.10	52.40	51.47	52.06	51.74	51.52
TiO ₂	0.36	0.24	0.22	0.24	0.19	0.24	0.22	0.17	0.27	0.19	0.19	0.28	0.22	0.27	0.19	0.19	0.19	0.28	0.22	0.17	0.27
Al ₂ O ₃	2.89	2.77	1.83	1.92	1.75	1.90	2.20	2.25	2.45	2.13	1.89	2.58	2.20	2.45	2.13	1.89	1.89	2.58	1.95	2.25	2.45
Cr ₂ O ₃	0.00	0.05	0.01	0.05	0.02	0.02	0.02	0.05	0.01	0.02	0.02	0.04	0.02	0.01	0.02	0.00	0.00	0.04	0.02	0.05	0.01
FeO*	9.04	12.55	9.61	11.11	11.58	11.73	9.59	9.55	10.62	9.48	9.10	10.56	9.59	10.62	9.48	9.10	10.56	10.56	9.27	9.55	10.62
MnO	0.33	0.39	0.32	0.58	0.54	0.45	0.41	0.40	0.42	0.33	0.37	0.36	0.41	0.42	0.33	0.37	0.36	0.36	0.31	0.40	0.42
MgO	12.39	13.76	12.91	12.51	12.61	12.68	12.70	12.53	12.76	13.11	13.31	12.65	12.70	12.76	13.11	13.31	12.65	12.65	13.20	12.53	12.76
CaO	21.91	17.28	21.28	20.19	19.66	19.31	21.53	21.35	20.70	21.29	21.65	20.85	21.35	20.70	21.29	21.65	20.85	20.85	22.02	21.35	20.70
CoO	0.00	0.00	0.00	0.00	0.00	0.00	0.00	0.06	0.00	0.01	0.04	0.00	0.00	0.00	0.01	0.04	0.00	0.00	0.01	0.06	0.00
NiO	0.02	0.00	0.00	0.00	0.01	0.01	0.00	0.00	0.00	0.03	0.01	0.01	0.00	0.00	0.03	0.01	0.01	0.01	0.01	0.00	0.00
BaO	0.09	0.04	0.03	0.00	0.00	0.00	0.00	0.03	0.00	0.00	0.03	0.00	0.00	0.00	0.00	0.03	0.00	0.00	0.05	0.03	0.00
Na ₂ O	0.55	0.42	0.60	0.65	0.60	0.65	0.67	0.72	0.59	0.57	0.53	0.61	0.67	0.59	0.57	0.53	0.61	0.61	0.52	0.72	0.59
K ₂ O	0.00	0.00	0.01	0.00	0.00	0.00	0.00	0.01	0.01	0.00	0.00	0.01	0.00	0.01	0.00	0.00	0.01	0.01	0.01	0.01	0.01
V ₂ O ₅	0.00	0.16	0.17	0.14	0.24	0.17	0.01	0.00	0.00	0.00	0.00	0.10	0.01	0.00	0.00	0.31	0.10	0.10	0.07	0.00	0.00
F	0.00	0.54	0.00	0.22	0.00	0.00	0.19	0.00	0.00	0.00	0.00	0.00	0.19	0.00	0.00	0.19	0.00	0.00	0.27	0.00	0.00
Cl	0.00	0.00	0.00	0.00	0.00	0.00	0.00	0.00	0.00	0.00	0.00	0.01	0.00	0.00	0.00	0.00	0.01	0.01	0.00	0.00	0.00
Total	98.17	98.89	99.13	99.32	99.03	98.91	99.27	98.86	99.35	99.46	100.02	99.53	99.99	98.86	99.35	99.46	100.02	99.53	99.99	98.86	99.35

NB. FeO* = total iron as FeO; - not determined.

Sample	MU-28		MU-28		MU-28		MU-28		MU-28	
	Lith.	GAB.	GAB.	GAB.	GAB.	GAB.	GAB.	GAB.	GAB.	GAB.
SiO ₂	50.63	50.55	51.11	50.38	49.60	-	-	-	-	-
TiO ₂	0.42	0.43	0.31	-	-	-	-	-	-	-
Al ₂ O ₃	3.38	2.76	2.93	2.99	3.04	-	-	-	-	-
Cr ₂ O ₃	0.09	0.09	0.08	-	-	-	-	-	-	-
FeO*	11.13	12.71	10.58	10.15	9.90	-	-	-	-	-
MnO	0.27	0.50	0.37	0.40	0.35	-	-	-	-	-
MgO	13.35	13.19	12.65	11.54	11.35	-	-	-	-	-
CaO	18.78	18.50	20.21	21.13	21.38	-	-	-	-	-
CoO	0.00	0.00	0.00	-	-	-	-	-	-	-
NiO	0.00	0.00	0.00	-	-	-	-	-	-	-
BaO	0.00	0.02	0.00	-	-	-	-	-	-	-
Na ₂ O	0.67	0.57	0.62	-	-	-	-	-	-	-
K ₂ O	0.23	0.00	0.01	-	-	-	-	-	-	-
V ₂ O ₅	0.58	0.44	0.41	-	-	-	-	-	-	-
F	0.13	0.17	0.08	-	-	-	-	-	-	-
Cl	0.00	0.00	0.00	-	-	-	-	-	-	-
Total	99.66	99.93	99.36	96.59	95.62					

NB. FeO* = total iron as FeO; - not determined.

Appendix 2.2 Orthopyroxene compositions in the gabbroic and dioritic rocks of Matuu-Masinga area, central Kenya. Lith.=lithologies: GAB = gabbro, DRT = diorite.

Sample Lith.	MU-5		MU-7		MU-7		MU-7		MU-7		MU-7		MU-28		MU-28		MU-28		MU-28	
	GAB.	GAB.	DRT.	DRT.	DRT.	DRT.	DRT.	DRT.	DRT.	DRT.	DRT.	DRT.	DRT.	GAB.	GAB.	GAB.	GAB.	GAB.	GAB.	GAB.
SiO ₂	51.35	51.07	51.81	51.76	51.63	51.93	51.56	51.05	51.76	51.79	51.59	51.16	51.83							
TiO ₂	0.11	0.25	0.07	0.08	0.06	0.09	0.06	0.08	0.10	0.20	0.10	0.07	0.06							
Al ₂ O ₃	1.46	1.88	1.10	1.06	1.18	1.00	1.02	1.39	1.19	1.11	1.13	1.19	1.36							
Cr ₂ O ₃	0.00	0.01	0.05	0.04	0.03	0.00	0.00	0.01	0.00	0.06	0.04	0.04	0.05							
FeO*	22.86	22.79	24.54	24.77	23.30	24.78	24.98	24.62	23.93	24.41	25.18	24.85	24.04							
MnO	0.81	0.72	1.08	0.92	1.03	1.08	1.12	0.95	0.84	0.79	0.73	0.80	0.78							
MgO	20.71	20.49	20.32	20.30	19.59	20.35	20.98	19.68	20.03	20.04	20.21	19.89	20.10							
CaO	1.17	0.96	0.59	0.81	2.70	0.49	0.50	0.55	1.26	1.43	0.54	0.53	1.33							
CoO	0.00	0.00	0.02	0.00	0.00	0.00	0.00	0.00	0.05	0.00	0.00	0.04	0.01							
NiO	0.01	0.00	0.02	0.00	0.01	0.00	0.01	0.01	0.02	0.08	0.00	0.00	0.00							
BaO	0.00	0.00	0.00	0.06	0.04	0.02	0.02	0.04	0.00	0.00	0.00	0.00	0.00							
Na ₂ O	0.06	0.06	0.02	0.01	0.07	0.01	0.00	0.03	0.03	0.02	0.01	0.01	0.04							
K ₂ O	0.01	0.00	0.02	0.00	0.00	0.00	0.00	0.00	0.00	0.01	0.01	0.01	0.00							
V ₂ O ₅	0.00	0.16	0.00	0.43	0.25	0.00	0.00	0.00	0.36	0.21	0.20	0.00	0.48							
F	0.15	0.15	0.18	0.19	0.05	0.00	0.00	0.04	0.20	0.10	0.00	0.00	0.04							
Cl	0.01	0.01	0.00	0.00	0.00	0.00	0.00	0.02	0.00	0.01	0.00	0.01	0.01							
Total	98.71	98.55	99.82	100.43	99.94	99.75	99.35	98.47	99.77	100.26	99.74	98.60	100.13							

NB. FeO* = total iron as FeO.

Appendix 2.3. Plagioclase compositions from the Matuu-Masinga area, central Kenya. Lith.= lithologies: DRT = diorite, GAB = gabbro, SYD = syeno-diorite, GRNT = granulite, AMP = amphibolite, GTE = granite, PEG = pegmatite.

Sample Lith.	MU-7 DRT	MU-7 DRT	MU-7 DRT	MU-7 DRT	MU-7 DRT	MU-7 DRT	MU-7 DRT	MU-7 DRT	MU-7 DRT	MU-7 DRT	MU-7 DRT
SiO ₂	58.21	58.41	59.90	60.00	59.75	59.91	60.80	60.86	60.20	59.66	58.46
TiO ₂	0.00	0.02	0.00	0.00	0.00	0.01	0.03	0.00	0.06	0.00	0.02
Al ₂ O ₃	25.74	25.44	24.65	24.65	24.86	24.67	24.56	24.47	25.01	25.44	25.84
Cr ₂ O ₃	0.04	0.00	0.00	0.00	0.00	0.01	-	-	-	-	-
FeO*	0.22	0.11	0.09	0.04	0.06	0.12	0.10	0.09	0.00	0.11	0.21
MnO	0.00	0.00	0.04	0.00	0.00	0.05	0.00	0.00	0.02	0.03	0.00
MgO	0.00	0.00	0.00	0.00	0.00	0.00	0.00	0.00	0.00	0.00	0.00
CaO	7.80	7.82	6.71	6.49	6.74	6.82	6.37	6.37	7.07	6.90	7.80
Na ₂ O	6.50	6.49	7.14	7.25	7.13	7.08	0.16	0.16	0.16	0.06	0.04
K ₂ O	0.27	0.35	0.25	0.28	0.36	0.38	0.28	0.39	0.30	0.31	0.23
NiO	0.00	0.05	0.00	0.00	0.05	0.00	-	-	-	-	-
BaO	0.00	0.00	0.04	0.04	0.00	0.00	0.13	0.03	0.08	0.00	0.05
SrO	-	-	-	-	-	-	6.88	6.73	6.61	6.35	5.98
Cs ₂ O	-	-	-	-	-	-	0.00	0.01	0.15	0.00	0.00
V ₂ O ₃	0.00	0.10	0.00	0.11	0.03	0.13	-	-	-	-	-
F	0.27	0.21	0.05	0.00	0.02	0.08	-	-	-	-	-
Cl	0.01	0.00	0.00	0.01	0.00	0.00	-	-	-	-	-
Total	99.07	99.00	98.87	98.87	99.00	99.26	99.31	99.11	100.01	99.21	98.91

FeO* - total iron as FeO; - not determined.

Sample Lith. Type	MU-26 AMP	MU-26 AMP	MU-26 AMP	MU-26 AMP	MU-26 AMP	MU-26 AMP	MU-26 AMP	MU-26 AMP	MU-26 AMP	MU-26 AMP	MU-28 GAB centre	MU-28 GAB rim	MU-28 GAB centre	MU-28 GAB rim
SiO ₂	55.60	55.57	57.98	56.24	57.12	58.30	58.02	57.12	56.89	58.76	59.51	59.45	58.40	58.40
TiO ₂	0.00	0.01	0.00	0.01	0.00	0.01	0.00	0.00	0.00	0.03	0.00	0.03	0.01	0.01
Al ₂ O ₃	27.59	27.59	26.00	26.90	26.69	26.19	26.27	26.36	26.22	25.86	25.15	25.26	26.10	26.10
FeO	0.03	0.00	0.00	0.08	0.01	0.01	0.05	0.08	0.02	0.12	0.16	0.18	0.13	0.13
MnO	0.00	0.00	0.02	0.06	0.00	0.00	0.04	0.00	0.00	0.00	0.07	0.00	0.01	0.01
MgO	0.00	0.00	0.00	0.00	0.00	0.00	0.00	0.00	0.00	0.00	0.00	0.00	0.00	0.00
CaO	9.85	9.90	8.23	9.29	8.69	7.91	8.08	8.34	8.26	7.71	7.05	7.05	7.67	7.67
Na ₂ O	5.25	5.21	6.10	5.61	5.89	6.17	6.13	6.14	5.94	0.11	0.15	0.16	0.02	0.02
K ₂ O	0.05	0.05	0.09	0.05	0.01	0.11	0.07	0.02	0.08	0.38	0.44	0.44	0.41	0.41
NiO	-	-	-	-	-	-	-	0.00	0.00	-	-	-	-	-
BaO	0.00	0.03	0.03	0.00	0.05	0.00	0.00	0.00	0.03	0.00	0.02	0.11	0.12	0.11
SrO	0.00	0.00	0.00	0.00	0.00	0.00	0.00	-	-	5.91	6.25	6.31	5.81	5.81
Cs ₂ O	0.00	0.00	0.00	0.00	0.06	0.01	0.16	-	-	0.12	0.00	0.08	0.00	0.00
F	-	-	-	-	-	-	-	0.09	0.06	-	-	-	-	-
Cl	-	-	-	-	-	-	-	0.00	0.00	-	-	-	-	-
Total	98.28	98.35	98.46	98.22	98.52	98.71	98.82	98.15	97.53	99.37	98.93	99.07	98.88	98.88

FeO* = total iron as FeO; - not determined.

Sample Lith.	MU-19 AMP	MU-19 AMP	MU-19 AMP	MU-10 SYD	MU-10 SYD	MU-10 SYD	MU-10 SYD	MU-10 SYD	MU-10 SYD	MU-10 SYD	MU-10 SYD	MU-10 SYD	MU-10 SYD	MU-29 GTE	MU-29 GTE	MU-29 GTE
SiO ₂	41.55	41.51	41.60	41.09	41.02	41.33	40.96	41.29	41.55	41.44	41.41	41.47	41.82			
TiO ₂	0.85	0.83	0.87	1.39	1.35	1.31	1.25	1.34	1.29	1.37	1.31	1.56	1.48			
Al ₂ O ₃	12.36	12.34	12.40	10.40	10.40	10.05	10.11	10.06	9.92	10.00	10.01	10.45	10.59			
Cr ₂ O ₃	0.02	0.00	0.02	0.00	0.02	0.03	0.00	0.04	0.00	0.03	0.00	0.00	0.07			
FeO'	18.22	18.18	18.46	20.52	21.09	21.09	20.54	21.01	20.49	20.93	20.93	19.24	19.17			
MnO	0.37	0.36	0.42	0.51	0.55	0.69	0.58	0.58	0.52	0.57	0.31	0.60	0.62			
MgO	8.84	8.81	8.87	8.19	8.03	8.08	8.10	8.18	8.03	8.06	8.00	8.87	8.98			
CaO	11.45	11.62	11.55	10.78	10.63	10.79	10.68	10.71	10.79	10.74	10.82	10.80	10.92			
Na ₂ O	1.23	1.27	1.29	1.62	1.57	1.48	1.54	1.54	1.57	1.58	1.51	1.59	1.56			
K ₂ O	1.07	1.08	1.11	1.62	1.64	1.63	1.65	1.60	1.58	1.62	1.57	1.56	1.51			
BaO	0.01	0.03	0.03	0.00	0.00	0.03	0.00	0.02	0.07	0.00	0.00	0.00	0.00			
CoO	0.00	0.00	0.00	0.00	0.00	0.00	0.00	0.00	0.00	0.01	0.00	0.01	0.00			
NiO	0.00	0.06	0.00	0.00	0.06	0.04	0.00	0.00	0.00	0.00	0.11	0.03	0.00			
V ₂ O ₅	0.15	0.12	0.00	0.10	0.31	0.11	0.00	0.00	0.00	0.06	0.04	0.13	0.00			
F	0.19	0.00	0.10	0.28	0.46	0.34	0.48	0.34	0.30	0.52	0.23	0.24	0.56			
Cl	0.03	0.03	0.03	0.21	0.19	0.19	0.17	0.18	0.24	0.17	0.20	0.15	0.16			
Total	96.34	96.24	96.75	96.55	97.32	97.19	96.06	96.89	96.35	97.10	96.74	96.71	97.43			

NB. FeO' = total iron as FeO.

Appendix 2.5 Biotite compositions from the Matuu-Masinga area, central Kenya. Lith.= lithologies: AMP = amphibolite, GAB = gabbro, SYD = syeno-diorite, GTE = granite.

Sample Lith.	MU-5 GAB	MU-5 GAB	MU-5 GAB	MU-7 DRT	MU-7 DRT	MU-7 DRT	MU-16 AMP	MU-26 AMP	MU-26 AMP	MU-26 AMP	MU-10 SYD	MU-10 SYD	MU-10 SYD	MU-10 SYD
SiO ₂	36.34	36.18	36.13	36.80	36.76	35.82	35.81	35.52	35.54	36.70	36.74	36.35	36.67	
TiO ₂	4.79	4.82	4.77	5.12	5.30	2.08	2.01	2.01	2.01	3.13	3.08	2.88	2.94	
Al ₂ O ₃	14.09	14.17	14.06	13.81	13.79	15.77	16.15	16.14	16.25	13.66	13.69	13.94	13.89	
Cr ₂ O ₃	0.02	0.08	0.02	0.03	0.00	0.03	0.00	0.03	0.00	0.06	0.00	0.00	0.00	
FeO	13.37	13.72	13.79	15.87	15.95	16.90	17.45	17.26	17.69	20.43	20.29	20.94	20.50	
MnO	0.03	0.06	0.03	0.21	0.05	0.22	0.58	0.60	0.53	0.31	0.29	0.34	0.23	
MgO	14.60	14.78	14.46	13.58	13.59	11.94	10.51	10.23	10.35	10.88	11.18	10.87	10.92	
CaO	0.01	0.00	0.03	0.00	0.00	0.07	0.06	0.02	0.08	0.03	0.03	0.02	0.03	
Na ₂ O	0.01	0.03	0.01	0.02	0.04	0.10	0.06	0.10	0.07	0.07	0.06	0.06	0.06	
K ₂ O	9.39	9.38	9.44	9.80	9.71	9.31	9.21	9.45	9.37	9.64	9.67	9.50	9.48	
BaO	0.88	0.90	0.97	0.37	0.23	0.36	0.17	0.27	0.20	0.00	0.00	0.04	0.05	
CoO	0.00	0.00	0.00	0.04	0.01	0.00	0.00	0.00	0.00	0.00	0.01	0.00	0.00	
NiO	0.02	0.00	0.02	0.01	0.00	0.00	0.02	0.02	0.00	0.00	0.00	0.00	0.00	
V ₂ O ₅	0.04	0.00	0.00	0.00	0.25	0.00	0.07	0.00	0.21	0.00	0.00	0.17	0.09	
F	0.50	0.63	0.47	0.55	0.65	0.08	0.00	0.00	0.00	0.65	0.65	0.82	0.89	
Cl	0.08	0.15	0.11	0.09	0.13	0.10	0.03	0.04	0.05	0.20	0.17	0.22	0.20	
Total	94.17	94.90	94.31	96.30	96.46	92.78	92.13	91.69	92.35	95.76	95.86	96.15	95.95	

NB. FeO' = total iron as FeO.

Sample Lith.	MU-29 GTE	MU-29 GTE	MU-6A GTE	MU-6A GTE	MU-8 GTE	MU-8 GTE	MU-8 GTE	MU-8 GTE	MU-8 GTE	MU-8 GTE	MU-8 GTE	MU-8 GTE	MU-8 GTE	MU-8 GTE	MU-8 GTE	MU-8 GTE	MU-8 GTE	MU-8 GTE	
SiO ₂	36.67	36.62	35.47	35.65	37.74	38.40	38.22	38.17	38.27	37.97	37.97	37.97	37.97	37.97	37.97	37.97	37.97	37.97	37.94
TiO ₂	3.15	3.13	3.41	3.42	2.84	0.67	1.82	2.83	0.42	3.02	2.88	2.80	2.80	2.80	2.80	2.80	2.80	2.80	1.90
Al ₂ O ₃	13.73	13.86	15.17	15.24	14.05	14.82	14.39	14.16	14.28	14.09	14.22	14.25	14.25	14.25	14.25	14.25	14.25	14.25	14.04
Cl ₂ O ₃	0.02	0.00	0.03	0.01	0.00	0.00	0.00	0.00	0.00	0.06	0.01	0.01	0.01	0.01	0.01	0.01	0.01	0.01	0.00
FeO*	18.46	18.18	20.42	20.97	17.68	15.40	15.71	17.04	14.77	16.77	16.99	17.24	17.24	17.24	17.24	17.24	17.24	17.24	15.22
MnO	0.31	0.40	0.38	0.35	0.14	0.22	0.45	0.10	0.24	0.08	0.08	0.11	0.11	0.11	0.11	0.11	0.11	0.11	0.35
MgO	12.27	12.24	8.11	8.19	12.53	15.37	14.62	12.57	15.67	12.31	12.54	12.33	12.33	12.33	12.33	12.33	12.33	12.33	14.19
CaO	0.00	0.00	0.01	0.00	0.01	0.00	0.01	0.00	0.02	0.00	0.00	0.00	0.00	0.00	0.00	0.00	0.00	0.00	0.01
Na ₂ O	0.05	0.05	0.06	0.06	0.05	0.06	0.08	0.05	0.04	0.07	0.05	0.04	0.04	0.04	0.04	0.04	0.04	0.04	0.08
K ₂ O	9.68	9.61	9.51	9.45	9.66	9.67	9.77	9.78	9.78	9.89	9.90	9.90	9.90	9.90	9.90	9.90	9.90	9.90	9.93
BaO	0.15	0.13	0.23	0.25	0.06	0.06	0.04	0.10	0.09	0.03	0.06	0.04	0.04	0.04	0.04	0.04	0.04	0.04	0.07
CoO	0.03	0.00	0.00	0.00	0.06	0.00	0.00	0.00	0.00	0.00	0.00	0.00	0.00	0.00	0.00	0.00	0.00	0.00	0.00
NiO	0.00	0.06	0.05	0.00	0.07	0.00	0.00	0.04	0.00	0.00	0.00	0.00	0.00	0.00	0.00	0.00	0.00	0.00	0.00
V ₂ O ₃	0.39	0.13	0.20	0.00	0.37	0.26	0.28	0.00	0.07	0.28	0.00	0.20	0.20	0.20	0.20	0.20	0.20	0.20	0.11
F	0.91	0.84	0.86	0.75	1.31	1.29	1.55	1.25	1.12	1.23	1.02	0.91	0.91	0.91	0.91	0.91	0.91	0.91	0.88
Cl	0.15	0.18	0.15	0.12	0.04	0.05	0.07	0.07	0.07	0.07	0.08	0.04	0.04	0.04	0.04	0.04	0.04	0.04	0.10
Total	95.93	95.43	94.06	94.46	96.61	96.27	97.01	96.16	94.84	95.87	95.80	96.02	96.02	96.02	96.02	96.02	96.02	96.02	94.82

NB. FeO* = total iron as FeO.

Appendix 2.7. Garnet, sphene and rutile compositions from the Matuu-Masinga area, central Kenya. Lith. = lithologies: AMP = amphibolite, GNRT = granulite, GAB = gabbro. Min. = mineral: grt = garnet, spn = sphene, rtl = rutile.

Sample Lith. Min.	MU-23 GRNT grt	MU-23 GRNT grt	MU-26 AMP spn	MU-23 GNTR spn	MU-23 GNRT spn	MU-20 GAB spn	MU-20 GAB spn	MU-20 GAB spn	MU-20 GAB spn	MU-20 GAB spn	MU-21 GAB spn	MU-21 GAB spn	MU-20 GAB spn	MU-20 GAB rtl	MU-20 GAB rtl	MU-20 GAB rtl
SiO ₂	36.26	36.03	29.94	31.98	30.17	29.70	30.13	29.91	30.04	29.92	29.61	29.92	30.04	0.00	0.00	0.02
TiO ₂	0.56	-	35.59	35.53	36.91	36.74	36.40	36.49	36.25	35.76	35.19	35.76	36.25	93.09	93.09	92.98
Al ₂ O ₃	10.69	9.87	1.49	1.47	1.57	0.88	1.10	0.94	0.90	1.56	1.68	1.56	0.90	0.05	0.05	0.06
Cr ₂ O ₃	0.00	-	0.02	0.00	-	0.00	0.03	0.18	0.19	0.03	0.00	0.03	0.19	0.79	0.79	0.87
FeO	18.43	19.80	0.90	1.01	1.86	0.44	0.34	0.23	0.24	0.55	0.49	0.55	0.24	0.07	0.07	0.16
MnO	0.95	0.91	0.12	0.03	-	0.01	0.08	0.00	0.00	0.03	0.00	0.03	0.00	0.00	0.00	0.00
MgO	0.00	-	0.00	0.00	-	0.00	0.00	0.00	0.00	0.00	0.00	0.00	0.00	0.00	0.00	0.00
CaO	28.95	29.47	28.45	28.44	28.82	27.98	28.37	28.46	28.44	28.19	27.83	28.19	28.44	0.10	0.10	0.05
CoO	0.00	-	0.00	0.02	-	0.00	0.02	0.00	0.01	0.00	0.00	0.00	0.01	0.00	0.00	0.00
NiO	0.00	-	0.05	0.01	-	0.01	0.02	0.00	0.00	0.01	0.00	0.01	0.00	0.00	0.00	0.00
BaO	0.00	-	0.35	0.32	-	0.32	0.42	0.38	0.23	0.37	0.38	0.37	0.23	0.93	0.93	0.87
Na ₂ O	0.01	-	0.01	0.01	-	0.00	0.00	0.01	0.00	0.02	0.02	0.02	0.00	0.02	0.02	0.02
K ₂ O	0.00	-	0.01	0.00	-	0.00	0.00	0.00	0.02	0.00	0.03	0.00	0.02	0.00	0.00	0.00
V ₂ O ₅	0.00	-	1.53	0.00	-	1.54	1.43	1.82	1.82	1.51	1.39	1.51	1.82	3.86	3.86	3.88
F	0.20	-	0.70	0.00	-	0.04	0.35	0.39	0.00	0.47	0.00	0.47	0.00	0.09	0.09	0.00
Cl	0.00	-	0.01	0.00	-	0.00	0.00	0.00	0.00	0.00	0.01	0.00	0.00	0.02	0.02	0.00
Total	96.07	96.08	99.17	98.82	99.33	97.66	98.69	98.81	98.14	98.42	96.63	98.42	98.14	99.02	99.02	98.91

NB. FeO* = total iron as FeO; - not determined.

Appendix 2.8. Apatite, calcite, ilmenite and magnetite compositions from the Matuu-Masinga area, central Kenya. Lith.= lithologies: DRT = diorite, AMP = amphibolite; GAB = gabbro, GRNT = granulite. Min.= mineral: Apt = apatite, Cc = calcite, Ilm = ilmenite, Mgn = magnetite.

Sample Lith. Min.	MU-7 DRT Apt	MU-7 DRT Apt	MU-7 DRT Apt	MU-7 DRT Apt	MU-5 GAB Apt	MU-5 GAB Apt	MU-5 GAB Apt	MU-19 AMP Cc	MU-19 AMP Cc	MU-19 AMP Cc	MU-19 AMP Cc	MU-19 AMP Ilm	MU-23 GRNT Mgn
SiO ₂	0.19	0.25	0.19	0.22	0.39	0.06	0.31	0.06	0.07	0.06	0.06	0.06	-
TiO ₂	0.01	0.01	0.02	0.00	0.01	0.00	0.00	0.01	0.01	0.00	0.01	46.98	-
Al ₂ O ₃	0.01	0.00	0.01	0.01	0.01	0.02	0.02	0.02	0.01	0.01	0.01	-	-
Cr ₂ O ₃	0.04	0.00	0.01	0.00	0.00	0.00	0.00	0.00	0.00	0.00	0.00	-	-
FeO*	0.14	0.05	0.14	0.06	0.04	0.04	0.04	0.03	0.06	0.03	0.02	49.82	95.33**
MnO	0.12	0.10	0.06	0.14	0.04	0.04	0.07	0.02	0.01	0.02	0.04	2.19	-
MgO	0.00	0.00	0.00	0.00	0.00	0.00	0.00	0.00	0.00	0.00	0.00	-	-
CaO	53.63	53.44	53.42	53.24	52.64	54.83	52.95	54.77	54.77	54.88	54.88	-	-
Na ₂ O	0.10	0.07	0.09	0.06	0.06	0.01	0.05	0.01	0.02	0.01	0.01	-	-
K ₂ O	0.00	0.00	0.00	0.00	0.00	0.00	0.00	0.00	0.00	0.00	0.00	-	-
BaO	0.00	0.04	0.00	0.00	0.14	0.01	0.00	0.01	0.02	0.01	0.00	-	-
CoO	0.01	0.01	0.03	0.00	0.02	0.02	0.00	0.02	0.00	0.06	0.06	-	-
NiO	0.00	0.00	0.02	0.00	0.03	0.01	0.01	0.00	0.00	0.01	0.01	-	-
V ₂ O ₃	0.00	0.00	0.00	0.00	0.00	0.00	0.00	0.20	0.25	0.00	0.00	-	-
F	2.19	1.91	2.36	2.18	1.39	2.45	2.65	2.49	2.49	2.17	2.17	-	-
Cl	0.38	0.31	0.30	0.30	0.28	0.08	0.28	0.08	0.08	0.10	0.10	-	-
P ₂ O ₅	42.72	42.69	42.65	42.72	43.25	-	42.81	-	-	-	-	-	-
CO ₃	-	-	-	-	-	43.40	-	43.45	43.45	43.35	43.35	-	-
Total	99.54	98.88	99.31	98.93	98.30	100.08	99.19	100.17	100.17	99.78	99.78	98.99	95.33

FeO* = total iron as FeO; ** = total iron as Fe₃O₄; - not determined.

Appendix 2.9. Chlorite and epidote compositions from Matuu-Masinga area, central Kenya. Lith.= lithologies: GTE = granite, AMP = amphibolite, GAB = gabbro. Min.= mineral: Chl = chlorite, Epd = epidote.

Sample Lith. Min.	MU-8 GTE Chl	MU-8 GTE Chl	MU-8 GTE Chl	MU-8 GTE Chl	MU-8 GTE Chl	MU-8 GTE Chl	MU-8 GTE Chl	MU-20 GAB Epd	MU-20 GAB Epd	MU-20 GAB Epd	MU-20 GAB Epd
SiO ₂	28.29	27.83	28.34	27.31	29.07	29.92	29.23	37.15	37.81	37.11	37.38
TiO ₂	0.08	0.02	0.07	0.03	0.05	0.04	0.07	0.12	0.02	0.08	0.03
Al ₂ O ₃	16.87	17.28	15.16	16.16	17.03	16.67	17.14	25.88	26.61	25.69	25.92
Cr ₂ O ₃	0.00	0.05	0.00	0.00	0.01	0.00	0.01	0.02	0.00	0.05	0.00
FeO*	35.17	35.32	33.88	35.26	33.56	31.84	32.47	7.93	7.35	7.90	8.22
MnO	0.12	0.12	0.06	0.08	0.08	0.01	0.09	0.09	0.03	0.11	0.06
MgO	7.10	6.15	9.83	7.01	7.59	7.51	6.34	0.00	0.00	0.00	0.00
CaO	0.18	0.12	0.13	0.14	0.19	0.36	0.24	23.28	23.31	23.47	23.32
Na ₂ O	0.07	0.06	0.04	0.05	0.07	0.06	0.05	0.01	0.00	0.00	0.00
K ₂ O	0.04	0.04	0.05	0.05	0.07	0.23	0.36	0.00	0.00	0.00	0.00
BaO	0.00	0.09	0.00	0.00	0.03	0.00	0.00	0.08	0.00	0.04	0.00
CoO	0.00	0.06	0.00	0.00	0.00	0.00	0.00	0.00	0.00	0.00	0.03
NiO	0.00	0.01	0.02	0.00	0.00	0.06	0.05	0.02	0.01	0.00	0.00
V ₂ O ₃	0.00	0.00	0.10	0.28	0.00	0.00	0.06	0.02	0.17	0.00	0.00
F	0.00	0.29	0.06	0.00	0.23	0.00	0.03	0.69	0.12	0.21	0.09
Cl	0.02	0.01	0.00	0.00	0.00	0.03	0.00	0.00	0.01	0.00	0.00
Total	87.94	87.45	87.74	86.37	87.98	86.73	86.14	95.29	95.44	94.66	95.05

FeO* = total iron as FeO.

Sample Lith. Min.	MX-21 GAB Epd	MX-21 GAB Epd	MX-21 GAB Epd	MU-26 AMP Epd	MU-26 AMP Epd	MU-26 AMP Epd	MU-26 AMP Epd	MU-26 AMP Epd	MU-26 AMP Epd
SiO ₂	36.89	37.23	36.40	36.60	36.60	36.97	36.83	37.10	36.93
TiO ₂	0.18	0.09	0.22	0.13	0.18	0.12	0.22	0.10	0.14
Al ₂ O ₃	23.39	23.37	23.42	22.48	22.52	23.02	22.57	22.51	22.65
Cr ₂ O ₃	0.02	0.07	0.00	0.00	0.04	0.00	0.00	0.00	0.00
FeO	11.02	11.02	11.24	11.30	11.53	11.18	12.05	12.10	12.10
MnO	0.15	0.14	0.12	0.29	0.21	0.23	0.10	0.15	0.17
MgO	0.00	0.00	0.00	0.00	0.00	0.00	0.00	0.00	0.00
CaO	22.97	22.90	22.87	22.75	22.56	22.40	22.81	22.99	23.10
Na ₂ O	0.00	0.00	0.00	0.02	0.00	0.00	0.01	0.00	0.00
K ₂ O	0.00	0.00	0.01	0.00	0.00	0.00	0.01	0.00	0.00
BaO	0.04	0.04	0.00	0.05	0.13	0.03	0.04	0.00	0.02
CoO	0.00	0.02	0.00	0.00	0.00	0.00	0.00	0.00	0.00
NiO	0.00	0.00	0.00	0.01	0.00	0.03	0.01	0.00	0.00
V ₂ O ₃	0.00	0.06	0.05	0.00	0.05	0.05	0.11	0.04	0.07
F	0.30	0.00	0.00	0.09	0.00	0.12	0.27	0.00	0.00
Cl	0.00	0.00	0.00	0.00	0.00	0.00	0.02	0.00	0.01
Total	94.96	94.94	94.33	93.72	93.82	94.15	95.05	94.99	95.19

Appendix 3.1. Geochemical analysis of the Mozambique belt intrusive rocks from Matuu- Masinga area, central Kenya. Major elements in weight %, trace elements in ppm.

Sample	MU-1A	MU-1B	MU-2	MU-3	MU-4	MU-5A	MU-5B	MU-6A	MU-6B
SiO ₂	74.4	64.11	52.56	49.5	51.7	48.84	44.12	70.44	69.04
TiO ₂	0.41	0.58	2.61	3.08	1.84	2.03	4.51	0.75	0.62
Al ₂ O ₃	12.83	15.42	14.36	13.73	18.37	14.99	12.54	13.43	13.8
FeOt	2.61	5.7	12.63	12.95	8.34	12.93	17.3	5.95	4.7
MnO	0.05	0.16	0.16	0.17	0.13	0.17	0.23	0.06	0.06
MgO	0.69	1.51	4.42	4.1	4.11	6.92	5.25	0.99	0.79
CaO	1.35	1.67	6.79	6.78	7.62	8.48	8.48	2.24	1.8
Na ₂ O	4.99	4.86	3.1	3.26	4.19	3.01	2.92	3.79	3.49
K ₂ O	1.5	2.46	2.21	2.3	1.04	0.77	0.87	4.38	4.51
P ₂ O ₅	0.05	0.08	1.18	1.17	0.56	0.56	2.15	0.24	0.23
Total	98.88	96.55	100.02	97.04	97.9	98.7	98.37	102.27	99.04
Nb	4	7	36	36	13	18	49	16	14
Zr	189	197	353	389	151	97	293	373	328
Y	27	35	45	43	23	33	61	45	33
Sr	192	225	920	981	1387	806	1137	336	257
Rb	22	35	41	47	5	7	3	96	94
Th	3	4	3	3	1	1	nd	16	10
Pb	8	16	14	15	8	8	8	18	19
Ga	11	18	22	22	24	23	24	18	18
Zn	40	61	161	157	103	133	264	82	72
Cu	26	48	2396	3229	1030	1450	5810	326	325
Ni	7	8	41	31	31	93	43	10	8
Co	5	10	46	37	24	58	48	7	10
Cr	24	35	74	15	54	133	183	34	223
Ce	27	35	118	123	54	55	176	163	105
V	46	76	209	228	111	212	320	61	29
Ba	361	519	1411	1507	1034	544	1333	1131	1341
Mg*	21	21	26	24	33	35	23	14	14

Samples:

MU-1A quartz feldspar gneiss

MU-1B quartz diorite

MU-2 medium grained gabbro dyke

MU-3 medium grained gabbro

MU-4 coarse grained gabbro

MU-5A fine grained meta-gabbro

MU-5B medium grained meta-gabbro

MU-6A coarse grained grey granite

MU-6B medium grained grey granite

Mg* = 100MgO/(MgO + FeOt)

FeOt = FeO + Fe₂O₃.

nd - not detected

Appendix 3.1.Cont.....

Sample	MU-7	MU-8	MU-10	MU-12	MU-13	MU-14	MU-15	MU-16
SiO ₂	53.23	70.43	59.69	69.8	70.75	68.48	47.39	54.85
TiO ₂	2.65	0.5	1.63	0.19	0.28	0.22	0.82	1
Al ₂ O ₃	14.88	13.79	13.33	15.67	15.54	16.09	15.63	15.62
FeO _t	11.1	3.34	10.52	1.19	1.37	1.15	12.69	9.92
MnO	0.13	0.04	0.18	0.02	0.02	0.02	0.37	0.17
MgO	3.71	0.58	1.75	0.26	0.31	0.19	5.67	4.88
CaO	6.58	1.35	3.96	1.15	1.1	1.27	14.44	7.71
Na ₂ O	3.34	3.57	3.46	4.8	4.72	5.17	2.55	3.13
K ₂ O	2.19	5.37	3.7	4.53	4.36	3.8	0.85	1.6
P ₂ O ₅	1.33	0.15	0.83	0.05	0.05	0.08	0.16	0.3
Total	99.14	99.12	99.05	97.66	98.5	96.47	100.57	99.18
Nb	23	7	52	1	1	3	1	4
Zr	259	386	584	94	140	125	37	93
Y	41	15	83	4	9	7	17	30
Sr	992	518	676	999	911	1399	348	469
Rb	32	81	75	73	72	78	8	23
Th	2	14	4	2	10	6	nd	1
Pb	13	41	31	26	57	58	16	10
Ga	23	16	24	17	18	18	17	17
Zn	136	45	218	31	34	38	79	88
Cu	2184	163	1363	41	32	60	371	501
Ni	42	5	1	3	3	2	69	35
Co	30	4	15	10	8	1	41	36
Cr	93	17	nd	11	5	3	220	90
Ce	87	190	261	11	27	19	11	26
V	178	35	85	17	26	20	261	219
Ba	1324	755	1841	1392	1121	1006	167	595
Mg*	25	15	14	18	18	14	31	33

MU-7 medium grained diorite

MU-16 coarse grained diorite

MU-8 coarse grained pink granite

MU-10 coarse grained syeno-diorite

MU-12 coarse grained granitoid gneiss

MU-13 medium grained granitoid gneiss

MU-14 medium grained granitoid gneiss

MU-15 medium grained meta-gabbro

Appendix 3.1.Cont.....

Sample	MU-17A	MU-20A	MU-20B	MU-23	MU-24	MU-28	MU-29
SiO ₂	74.5	45.38	49.87	38.9	48.76	51.14	65.54
TiO ₂	0.22	1.45	0.42	0.84	0.49	2.84	1.02
Al ₂ O ₃	15.55	11.48	18.85	23.77	14.53	15.34	14.02
FeO _t	1.79	14.99	9.8	12.52	10.6	12.09	6.31
MnO	0.03	0.19	0.12	0.17	0.18	0.16	0.09
MgO	0.43	12.41	3.44	0.11	10.91	4.73	1.15
CaO	1.58	12.69	17.85	25.52	13.42	7.92	2.62
Na ₂ O	5.8	1.39	0.82	0.15	1.91	3.4	3.4
K ₂ O	2.58	0.61	0.2	0.05	0.72	1.65	4.45
P ₂ O ₅	0.07	0.09	0.04	0.23	0.05	1.54	0.4
Total	102.55	100.68	101.41	102.26	101.57	100.81	99
Nb	2	1	nd	4	1	25	26
Zr	80	24	64	242	19	290	589
Y	5	21	18	48	11	42	50
Sr	889	116	975	1032	235	1223	411
Rb	45	2	2	1	3	23	92
Th	3	1	3	7	1	1	9
Pb	36	4	20	19	4	12	21
Ga	19	13	26	33	12	22	20
Zn	31	82	32	7	121	137	120
Cu	68	188	48	470	92	2782	571
Ni	2	87	45	nd	76	47	8
Co	6	61	26	9	52	32	12
Cr	9	274	41	21	168	107	19
Ce	10	1	10	38	2	98	242
V	26	380	206	170	220	187	72
Ba	874	111	84	257	97	1379	1410
Mg*	19	45	26	1	51	28	15

- MU-17A fine grained quartz feldspar gneiss
- MU-20A coarse grained meta-gabbro
- MU-20B coarse grained meta-gabbro
- MU-23 medium grained plagioclase-pyroxene-garnet gneiss
- MU-24 medium grained amphibolite
- MU-28 medium grained meta-gabbro
- MU-29 coarse grained porphyritic granite